Petroleum Reservoir Performance Evaluation Based on Compositional Grading Models

IKECHI IGWE, *B.Tech., PGD, MSc, M.Tech.*

This thesis is submitted in partial fulfilment of the requirements for the award of the degree

of

Doctor of Philosophy

of the

University of Portsmouth

United Kingdom

September 2020

Abstract

Analysis of the technical implications of initialising reservoir simulation models with and without compositional grading (CG) models on realistic reserves estimates and reservoir performances prediction have been considered. The mathematical framework for the compositional grading modelling is based on one-dimensional zero-mass-flow stationary state assumption. Computer Modelling Group's WinProp, was used for the fluid modelling while Computer Modelling Group's compositional reservoir simulator, GEM, was used for the reservoir modelling and simulation. In the absence of historical production data, Computer Modelling Group's CMOST was used to perform uncertainty assessment for the validation of models results and for sensitivity analysis. The effect of various equations of state on the performances of initialised reservoir models and the effect of changes in temperature gradient on the performances of applied nonisothermal CG initialised reservoir models are also reported.

The research results suggests that inadequate account or complete neglect of compositional grading effect in reservoir simulation model initialisation has significant technical consequences. The results shows that constant composition (without CG) initialised reservoir model overestimated the original oil in-place by 13.86 % more than the isothermal model, 24.37 % more than the zero thermal CG model, 24.44 % more than the Haase;s thermal diffusion CG model, and 24.41 % more than the Kempers model. However, it underestimated original gas in-place by 12.73 % less than the isothermal CG model, 21.24 % less than the zero thermal diffusion CG model, 21.35 % less than the Haase's thermal diffusion CG model, and 21.31 % less than the Kempers thermal diffusion CG initialised reservoir model. The results of the sensitivity analysis shows that for all the initialised reservoir models, water saturation (which indirectly accounts for hydrocarbon saturation) with 82-88 % main effects is the most sensitive input parameter responsible for the estimated reserve volumes. The observed differences in in-place volumes estimated by the various CG models are due to the influence of the CG models on the reservoir fluid formation volume factor, which made the hydrocarbon saturation (compositions of various components) to either increase or reduce in the gas and oil phases, respectively. Analysis of the effect of various equations of state (EOSs) on the performances of initialised reservoir models suggest that, although, the choice of applied EOSs is not very critical to the efficient performances of reservoir models initialised without CG models, each EOSs had noteworthy different impact on the performances of

reservoir models initialised with CG models. Therefore, to effectively predict the performances of compositionally sensitive reservoir, it is important that a sensitivity analysis be carried out to determine the EOS that will guarantee optimal performance. Increasing the temperature gradient in nonisothermal CG initialised reservoir models from 0.002 ^{o}F/ft to 0.5 ^{o}F/ft caused a 30.69 % decrease in the OOIP estimated by zero (passive) thermal diffusion CG initialised reservoir model; 34.14 % increase in OOIP estimated by Haase's thermal diffusion CG initialised reservoir model; and 38.34 % decrease in the OOIP estimated by the Kempers thermal diffusion CG initialised reservoir model. A further increase in the temperature gradient from 0.5 ^{o}F/ft to 2.5 ^{o}F/ft caused a 22.48 % increase in the OOIP estimated by the Kempers thermal diffusion CG initialised reservoir model; 61.43 % increase in OOIP estimated by Haase's thermal diffusion CG initialised reservoir model; and 44.73 % decrease in the OOIP estimated by zero thermal diffusion CG initialised reservoir model. Therefore, temperature gradient and its associated thermal diffusion factor can significantly influence the performances of nonisothermal CG initialised reservoir models. Hence, need to adequately account for thermal diffusion factor during reservoir simulation model initialisation.

The results of this work provides a new insight into the impact of neglecting compositional grading in field development studies and should encourage field managers, and in particular those of Niger Delta, to put more weight into the investigation of compositional grading effects and to support research works in this area.

Declaration

Whilst registered as a candidate for the above degree, I have not been registered for any other research award. The results and conclusions embodied in this thesis are the work of the name candidate and have not been submitted for any other academic award. Some of the results presented in this thesis have already been published.

IKECHI IGWE

14/09/2020.

Contents

List of Figures

List of Tables

Abbreviations and Symbols

Abbreviations

AAD	Average Absolute Deviation
AD	Absolute Difference
AIAA	American Institute of Aeronautics and Astronautics
AIS	Adaptive Importance Sampling
API	American Petroleum Institute
AMV	Advanced Mean Value
ASME	American Society of Mechanical Engineers
BHP	Bottom Hole Pressure
BIC	Binary Interaction Coefficient
CCE	Constant Composition Expansion
CG	Compositional Grading
CGS	Compositional Grading Simulation
CMG	Computer Modelling Group
CVD	Constant Volume Depletion
DL	Differential Liberation
EOS	Equation of State
EOSs	Equations of State
FORM	First Order Reliability Methods
GCE	Gravity Chemical Equilibrium
G&D	Graboski and Daubert
GOC	Gas-Oil Contact
GOR	Gas-Oil Ratio
HC	Hydrocarbon
LSFEM	Least-Squares Finite-Element Method
MCS	Monte Carlo Simulation
MD	Molecular Dynamics
MW	Molecular Weight
NHT	Net Heat of Transport
OGIP	Original Gas In-Place
OOIP	Original Oil In-Place
poro	Poeosity
PR	Peng and Robinson
PR-EOS	Peng and Robinson Equation of State
PVT	Pressure–Volume–Temperature
RF	Recovery Factor
RK	Redlich and Kwong
STG	Surface Gas Rate
STO	Surface Oil Rate
STW	Surface Water Rate
SRK	Soave-Redlich-Kwong
SRK EOS	Soave-Redlich-Kwong Equation of State
TDF	Thermal Diffusion Factor
UA	Uncertainty Assessment
U.S. DOE	U.S. Department of Energy
vdW	van der Waals
XFT	Offset of the simulation grid origin in the x-direction
YFT	Offset of the simulation grid origin in the y-direction

ZFT	corner point depths for corner point grids
ZDEPTH	Keyword for global composition versus depth
1D	One-Dimensional
2D	Two-Dimensional
3D	Three-Dimensional

Symbols

a	Intermolecular attractive force
B	Formation volume factor
b	Intermolecular repulsive force
b_i	PR co-volume of component *i*
D_{ij}	Molecular diffusion coefficient
D_i^P	Pressure diffusion coefficient
D_i^T	Thermal diffusion coefficient
c	Volume correction constant or total molar density
f_i	Fugacity of component *i*
G	Molar Gibbs free energy
g	Acceleration due to gravity
H or H_m	Molar enthalpy of the mixture
H_i	Molar enthalpy of component *i*
h	Depth, reservoir thickness or elevation above arbitrarily chosen datum
h^o	Reference depth
h_{GOC}	Gas oil contact location
J	Diffusion flux
J_{Gi}	Effect of gravity
J_{Ti}	Thermal diffusion factor
k	Permeability
k_{rg}	Relative permeability to gas
k_{ro}	Relative permeability to oil
k_{rog}	Relative permeability to oil in oil-gas system
k_{rw}	Relative permeability to water
K_T	Column vector of the thermal diffusion ratios in a multicomponent mixtures
k_{Ti}	Thermal diffusion ratio for component *i*
δ_{ij}	The Kronecker delta
α	A function introduced to fit the vapour pressure data of petroleum mixture
$L=[L_{ij}]$	Matrix of the phenomenological coefficients
μ	Fluid viscosity
μ_i	Chemical potential of component *i*
$\nabla\mu_i$	Chemical potential gradient of component *i*
μ_i^o	Chemical potential of component *i* at the reference state
β_c	Transmissibility conversion factor
φ_i	Fugacity coefficient of component *i*

φ_i^h	Fugacity coefficient of component *i* at a certain depth
$\varphi_i^{h^o}$	Fugacity coefficient of component *i* at a reference depth
∇p	Pressure gradient
∇p_R	Reference sample reservoir pressure gradient
∇p_s	Reference sample saturation pressure gradient
∇T	Temperature gradient
$\nabla \mathrm{x}_i$	Mole fraction of component *i* gradient
ΔU_i^*	Partial molar activation energy for component *i* in the mixture
ΔU_m^*	Function of the viscosity-to-density ratio
$\nabla \bar{U}_i$	Partial molar internal energy departure of component *i*
$\nabla U_i^{vap.}$	Energy of vaporisation
$\nabla U_i^{vis.}$	Energy of viscous flow of pure component *i*
M	Molecular weight of mixture
M_i	Molecular mass or weight of component *i*
M_k	Molecular weight of component *k,*
n_k	Mole fraction of component *k*
P	Pressure
p_{cow}	Capillary pressure between oil and water phases
P_g	Gas pressure
P_o	Oil pressure
P_w	Water pressure
P^o	Reference pressure
p_s^o	Reference saturation pressure
p_R^o	Reference reservoir pressure
p_i^h	Pressure at a depth
$p_i^{h^o}$	Pressure at a reference depth
Q	Column vector
q_w	Well rate
Q_i^*	Net heat of transport of component *i*
T	Temperature
T_r	Reduced temperature
N or n	Number of components
n	Number of moles
°C	Degree centigrade
°C/m	Degree Centigrade per metre
°F	Degree fahrenheit
P_c	Critical pressure
P_T	Pressure at the top of the hydrocarbon column
P_s	Saturation pressure
P_{sB}	Saturation pressure at the bottom of the hydrocarbon column

P_{sT}	Saturation pressure at the top of the hydrocarbon column
R	Universal gas constant
r	Radial distance
r_w	Well radius
s_i	Shift parameter of component *i*
S_i	Partial molar entropy of component *i*
s_g	Gas saturation
s_w	Water saturation
V	Volume
$\overline{V_k}$	Partial molal volume of component *k*
$\overline{\underline{V}}_k$	Residual partial molal volume of component *k*
V_m	Molar volume
v	Molar volume
v^*	Linearly translated volume
v^L	Molar volume of the liquid phase
v^V	Molar volume of the vapour phase
$v^L{}_{corr}$	Corrected volumes of the liquid phase
$v^V{}_{corr}$	Corrected volumes of the vapour phase
$\overline{\mathrm{v}}_i$	The partial molar volume of component *i*
ρ	Mass density
ω	Acentric factor
δ_{mn}	Binary interaction coefficient
wt %	Percentage weight
x *or* x	Mole fraction
x_i	Mole fraction of components *i*
χ_m	Mole fraction of components *m*
χ_n	Mole fraction of components *n*
Z	Compressibility factor/fluid composition
z_B	Composition at the bottom of hydrocarbon column
z_T	Composition at the top of hydrocarbon column
Z^o	Reference fluid composition
z_i^h	Composition of component *i* at a certain depth
$z_i^{h^o}$	Composition of component *i* at a reference depth

Acknowledgements

I wish to express my gratitude to my supervisor, Dr. Jebraeel Gholinezad, for his guidance, suggestions and comments throughout my research work. I also wish to thank my second supervisor, Dr. Mohamed Hassan, for his support and advises.

I am very grateful to the PSC Division of the National Petroleum Investment Management Services (NAPIMS) Nigeria and Chevron Nigeria Limited for providing the data for this work. Time will not fail me to acknowledge the role played by Engr. Tamunotonye John Adegbenro Allison and Engr. Frank Ogbuagu, in facilitating the release of the research data.

It is my pleasure to thank the Tertiary Education Trust Fund (TETFund), Nigeria and the Rivers State University, Nigeria, for sponsoring this research work.

Many thanks to the staff and student of Petroleum Engineering, School of Energy and Electronic Engineering (formerly School of Engineering) and to the Faculty of Technology, University of Portsmouth. The research experience you offered me is worth its weight in gold. I also wish to thank the Computer Modelling Group (CMG) for their partnership with the University of Portsmouth, which made the applied software available for this research.

I would like to acknowledge my wife, Emilia, my mother, Grace, my brothers and sisters for their very kind support during the course of this research. I am sincerely grateful to all my friends for their moral support and prays for my family and I.

Dedication

To God Almighty and to my children – Iknebubechim and Jachinma.

CHAPTER 1

INTRODUCTION

1.1 Research Background

To efficiently produce reservoir fluids from the reservoir to the surface, it is necessary to know the compositions of the fluids, the behaviour of the fluids at reservoir and surface conditions and the processes and factors responsible for the established behaviour of the fluid systems. These tasks can be achieved with the help of reservoir simulation study.

Most compositional reservoir simulation practices assumes that the compositions of the various fluid components are the same at all locations within the reservoir system. However, studies have shown that the constant composition assumption is incorrect and unrealistic as it may ignore the occurrences of some physical processes such as gravitational segregation of components, thermal diffusion causing compositional gradient in opposition to gravity effect, natural convection induced by horizontal temperature difference, and biodegradation of hydrocarbon fluids, in some reservoirs (Hoier and Whitson, 2000; Bogatyrev et al., 2015; Nikpoor et al., 2013a, 2016; Pedersen and Hjermstad, 2015). Several research efforts have shown that gravitational force, temperature gradient, and thermal diffusion, amongst other factors, contributes significantly to distribution and gradation of hydrocarbon fluid compositions in the some reservoirs (Hamoodi et al., 1994; Hoier and Whitson, 2000; Leahy-Dios, 2008; Nikpoor et al., 2011, 2013a; Bogatyrev et al., 2015; Pedersen and Hjermstad, 2015; Nikpoor et al., 2016). This compositional variation with depth is what is known as compositional grading (CG) or compositional gradient. CG in petroleum reservoirs will give rise to variation in other fluid properties, such as gas-oil ratio (GOR), saturation pressure, density, molecular weight (Whitson and Belery, 1994; Pedersen and Hjermstad, 2015; Nikpoor *et al.*, 2016). Therefore, to accurately estimate in-place volumes and predict reservoir performances, it is necessary to adequately account for CG in reservoir simulation model initialisation. This will require coupling reservoir simulation models with CG models that adequately accounted for the factors responsible for observed compositional variation with depth in the reservoir of interest. The effect of gravity alone is simulated using the isothermal CG model while the combined effect of gravity, temperature gradient and thermal diffusion are simulated based on nonisothermal CG

models – zero thermal diffusion model; Haase's thermal diffusion model; and Kempers thermal diffusion model.

1.2 Problem Statement and Research Gaps

It has been reported that reservoir performance indicators such as original hydrocarbon in-place and cumulative oil and gas productions can either be overestimated or underestimated (depending on the type of reservoir fluid) if CG is not adequately accounted for or completely ignored in reservoir simulation model initialisation (Favang et al., 2000; Jaramillo and Barrufet, 2001). Therefore, technical decisions made based on production forecast derived from models that ignored or inadequately accounted for CG effect, will inevitably lead to detrimental technical consequences. For instance, field development decisions based on the performances of initialised reservoir models that inadequately accounted for CG or completely ignored CG effect, will lead to wasted investment in the design and procurement of oversized surface and subsurface oil production handling facilities and equipment. That is, if such reservoir model significantly overestimated oil production. Such development decisions will also mean the design or procurement of undersized surface handling facilities for gas production since the same initialised reservoir model will definitely underestimate cumulative gas production. This problem could lead to more adverse technical consequences such as loses in production or complete operational shutdown due to limited surface handling capacity for the unexpected high volume of produced gas. It could also lead to environment issues such as gas flaring, which is still ongoing in some Nigeria oil and gas fields.

Therefore, to accurately estimate in-place volumes and reservoir performances, it is necessary to initialise applied reservoir simulation model with CG model that adequately accounts for the factors responsible for CG in the reservoir system (Favang et al., 2000). Available literature indicates limited application of CG models for reservoir model initialisation, with isothermal CG models as the main CG model that has been applied for this purpose (Whitson et al., 1999; Favang et al., 2000; Jaramillo and Barrufet, 2001; Liu et al., 2001; Vo, 2010; Mokhtari and Ashoori, 2013). However, it has been shown that gravity effect alone and the constant temperature assumptions by isothermal CG model are likely inappropriate since temperature gradient and its concomitant thermal diffusion

effect also contribute to compositional variations with depth in the reservoir (Hoier, 1997; Hoier and Whitson, 2000; Nikpoor et al., 2013a; Pedersen and Hjermstad, 2015).

Therefore, by using nonisothermal CG models that accounts adequately for the combine effects of gravity, temperature gradient, and thermal diffusion to initialise reservoir simulation models, this research effort seeks to contribute to knowledge by elucidating the technical implications of initialising reservoir simulation models with and without CG models, on accurate reserves estimation and reservoir performances prediction. This is the main thrust of this current research effort.

Sensitivity analysis of reservoir simulation outcomes are intended to show what variables in the various initialised reservoir models are mostly responsible for observed differences in reserves estimates and predicted reservoir performances. Therefore, sensitivity analysis outcomes provides the premise for establishing the relationship between observed compositional variations with depth, the various CG initialised reservoir models, and observed differences in reserves estimates. This is another major novel contribution of this work to knowledge. Also, the analysis of the effect of various EOSs on the performances of CG initialised reservoir models and the effect of changes in temperature gradient on the performances of applied nonisothermal CG initialised reservoir models are novel contributions of this work to knowledge.

Efficient and effective pressure maintenance option is very important for optimal field development strategy and reservoir performance optimisation. Jaramillo and Barrufet, (2001) posited that CO_2 injection (pressure maintenance) improved the performances of isothermal CG initialised reservoir model more than it did on reservoir model initialised without CG model. However, there is a limited report of the effect of CO_2 or separator gas injection on the performances of nonisothermal CG initialised reservoir model in the literature. Hence, this work seeks to investigate the comparative effects of water and separator gas injections, on the performances of reservoir models initialised with constant composition fluid model, isothermal CG model, and nonisothermal CG models.

1.3 Research Questions

The research concept, methodology, and obtained results were motivated by the following major research questions, which highlights the research main areas of focus:

- What are the technical implications of initialising reservoir simulation models with and without CG models?
- What input variables in the various initialised reservoir simulation models are mostly responsible for observed differences in the estimated in-place volumes?
- Which pressure maintenance option, water injection or gas cycling, is an optimal pressure maintenance option for CG initialised reservoir model?
- What are the effects of different EOSs on the performances of the various initialised reservoir models?
- What are the effects of changes in temperature gradient on the performances of nonisothermal CG initialised reservoir models?

1.4 Aims and Objectives

The aim of this research are to evaluate the technical implications of initialising reservoir simulation models with and without CG models, on realistic reserve estimates and reservoir performances prediction. This research aim would be achieved through the following objectives:

1. To evaluate the technical implications of initialising reservoir simulation models with and without CG models, under water and separator gas injection scenarios.
2. To determine the input parameters in the various initialised reservoir model that are mostly responsible for observed differences in reserves estimates and predicted reservoir performances, thereby, establish the relationship between observed CG, the various CG initialised reservoir models, and observed differences in reserves estimates.
3. To evaluate the effects of different EOSs on the performances of the various initialised reservoir models.
4. To investigate the effects of changes in temperature gradient on the performances of nonisothermal CG initialised reservoir models.

The development of a new empirical model is beyond the scope of this Ph.D work.

1.5 Research Scope and Limitations

Applied methodology is limited to modelling and simulation using Computer Modelling Group's simulators for the fluid modelling, geologic modelling, dynamic reservoir modelling and simulation, uncertainty assessment, and sensitivity analysis. In the absence of historical production data, uncertainty assessment was used for the validation of the

initialised reservoir simulation models results. Another inherent limitation is the unavailability of the study reservoir actual geological map. Hence, the geological surfaces or horizons (top and bottom maps), which also defined the geomodel outer boundaries, were generated from correlation of formation tops from available well logs based on inverse distance estimation method. Static CG models considered are the isothermal, zero thermal diffusion, Haase's thermal diffusion, and Kempers thermal diffusion CG models, respectively. The mathematical framework for the CG modelling is based on one-dimensional zero-mass-flow stationary state assumption. The primary research data were obtained from high shrinkage black oil reservoir systems located offshore Nigeria. Obtained results can only be attributed to the study reservoir systems as other reservoir system may behave differently.

1.6 Thesis Layout

This thesis consists of five chapters:

- **Chapter 2 – Literature Review:** in order to establish the research gaps, extensive review of related literature was carried out and presented in this chapter. Discussions on related topics and fundamental principles associated with the research area are also presented in chapter 2.
- **Chapter 3 – Methodology**: the applied research data, methods, and procedures were presented and explained in chapter 3.
- **Chapter 4 – Results and Discussions:** the results obtained by applying the research data, methods and procedures stated in chapter 3 were presented and discussed in chapter 4.
- **Chapter 5 – Conclusions and Future Works:** this chapter presents a summary of the major research findings, relates them to the research aim and objectives. Also recommended in chapter 5 are future research works triggered by the current research results and limitations.

CHAPTER 2

LITERATURE REVIEW

2.1 Petroleum Reservoir System

The contained fluids in some petroleum reservoirs could be a combination of crude oil, natural gas, and water, as shown in Figure 2.1. Crude oil and natural gas are the hydrocarbon fluids of interest to the petroleum industries. These reservoir fluids can be produced (extracted) to the surface using different recovery methods shown in Figure 2.2. Figure 2.2 shows that the first production phase (phase 1) depends on primary recovery methods, which relies on the natural energy of the reservoir and artificial lift methods to drive reservoir fluids to the surface. In Phase 2 production history, secondary recovery methods – water injection/flooding and immiscible gas injection are the driving force responsible for the production reservoir fluids. After the economic limit of the primary and secondary recovery methods have been reached, tertiary recovery methods also known as enhanced oil recovery methods are deployed to producing residual hydrocarbon fluids from the reservoir. This is the final phase (phase 3) of the production history of a petroleum reservoir. Various tertiary recovery methods have been listed in Figure 2.2.

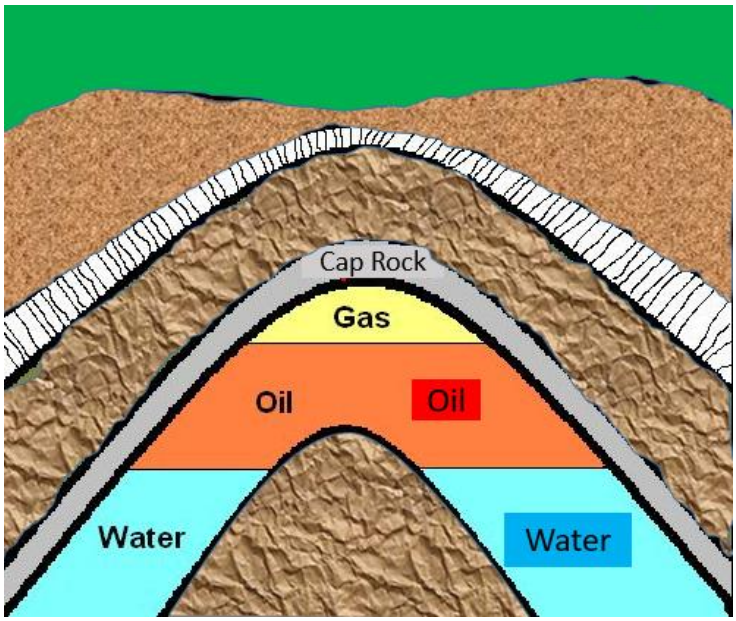

Figure 2.1: Schematic of a Cross-Section of a Petroleum Reservoir

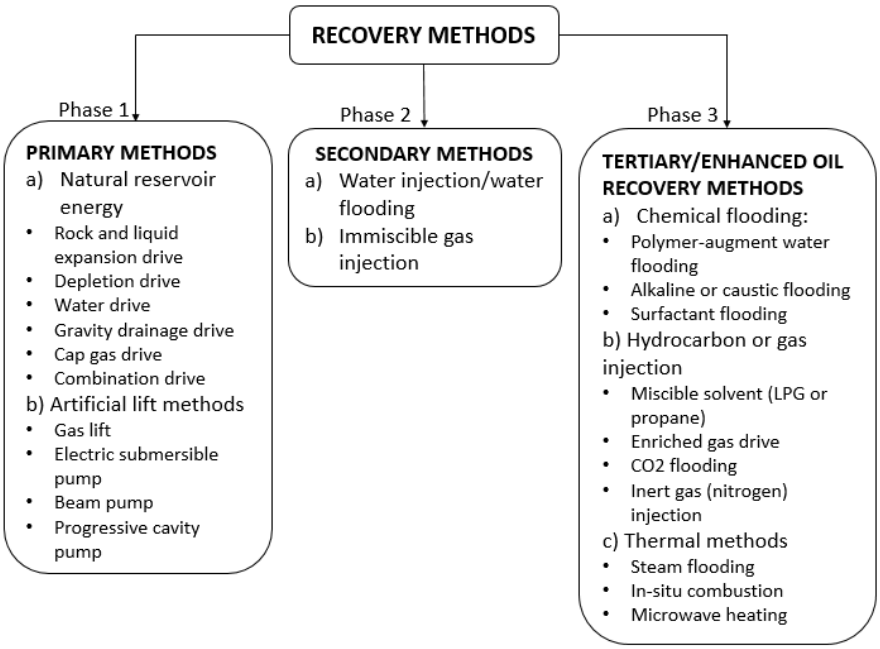

Figure 2.2: Production History of a Petroleum Reservoir

Hydrocarbon fluids consist of several hydrocarbon and non-hydrocarbon components, ranging from the light molecular weight components such as methane (C_1) to the heavy plus fractions. The compositions of the various components in the oil and gas phases, respectively, differs due to certain reservoir conditions (such as gravity and temperature). To effectively and efficiently produce these reservoir fluids from the reservoir to the surface as shown in Figure 2.3, it is necessary to know the compositions of the fluids, the behaviour of the fluids at reservoir and surface conditions and the processes and factors responsible for the established behaviour of the fluid systems. These tasks could be achieved with the help of reservoir simulation study.

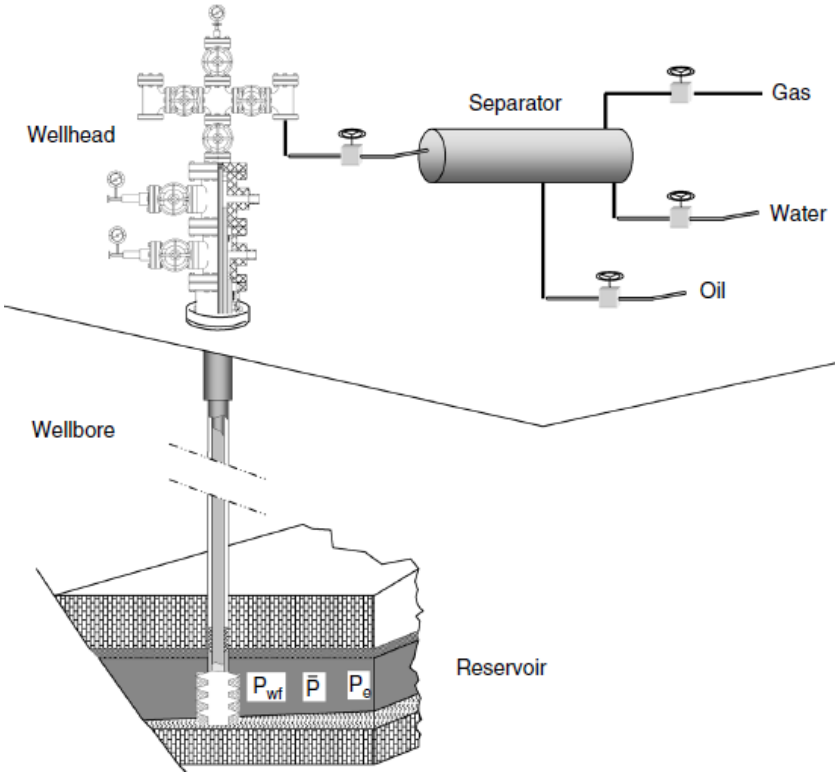

Figure 2.3: Schematic of a Petroleum Production System (Guo, 2011)

Reservoir simulation models (simulators) are classified as either black oil simulators or compositional simulators. In black oil simulator, oil and gas phases are represented by two components: one component is oil and the other is gas. The physical properties (like formation volume factors, gas oil ratio, and viscosity) are a function of pressure only. In the contrary, oil and gas are represented as multicomponent mixtures in compositional simulators. The oil phase and the gas phases are composed of different amounts of the same components. The compositions that are present in each phase are a function of pressure and temperature, and are also as a result of mass transfer occurring through the interface between the two phases (oil and gas). The built reservoir simulation model consists of mathematical models (equations) that represents different physical processes occurring in the reservoir, subject to certain constraint and conditions (Ezekwe, 2010). For example, the material balance equation accounts for the amount of fluid in the reservoir with respect to time, fluid flow equation describes flow processes in the reservoir, and energy balance equation describes the thermal processes occurring in the reservoir system.

2.2 PVT Analysis

Pressure–Volume–Temperature (PVT) analysis of reservoir fluids is essential for proper characterisation of petroleum reservoirs and adequate evaluation of their volumetric performances at various perturbations. Such evaluation will aid development of better reservoir management plan. In order to conduct PVT analysis of any reservoir fluid, a representative fluid sample is either taken from a reference depth in reservoir (bottom hole sampling) or at the surface (recombined oil and gas surface sampling). The collected sample is then transported to a PVT laboratory for standard PVT experiments. Compositional analysis, flash liberation, constant composition expansion (CCE), differential liberation (DL), and constant volume depletion (CVD), are standard experiments performed by PVT laboratories on reservoir fluids (Whitson and Brule, 2000). These standard experiments provide suitable PVT fluid properties (data) needed to study and understand the behaviour of the fluids in the reservoir, within the wells, in the piping system, and at surface conditions (Schlumberger, 2005). PVT fluid properties are also need to estimate: well stream composition as a function of time, completion design, possible miscibility effects due to gas injection, surface facility specification, contaminants (H_2S, CO_2 and N_2) concentration in produced fluids (Schlumberger, 2005). These PVT fluid properties (physical properties) include the oil and gas formation volume factor, fluid compressibility factor, solution gas oil ratio, fluid density and specific gravity, fluid viscosity and API gravity, saturation pressures, mole percent and molecular weight of components, etc. It is expected that fluid samples collected at different depths in a particular reservoir should have similar quality and exhibit similar characteristics but near-critical reservoirs have exhibited major variation in fluid compositions along the hydrocarbon column (Ahmed, 2007). Such compositional grading are primarily predicted from standard PVT experiments such as CCE and CVD experiments. The data needed for subsequent numerical simulation of PVT experiments and compositional grading are also generated from PVT laboratory experiments (Ahmed, 2007).

However, these PVT experiments are relatively expensive and the uncertainty in the accuracy of the results is also a major concern (Ahmed, 2007). Reservoir simulation models when adequately turned are capable of simulating the PVT properties of reservoir fluids, and can consequently save significant time and expenses by eliminating the need to performing a complete set of experimental PVT test on each and every new reservoir fluid (Ahmed, 2007). Also, with only one sample collected at a reference depth in the

reservoir, reservoir simulation can predict with certain degree of accuracy the composition and PVT properties of the reservoir fluid at different depths along the hydrocarbon column, thereby saving time, expense and improving the overall economy of the field. Therefore, the major reason for implementing reservoir simulation is economics.

2.2.1 Equation of State Model

An equation of state (EOS) is a semi-empirical relationship of pressure, volume, and temperature which describe the phase behaviour of pure substances. The application of EOS to multicomponent systems such as hydrocarbon mixtures requires an extra variable – composition, and a suitable mixing rule (Danesh, 1998). Mixing rules enable the description of the prevailing forces between molecules of different substances in the mixture (Danesh, 1998). Despite the fact that equilibrium conditions can be scrupulously determined thermodynamically, the accuracy of phase equilibrium prediction depends mainly on the capability of the EOS and the concomitant mixing rule (Danesh, 1998).

Most of the phase equilibrium calculations implemented for hydrocarbon mixtures were based on cubic EOS which dates back to the renowned work of van der Waals (vdW) in 1873 (Van Der Waals and Rowlinson, 2004; Pedersen et al., 2006). Redlich and Kwong, (RK) EOS was the first cubic EOS to gain extensive application in 1949 (Redlich and Kwong, 1949; Pederson et al., 2006). They introduced a temperature dependency to the attraction parameter "α" of the vdW EOS. Several other modifications of the vdW EOS have been reported in the literature (Thiele, 1963; Carnahan and Starling, 1972; Chien et al., 1983; Adachi and Lu, 1984; Lin et al., 1985; Watson et al., 1986; Wei and Sadus, 2000; Span et al., 2001; Tian and Gui, 2003). The RK EOS was further modified by Soave, and Peng and Robinson (Soave 1972; Peng and Robinson 1976; Robinson and Peng, 1978). Soave modified the RK EOS by replacing the temperature dependency of the attractive term in RK EOS with Pitzer's acentric factor to develop the original Soave-Redlich-Kwong (SRK) equation of state (Zudkevitch and Joffe, 1970; Joffe *et al.*, 1970; Soave, 1972). The acentric factor was introduced to enable prediction of hydrocarbon vapour pressure. Graboski and Daubert also modified the original SRK EOS by formulating a new expression for the constant "α" (Graboski and Daubert, 1978). This new modification is known as SRK (G&D) EOS. Peng and Robinson (PR) modified the SRK EOS by proposing an improved expression for the attractive term primarily to improve liquid density prediction (Zudkevitch and Joffe, 1970; Joffe *et al.*, 1970;

McCain, 1990). PR EOS shows performance analogous to SRK EOS, although, it is usually superior in calculating liquid densities of particularly nonpolar substances (Danesh, 1998). Several other modifications mainly aimed at improving performances of the various cubic EOSs have been reported in the literature (Harmens and Knapp 1980; Schmidt and Wenzel 1980; Patel and Teja 1982; Péneloux, et al., 1982; Mathias, 1983; Yu and Lu, 1987; Valderrama, 1990; Twu et al., 1991; Tsai and Chen, 1998; Ahlers and Gmehling, 2001; Cismondi and Mollerup, 2005; Haghtalabet al., 2010; Abudour et al., 2012; Burgess et al., 2013; Mahmoodi, 2016; Privat et al., 2016).

While an EOS mainly generates volumetric data, its main application in engineering is through its coupling with thermodynamic models in estimating phase behaviour and physical properties of fluids (Danesh, 1998). CG models are typical examples of such thermodynamic relations, which are usually coupled with EOS to predict hydrocarbon compositional variation and physical properties variation with depth in oil and gas reservoirs. The Peng-Robinson (PR) EOS used in this current research for PVT modelling of the reservoir fluid is stated thus:

$$p = \frac{RT}{v-b} - \frac{a\alpha}{v(v+b)+b(v-b)} \tag{2.1}$$

For pure components, the parameters a (the intermolecular attractive force) and b (the intermolecular repulsive force) are determined by applying critical properties (T_c and P_c):

$$a = \Omega_a \frac{R^2 T_c^2}{P_c} \tag{2.2}$$

$$b = \Omega_b \frac{R\ T_c}{P_c} \tag{2.3}$$

$$\alpha = \left[1 + k\left(1 - \sqrt{T_r}\right)\right]^2 \tag{2.4}$$

$$k = 0.37464 + 1.54226\omega - 0.26992\omega^2 \quad \text{for } \omega < 0.49 \tag{2.5}$$

$$k = 0.3796 + 1.485\omega - 0.1644\omega^2 + 0.01667\omega^3 \text{ for } \omega > 0.49 \tag{2.6}$$

$$T_r = \frac{T}{T_c} \tag{2.7}$$

Where R is the universal gas constant, v is the molar volume, T_c is critical temperature, P_c critical pressure, T_r is reduced temperature and ω is the acentric factor of the species. α is a function introduced to fit the vapour pressure data of petroleum mixture.

The multipliers:

$\Omega_a = 0.45724$

$\Omega_b = 0.0778$

Eq. 2.1 can be expressed in polynomial form thus:

$$A = \frac{a\alpha p}{R^2 T^2} \tag{2.8}$$

$$B = \frac{bp}{RT} \tag{2.9}$$

$$Z^3 - (1-B)Z^2 + (A - 2B - 3B^2)Z - (AB - B^2 - B^3) = 0 \tag{2.10}$$

$$Z = \frac{pv}{RT} \tag{2.11}$$

Where Z is the compressibility factor.

For mixtures and hydrocarbon systems intended for use in this current research, the parameters a and b are determined thus:

$$a = \sum_{m=1}^{N}\sum_{n=1}^{N} a_{mn} x_m x_n \tag{2.12}$$

$$a_{mn} = \sqrt{a_m a_n}(1 - \delta_{mn}) \tag{2.13}$$

$$b = \sum_{m=1}^{N} b_m x_m \tag{2.14}$$

Where δ_{mn} is the binary interaction coefficient (BIC), x_m and x_n are the mole fraction of components *m and n*, respectively. $\delta_{mn} = \delta_{nm}$ and $i \equiv m \equiv n = 1,2,3,...N$.

A fourth parameter, volume correction constant, was introduced to the PR EOS to improve the volumetric prediction accuracy (Jhaveri and Youngren, 1988). The volume correction constant *c* is expressed thus:

$$c = s_i b_i \tag{2.15}$$

Where s_i is the shift parameter (dimensionless parameter), characteristic of each component and b_i is the PR co-volume of component *i*.

The corrected fluid phase volumes are express thus:

$$v^L{}_{corr} = v^L - \sum_{i=1}^{N} \left(x_i c_i \right) \tag{2.16}$$

$$v^V{}_{corr} = v^V - \sum_{i=1}^{N} \left(y_i c_i \right) \tag{2.17}$$

Where v^L and v^V are molar volume of the liquid and vapour phases, respectively, $v^L{}_{corr}$ and $v^V{}_{corr}$ are the corrected volumes of the liquid and vapour phase, respectively.

The Soavo-Redlich-Kwong (SRK) EOS also used in this work is given as follow:

$$p = \frac{RT}{V_m - b} - \frac{a\alpha}{V_m (V_m + b)} \tag{2.18}$$

Where,

$$a = \frac{0.42747 R^2 T_c^2}{p_c} \tag{2.19}$$

$$b = \frac{0.08664 R T_c}{p_c} \tag{2.20}$$

$$\alpha = (1 + (0.480 + 1.574\omega - 0.176\omega^2)(1 - T_r^{0.5}))^2 \tag{2.21}$$

$$T_r = \frac{T}{T_c} \tag{2.22}$$

V_m = molar volume.

The expression for α due to the work of Graboski and Daubert is given as:

$$\alpha = (1+(0.48508+1.55171\omega-0.15613\omega^2)(1-T_r^{0.5}))^2 \quad (2.23)$$

For hydrogen,

$$\alpha = 1.202\exp(-0.30288T_r) \quad (2.24)$$

The SRK EOS can be written in the polynomial form as:

$$A = \frac{a\alpha P}{R^2T^2} \quad (2.25)$$

$$B = \frac{bP}{RT} \quad (2.26)$$

$$0 = Z^3 - Z^2 + Z(A-B-B^2) - AB \quad (2.27)$$

Where the parameters are as defined in Eq. 2.1–2.11.

2.2.2 EOS Tuning Procedure

Simulated PVT data based on EOSs often deviates significantly from measured PVT data. The deviation is attributed to factors such as:

- Heavy lumping required for proper simulation of complex compositional reservoir fluid system (excessive lumping downgrades the accuracy of simulation results)
- Inherent limitations of EOS to accurately predict volumetric properties and phase behaviour of hydrocarbon (HC) mixtures and
- Characterisation of multiple components to the same pseudo components requires tuning to get an acceptable match of PVT data (Whitson *et al.*, 1999; Coats, 1985).

EOS tuning procedure is actually a trial and error technique requiring adjustment of the value of component parameters to minimise the deviation between measured and simulated PVT data. The tuning procedure proposed by Whitson *et al.* (1999) is stated thus:

- Tuning variables like plus fraction, heavy components molecular weight, critical properties, and BIC, with very significant effect are initially considered
- BIC between heavy HC ends and non-HC components should be regressed in fluid systems with significant amount of non-HC components
- Only few variables are regressed
- Physical properties of light components are not tuned (components < C_6 are usually well defined)

Coats (1985) described the specific effect of tuning EOS variables as follows:

- Tuning BIC of HC pairs controls the saturation pressure prediction
- Regressing critical properties (temperature and pressure) impacts saturation pressure and vapour-liquid equilibrium estimation
- Dew point pressure and curve are regulated by tuning the critical pressure and temperature of heaviest component
- Critical z-factor impacts viscosity prediction
- Volume shift parameter impacts density prediction

2.2.3 Gas-Oil Contact Prediction

Gas-oil contact (GOC) is the depth along the HC column at which HC mixture transit from a bubble point liquid to a dew point gas. Instability in CG calculations is established when the saturation pressure (P_s) at the GOC is equal to the reservoir pressure, resulting to saturated GOC. Undersaturated GOC occurs when the reservoir pressure is higher than the P_s at the GOC, especially in near-critical reservoirs (Whitson and Belery, 1994; Danesh, 1998). This will result to a stable CG calculation. Since no sharp change in trend is observed for an undersaturated GOC, the properties of the fluid phases at that depth are the same (critical mixture) (Whitson and Belery, 1994). Locating the exert point where these transitions occur requires a trial-and-error procedure. Whitson and Belery (1994) recommended three methods for the estimation of saturated GOC: stability analysis; negative flash calculation; or saturation pressure calculations. For a transition from gas to oil through a critical mixture (undersaturated GOC), only saturation pressure calculations can be used to predict the GOC (Whitson and Belery, 1994).

Whitson and Belery (1994) proposed the following algorithm for predicting both saturated and undersaturated GOCs. The algorithm starts with the calculation of the composition and pressure at the top of the HC column (z_T and P_T) and the bottom of the HC column (z_B and p_B), followed by the calculation of saturation pressure at the top and bottom of the HC column (P_{sT} and P_{sB}), respectively. If the bubble point pressure and the dew point pressures, respectively, are the same at that location, then no GOC exist. Hence, a search for the GOC location is done using either a straight forward algorithm such as the interval halving method for saturation type GOC, or some other existing algorithms (Michelsen, 1984; 1985; 1994). A simple method that can approximately estimate the location of both types of GOC, was proposed by Høier and Whitson (2000). They opined that GOC location $\left(h_{GOC}\right)$ can be estimated from the reference sample reservoir pressure gradient, ∇p_R, and reference sample saturation pressure gradient, ∇p_s, based on the following gradient model:

$$h_{GOC} = h^o - \frac{p_s^o - p_R^o}{\nabla p_s - \nabla p_R} \tag{2.28}$$

Where;

h^o, p_s^o and p_R^o are the reference depth, saturation pressure and reservoir pressure, respectively.

2.3. Compositional Grading Theory

CG also known as compositional gradient or compositional variation with depth, is the variation in mole percent or fraction of both hydrocarbon and non-hydrocarbon components along the fluid column in petroleum reservoirs. Some studies have shown that in additional to vertical compositional variation widely reported in the literature, horizontal compositional variations occurs in some reservoirs, mainly due to flow processes (Jacqmin, 1986, 1987; Moser, 1986; Riley and Firoozabadi, 1998; Gibson *et al.*, 2006; Thomas, 2007). Compositional grading in petroleum reservoirs will give rise to variation in other fluid properties, such as GOR, saturation pressure, density, molecular weight (Whitson and Belery, 1994; Pedersen and Hjermstad, 2015; Nikpoor *et al.*, 2016).

Compositional variation with depth in petroleum reservoirs is attributed to several natural processes occurring in the petroleum reservoir system (Høier and Whitson, 2000), which include the following:

1. Gravitational force causing the heavier components to segregate towards the hot bottom section and lighter components towards the cold top zone (Sage and Lacey, 1939; Schulte, 1980; Whitson and Belery, 1994).
2. Thermal diffusion causing compositional gradient in opposition to gravity effect – separates heavier components towards the low temperature zone (top) and lighter components like methane towards the high temperature zone (bottom) (Chaback and LIRA-GALEANA 1992; Whitson and Belery, 1994).
3. Natural convection induced by horizontal temperature difference in highly permeable or fractured reservoirs can alter the compositions vertically and horizontally (Rabinowicz *et al.*1985; Jacqmin, 1987; Ghorayeb and Firoozabadi, 2000).
4. Incomplete migration and non-equilibrium distribution of components throughout the reservoir may cause compositional variation with time and location. It takes some 10s of millions of years for fluid molecules to diffuse over distance of reservoir kilometres (England *et al.*, 1987; Whitson and Belery, 1994).
5. Water drive mechanism with dynamic aquifer flux partially contacting the lateral extent of the reservoir thereby creating a sink, which continuously depletes the lighter components such as methane (Høier and Whitson, 2000).
6. Asphaltene precipitation during hydrocarbon migration may cause the distribution and localisation of varying fluid types with respect to the permeability of the layers (Schulte, 1980; Ratulowski *et al.*, 2000).
7. Hydrocarbon fluids migrating differentially from multiple source rocks into different layers and geological parts (Høier and Whitson, 2000).
8. Biodegradation of hydrocarbon fluids in the reservoir producing contaminants such as H_2S while depleting some hydrocarbon components at the hot bottom zone of the reservoir (Temeng *et al.*, 1998).
9. Reservoir compartmentilisation such as sealing faults and shale breaks as well as partial barriers may limit fluid and pressure communications between various sections of the reservoir (Smalley *and* England 1994; Nasrabadi *et al.*, 2008)

10. Capillary effects in low temperature reservoirs opposing gravity effect in two-phase fluid system will produce a transition zone from oil to gas rather than a clear gas-oil contact (GOC) (Lee, 1989; Thomas, 2007; Wheaton, 1991).

Researchers have been able to simulate the effects of gravity, thermal diffusion, natural convection and molecular diffusion using theoretical and numerical models. The other natural processes seems too complex to be modelled empirically or numerically. The effect of gravity is simulated using the isothermal gravity-chemical equilibrium (GCE) model while thermal diffusion effect is simulated based on nonisothermal models. Natural convection and diffusion are simulated based on numerical frameworks. A critical review of the various research efforts on compositional grading based on isothermal GCE model and nonisothermal models is presented in this current research work.

2.3.1 Isothermal Reservoirs

Isothermal reservoirs are those in which temperature fields at all locations are assumed to be constant. A petroleum reservoir system with no substantial thickness will consist of hydrocarbon components that at thermodynamic equilibrium have the same chemical potentials no matter their locations in the reservoir (Pedersen and Hjermstad, 2006). For systems with significant thickness, the effect of height potential or the force of gravity must be accounted for. This height potential effect, for an isothermal reservoir will result in an equilibrium state where the components with high molecular weight will move towards the bottom of the reservoir and those with low molecular weight will migrate to the top (Pedersen and Hjermstad, 2006). The procedure for estimating compositional gradient for an isothermal petroleum reservoir was provided by Schulte (1980). The effect of gravity is simulated using the isothermal GCE model.

2.3.2 Non-Isothermal Reservoirs

Thermodynamic equilibrium conditions are seldom the case in most petroleum reservoirs. Petroleum reservoirs with a characteristic temperature gradient are regarded as non-isothermal reservoirs and will not be at thermodynamic equilibrium. Pedersen and Hjermstad (2006) suggested a typical vertical temperature gradient of 0.02 ^{o}C/m. This will result to heat and molecular transfers between the top and bottom sections of the reservoir system. Pedersen and Hjermstad (2006) opined that at stationary conditions (zero mass flux), compositional gradient is estimated via component fugacities, molecular weights and absolute enthalpy per unit mass (heat content). The effect of temperature

gradient on CG in reservoirs at stationary conditions have been modelled based on irreversible thermodynamic processes (non-isothermal models) by many research efforts (Dougherty and Drickamer, 1955; Holt *et al.*, 1983; Belery and da Silva, 1990; Whitson and Belery, 1994; Pedersen and Lindeloff, 2003; Pedersen and Hjermstad, 2006; Nikpoor *et al.*, 2011, 2013a; Pedersen and Hjermstad, 2015; Nikpoor *et al.*, 2016).

Several studies have reported a significant compositional grading in the Brent field, North Sea (Bath *et al.*, 1980; Schulte, 1980; Bath *et al.*, 1983). The compositional gradient observed in the Brent formation of the Brent field, according to these authors, exhibited transition from gas to oil at saturated gas oil contact (GOC). Also observed was a transition from gas to oil without GOC (Bath *et al.*, 1980; Schulte, 1980; Bath *et al.*, 1983). They reported that the transition rather occurred at a depth with the critical temperature equal to the reservoir temperature and critical pressure less than the reservoir pressure – undersaturated GOC. The Statfjord formation in the Brent field is a typical example of a reservoir with an undersaturated GOC and compositional gradient (Bath *et al.*, 1980; Schulte, 1980; Bath *et al.*, 1983).

2.4. Advances in Compositional Grading Modelling

2.4.1 Isothermal Model

Compositional variation with depth in petroleum reservoirs was originally modelled and simulated assuming constant reservoir temperature (isothermal) condition. Isothermal model formulation for the simulation of compositional grading due to gravitational force was initially presented by Gibbs (1906), and is known as the Gravity-Chemical Equilibrium (GCE) model, stated thus:

$$\mu_i\left(P,Z,T\right)=\mu_i\left(p^o,Z^o,T\right)-M_i g\left(h-h^o\right) \tag{2.29}$$

$$d\mu_i = RTd\ln\left(f_i\right) \tag{2.30}$$

$$f_i = f\left(Equation\ of\ State\right) \tag{2.31}$$

Where,

P is the pressure, T is the temperature, Z is the fluid composition, M_i is the molecular mass of component i, μ_i is the chemical potential of component i, h is the depth,

P^o, Z^o, h^o is the reference pressure, fluid composition, and depth, respectively, R is the universal gas constant, f_i is the fugacity of component i, and g is acceleration due to gravity. The novel model presented by Gibbs (1906), prompted several investigations in the study of compositional grading in petroleum reservoirs.

Muskat (1930) proposed an exact solution algorithm to Eq. (2.29) based on a simplified Equation of State (EOS). The resultant numerical solution, due to the oversimplification of the EOS, resulted to the deceptive opinion of negligible gravity effect on compositional grading in petroleum reservoirs.

Similar investigation by Sage and Lacey (1939) also assessed CG using Eq. (2.29) but with a different and more accurate EOS model for binary hydrocarbon liquid and gas, respectively:

$$\left(\frac{\partial n_k}{\partial h}\right)_T = \frac{\frac{M\overline{V_k}}{V} - M_k}{\frac{RT}{n_k} - \int_{p^o}^{p}\left(\frac{\partial \underline{\overline{V}}_k}{\partial n_k}\right)_{T,P,h,n_m} dP} \qquad (2.32)$$

Where n_k is the mole fraction of component k, h is the elevation above an arbitrarily chosen datum, M is average molecular weight, M_k is the molecular weight of component k, R is universal gas constatnt, T is temperature, P is pressure, V is volume, $\overline{V_k}$ is partial molal volume of component k, $\underline{\overline{V}}_k$ is residual partial molal volume of component k. Their result shown in Figure 2.4 indicated compositional grading in the reservoir systems. It shows that the mole percent of methane varies with depth. Sage and Lacey (1939) also made a major observation that compositional grading are more significant in reservoir systems close to the critical condition.

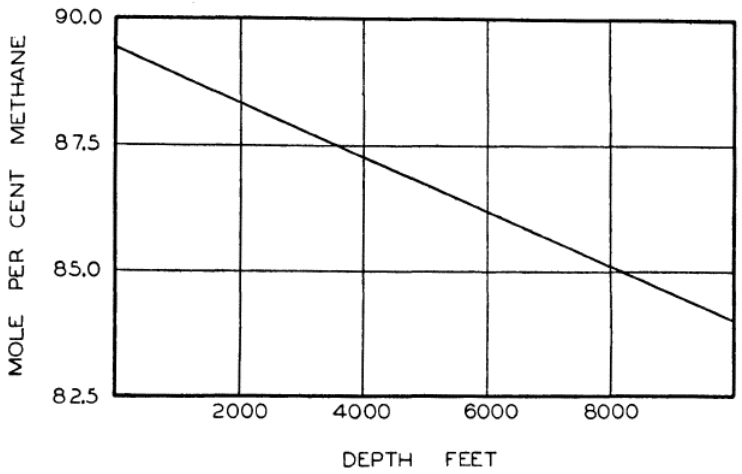

Figure 2.4: Calculated Effect of Depth upon Composition of Gaseous Mixture of Methane and N-Butane (Sage and Lacey, 1939)

Schulte (1980) reported that there was no research advancement with respect to modelling compositional variation with depth in any petroleum literature from 1938 to 1980. Some references which do exist during this period only made mention of reservoirs displaying compositional grading. These references are well cited by Schulte (1980). The research effort presented by Schulte (1980) seems to be the foremost to calculate Eq. (2.29) using cubic EOS. The novel report demonstrates that compositional grading can be created and stabilized by gravity segregation along the fluid column in reservoir systems. The calculation procedure employed by Schulte (1980) uses the Soave and Peng-Robinson (PR) EOS. The result presented in Figure 2.5 illustrates that gravity forces caused observed compositional gradient of aromatics and methane in investigated reservoir system.

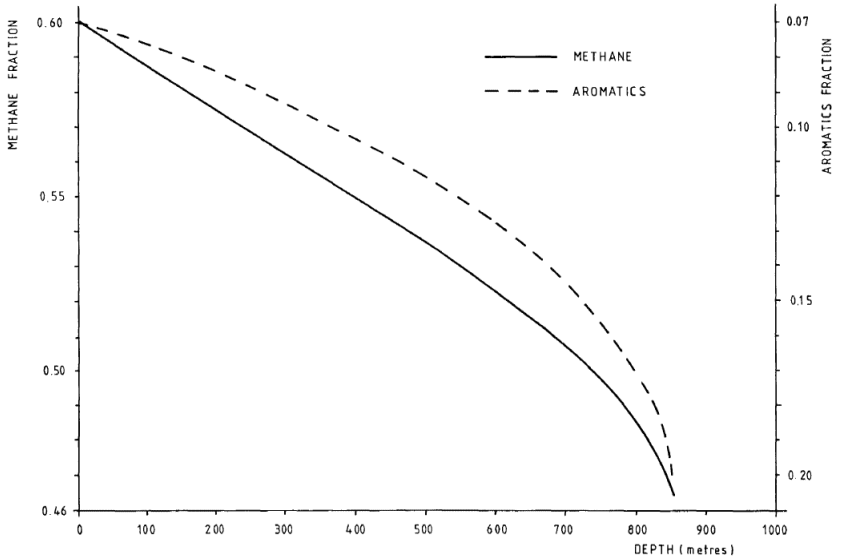

Figure 2.5: Methane fraction and aromatics fraction as a function of depth (Schulte, 1980)

Also in the year 1985, Montel and Gouel (1985) proposed a method for predicting compositional grading in petroleum reservoirs. Their method considered gravity effect only, and it can predict fluids phase behaviour along the fluid column assuming stationary state conditions. The proposed algorithm is an iterative calculation which depends on the fugacity of each component at various depth. Montel and Gouel (1985) stated that if pressure, temperature and overall composition are known at a reference depth, the compositional grading, GOC, including physical state change with depth could be predicted. Montel and Gouel (1985) also suggested the inclusion of thermal diffusion coefficient to optimize thermodynamic fitting for better predictions.

Hirschberg (1988) investigated the relationship between compositional grading prompted by gravity and reservoir fluid phase behaviour. He proposed a simple two-component (assphaltenes and light oil) molecular model, which enables the prediction of asphaltene segregation with depth. The model is valid for asphaltene content ≤10 wt % asphaltene and temperature ≥60°C ≤ 140 °F (Hirschberg, 1988). He observed that for the heavy oils (stock tank oil gravity ≤ 35 °API), compositional variations with depth are mainly due to asphaltene segregation. Strong gravity segregation was report for the light oil (stock tank oil gravity ≥ 35 °API) and near-critical conditions fluids (Hirschberg, 1988). Hirschberg (1988) posited that the lighter the oil and the higher the asphaltene content, (for example, 30°API and 5 wt % asphaltene), the greater the observed compositional variation with depth. He therefore, inferred that under gravity effect, heavy polar components (asphaltene content ≤ 35 °API) play major role in compositional gradient in oil reservoirs, especially in heavy oil reservoirs (≤ 35 °API) where aspaltene segregation is the overriding effect.

Riemens *et al.* (1988) employed a thermodynamic model to estimate the compositional gradient of Birba field, south of Oman. They reasoned that the prediction of reservoir fluid compositional gradient and properties variation with depth in a reservoir can be made by assuming thermodynamic equilibrium in the gravity field (isothermal GCE), which imply constant temperature throughout the reservoir. The results presented show that gravity force generated compositional gradient along the fluid column, resulting to the presence of significantly undersaturated oil just 650 ft below the gas cap. The model was validated using field tests (Riemens *et al.*, 1988).

Kord and Zobeidi (2007) investigated the effect of compositional gradient on characterisation of an Iranian oil reservoir. Isothermal and non-isothermal models were used to predict the compositional gradient of the reservoir. Kord and Zobeidi (2007) observed that the isothermal GCE model shows the best match with the measured data as illustrated in Figures 2.6 and 2.7 for C_1 and C_{7+} gradations, respectively. Castro *et al.* (2009) also applied isothermal compositional grading model to define reservoir compartmentalisation in Magrosa B formation in the middle Magdalena Valley Basin, Lisama filed, Colombia. These authors did not apply their models to predicting original hydrocarbon in-place and reservoir performance.

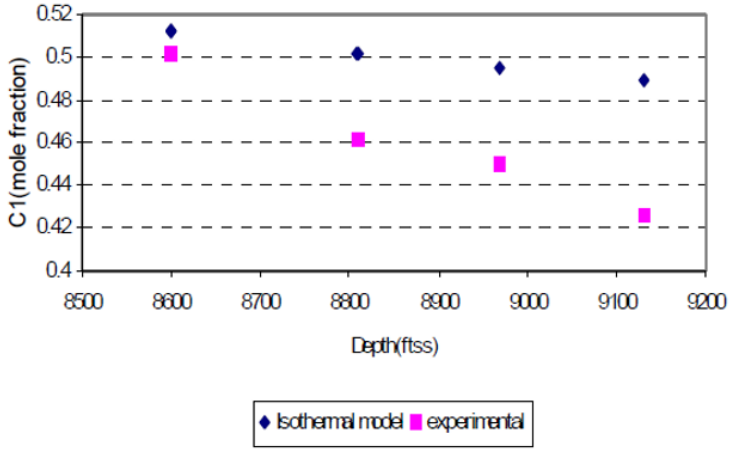

Figure 2.6: Experimental and Isothermal Model Simulated C_1 Mole % Variation with Depth (Kord and Zobeidi, 2007)

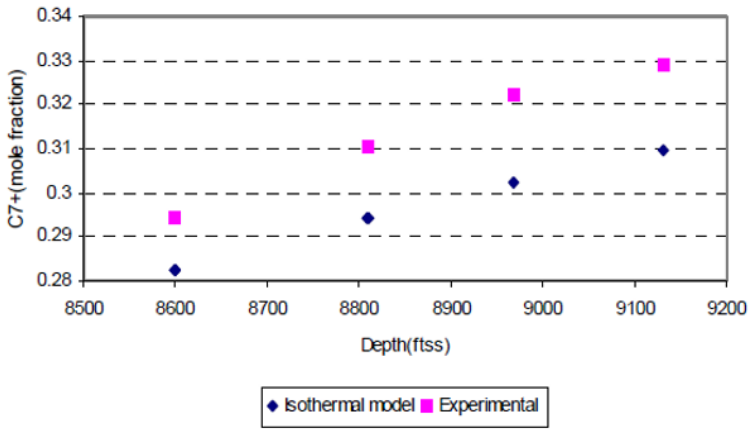

Figure 2.7: Experimental and Isothermal Model Simulated C_{7+} Mole % Variation with Depth (Kord and Zobeidi, 2007)

In the course of sourcing for CG data for this current work from oil and gas companies operating in Nigeria, it was discovered that CG phenomena in Nigeria oil fields have not been adequately investigated and reported in the literature. Some of the reported CG related research efforts from the region includes the work of Joseph and Imo-Jack (2013).

They presented the use of compositional model to predicting the presence of oil-rim in Niger Delta reservoirs. The model was initially standardised with data from various reservoirs with known GOC, then applied to the research data. Joseph and Imo-Jack (2013) observed that the model results significantly agree with log, amplitude, and core data. It is important to note that the results were based on isothermal model since there was no thermal gradient term nor thermal diffusion term in the model presented. Although, the algorithm for predicting fluid compositional grading was presented, no compositional grading result was presented. Only predicted GOCs and pressure gradients were presented. Eyitayo *et al.* (2017) also used compositional grading simulation (CGS) to predict GOCs in various Niger Delta reservoirs. The simulation results were validated with log results. Their result presented in Figure 2.8 shows that within a fluid column and the availability of reliable experimental PVT data, CGS is a credible and cost-effective tool for predicting GOC for optimum field development plan.

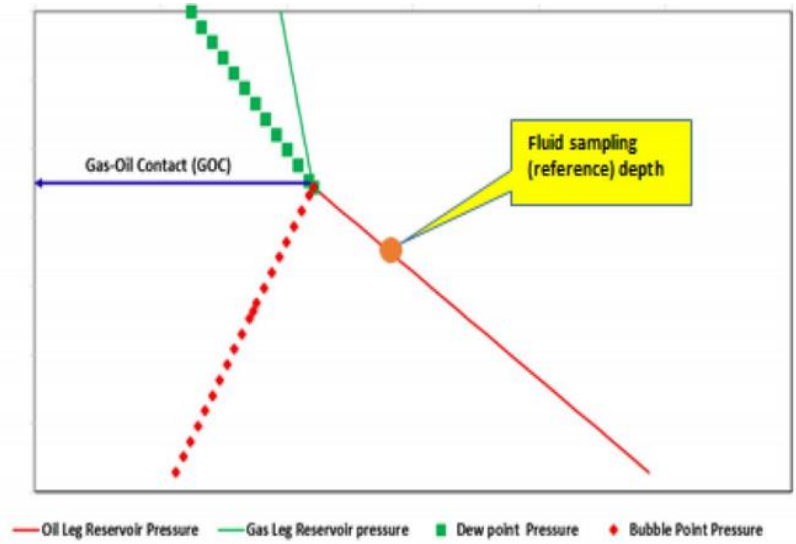

Figure 2.8: Determination of GOC from CGS (Eyitayo *et* al., 2017)

Mohammadi *et al.* (2014) developed an isothermal model for outlier detection in experimental compositional grading data set of reservoir fluid. The algorithm used by the authors was based on statistical Hat matrix and Williams plot, from which the residuals of a compositional grading outcome generated the probable outlier detection. The results show that the developed model for estimation of compositional grading has wide range of applicability. Although Mohammadi *et al.* (2014) agreed that thermal gradient cause heat flow between various points of the reservoir, but relied on the thermodynamic equilibrium assumption of gravity segregation as the basis for the isothermal compositional grading thermodynamic model. They opined that the effects of temperature

on compositional variation may be negligible compared with effects of gravity. The calculations of heat flux, heat diffusions and their effects on residual enthalpies and finally on chemical potential of components throughout the reservoir, greatly increase the complexity of non-isothermal model (Mohammadi *et al.*, 2014).

2.4.2 Non-Isothermal Models

Different existing non-isothermal models are reviewed in this section. The first point to note is that the difference between some non-isothermal models is just in the method of estimating the thermal diffusion coefficient. Dougherty and Drickamer (1955) presented a theory for the measurement of thermal diffusion coefficient on series of binary mixtures of isomers, based on the thermodynamics of irreversible processes. The theoretical model was formulated using molecular weight, molar volume, activation energies for viscous flow, and additional thermodynamic properties. They obtained a more adequate expression for the energy of transport term, which was previously considered to be a fraction of the cohesive force of the molecules. The energy of transport was adequately expressed in terms of activation energy for molecular transport, and most appropriately estimated from viscosity measurements. The activation energy, according to Dougherty and Drickamer (1955), is the energy required to transport molecules from one equilibrium position to an activated state where no further energy is required for transport to the next equilibrium position. Dougherty and Drickamer (1955) assumed a stationary centre of mass for the system because, in the real experiment, the velocity of centre of mass is insignificantly small. The results were qualitatively valid when compared with previous model results.

Holt *et al.* (1983) modelled the effect of gravity and temperature fields on reservoir fluid components based on irreversible thermodynamics, assuming a stationary state reservoir system. The effect of gravity force was calculated using predicted liquid data while that of temperature was investigated using diffusion factor (Holt *et al.*, 1983). The authors concluded that both gravity and temperature effects could explain the observed compositional gradient in the Valhall field, North Sea, used for the study. Holt *et al.* (1983) stated that the two effects of gravity and temperature contributed to 10 % of the observed compositional gradient in this field. It was also observed that temperature effect might be large for near-critical oil reservoir (Holt *et al.*, 1983). This work was limited to compositional grading of binary system of methane and solvent.

Belery and da Silva (1990) proposed the combination of the effects of gravity and thermal diffusion for a stationary system. They adopted the thermal diffusion coefficient model proposed by Dougherty and Drickamer (1955) and modified it to account for multicomponent mixtures. Their novel gravity-thermal diffusion model revealed that thermal diffusion has significant effects on compositional variation with depth.

Bedrikovetsky (1993) formulated a mathematical framework for the investigation of compositional grading in petroleum reservoir. The proposed mathematical framework combined gravity, thermal diffusion, and capillary effects to form a complex equation. The mathematical framework was only implemented for simplified conditions such as ideal EOS and binary mixtures. Multicomponent systems were not considered.

Faissat *et al.* (1994) provided a theoretical background to the study of the effects of gravity on compositional gradient in porous medium based on the thermodynamics of irreversible processes. They show that the models proposed by Haase (1969) and Kempers (1989) on thermal diffusion are ideal cases of static thermal diffusion since the coupling coefficients are equal to equilibrium quantities such as enthalpy or entropy. Faissat *et al.* (1994) observed that the coupling coefficient, in reality, do not reduce to pure thermostatic quantities but rather, are related to the microscopic transport of each species. Hence, suggesting the need for kinetic model for the thermal diffusion coefficient. They also opined that the thermal diffusion coefficient should also depend on the characteristics of the reservoir system.

Whitson and Belery (1994) formulated methods for estimating the one-dimensional (1D), compositional gradient induced by gravity and thermal diffusion effects. The proposed isothermal model is based on Gibbs equation. They used the PR and Soave-Redlich-Kwong (SRK) cubic EOS as thermodynamic models for fluid characterization. The volumetric deficiencies of the EOS were corrected using volume translation method, which is done by estimating a linearly translated volume v^* by adding a constant c to the molar volume v, estimated from the EOS. That is:

$$v^* = v + c \tag{2.33}$$

Belery (1994) used Eq. 2.34 to investigate the effect of thermal diffusion on compositional grading.

$$\frac{dz_i}{dh} = -k_{Ti} \frac{d \ln T}{dh} \tag{2.34}$$

Where z_i is the composition of component *i*, *T* is the system temperature, and *h* denotes depth. The term k_{Ti} is the thermal diffusion ratio for component *i*, and is used in Eq. 2.34 for estimating the contribution of thermal diffusion to compositional grading. The results show that without thermal diffusion influence, a temperature gradient of 0.055 ^{o}C/m induced an inconsequential compositional gradient compared to the isothermal GCE predictions. Whitson and Belery (1994) observed the tendency of thermal diffusion effect to enhance or reverse the compositional gradient estimated by the isothermal GCE model. It was also observed that negative thermal diffusion ratio tend to generate substantial downward methane movement, resulting to mechanical instability, with induced convection as the overall consequence. Whitson and Belery (1994) noted that the isothermal GCE problem is no longer one-dimensional when there is convection. The lack of compromise for how to formulate the thermal diffusion problem was also mentioned. Alternative formulations, other than the zero net flux evaluated, should be tested for the investigation of compositional gradient (Whitson and Belery, 1994).

Biswas and Carey (1998) presented a Least-Squares Finite-Element Method (LSFEM) to estimate areal compositional variation in large petroleum reservoirs. They developed a 2D model by combing Darcy's law, energy and mass balance relations for multicomponent reservoir system. Biswas and Carey (1998) opined that the effect of convection in the reservoir may be small since the areal extent is very large compared to the thickness. They also assumed a stationary state but with significant net energy flux. Biswas and Carey (1998) estimated the fluxes and thermodynamic properties of the system from nonequilibrium thermodynamics and PR-EOS, respectively. The results was validated with finite-difference solutions of similar problem. It show that compositional segregation of hydrocarbon components increased with temperature. Biswas and Carey (1998) concluded that a nonisothermal condition enhances mass diffusion of components in the reservoir system.

Hoier and Whitson (2000) applied calculation methods and algorithms to model static one-dimensional compositional variations with depth based on isothermal and various non-isothermal gradient models. The results shows that thermal diffusion impedes gravity, causing compositional grading smaller than estimated by isothermal model. The

author found that saturated, near-saturated, and near-critical reservoir fluids exhibited enormous compositional variations than extremely undersaturated reservoirs. They observed that variation in fluid properties with depth such as fluid density, saturation pressure, API gravity, mixture molecular weight, and producing GOR are directly related to the compositional variations. The effect of thermal diffusion on compositional grading based on Haase's, Kempers, and Dougherty and Drickamer (extended to multicomponent systems by Belery and da Silva) models were presented (Høier, 1997; Høier and Whitson, 2000). The performances of the nonisothermal models to accurately predict compositional gradient were compared with isothermal model results as shown in Figures 2.9 and 2.10, which indicates that isothermal model predicted greater compositional gradient than the nonisothermal models.

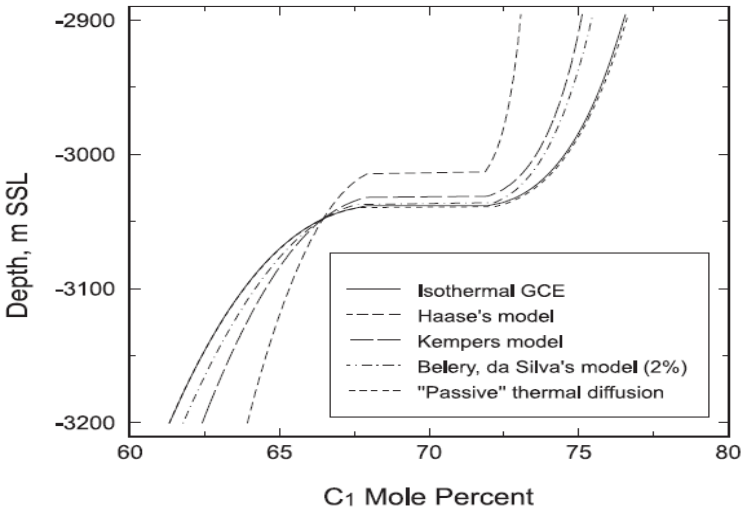

Figure 2.9: Predicted Variation C_1 in Near Critical Oil System Based on Isothermal and Different Nonisothermal Models (Hoier and Whitson, 2000)

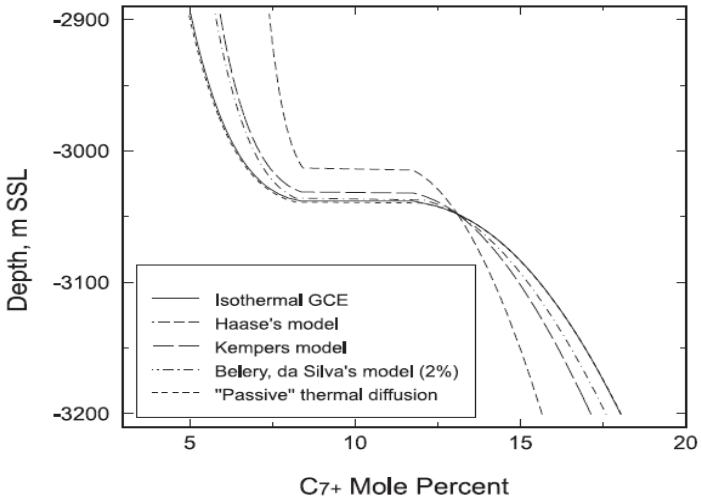

Figure 2.10: Predicted Variation C_{7+} in Near Critical Oil System Based on Isothermal and Different Nonisothermal Models (Hoier and Whitson, 2000)

Firoozabadi et al. (2000) presented the first known theoretical framework for the estimation of thermal diffusion coefficient in non-ideal multicomponent mixtures. Theoretical model was developed for thermal diffusion coefficient in ideal and non-ideal multicomponent systems, based on thermodynamics of irreversible processes and molecular kinetic methodology combining precise effect of non-equilibrium properties (net heat of transport and molecular diffusion coefficient), and of equilibrium properties of the mixture, determined by the Peng-Robinson equation of state (Firoozabadi *et al.*, 2000). The model successfully predicted thermal diffusion coefficients of binary mixtures for which experimental data were available, but its accuracy could not be validated in multicomponent mixtures due to unavailability of experimental data (Firoozabadi *et al.*, 2000). The model also shows that it is unnecessary to adopt sign convection for thermal diffusion coefficient in binary and higher mixtures since by thermodynamic stability analysis it has been proven that when thermal diffusion coefficient is positive, the components move to the cold zone in binary mixture (Firoozabadi *et al.*, 2000). Further experimental investigation of thermal diffusion coefficients in multicomponent mixtures was also recommended by Firoozabadi *et al.* (2000) to close the gap in experimental data in this research area.

In the year 2003, Pedersen and Lindeloff (2003) presented a model based on thermodynamics of irreversible process for predicting compositional gradient in two high pressure gas condensate reservoirs with a vertical temperature gradient. By assuming a stationary state condition with zero heat flux in the reservoir, they used the partial molar enthalpies of the components to show the effect of temperature gradient. Binary components of C_1-C_3 and C_I-nC_4 were used for the model. The model results was validated using measured data. It shows that C_1 will move to the warmer bottom section in the presence of C_3 or nC_4 while temperature gradient will cause the concentration of C_1 to surge in the colder top section of the reservoir. This observed inconsistency in the transport behaviour of C_1 is due to the development in specific energy with molecular weight. C_1 has a higher specific enthalpy than C_3 and nC_4, which result in the segregation of C_1 towards the bottom warmer section of the reservoir in the binary mixture containing one of the components C_3 of nC_4. In petroleum reservoirs containing significant plus fraction (C_{7+}) content, C_1 will segregate towards the colder top section of the reservoir if the specific enthalpies of the C_{7+} components exceed that of C_1 (Pedersen and Lindeloff, 2003). Their results presented in Figures 2.11 and 2.12 shows that a temperature gradient

of 0.01 ºC/m and an ideal gas enthalpy greater than zero resulted in a better match with measured data.

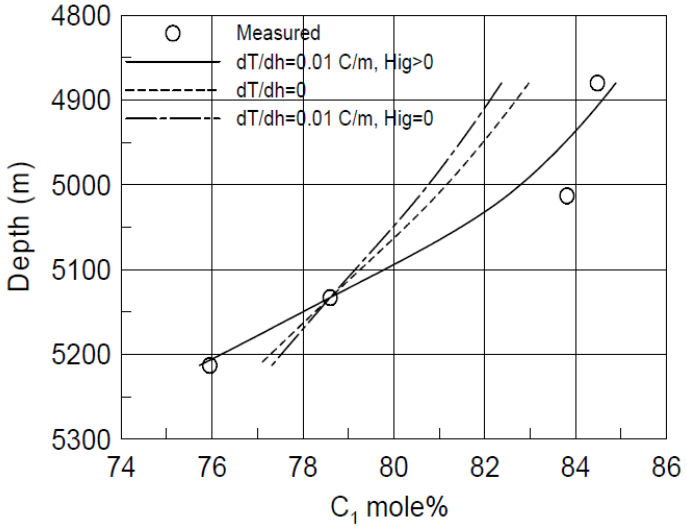

Figure 2.11: Measured and Simulated C_1 Mole % Variation with Depth (Pederson and Lindeloff, 2003)

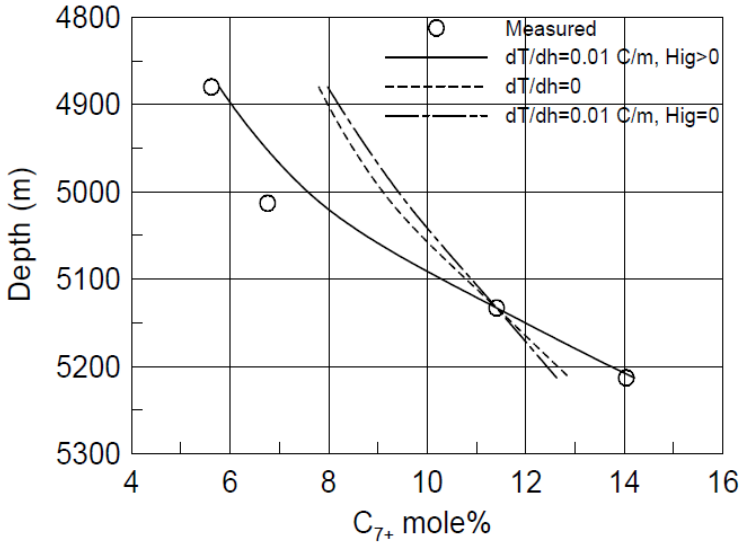

Figure 2.12: Measured and Simulated C_{7+} Mole % Variation with Depth (Pederson and Lindeloff, 2003)

Ghorayeb, *et al.* (2003) formulated a theoretical model to explain the strange variation in density and component distribution with depth, respectively, both in the hydrocarbon column and along the wells in the Yufutsu gas-condensate field. The model was based on thermodynamics of irreversible processes. The results show that thermal diffusion segregated heavy components of the reservoir fluid system towards the top and cold zone of the hydrocarbon column, counteracting pressure and molecular diffusion. This gave rise to the unusual trend observed in the reservoir system, where heavy fluid components were observed floating on the top of light fluid system. Ghorayeb, *et al.* (2003) concluded

that thermal diffusion was the major factor affecting density and component variation with depth.

Leahy-Dios (2008) experimentally and theoretically investigated Fickian and thermal diffusion coefficients in alkane-alkane and alkane-aromatic liquid binary mixture. The model results shows that modelling thermal diffusion by equilibrium thermodynamics alone may not be an adequate methodology (Leahy-Dios, 2008). Despite the various novel results presented by this research effort, Leahy-Dios (2008) stated that the new model approach lacks further comparison with experimental data. Hence, need for further investigations on molecular and thermal diffusions phenomena in non-ideal multicomponent systems.

A novel molecular dynamics (MD) simulation scheme and thermodynamic model based on EOS were proposed to study isothermal and non-isothermal segregation of isotopic mixtures in convection free systems (Galliero and Montel, 2008; Galliero and Montel, 2009). Both methods were applied and compared on a rich CO_2 gas mixture. The results show a slight overestimation of compositional gradient by the EOS base isothermal model compared to the MD based isothermal scheme (Galliero and Montel, 2008; Galliero and Montel, 2009). The EOS model significantly matched the MD results in the non-isothermal segregation instance as shown in Figure 2.13 (Galliero and Montel, 2008; Galliero and Montel, 2009). These results suggest that nonisothermal models are very suitable for accurate description of CG in some reservoirs.

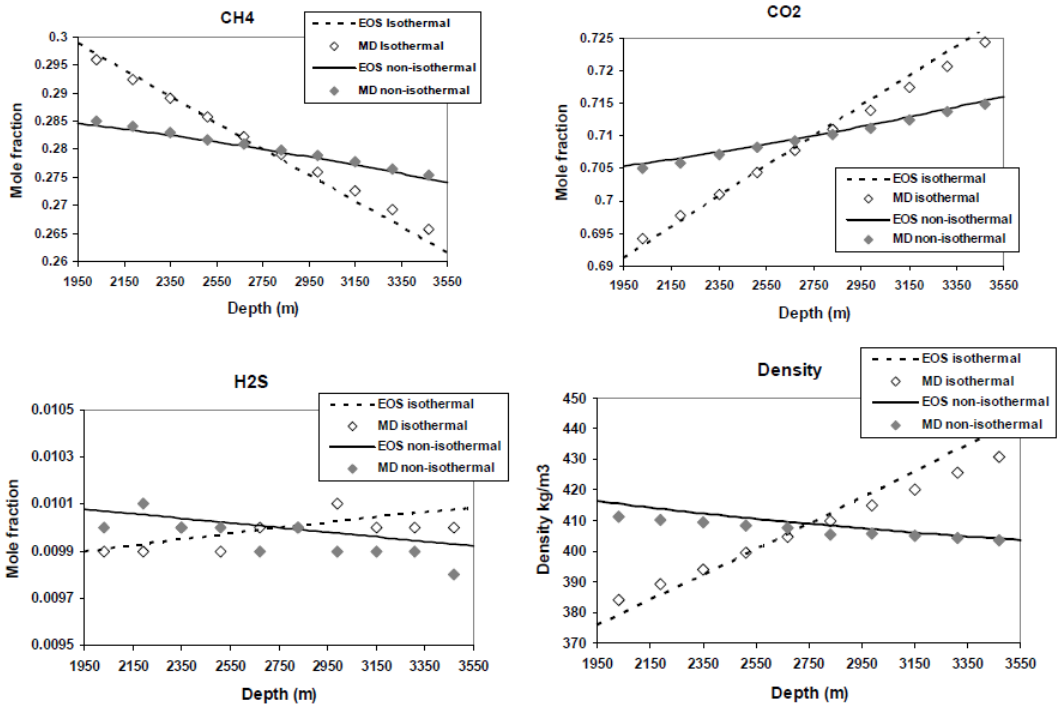

Figure 2.13: Thermogravitational Profiles within Acid Gas Reservoir Fluid Column: Comparison between MD Simulation and EOS Calculation (Galliero and Montel, 2008; Galliero and Montel, 2009)

Nikpoor *et al.* (2011; 2013a; 2016) considered the effect of GCE and thermal diffusion on reservoir fluid compositional variation and pressure gradient and on the prediction of GOC in reservoirs. They proposed a model for the prediction of plus-fraction molecular weight (MW) in a non-isothermal reservoir system based on continuous thermodynamics and the theory of irreversible processes. Nikpoor *et al.* (2016) also proposed a method that can accurately predict the location of GOC. The results show that the developed models satisfactorily predicted compositional gradient, GOC location, and plus-fraction MW change. Nikpoor and Chen (2013) also proposed a new method for the modelling of compositional gradient along the gas-oil transition zone in petroleum reservoirs.

Nikpoor *et al.* (2013b) evaluated the performance of six (6) different methods of predicting compositional gradient in a non-isothermal two-phase reservoir. The methods include:

1. Isothermal model with no plus fraction change with depth – MATLAB code;
2. Isothermal model with no plus fraction change with depth – CMG 2006 software,
3. Isothermal model with plus fraction change with depth – MATLAB code,
4. Firoozabadi's NHT model (non-isothermal) with plus fraction change with depth – MATLAB code,
5. Kempers NHT model (non-isothermal) and
6. Haase's NHT model (non-isothermal).

Nikpoor *et al.* (2013b) showed that only methods 3 and 4 generated the most satisfactory results with method 4 being the most efficient. They inferred that the variation in plus fraction mole percent with depth and temperature gradient effect cannot be ignored in compositional gradient estimations. Nikpoor *et al.* (2013b) concluded that the effect of the numerical algorithm on the model results is too insignificant.

Pedersen and Hjermstad (2015) evaluated compositional grading data of five North Sea reservoir fluids sampled at different depths. The observed compositional gradient cannot be described by gravity segregation alone, according to the authors. They observed the highest compositional gradient in reservoir that is very rich in asphaltane contents. Pedersen and Hjermstad (2015) simulated the compositional grading of the five reservoir fluid samples using Haase's (1969) model, in which specific enthalpy of each component reflects the effect of temperature gradient. The results from one of the reservoirs are presented in Table 2.1, which shows that the compositions of lighter fluid components decreased with depth while those of heavier components increased with increasing depth.

Table 2.1: Measured and Simulated Compositional Variation with Depth a Reservoir System (Pedersen and Hjermstad, 2015)

Components	Depth = 0 m			Depth = 175 m (Reference Depth)		
	Exp mol%	Sim mol%	% Deviation	Exp mol%	Sim mol%	% Deviation
Inorganics	1.76	1.71	-3.0	1.11	1.11	0.0
C1	75.66	75.73	0.1	50.04	50.04	0.0
C2-C6	18.12	18.74	3.4	23.44	23.44	0.0
C7+	4.45	3.83	-14.1	25.41	25.41	0.0
Components	Depth = 204 m			Depth = 228 m		
	Exp mol%	Sim mol%	% Deviation	Exp mol%	Sim mol%	% Deviation
Inorganics	1.12	1.10	-1.9	1.09	1.09	0.0
C1	49.88	49.47	-0.8	48.89	49.04	0.3
C2-C6	23.35	23.24	-0.5	23.49	23.05	-1.8
C7+	25.64	26.19	2.1	26.53	26.81	1.1
Components	Depth = 327 m					
	Exp mol%	Sim mol%	% Deviation			
Inorganics	1.20	1.05	-12.1			
C1	45.66	47.33	3.6			
C2-C6	24.61	22.14	-10.0			
C7+	28.53	29.48	3.3			

Kiani *et al.* (2015) investigated the impact of fluid characterisation on compositional grading in a volatile oil sample from an oil field south of Iran based on isothermal and non-isothermal models, respectively. The non-isothermal models implemented include zero thermal diffusion model, Hasse's model, and Kemper model. According to the authors, the results of the models presented in Figure 2.14 shows that isothermal model and zero diffusion model are more suitable for the investigated case than the other non-

isothermal models that indicated contrasting prediction with isothermal model. They suggested that the observed performance of the non-isothermal models could be due to the change in sign of thermal diffusion ratio in the range of depth investigate which will cause thermal diffusion ratio to dominate gravity effect. Kiani *et al.* (2015) also observed that by reducing the effect of thermal diffusion factor (TDF) with certain multiplier coefficients, non-isothermal models approached isothermal model behaviour. This, they said was more rapid in Kempers model than in Hasse's model since the TDF calculated in the Kempers model was lesser. The model results also shows that splitting procedure and the splitting of the plus fraction to more pseudo-components does not influence the prediction of hydrocarbon compositional variation (Kiani *et al.*, 2015).

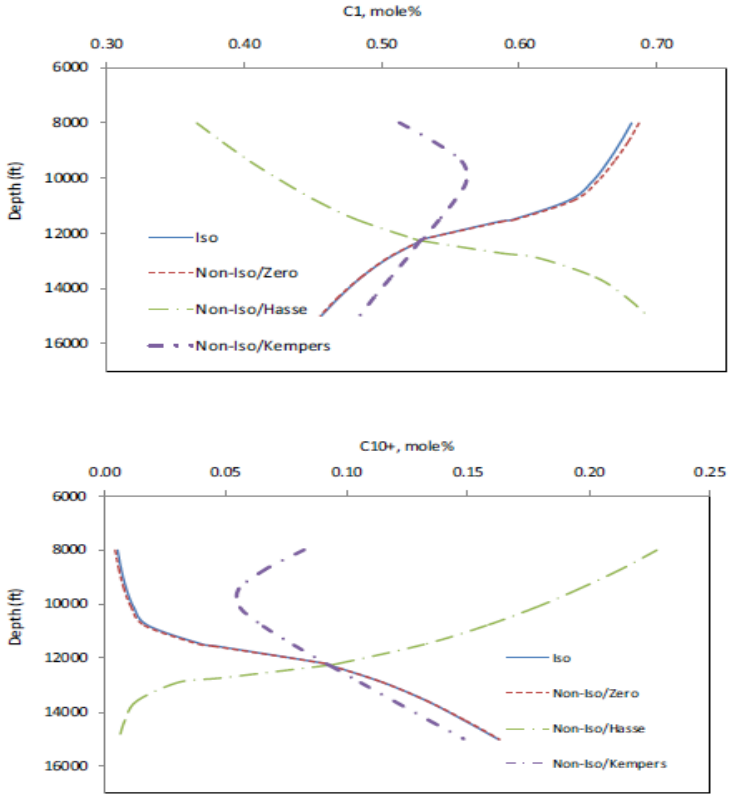

Figure 2.14: Prediction of Methane and C_{10+} Compositional Grading with Four Available Models (Kiani *et al.*, 2015)

2.5 Mathematical Framework for CG Modelling

The mathematical frameworks for the estimation of compositional variation with depth in petroleum reservoirs under the influence of chemical potential, gravitational force, and thermal diffusion were presented by Montel and Gouel (1985); Montel (1993); Faissat et al. (1994); Høier and Whitson (2000). The one-dimensional zero-mass-flow stationary state model proposed by Høier and Whitson (2000) can be written as shown in Eq. 2.35 for the combined effects of gravity and thermal diffusion:

$$\nabla \mu_i = M_i.g - S_i \nabla T - J_{Ti} \frac{\nabla T}{T} \tag{2.35}$$

In Eq. 2.35, μ_i is the chemical potential of component i, ∇T is the temperature gradient, T is the system temperature, J_{Ti} denotes thermal diffusion factor, M_i is the molecular weight of component i, and g is acceleration due to gravity. The term S_i is the partial molar entropy of component i, and is expressed thus:

$$S_i = -\left(\frac{\partial \mu_i}{\partial T} \right) \tag{2.36}$$

The derivation of Eq. 2.35 is presented in Appendix A. One necessary constraint to the application of Eq. 2.35 either in the form of isothermal model or non-isothermal models, is that the sum of the molar compositions of all fluid components at a given depth along the hydrocarbon column must add up to one (unity). That is:

$$\sum_{i=1}^{n} z_i(h) = 1 \tag{2.37}$$

where n is the number of components and z_i is the overall composition of component i. Hence, there are $n+1$ variables at any given depth along the hydrocarbon column. To determine the pressure and molar compositions at any depth will consequently require solving $n+1$ equations consisting $n+1$ variables, with suitable EOS. Eq. 2.35 is the compositional grading model used in this work.

2.5.1 Isothermal CG Model

Isothermal CG model assumes thermodynamic equilibrium conditions in the reservoir. It neglects the effect of thermal gradient and thermal diffusion ($J_{Ti} = 0$). Thus, gravity force is the only factor responsible for the distribution of fluid compositions in the reservoir, causing lighter components like methane to migrate towards the top of the reservoir and heavier components to move towards the bottom section. Eq. 2.35 can be mathematically transformed to an isothermal model by expressing component chemical potential in terms of molar Gibbs free energy and hydrostatic equation (which relates pressure and position). The chemical potential of a pure substance is equal to the molar Gibbs free energy, and its variation with temperature and pressure is given thus:

$$d\mu_i = dG = -SdT + VdP \tag{2.38}$$

At constant temperature $(dT = 0)$, Eq. (2.38) transforms to:

$$d\mu_i = VdP \tag{2.39}$$

Eq. 2.39 can be integrated as a function of pressure based on a set reference state. For an ideal gas, the reference state depends only on pressure, and is set at 1 bar. Hence,

$$\int_{\mu^o}^{\mu} d\mu_i = \int_{p^o}^{p} Vdp \tag{2.40}$$

For ideal gas,

$$V = \frac{RT}{P_i} \tag{2.41}$$

$$\int_{\mu^o}^{\mu} d\mu_i = \int_{p^o}^{p} \frac{RT}{p_i} dp \tag{2.42}$$

$$\mu_i - \mu_i^o = RT \ln\left(\frac{p_i}{p_i^o}\right) \tag{2.43}$$

The hydrostatic equation relating pressure and position is written thus:

$$Vdp + M_i g dh = 0 \tag{2.44}$$

Combining Eqs. 2.39, 2.43 and 2.44, gives:

$$RT \ln\left(\frac{p_i}{p_i^o}\right) = -M_i g dh \tag{2.45}$$

$$\ln\left(\frac{p_i}{p_i^o}\right) = \left[-\frac{M_i g dh}{RT}\right] \tag{2.46}$$

Integrating Eq. 2.46 from a reference depth h^o to h gives:

$$p_i(h) - p_i(h^o) = \exp\left[-\frac{M_i g\left(h - h^o\right)}{RT}\right], i = 1, ..., n \tag{2.47}$$

Eq. 2.47 is the isothermal GCE compositional grading model for an ideal gas (or pure substance). For real gas, the integral, $\int_{p^o}^{p} V dp$ cannot be calculated because there is no simple expression for a real gas molar volume. To ensure that the chemical potential of a real gas is similar to that of an ideal gas, the pressure terms in Eq. 2.47 are replaced with a quantity called fugacity, which gives better approximation of the chemical potential of real gases than estimates made using the ideal gas law. Hence, based on component fugacity. Eq. 2.47 is written thus:

$$f_i(h) = f_i(h^o)\exp\left[-\frac{M_i g\left(h-h^o\right)}{RT}\right], i = 1,...,n \qquad (2.48)$$

The fugacity of component i can be estimated based on the overall composition of the species, thus:

$$f_i = p_i z_i \varphi_i \qquad (2.49)$$

Therefore, Eq. (3.48) can be rewritten thus:

$$\left(\varphi_i^h z_i^h p_i^h\right) = \left(\varphi_i^{h^o} z_i^{h^o} p_i^{h^o}\right)\exp\left(-\frac{M_i g(h-h^o)}{RT}\right), i = 1,...,n \qquad (2.50)$$

In Eq. 2.38 – 2.50, μ_i is the chemical potential of component *i* in the mixture, μ_i^o is the chemical potential of component *i* at the reference state, *G* is the molar Gibbs free energy M_i is the molecular weight of component i, *V* is the molar volume, g is acceleration due to gravity. f_i is the fugacity of component i, h^o is the reference depth, h is the depth of interest, R is the universal gas constant, p_i is the pressure of component i, p_i^o is the pressure of component i at the reference state, and φ_i is the fugacity coefficient of component i. Eq. 2.50 is the isothermal GCE model applied in this work to simulate compositional variation with depth.

2.5.2 Non-isothermal models

Thermodynamic equilibrium conditions are seldom the case in most petroleum reservoirs. Petroleum reservoirs with a characteristic temperature gradient are referred to as non-

isothermal reservoirs and will not be at thermodynamic equilibrium. The presence of temperature gradient in the reservoir will lead to the migration of heavier components to the top of the reservoir and lighter fluid components to the hot bottom zone. Therefore, thermal diffusion opposes the effect of gravity. Non-isothermal models considered in this work are the zero thermal diffusion model, Haase's thermal diffusion model, and Kempers thermal diffusion model.

- ***Zero (Passive) Thermal Diffusion Model***

Zero or passive thermal diffusion model is a hypothetical model in which the thermal diffusion factor (J_{Ti}) in Eq. 2.35 is assumed to be negligible even though thermal gradient exist in the system ($J_{Ti} = 0,\ \nabla T \neq 0$). The temperature, T at a depth (h), was estimated from the knowledge of temperature gradient (∇T). By assuming J_{Ti} = 0 but accounting for thermal gradient, Eq. 2.35 is expressed thus for passive thermal diffusion CG model:

$$\left(\varphi_i^h z_i^h p_i^h\right) = \left(\varphi_i^{h^o} z_i^{h^o} p_i^{h^o}\right) \exp\left(-\frac{M_i g(h-h^o}{RT}\right) - \frac{\nabla T}{T} \qquad (2.51)$$

Some further simplifications for the case where J_{Ti} = 0 were made by de Oliveira Padua (1997):

$$\left(\varphi_i^h z_i^h p_i^h\right) = \left(\varphi_i^{h^o} z_i^{h^o} p_i^{h^o}\right) \exp\left(-\frac{M_i g(h-h^o) + S_i.(dT/dh)}{RT}\right) \qquad (2.52)$$

de Oliveira Padua applied the solution technique formulated by Whitson and Belery for isothermal models, based on analytical solution of the depth integral.

- ***Haase's Thermal Diffusion Model***

The basic difference between the various non-isothermal models is the method applied in estimating the thermal diffusion coefficient, (J_{Ti}) in Eq. 2.35. The J_{Ti} for Haase's thermal diffusion model is based on centre of mass assumption and is stated thus:

$$J_{Ti} = M_i\left(\frac{H}{M} - \frac{H_i}{M_i}\right) \qquad (2.53)$$

Hence, Haase's thermal diffusion CG model is expressed as:

$$\left(\varphi_i^h z_i^h p_i^h\right) = \left(\varphi_i^{h^o} z_i^{h^o} p_i^{h^o}\right) \exp\left(-\frac{M_i g(h-h^o}{RT}\right) - M_i\left(\frac{H}{M} - \frac{H_i}{M_i}\right)\frac{\nabla T}{T} \quad (2.54)$$

where

$$M = \sum_i x_i M_i \quad (2.55)$$

$$H = \sum_i x_i H_i \quad (2.56)$$

M is molecular weight of the mixture, H is molar enthalpy of the mixture, M_i is the molecular weight of component i in the mixture, H_i is the partial molar enthalpy of component i in the mixture, x_i is the mole fraction of component i.

- ***Kempers Thermal Diffusion Model***

Kempers thermal diffusion model depends on the centre of volume assumption for thermal diffusion coefficient prediction. The J_{Ti} is expressed thus:

$$J_{Ti} = V_i\left(\frac{H}{V} - \frac{H_i}{V_i}\right) \quad (2.57)$$

Hence, Kempers thermal diffusion CG model is expressed as:

$$\left(\varphi_i^h z_i^h p_i^h\right) = \left(\varphi_i^{h^o} z_i^{h^o} p_i^{h^o}\right) \exp\left(-\frac{M_i g(h-h^o}{RT}\right) - V_i\left(\frac{H}{V} - \frac{H_i}{V_i}\right)\frac{\nabla T}{T} \quad (2.58)$$

where,

$$V = \sum_i x_i V_i \quad (2.59)$$

where, V is the molar volume of the mixture, V_i is the partial molar volume of component i in the mixture.

- ***Soret effect ($J_{Gi} = 0$)***

Temperature gradient can induce a compositional gradient by thermal diffusion in the absence of gravity. This effect is often referred to as Soret effect, and is expressed thus:

$$\sum_{k=1}^{n-1}\left(\frac{\partial \mu_i}{\partial x_k}\right)_{p,T,\mathrm{x}_{j=k}} \nabla \mathrm{x}_k = -J_{Ti}\frac{\nabla T}{T} \quad (2.60)$$

Thermal diffusion can be expressed in terms of the dimensionless thermal diffusion ratio k_{Ti}, defined thus:

$$\nabla x_i = -k_{Ti} \frac{\nabla T}{T} \tag{2.61}$$

Eq. 2.61 represents a balance of fluxes associated with compositional gradient governed by Fick's law and thermal diffusion (Høier and Whitson, 2000).

- ***Non-isothermal CG models solution technique***

According to Høier and Whitson (2000), Solution to the non-isothermal models uses successive substitutions accelerated with General Dominant Eigenvalue Method for composition, and successive substitution for pressure. Gaussian elimination is used in the inversion process to estimate ∇x_i.

2.5.3 Diffusive flux based CG model

Ghoroyeb et al. (2003) presented another theoretical model based on the concept of thermodynamics of irreversible processes to describe CG. The proposed model relied on the diffusion flux (*J*) *presented* by Ghoroyeb and Firoozabadi (2000b) and the thermal diffusion factors presented by Firoozabadi et al. (2000). The model is expressed thus:

$$J = -c(D^M.\nabla x + D^T.\nabla T + D^P.\nabla_P) \tag{2.62}$$

where,

$$D^M = [D_{ij}] \tag{2.63}$$

$$D^T = (D_1^T, ..., D_{n-1}^T) \tag{2.64}$$

$$D^P = (D_1^P, ..., D_{n-1}^P) \tag{2.65}$$

and

$\nabla x = (\nabla x_1, ..., \nabla x_{n-1})$; c and x_i ($i=1,...n-1$) are the total molar density and mole fraction of component *i*, respectively. D_{ij} is the molecular diffusion coefficient, D_i^T is the thermal

diffusion coefficient, and D_i^P is the pressure diffusion coefficient. Eq. 2.62 can also be expressed thus:

$$J = -c(D.M.L.W.F.\nabla \mathrm{x} + D.K_T \nabla T + D.M.L.V\nabla_P) \qquad (2.66)$$

where $L = [L_{ij}]$ is the matrix of the phenomenological coefficients (Ghoroyeb and Firoozabadi, 2000b). The other symbols in Eq. (2.66) are defined thus:

$$D = [D_{ij}] = \left[\frac{RL_{ii}}{cM_i M_n x_i x_n} \delta_{ij} \right] i, j = 1, ..., n-1 \qquad (2.67)$$

$$F = [F_{ij}] = \left[\left. \frac{\partial \ln f_i}{\partial x_j} \right|_{\mathrm{x}_j, \mathrm{T,P}} \right] i, j = 1, ..., n-1 \qquad (2.68)$$

$$M = [M_{ij}] = \left[\frac{M_i x_i}{L_{ii}} \delta_{ij} \right] i, j = 1, ..., n-1 \qquad (2.69)$$

$$W = \left[W_{ij} \right] = \left[\frac{M_j x_j + M_n x_n \delta_{ij}}{M_j} \right] i, j = 1, ..., n-1 \qquad (2.70)$$

In Eq. 2.66–2.70, R is the universal gas constant, f_i is the fugacity of component *i*, and δ_{ij} is the Kronecker delta. The subscript x_j is defined by $(x_1, ..., x_{j-1}, x_{j+1}, ..., x_{n-1})$. K_T denotes the column vector of the thermal diffusion ratios in a multicomponent mixtures. Firoozabadi *et al.* (2000) expressed K_T as:

$$K_T = \frac{M_n x_n}{RT^2} M.L.Q \qquad (2.71)$$

where Q is the column vector expressed thus:

$$Q \equiv \left[\frac{Q_i^*}{M_i} - \frac{Q_n^*}{M} \right] i = 1, ..., n-1 \qquad (2.72)$$

Q_i^* = the net heat of transport of component *i*, given by Firoozabadi *et al.* (2000) as follow:

$$Q_i^* = \frac{\nabla \bar{U}_i}{\tau_i} + \left[\sum_{j=1}^{n} \frac{x_j \nabla \bar{U}_j}{\tau_j} \right] \frac{\bar{\mathrm{v}}_i}{\sum_{j=1}^{n} x_j \bar{\mathrm{v}}_j}, i = 1, ..., n-1 \qquad (2.73)$$

where,

$\nabla \bar{U}_i$ = the partial molar internal energy departure of component *i*,

$$\tau_i = \frac{\nabla U_i^{vap.}}{\nabla U_i^{vis.}} \qquad (2.74)$$

$\nabla U_i^{vap.}$ = the energy of vaporisation

$\nabla U_i^{vis.}$ = the energy of viscous flow of pure component *i*, and

$\bar{\mathrm{v}}_i$ = the partial molar volume of component *i*.

Substituting Eq. 2.71 into Eq. 2.66 gives:

$$J = -c(D.M.L.W.F.\nabla \mathrm{x} + \frac{M_n x_n}{RT^2} D.M.L.Q\nabla T + D.M.L.V\nabla_P) \qquad (2.75)$$

At steady state conditions, the thermal diffusion flux disappears; and Eq. (2.75) reduces to:

$$W.F.\nabla \mathrm{x} + \frac{M_n x_n}{RT^2} Q\nabla T + V\nabla_P = 0 \qquad (2.76)$$

At isothermal conditions; Eq. 2.76 reduces to:

$$W.F.\nabla \mathrm{x} + V\nabla_P = 0 \qquad (2.77)$$

Given pressure and composition at depth z^{m-1}, Eq. 2.76 can be written at depth z^m to find the unknowns using a forward first-order finite-difference method (Ghoroyeb *et al.*, 2003) thus:

$$\sum_{j=1}^{n-1}\sum_{k=1}^{n-1} W_{ik}F_{kj}(x_j^m - x_j^{m-1}) + \rho g V_i(z^m - z^{m-1}) + \frac{M_n x_n}{RT^2} Q_i(T^m - T^{m-1}) = 0, i = 1,...,n-1 \quad (2.78)$$

In Eq. 2.78, the superscript *m* and *m-1* denote the grids *m* and *m-1* in the vertical direction (assuming pressure and composition are known at grid *m*). According to Ghoroyeb *et al.* (2003), Eq. 2.78 is solved based on Newton method. Given p^{m-1}, and x_i^{m-1}, i = 1,…,n-1 at depth z^{m-1}, the initial guess for solution at z^m, for p^m and x_i^m is assumed as p^{m-1} and x_i^{m-1}, respectively. This solution procedure converges quadratically everywhere in the vertical column but at the vapour-liquid interface due to the discontinuity of composition and pressure across the vapour-liquid interface (Ghoroyeb *et al.*, 2003).

2.6 Reservoir Performance Evaluation Based on CG

Wheaton (1991) developed a theoretical framework to estimate compositional variation with depth in several North Sea reservoirs. The theoretical framework incorporated the effect of capillary pressure into the isothermal GCE model. Wheaton (1991) simulated some hypothetical reservoirs using the developed isothermal GCE model with results suggesting that neglecting compositional grading may result in inadequate prediction of initial hydrocarbon in place. He explained that the error in such inadequate prediction could be about 20 %, even in reservoirs with minimal changes in compositional gradient. Wheaton (1991) posited that the observed error could be minimized by obtaining fluid composition data from the middle of the reservoir. This theoretical model presented by Wheaton (1991) was not validated with field data and did not account for the effect of thermal diffusion.

Whitson et al. (1999) presented a review of the major PVT data governing recovery and well performance of gas condensate reservoirs. The importance of phase behaviour to gas cycling operation was also presented. Equation of state modelling of gas condensate reservoir, complex fluid systems with strong changes in compositions and PVT properties were presented (Whitson et al., 1999). The publication was limited to the assessment of the effect of compositional variation on in-place surface volumes, prediction of gas-oil contact, and impact of compositional variation on recoveries based on isothermal GCE assumption. The effect of thermal gradient was not considered. The result shown in Figure

2.15, indicates that gas injection resulted in more condensate recoveries than pressure depletion alone.

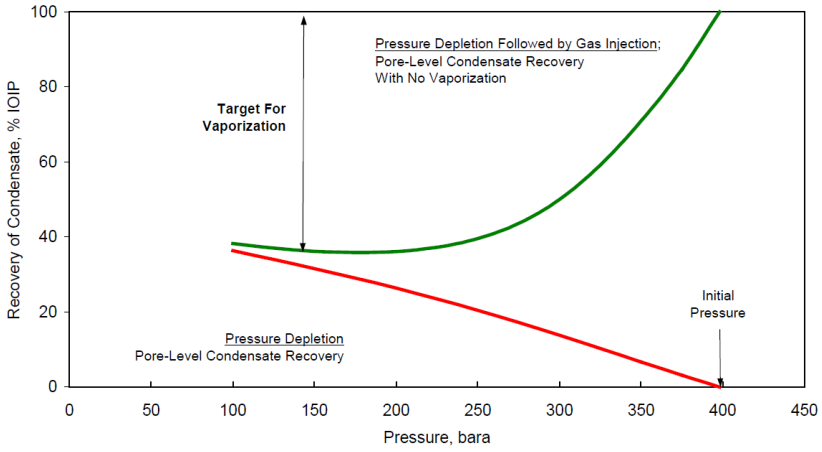

Figure 2.15: Condensate Recoveries for Pressure Depletion and Gas Cycling Below the Dewpoint in a Saturated Reservoir (Whitson et al., 1999)

Favang et al. (2000) compared the capability of black-oil PVT initialised reservoir simulation model, constant composition initialised reservoir model, and isothermal CG initialised reservoir model to estimate initial fluid in-place accurately, under depletion and gas injection scenarios using ECLIPSE reservoir simulator. They used a "generic" reservoir from the North Sea. The reservoir fluid system vary compositionally with depth from a medium-rich gas condensate upstructure, through an undersaturated critical fluid system at the GOC, to a volatile oil at the bottom structure. Their simulation results presented in Figure 2.16 illustrates that reservoir performances can be predicted accurately by initialising with the correct compositional gradient. Favang et al. (2000) posited that in a compositional model, CG should be predicted from EOS model devoid of pseudoisation. Their work did not consider nonisothermal CG models.

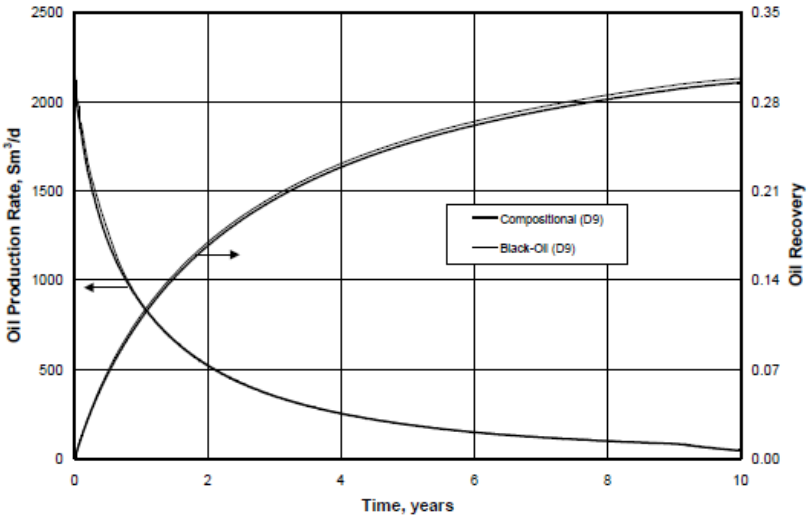

Figure 2.16: Comparison of the Performances of Compositional Model and Black Oil Model under Depletion Case for Reservoir with Compositional Gradient (Favang et al., 2000)

Liu *et al.* (2001) presented a compositional simulation model to evaluate field development problems and future hydrocarbon production of a gas condensate reservoir. The model was based on compositional grading and reservoir compartmentalisation, which are the two main concerns with the reservoir they investigated. The compositional grading aspect of the model was based on isothermal GCE assumption. Non-isothermal conditions were not considered.

Jaramillo and Barrufet (2001) studied the effect of gravitational compositional gradients on oil reserve estimation in various reservoir fluid systems from the Cusiana field, Colombia, based on isothermal GCE model. The results revealed the inconsistencies in original hydrocarbon in-place volumes and cumulative oil productions that occurred when compositional grading is ignored. Jaramillo and Barrufet (2001) observed that original hydrocarbon in place can be either underestimated or overestimated (depending on the type of reservoir fluid system), if compositional grading is not considered. Their results presented in Table 2.2, shows that for volatile oil reservoir, model without CG estimated low OOIP and high OGIP while model with CG predicted high OOIP and low OGIP. Similar trends were observed in two-phase reservoir system. However, in gas condensate reservoir, model without CG, estimated high OOIP and low GOIP while model with CG, estimated low OOIP and High OGIP. These trends indicates the possibility of different reservoir systems behaving differently under CG simulation. This work, again, was based on isothermal GCE model. The economic outlook of the predicted results were not also presented.

Table 2.2. Original Hydrocarbon In-Place for Three Reservoirs (Jaramillo and Barrufet, 2001)

Volatile Oil Reservoir		
Compositional Gradient	**Original Oil Volume (MMstb)**	**Original Gas Volume (MM Mscf)**
No	14.619742	36.379911
Yes	16.64119	33.270291
Gas Condensate Reservoir		
Compositional Gradient	**Original Oil Volume (MMstb)**	**Original Gas Volume (MM Mscf)**
No	14.544608	36.192947
Yes	9.452134	42.887076
Two-Phase Reservoir		
Compositional Gradient	**Original Oil Volume MMstb)**	**Original Gas Volume (MM Mscf)**
No	13.309239	38.042961
Yes	13.616491	37.577882

Luo and Barrufet (2004) investigated how compositional grading does influence production performance during development of near-critical reservoirs. Their simulation study was based on isothermal GCE model. Luo and Barrufet (2004) used both coarse and fine grids in the vertical direction for the simulation study. The results indicates that compositional grading has substantial effect on accurate prediction of hydrocarbon in-place volumes and fluid properties. The results also shows that compositional grading has some effects on gas-injection recovery, resulting in improved recovery. However, carrying out this simulation study based on nonisothermal models and with actual reservoir (synthetic reservoir was used by the authors) will enable the evaluation of the effect of thermal diffusion in compositional gradient reservoir on in-place fluid and reservoir performance predictions.

Vo (2010) investigated the impact of compositional grading on the flow behaviour of gas-condensate production system based on numerical simulations and series of laboratory experiments. The study shows that hydrocarbon compositions vary considerably during depletion. It was observed that the composition of gas-condensate mixture varies locally due to difference in mobilities caused by relative permeability. He posited that the net composition near the wellbore gets richer in heavy components, forcing the phase envelop to shift to the right. The result also established that fluids very close to the wellbore can transit from retrograde gas to a volatile oil, via a critical composition process (Vo and Horn, 2015). The study shows that immobile water in the reservoir has no relevant effect on the compositional grading of gas composite mixture. The pressure depletion processes

for both the simulation model and experimental methods were based on isothermal conditions. Non-isothermal conditions were not considered.

Mokhtari and Ashoori (2013) investigated the effect of compositional grading in the development of an Iranian oil reservoir with low shrinkage undersaturated oil of API gravity of 30. The authors used two simulation models, one that accounts for compositional variation, and the other for uniform fluid condition without accounting for compositional variation. The two models were compared by evaluating the effect of compositional gradient on estimations of original hydrocarbon in-place (OHIP) and recovery factor. The results shows that the model, which accounted for compositional grading produced a more realistic simulation model and resulted in high recovery as shown in Figures 2.17. Although a complex model will require longer simulation run time, the severe difference between the two cases, compensates very well for the complexity and increased simulation run time (Mokhtari and Ashoori, 2013). The simulation model presented by Mokhtari and Ashoori (2013) was based on isothermal GCE model. Thermal diffusion or non-isothermal models were not considered. Hence, the need for this current research work.

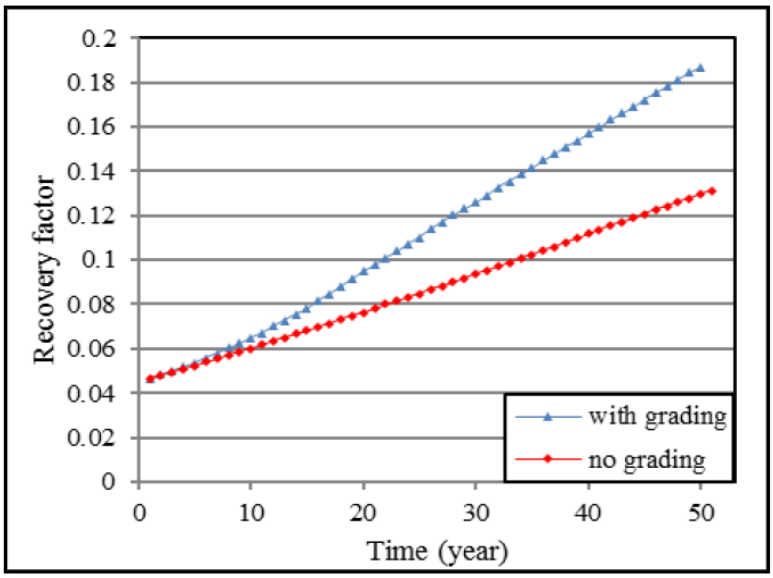

Figure 2.17: Recovery Factor for CO_2 Injection (Mokhtari and Ashoori, 2013)

2.7 Procedure for Mathematical Model Verification and validation

A Mathematical Model consists the conceptual model, mathematical equations, and modelling data required to describe the physical system of interest. Mathematical Model will normally take the form of the partial differential equations (PDEs), constitutive equations, geometry, initial conditions, and boundary conditions needed to

mathematically describe the reality of interest (Thacker et al., 2004). Irrespective of the modelling framework or solution technique applied, the performance measures extracted from a model will only have some bearing on the real physical system represented if the model is a good representation of the system (Hillston, 2003). Hillston (2003) posited that although, what constitutes a good model is subjective, from a performance point of view, the criteria for judging the goodness of models will be based on how accurately measures mined from the model correspond to the measures which would be obtained from the represented physical system (Hillston, 2003). A mathematical model is more abstract than the physical system it represents. Abstractions and assumptions are inevitably made to build it, exclude unnecessary detail and allow us to concentrate on the elements within the system, which are important from a performance point of view. Conversely, having made such assumptions, concerns about the goodness of the model must be addressed (Hillston, 2003).

Model verification and validation are the two major processes for quantifying and building credibility in mathematical models (determining how good a mode is). Model verification is the process of establishing that a model implementation accurately represents the conceptual description of the model and the solution to the model while validation is the process of determining the degree to which a model is an accurate representation of the physical system from the perspective of the intended uses of the model (AIAA, 1998; U.S. DOE, 2000; ASME, 2006). A schematic of model verification and validation processes is shown in Figure 2.18 This diagram provides a basic illustration of the modelling and simulation activities (black solid lines) and the assessment activities (red dashed lines) involved in model verification and validation (Thacker et al., 2004).

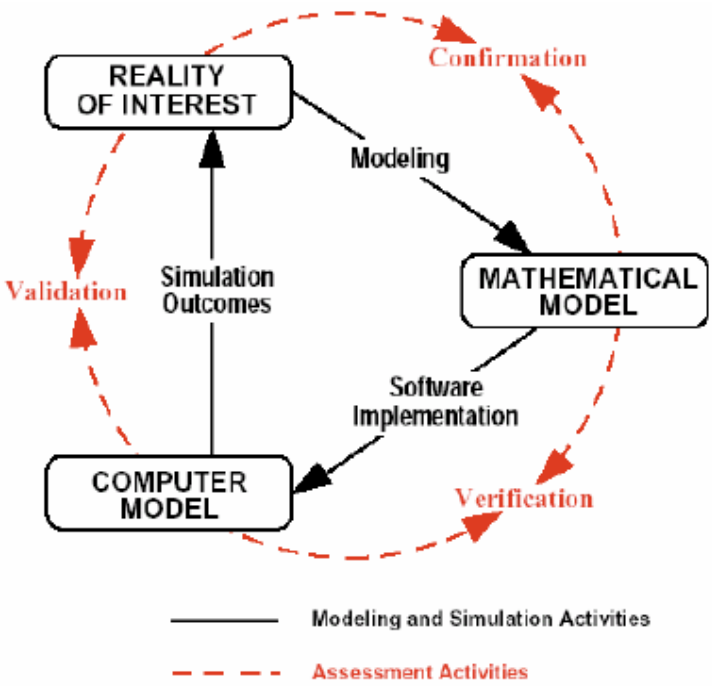

Figure 2.18: A schematic of model verification and validation processes (Schlesinger, 1979).

Despite the fact that Figure 2.18 is effective for collaborating the major concepts involved in model verification and validation processes, numerous important activities are not shown. According to Thacker et al. (2004), Figure 2.18 does not evidently represent:

i. the various activities involved in designing, performing, and presenting experimental results;
ii. the parallel and cooperative role of experimentation and simulation,
iii. the quantification of uncertainties in both experimental and simulation outcomes, and
iv. an objective mechanism for improving agreement between experiment and simulation. Figure 2.19 magnifies on Figure 2.18, providing more detail to addressing these and other inadequacies.

As shown in Figure 2.19, the right branch demonstrates the process of developing and exercising the model, and the left branch shows the process of obtaining appropriate and high-quality experimental data through physical testing. The closed boxes denote objects or data, connectors in black solid lines denote modelling or experimental activities, and the connectors in dashed red lines denote assessment activities (Thacker et al., 2004).

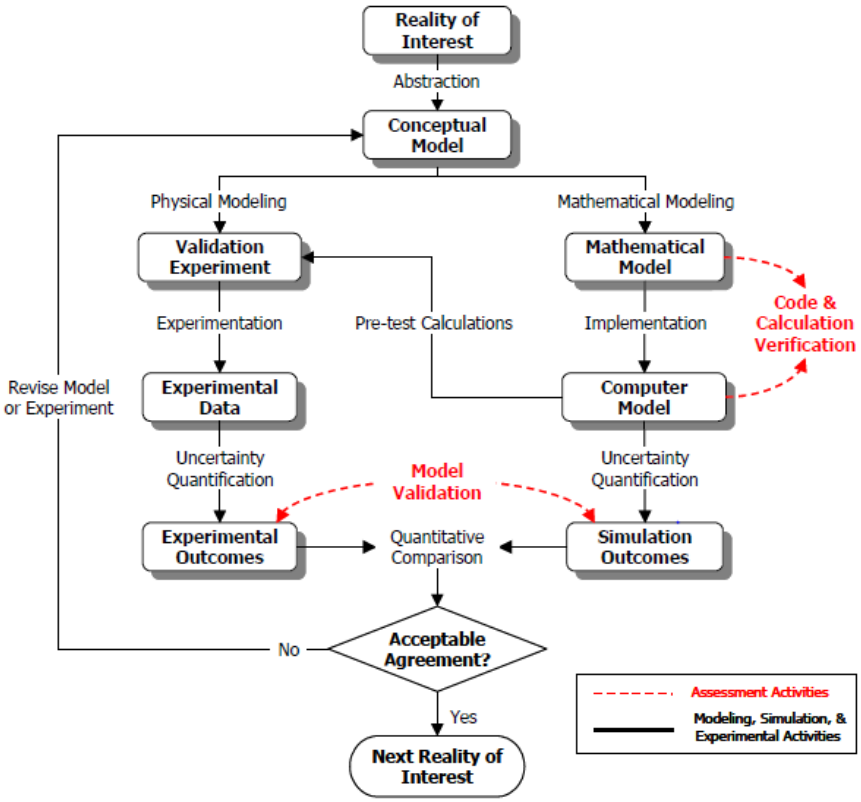

Figure 2.19: Detailed model development, verification, and validation process (Thacker et al., 2004).

2.7.1 Model Verification Procedure

Model verification is like debugging the mathematical model to ensure that it performs what it was intended to do. The following procedures are involved in model verification:

Antibugging. This involves including additional checks and outputs in a mathematical model that could be used to capture existing bugs. Antibugging features do not play any role in representing the physical system and in performance measures calculations. Their only usefulness is in checking the behaviour of the mathematical model. Maintaining counters within a simulation model is a common type of antibugging feature, which keep track of the entities that are generated and terminated during the execution of the model (Hillston, 2003).

Structured walk-through/one-step analysis. This involves explaining the model to someone else or to a willing audience with the intent of making the modeller focus on various aspects of the model and therefore discover shortcomings in the initial model implementation. By studying the model carefully and trying to explain how it works, the modeller may discover some bugs (Hillston, 2003).

Continuity testing. Continuity testing involves solving a mathematical model several times for somewhat different values of input variables. Considering any one variable, a somewhat change in input should generally produce only a slight change in the output. Any sudden changes in the output are taken to be a sign of a possible error, which should be investigated unless such changes represent the behaviour of the physical system (Hillston, 2003).

Degeneracy testing. According to Hillston (2003), degenerate cases for a model are those values of input variables which are at the extremes of the model's intended range of representation. Degeneracy testing involves checking that the model works for the extreme values of system and input variables. Although extreme cases may not represent typical cases, degeneracy testing can help the model developer to discover bugs that would not otherwise have been discovered (Hillston, 2003).

Consistency testing. It is a reasonable assumption that similarly loaded systems will exhibit similar characteristics, even if the arrangement of the workload varies, for most models and systems. Consistency tests are used to check that a model produces similar results for input variable values that have similar effects. If the model output shows a noteworthy difference, it should be possible to explain the difference from more detailed knowledge of the system, otherwise, the possibility of a modelling error should be investigated (Hillston, 2003).

2.7.2 Model Validation Procedure

One of the various procedures used to establish or reject the validity of a mathematical model is the one that starts with the assumptions that (Urbina et al. 2005):

i. calibration of the parameters of the mathematical model is permissible (and sometimes necessary), and

ii. the issue of interpolation among and extrapolation outside the set of validation experiments, respective, can be resolved.

According to Urbina et al. (2005), the validation process involves three kinds of activities: calibration, validation comparisons, and predictions. The validation may commence with some preliminary specifications (Urbina et al., 2005):

- *Specify the model use/purpose, and the response measures of interest. Model use/purpose should indicate whether the model is intended for use in preliminary/intermediate/advanced analysis and prediction. Measures of interest are the quantities the mathematical model was constructed to predict.*

- *Specify validation metrics and domain of comparison. The metric defines the way in which the model/experiment comparison will be made, for example, differences of response measures. Domain of comparison indicates ranges of excitation, boundary conditions, etc., within which validation comparisons are to be carried out.*

- *Specify calibration experiments. Physical experiments to be used to calibrate the mathematical model parameters (that is, identify the model parameters) must be defined.*

- *Specify validation experiments. These identify physical system environments, boundary conditions, etc., whose responses must be satisfactorily predicted by the mathematical model in order for the model to be deemed adequate. They may involve interpolation among and/or extrapolation outside the points in environment/parameter space where calibration was performed.*

- *Specify adequacy criteria. These define the degree of accuracy the model-predicted measures of interest relative to experimentally inferred measures of interest required of the mathematical model.*

Following the definition of the preliminary specifications, calibration of the model may be executed thus:

- Do calibration experiments. Measure physical system responses and, where applicable, excitations.

- Calibrate parameters of mathematical model using experimental data.

Validation Metrics. Execution or simulation of a mathematical model generate mammoth amount of data from which to select. The selection of the simulation outcome should foremost be driven by application requirements. For example, if a design requirement is that the peak strain at specified location should not exceed some value,

then the model validation should focus on comparison of measured and computed strains at that location (Thacker et al., 2004).

Features of experimental data and model outputs must be prudently selected. A feature may be simple, such as the maximum response for all times at a specific location in the computational domain, or more complex, such as the complete response history at a specific location, modal frequencies, mode shapes, peak amplitudes, signal decay rates, and temporal moments. In some instances, a feature can be used directly as a validation metric; in other instances, the feature must be processed further into a form more appropriate for comparison with experimental data (Thacker et al., 2004).

A validation metric is the basis for comparing features from experimental data with model predictions (Trucano et al, 2001). Validation metrics are determined during the requirements phase of the conceptual model development and integrate numerical and experimental uncertainty. If the error, e, between experimental data, y, and model prediction, y^*, is given by $e = y - y^*$, a simple metric could be the expected value of the error, $E(e)$, or the variance of the error, $V(e)$. Other metrics could include, for example: $P(e > 0)$, where P is the probability; the 95 % of the probability distribution of e; or a hypothesis test such as $E(e > 0)$, where the validation metric is a pass/fail decision of whether or not the model is contradicted by the data (Thacker et al., 2004).

According to Thacker et al. (2004), validation metrics must be determined during the validation requirement phase of the conceptual model development and should comprise estimates of the numerical and experimental error. In selecting the validation metric, the main concern should be what the model must predict relative to the types of data available from the experiment. Furthermore, the metrics should offer a measure of agreement that includes uncertainty requirements (Thacker et al., 2004).

Validation experiments. Traditional experiments are performed to improve essential understanding of physical behaviour, improve mathematical models, estimate values of model parameters, and assess system performance (Thacker et al., 2004). Data from traditional experiments are usually inadequate for purposes of model validation because of lack of control or documentation of some experimental parameters or inadequate measurement of specimen response. Therefore, for model validation, it will typically be necessary to perform experiments devoted to model validation (Thacker et al., 2004).

Contrary to traditional experiments, validation experiments are performed to generate high-quality data for the purpose of evaluating the accuracy of model predictions (Thacker et al., 2004). A validation assessment is a physical realization of an initial boundary value problem. To qualify as a validation assessment, the specimen geometry, initial conditions, boundary conditions, and all other model input variables must be stated accurately (Thacker et al., 2004). The response of the test specimen to the loading must be measured with high measurable accuracy. Data collected during the test should include the applied loads as well as initial conditions and boundary conditions that might change during the assessment. Additionally, all given input, test conditions, and measurements must be fully documented. Ideally, this approach provides as many constraints as possible, requiring few, if any, assumptions on the part of the modeller (Thacker et al., 2004).

Experimental data consist of the standard against which the model outputs are compared. Hence, it is critical to determine the accuracy and precision of the data from experiments. Uncertainty in the measured quantities should be estimated so that the predictions from the model can be realistically assessed. Uncertainty and error in experimental data include variability in test fixtures, environmental conditions, and measurements (Thacker et al., 2004).

Uncertainty Quantification. It is generally known and accepted that uncertainties, whether random or systematic, arise because of the intrinsic randomness in physical systems, modelling idealisations, experimental variability, measurement inaccuracy, and cannot be ignored (Thacker et al., 2004). This fact obfuscates the already challenging process of model validation by creating a situation in which neither the simulated nor the observed behaviour of the system is known with certainty (Thacker et al., 2004).

Thacker et al., (2004) stated that when the variability in mathematical model input parameters has been established, this variability can be propagated through the simulation to determine an expected variability on the simulation output quantities. Sampling-based propagation methods such as Monte Carlo and Latin Hypercube are straightforward, although inept, techniques for distributing variabilities. These methods draw samples from the input parameter populations, evaluate the deterministic model using these samples, and then build a distribution of the appropriate response quantities (Thacker et al., 2004). Sampling methods can be made more efficient by the use of local response

surface approximations such as metamodel and reduced-order model, of the model being studied (Thacker et al., 2004). Nevertheless, the error involved in the use of a response surface must also be estimated. Sensitivity-based methods that are more efficient than sampling-based methods may also be used to propagate input uncertainties to uncertainties on the response quantities. Well known sensitivity-based methods include the First Order Reliability Methods (FORM), Advanced Mean Value (AMV), and Adaptive Importance Sampling (AIS) (Thacker et al., 2004).

Validation Requirements and Acceptable Agreement. The final step in the validation process is to compare values of the metrics chosen to measure the agreement between model outputs with the experimental data and to make an assessment of model accuracy (Thacker et al., 2004). The determination of whether or not the validated system-level model is adequate for its intended use is a programmatic decision and involves both technical and nontechnical requirements such as schedule, availability, financial resources and public perception. Stakeholders who are not part of the validation team will typically determine these nontechnical requirements. Consequently, the interpretation of adequacy is restricted here to include only the acceptable agreement between experimental and simulation outcomes (Thacker et al., 2004). A sensitivity analysis of the complete system can be used to identify the importance/contribution of each model, which can then be used to establish corresponding accuracy requirements (Thacker et al., 2004).

According to Thacker et al., (2004), the required accuracy between simulation and experimental outcomes should be determined before the comparison is made. It is rational to expect that the accuracy objective for unit problems will be more rigorous than for the complete system because of the simpler nature of unit problems. For example, a 2% accuracy expectation might be established for a unit model that predicts the axial deformation of a bolt in tension, whereas the accuracy expectation might be 5% or more for a model that predicts the dynamic response of the bolt under combined loadings.

CHAPTER 3

METHODOLOGY

3.1 Summary of Research Milestones

Evaluation of the technical implications of initialising reservoir simulation models with and without CG models on realistic reserves estimates and reservoir performances prediction based on constant composition fluid model, isothermal CG model, passive thermal diffusion CG model, Haase's thermal diffusion CG model, and Kempers thermal diffusion CG model, have been considered. The comparative analysis of the implications of these fluid models on the performances of their respectively initialised reservoir models is intended to divulge the individual and combine effects of gravity, temperature gradient, and thermal diffusion on accurate and realistic reserve estimates and reservoir performances prediction. In the absence of historical production data, uncertainty assessment outcomes were used for the validation of the initialised reservoir simulation models results. Sensitivity analysis of reservoir simulation outcomes were intended to show what variables in the various initialised reservoir models are mostly responsible for observed differences in reserves estimates and predicted reservoir performances. Therefore, sensitivity analysis outcomes provided the premise for establishing the relationship between observed compositional variations with depth, the various CG initialised reservoir models, and observed differences in reserves estimates, which is another major contribution of this work to knowledge. Also, the effect of various EOSs on the performances of CG initialised reservoir models and the effect of changes in temperature gradient on the performances of applied nonisothermal CG initialised reservoir models were also reported. The flowchart showing various research activities and major milestones implemented in order to achieve the research aim and objectives is presented in Figure 3.1.

The Computer Modelling Group's (CMG) equation of state multiphase equilibrium property simulator, WinProp, was used for the reservoir fluid modelling and simulation while Computer Modelling Group's compositional reservoir simulator, GEM, was used for the reservoir simulation study. In the absence of historical production data, Computer Modelling Group's CMOST was used to perform uncertainty assessment for the validation of the initialised reservoir models. CMOST was also used for sensitivity analysis.

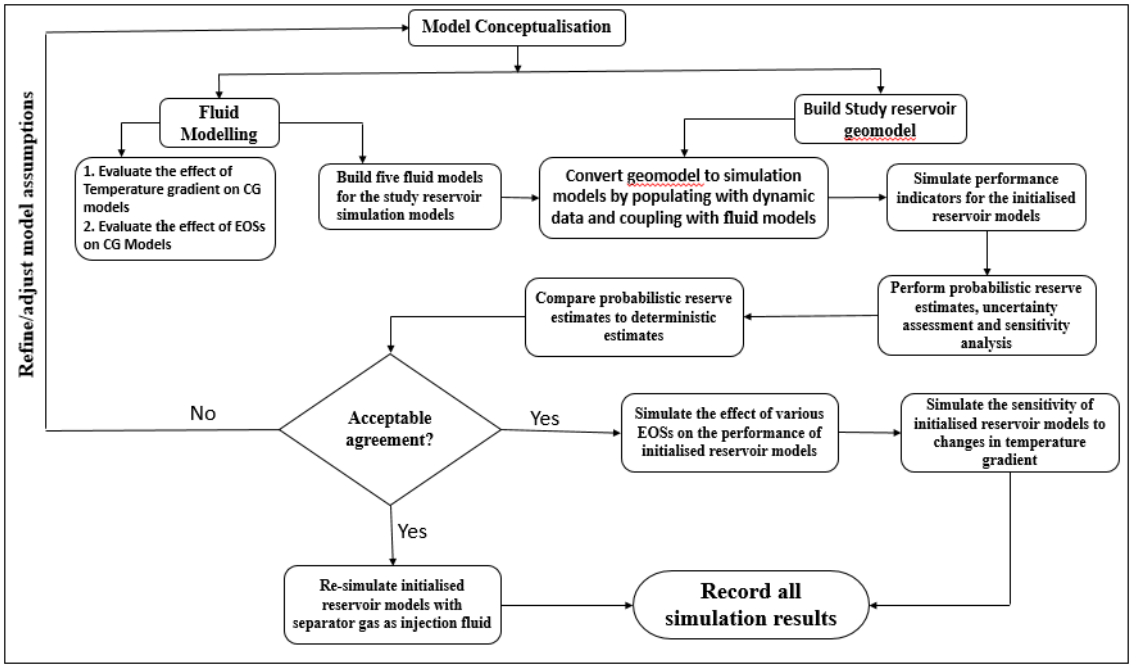

Figure 3.1: Flowchart of Research Milestones

3.2 Sources of Research Data

There are two categories of data sources available to this research work, namely: primary and secondary data sources, respectively.

3.2.1 Primary Data Source

Chevron Nigeria limited, an international oil and gas producing company based in Nigeria, in partnership with the Nigerian National Petroleum Corporation, was the source of the primary data. These primary data set was obtained from a Nigerian offshore high shrinkage black oil reservoir as described in section 3.3, and used for the reservoir simulation study (in building five fluid models. Geomodel, and initialised reservoir simulation models). Research data obtained from this primary data source are:

- **Fluid (PVT) data**. The PVT data characterised in section 3.3 and presented in Table 3.2 was used for building the five fluid models, which was used for the reservoir simulation study.
- **Reservoir data**. Relevant reservoir data obtained from the primary data source are presented in Table 3.8, in section 3.9. Tables 3.9 and 3.10 (section 3.9) shows the water-oil relative permeability table and the gas-oil relative permeability table, respectively.
- **Geological and geophysical data**. Geological and geophysical data collected from the primary data source include well logs, well trajectories, and well (formation) tops, from six (6) wells. Thirty seven (37) well logs were available

from the six (6) wells. These data were stored as electronic data files and are compatible with CMG GEM simulator used for the simulation study. These data were used in building the study reservoir geomodel as described in section 3.7.1.

3.2.2 Secondary Data Sources

Two sets of secondary data were obtained from two different sources. The first set is a PVT data of a black oil reservoir obtained from Chevron Nigeria limited in partnership with the Nigerian National Petroleum Corporation. This PVT data set is used for simulating the effect of temperature gradient on observed CG as explained in section 3.5 and presented in Table 3.4. The second set of secondary data is also a PVT data obtained from Pedersen and Hjermstad (2015) and used for simulating the effect of EOSs on the performances of CG models as described in section 3.6. This PVT data set are presented in Table 3.5 and Table 3.6, in section 3.6.

3.3. Reservoir Fluid Characterisation

PVT data from the primary data source mentioned in section 3.2.1, was characterized in this section. The reservoir fluid sample data was compared to black oil and volatile oil as classified by McCain (1990). Although, the heptane plus mole percent of the research sample is greater than 20 %, every other fluid identification criteria shown in Table 3.1, confirmed the fluid sample to be a high shrinkage black oil. The phase envelop of the fluid sample is presented in Figure 3.2. The reservoir fluid composition and related reservoir data used for the research are presented in Table 3.2.

Table 3.1: Comparison and Identification of Reservoir Fluid Sample, Modified from McCain (1990)

Parameter	Unit	Black Oil	This Research Sample	Volatile Oil
Producing GOR	scf/STB	≤ 2000	1147	2000 - 3300
Stock-tank Oil Gravity	Deg. API	<45	41.9	≥ 40
Oil formation volume factor	res bbl/STB	≤ 2.0	1.71	> 2.0
Heptane Plus	Percent	< 20	27.49	12.5 - 30

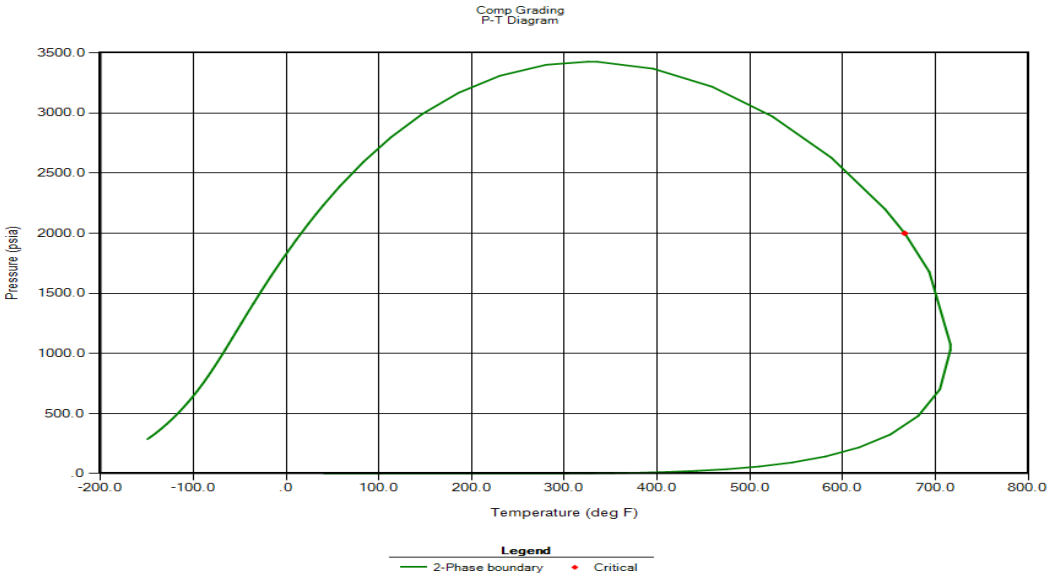

Figure 3.2: 2-Phase Envelop of Reservoir Fluid System

Table 3.2: Study Reservoir Fluid Composition and Properties

Component	**Mole fraction**
CO_2	0.0143
C_1	0.4608
C_2	0.0518
C_3	0.0648
iC_4	0.0211
nC_4	0.0354
iC_5	0.0194
nC5	0.0195
C_6	0.0380
C_{7+}	0.2749
Total	**1.000**
C_{7+} Molecular weight (g/mol)	200
C_{7+} specific gravity	0.8347
Reference depth (ft)	7655
Saturation pressure (psia)	3391.64
Reservoir pressure (psia)	3487
Reservoir temperature (^oF)	230
Depth to top of sand (ft)	7398
Depth to bottom of sand (ft)	7996
Oil formation volume factor, Bo	1.71
Solution gas-oil ratio, Rs (SCF/STB)	1147

The reference reservoir fluid data presented in Table 3.2 was characterised based on 1978 modification of Peng and Robinson EOS (PR 1978) using CMG *WinProp* version of 2017. The heptane plus fraction was defined using the molecular weight and specific gravity. Critical temperature and pressure, acentric factor, and molecular weight of the

heptane plus fraction were selected for the tuning of the EOS fluid model. This is to ensure accurate prediction of saturation pressure and vapour-liquid equilibrium (VLE) properties such as density and GOR.

The Agarwal *et al.* (1990) regression procedure is what *WinProp* uses to tune EOS. This procedure ensures that the most sensitive parameter amongst selected parameters is regressed first. Only a small number of parameters are regressed per time. Subset of five (5) parameters is the default, although, modification in the number of parameters is allowed. When a parameter reaches its upper or lower bound allowed or it no longer contribute to improving the regression, it is substituted by a new parameter from the selected list. *WinProp* has the capacity to handle large selected parameters, regressing a small number per time, from the most sensitive parameters to the least sensitive. Table 3.3 presents the specified regression parameters for EOS tuning applicable to this work. It also shows that critical properties and molecular weight of C_{7+} are the most sensitive parameters while the C_{7+} and CO_2 interaction coefficient is the least sensitive parameter. A convergence tolerance of 1E-06 was specified with a maximum number of iteration set to 200.

Table 3.3: Regression Parameters for Tuning EOS

No.	Variable	Value	Lower Bound	Upper Bound
1	1st Set Critical Pressure: C7+	17.33415165	15.943	25.865
2	1st Set Critical Temperature: C7+	722.7438208	567.86	851.79
3	1st Set Acentric Factor: C7+	0.592756541	0.40483	0.6274
4	1st Set Molecular Weight: C7+	200	177.6	266.39
5	1st Set HC Inter. Coeff. Exp.	1.2	0	1.8
6	1st Set Int. Coeff.: C7+, CO_2	0	0	0.2

3.4. CG Simulation Procedure

The flowchart for CG modelling steps using CMG's Winprop version of 2017 simulator, is presented in Figure 3.3. CG simulation process using CMG's Winprop involve specifying parameters that would enable the various CG models predict PVT related fluid properties with respect to depth. These parameters include the sample reference depth, the reservoir tops, and number of calculation interval along the hydrocarbon column. The reference temperature and pressure must be specified. It is also required to specify at least two key components at a time. The keyword **ZDEPTH* is also specified to enable generation of the global composition versus depth table for the initialisation of the CMG's compositional reservoir simulator (GEM). In order to couple the CG models into the

dynamic reservoir models, the CMG GEM EOS Model is included in the dataset and completed appropriately. This CMG GEM EOS Model enables *WinProp* to write out the CG model results in a file format suitable for CMG's GEM and importable into GEM dataset (components section) using Builder. The simulator default convergence tolerance of 1E-06 and 99 maximum number of iterations were adopted.

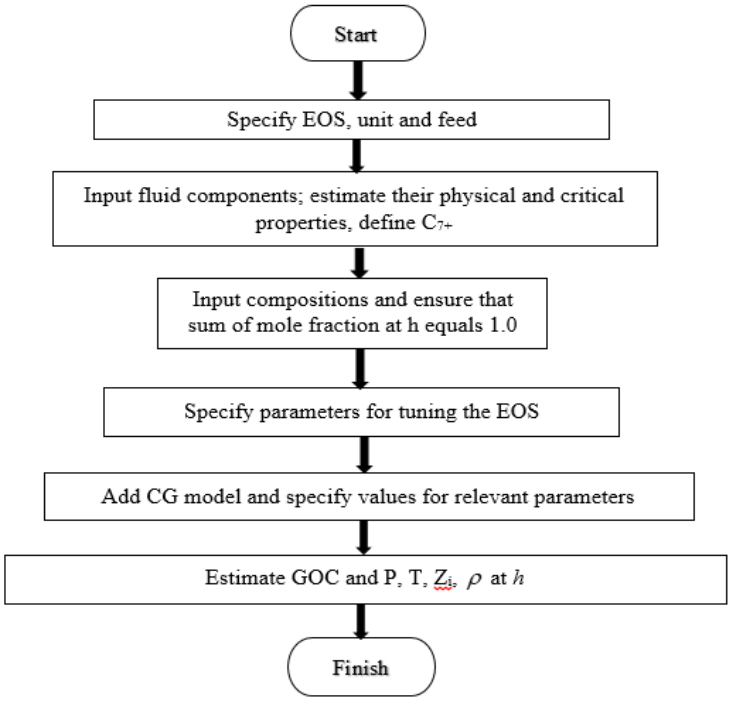

Figure 3.3: Flowchart of CG Modelling Steps Using CMG's Winprop

The nonisothermal CG models requires in additional to the above specified data, specification of the temperature gradient to account for the effect of thermal diffusion. A temperature gradient of 0.002 ^{o}F/ft was used for the nonisothermal models selected for this research. The decision to use 0.002 ^{o}F/ft as the temperature gradient for the nonisothermal models was based on rigorous sensitivity analysis. 0.002 ^{o}F/ft is the maximum temperature gradient at which the reservoir fluid data mimics the actual reservoir behaviour – exhibiting saturated GOC with clearly marked gas cap. Beyond 0.002 ^{o}F/ft, the fluid sample exhibited undersaturated GOC (without a clearly marked gas cap), which was contrary to the original reservoir conditions. CMG's Winprop was also prompted to use thermal diffusion coefficient models directly to estimate the effect of thermal diffusion on component distribution, rather than manually entering constant thermal diffusion coefficient term or multiplying factors, respectively, for each component.

Four (4) CG fluid models were built for this research in addition to the constant composition model (without CG) built in section 3.3: one (1) isothermal model, and three (3) nonisothermal models – passive (zero) thermal diffusion model, Haase's thermal diffusion model, and Kempers thermal diffusion model. Each CG models was executed and the simulation outputs recorded.

3.5 Effect of Temperature Gradient on CG

To further investigate the effect of thermal diffusion or temperature gradient on CG phenomena, another high shrinkage black oil reservoir fluid sample from Nigeria (The first set secondary PVT data obtained obtained from Chevron Nigeria limited in partnership with the Nigerian National Petroleum Corporation), that is more sensitive to a limited range of temperature gradients, was used. The composition and properties of this reservoir fluid system are presented in Table 3.4. The CMG's WinProp, was used for the reservoir fluid modelling and simulation. To investigate the effect of temperature gradient, the value of the temperature gradient in each of the nonisothermal CG models (Zero thermal diffusion model, Haase's thermal diffusion model, and Kempers thermal diffusion model) were varied from a minimum value of 0.002 ^{o}F/ft to a maximum value of 0.02 ^{o}F/ft. The effect of the variation in temperature gradient on GOC estimate, reservoir and saturation pressure gradient behaviour, methane (C_1) and dodecane plus (C_{12+}) fraction gradation, respectively, as predicted by the various nonisothermal models were considered.

Table 3.4: Fluid Sample and Properties at 6115 ft Reference Depth, Used for Evaluating the Effect of Temperature Gradient on CG

Component	Mole Fraction
N_2	0.0009
CO_2	0.0220
CH_4	0.4788
C_2H_6	0.0772
C_3H_8	0.0519
iC_4	0.0102
nC_4	0.0230
iC_5	0.0107
nC_5	0.0109
C_6	0.0193
C_7	0.0388
C_8	0.0384
C_9	0.0356
C_{10}	0.0239
C_{11}	0.0141
C_{12+}	0.1443
Total	**1.000**
C_{12+} MW (g/mol)	286.0
C_{12+} Density (g/ft^3)	0.8210
Saturation Pressure (psia)	3460.0
Reservoir Press. (psia)	3670.0
Reservoir Temp. (^{o}F)	265.0
Depth to Top (ft)	4873
Depth to Bottom (ft)	9873

3.6 Effect of EOSs on the performances of CG models

A PVT data of a reservoir fluid and related reservoir properties at a reference depth as reported by Pedersen and Hjermstad (2015) – the second secondary data source described in section 3.2.2, is used for simulating the effect of EOSs on the performances of CG models. The reservoir fluid composition and properties at a reference (sample) depth of 175 m are presented in Table 3.5 while Table 3.6 shows the measured (experimental) C_1 and C_{10+} mole percentage at different depths in the study reservoir.

Table 3.5. Reservoir Fluid Composition at a Reference Depth of 175 m (Pedersen and Hjermstad, 2015)

Component	**Mole %**
N_2	0.42
CO_2	0.69
C_1	50.04
C_2	7.85
C_3	6.77
iC_4	1.04
nC_4	3.2
iC_5	1.16
nC_5	1.55
C_6	1.88
C_7	3.5
C_8	3.75
C_9	2.28
C_{10+}	15.88
C_{10+} molecular weight (MW)	196
C_{10+} specific gravity	0.85
Reservoir pressure (kPa)	28400
Reservoir temperature (^oC)	93
Saturation pressure (kPa)	27200
Depth to top of reservoir (m)	0
Depth to bottom of reservoir (m)	327

Table 3.6. Measured (experimental) C_1 and C_{10+} Mole % at Different Depths in The Reservoir (Pedersen and Hjermstad, 2015)

	Depth (m)				
	0	175	204	228	327
Components	**mole %**				
C_1	75.66	50.04	49.88	48.89	45.66
C_{10+}	1.57	15.88	16.11	16.70	17.66

Modelling the influence of EOSs on the performances of isothermal and non-isothermal CG models was executed using WinProp version of 2017. The modelling process starts with the selection of EOS, specification of unit and feed (mole or mass). The four EOSs considered are the PR 1976 EOS with 1976 expression for the constant "α", PR 1978 EOS with 1978 expression for the constant "α", the original SRK EOS, and SRK EOS with the constant "α" proposed by Graboski and Daubert (SRK (G&D)). These EOSs are the only EOSs compactable with the applied commercial simulator – CMG WinProp. they are the most commonly used EOSs in the petroleum industry due to their applicability to multicomponent systems (Firoozabadi 1988; Esmaeilzadeh et al. 2005; Ashour et al. 2011). The next step in the simulation process involves selection of the reservoir fluid components and estimation of their respective physical and critical

properties. The decane plus fraction (C_{10+}) was defined using its molecular weight and specific gravity.

Thereafter, the composition of each fluid component either in mole fraction or in percentage, is specified. During this step, the model constraint stated in Eq. 2.37, is complied with by ensuring that the sum of the mole fraction of all fluid components equals unity or 100 %. Regression (tuning) of the EOSs parameters is implemented subsequently. The objective of regression is to minimize the square error between EOS predicted results and the experimental values. WinProp uses the Agarwal et al. (1990) regression procedure to tune the EOSs. This procedure ensures that the most sensitive parameter amongst selected parameters is regressed first. Regression parameters used include the critical pressure and temperature of C_{10+}, acentric factor of C_{10+}, molecular weight of C_{10+}, hydrocarbon interaction coefficient exponent, and the interaction coefficient between C_{10+} and CO_2. The simulator default convergence tolerance of 1E-06 and 99 maximum number of iterations were adopted.

Parameters required for the calculation of saturation pressure, liquid densities, and phase stability were then specified. These parameters include the temperature at which the saturation pressure is to be calculated, initial saturation pressure estimate, and experimental value of the saturation pressure that can be matched by tuning. The final step in the modeling process is the coupling of selected CG models (isothermal model, zero thermal diffusion model, Haase's thermal diffusion model, and Kempers thermal diffusion model) with the EOS model and specification of values for the various parameters in the CG models. A vertical temperature gradient of 0.025 ^{o}C/m that was proposed by Pederson and Hjermstad (2015) was applied to the non-isothermal models. Finally, the coupled models are executed separately and the simulation results recorded.

Statistical analysis of the results based on percentage average absolute deviation (% AAD) was performed to determine the error between simulation results and the experimental (measured) values. The lower the calculated % AAD, the less the calculated error, hence, the more suitable the related EOS is to the applied CG model. The mathematical expression of the % AAD is presented in Eq. 3.1:

$$AAD = 100 \times ABS\left[\frac{\sum_{i=1}^{N}\left((n_{i(model)} - n_{i(\exp)})/n_{i(\exp)}\right)}{N}\right] \quad (3.1)$$

Where $n_{i(model)}$ is the model predicted mole fraction of component *i* with respect to depth, $n_{i(\exp)}$ is the experimental (measured) mole fraction of component *i* with respect to depth, and *N* is the number of sample points (observations).

3.7 Geologic (Static) Modelling

CMG Builder was used in this research to construct the geologic model from analysis and interpretation of seismic and well log data, respectively. CMG Builder is a Microsoft Window based software tool that supports creation of simulation datasets for all CMG simulators (CMG Manual, 2017).

3.7.1 Model Assumptions

i. The geological surfaces or horizons (top and bottom maps), which also defined the geomodel outer boundaries, were generated from correlation of formation tops from available well logs based on inverse distance estimation method. Hence, the built geomodel is only synthetic due to none availability of actual field surface map.

ii. Permeability distribution (Permeability I and permeability J) was based on Gaussian geostatistical simulation.

iii. There was no aquifer definition or support for the study reservoir and report from the industry shows that the reservoir was placed under water injection pressure-maintenance from initial production period.

3.7.2 Boundary Conditions

- **Outer Boundary condition**

  Since all gradients across the reservoir outer boundary are equal to zero, a no-flow outer boundary conditions exist at the reservoir boundary. This is mathematically expressed as:

$$\frac{\partial p_o}{\partial n} = \frac{\partial p_g}{\partial n} = \frac{\partial p_w}{\partial n} = 0 \quad (3.2)$$

Where n is the direction normal (perpendicular) to the reservoir boundary; P_o is the oil pressure; P_g is the gas pressure; and P_w is the water pressure. Eq. 3.2 is a Neumann-type boundary condition (boundary conditions that specify derivative on a boundary).

- **Inner Boundary conditions**

  Darcy's law is used to generate Nuemann-type boundary conditions for specified production and injections well rates as follow:

$$\left.\frac{\partial p}{\partial r}\right|_{r=r_w} = -\frac{\mu B q_w}{2\pi\beta_c khr_w} \tag{3.3}$$

Where p is pressure; r is radial distance; r_w is well radius; μ is fluid viscosity; B is the formation volume factor; q_w is the well rate; β_c is the transmissibility conversion factor; k permeability; h is the reservoir thickness. Well behaviours have been specified in section 3.8.2 and in Table 3.12.

3.7.1 Geomodelling Process

The reservoir simulator setting was specified by selecting the simulator type (in this case, GEM), working unit (field), and porosity (single porosity). The simulation start date was also specified. Builder static model task manager was used in creating the geologic model. Three major steps were involved: importing the well trajectories, well logs, and formation tops. The second step involve creating geological maps or horizons. Top and bottom maps associated with the top and bottom markers, respectively, were created based on the inverse distance estimation method. A 2D corner-point-grid system was created for one geologic unit and the dimensions presented in Table 3.7. Ten (10) vertical layers were added to the 2D grid to create the 3D grid model. The last step in the creation of the geologic model involve assigning the created contour maps to the built 3D grid model, thereby generating the actual reservoir topology presented in Figure 3.4, which is the geologic (static) model of the study reservoir with 26 x 54 x 10 gridblocks (14040 grid cells).

Table 3.7: Grid System Dimension

Parameter	Value
Origin X	836538
Origin Y	633816
Rotation	0
Size X	3900
Size Y	6480
Delta X	150
Delta Y	120
NX	26
NY	54
No. of cells per layer	1404

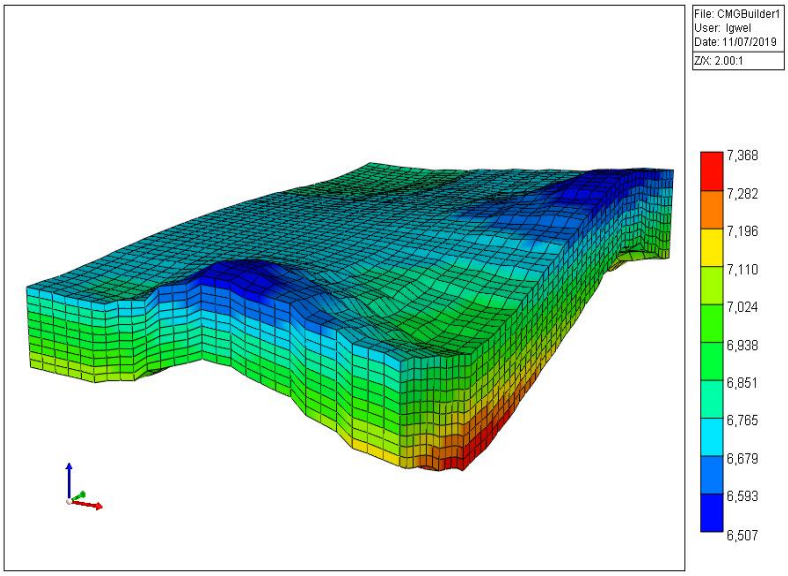

Figure 3.4: Completed 3D Geologic Model of the Study Reservoir

3.9 Reservoir Simulation Models

CMG's Builder was used in building the various reservoir simulation models based on GEM simulator (CMG's compositional simulator). Relevant reservoir data obtained for this work are presented in Table 3.8. Tables 3.9 and 3.10 shows the water-oil relative permeability table and the gas-oil relative permeability table, respectively.

Table 3.8: Study Reservoir Parameters

Parameter	Value
Permeability , mD	52-125
Porosity, fraction	0.16-0.25
Vertical/Horizontal Permeability Ratio	0.1
Rock Compressibility, psia-1 @ 3000 psia	0.000003
Initial Reservoir Pressure, psia	3487
Initial Reservoir Temperature, ^{o}F	230

Table 3.9: Oil-Water Relative Permeability Table

S_w	K_{rw}	K_{row}	P_{cow}
0.20000	0.00000	0.78000	13.000
0.22000	0.00000	0.70692	4.5530
0.30571	0.000354	0.44518	3.0259
0.39143	0.005664	0.25763	2.1088
0.47714	0.028676	0.13190	1.3772
0.56286	0.090629	0.055647	0.67359
0.64857	0.22126	0.016488	0.14427
0.73429	0.45881	0.002061	-1.4163
0.82000	0.85000	0.000000	-8.0518
1.00000	1.00000	0.000000	-23.463

Table 3.10: Gas-Oil Relative Permeability Table

S_g	K_{rg}	K_{rog}
0.00000	0.0000	0.78000
0.01000	0.0000	0.72182
0.10143	0.048595	0.33396
0.19286	0.13745	0.13421
0.28429	0.25251	0.043978
0.37571	0.38876	0.010436
0.46714	0.54331	0.001374
0.55857	0.7142	4.29E-05
0.65000	0.9000	0.00000
0.80000	0.9000	0.00000

The geologic model was converted to a dynamic reservoir model by populating the grid blocks with dynamic data. There was no need for upscaling since the geomodel was constructed with few thousand grid blocks that sufficiently represent the actual reservoir and satisfied the study objective. The objective of the reservoir simulation study is to investigate the technical implications of initialising reservoir simulation models with and without CG models. A corner point grid system representing a sector model of the study reservoir with 14,040 grid cells and the available geological, geophysical, and engineering data were sufficient for this purpose. The values of reservoir properties provide in Table 3.8 were specified in the array property node of the reservoir model. Permeability distribution (Permeability I-direction and permeability J-direction) was based on Gaussian geostatistical simulation as shown in Figures 3.5 and 3.7, respectively, and ranges from 52–125 mD. Gaussian geostatistical-simulation accounts for the uncertainty associated with some reservoir properties (permeability and porosity). Figure 3.6 compares the uncertainties in the Gaussian geostatistical-simulation model generated permeability distribution with actual horizontal variogram while Figure 3.8 shows that of

vertical permeability. Analysis of these uncertainties presented in Table 3.11, indicated zero nugget effects for both horizontal permeability and vertical permeability realisations generated with the Gaussian geostatistical-simulation model, which suggest that Gaussian geostatistical-simulation accounted for the uncertainties in the actual property distribution and minimised the observed measured error. Permeability K was set equals permeability I*0.1. Rock compressibility of 3.00e-06 psi^{-1} was also specified. The reservoir porosity ranges from 0.16–0.25, with an average porosity of 0.205. There was no aquifer definition or support for the study reservoir and report from the industry shows that the reservoir was placed under water injection pressure-maintenance from initial production period.

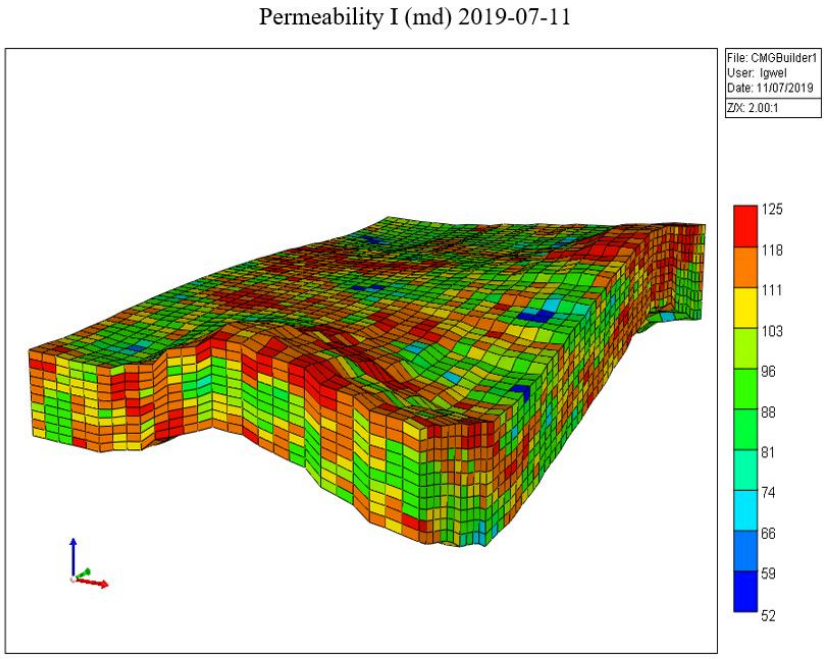

Figure 3.5: Gaussian Geostatistical Realisation of Horizontal Permeability (Perm I) Distribution

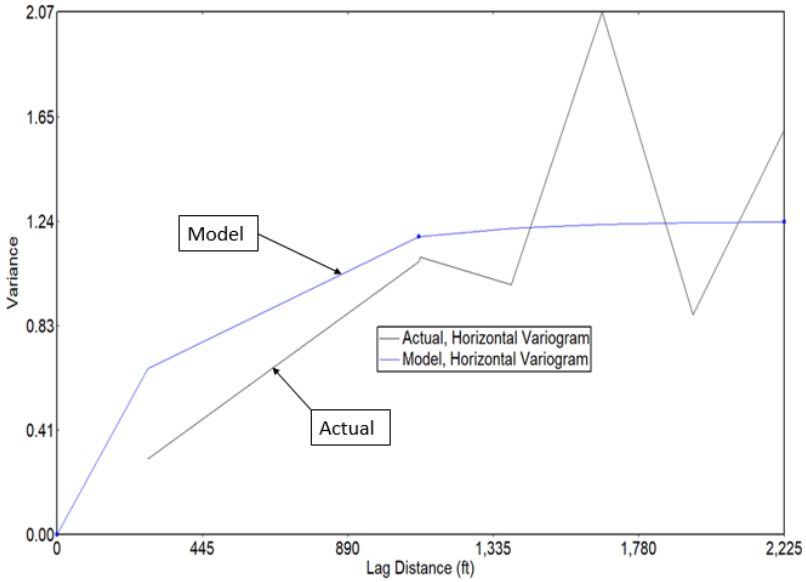

Figure 3.6: The Match of Gaussian geostatistical-simulation Model Generated Permeability Distribution with Actual Horizontal Variogram

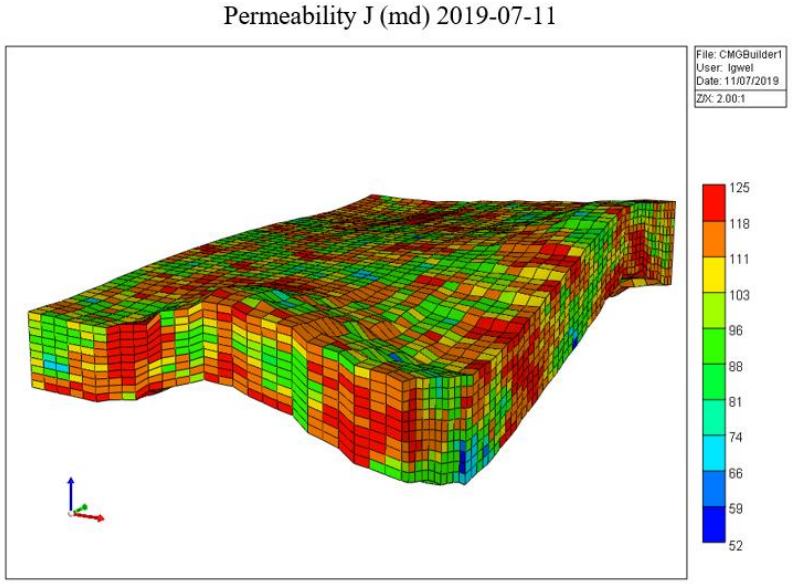

Figure 3.7: Gaussian Geostatistical Realisation of Permeability in the J-Direction (Perm J) Distribution

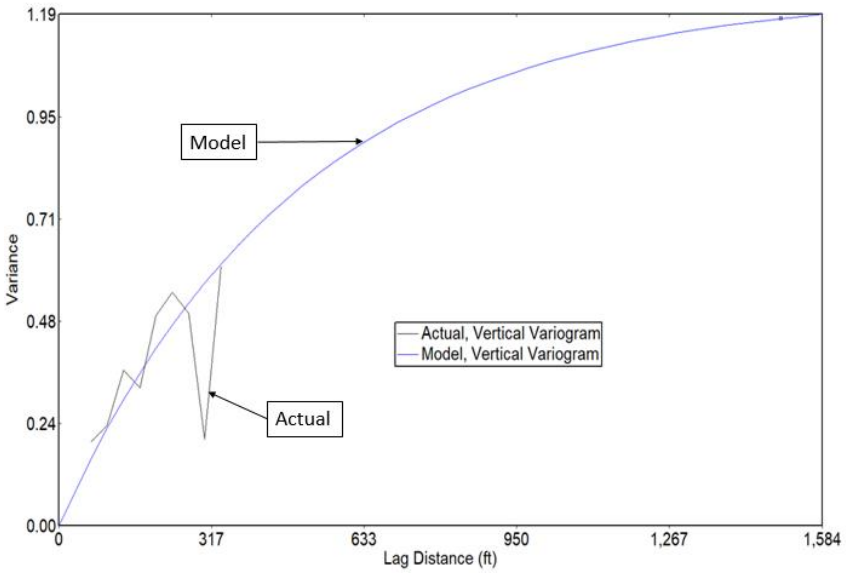

Figure 3.8: The Match of Gaussian geostatistical-simulation Model Generated Permeability Distribution with Actual Vertical Variogram

Table 3.11: Uncertainty Analysis of Gaussian geostatistical-simulation Model Generated Permeability Distribution

Parameter	Horizontal Variogram	Vertical Variogram
Nugget	0.000	0.000
Sill	1.241	1.241
Range	1107.847	1497.982

3.8.1 Coupling Fluid models with Reservoir Model

The coupling of the CG models (PVT models) into the reservoir model was implemented in the component section of Builder tree view. The constant composition fluid model built in section 3.3 and the various CG models built in section 3.4 were coupled individually with the reservoir model. Therefore, five (5) initialised dynamic reservoir models were built – constant composition, isothermal CG, Zero thermal diffusion CG, Haase's thermal diffusion CG, and Kempers thermal diffusion CG initialised reservoir model, respectively. The composition of each component as they vary with depth were specified for the various reservoir models. The reservoir gridblock temperature with respect to depth were also specified for the nonisothermal CG initialised models.

The oil-water and gas-oil relative permeability tables presented in Tables 3.9 and 3.10, respectively, were specified and the relative permeability curves generated. The oil-water and gas-oil relative permeability curves are shown in Figures 3.9 and 3.10, respectively. Figures 3.9 indicates that the relative permeability to oil (k_{ro}) decreases with increasing water saturation (s_w) while relative permeability to water (k_{rw}) increases with increasing s_w. The relative permeability to gas (k_{rg}) increased linearly with gas saturation (s_g) while

the relative permeability to oil in oil-gas system (k_{rog}) decreased with increasing s_g. as shown in Figures 3.10. Generated capillary pressure curve presented in Figure 3.11 shows that the capillary pressure between oil and water phases (p_{cow}) decreases with increasing water saturation (s_w) and that water is the wetting phase in the reservoir. The simulator recommended separator conditions for calculation of initial fluid-in-place was also specified.

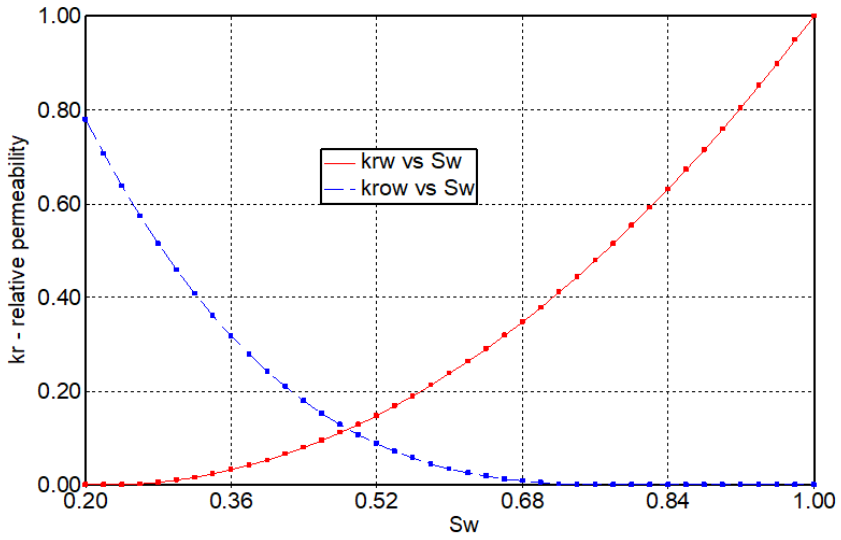

Figure 3.9: Oil-Water Relative Permeability Curve

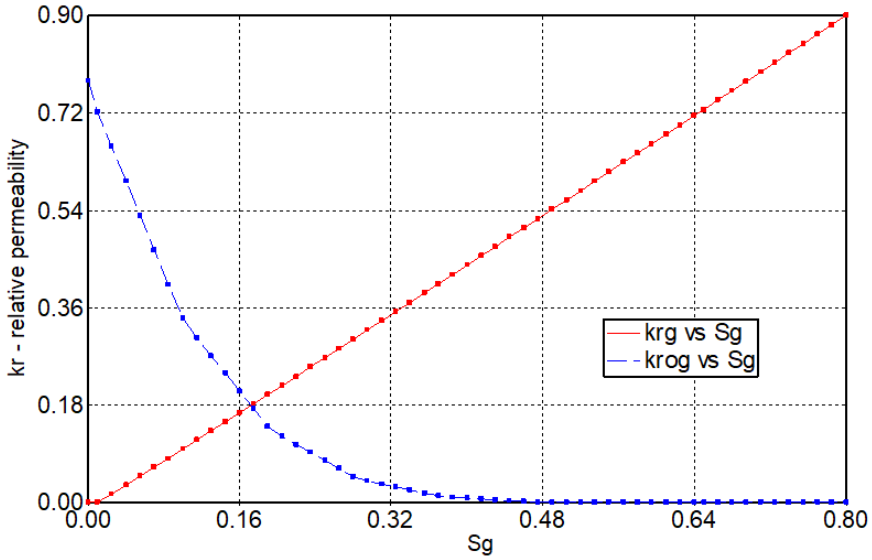

Figure 3.10: Gas-Oil Relative Permeability Curve

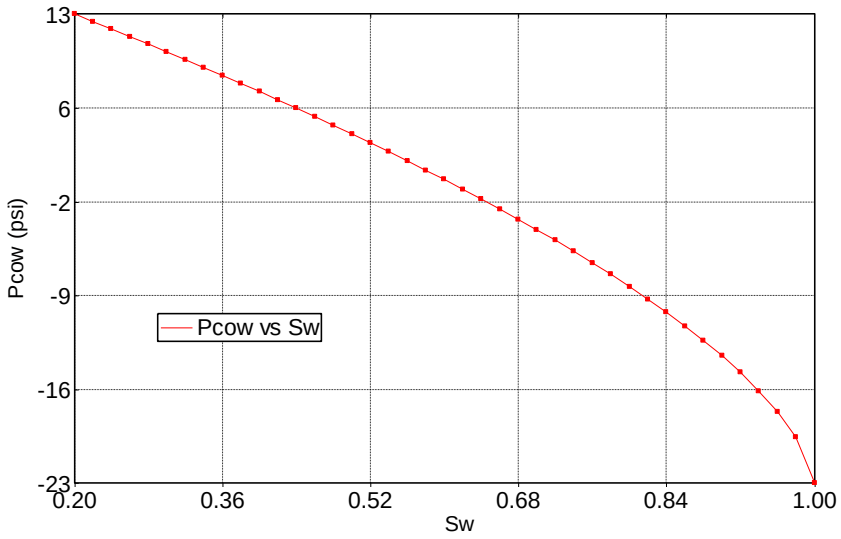

Figure 3.11: Capillary Pressure Curve

3.8.2 Wells and Recurrent

Six (6) wells were defined, four producers and two injection wells. They were manually completed across the ten (10) reservoir grid layers along the original well trajectories. Well completion data from industrial source was not provided. Hence, the need to manually complete the wells using the well trajectory perforation intervals. Two operate well constraints were set for the four (4) producers. The first is a maximum surface oil rate (STO) and secondly, a minimum bottom hole pressure (BHP). The values of the constraints for each producer well are presented in Table 3.12. Well-6 and well-7 were defined as injectors. The well locations and completions are indicated in Figure 3.12. Two simulation scenarios were executed based on two types of injection fluid – water injection scenario and separator gas injection scenario. A maximum bottom hole pressure (BHP) of 4100 psi and surface water rate (STW) of 15170 bbl/day were set as the first and second operate constraints, respectively for Well-6 while a maximum BHP of 4100 psi and STW of 5170 bbl/day were set as the first and second operate constraints, respectively for Well-7 (water injection scenario). Maximum BHP of 2700 psi and maximum surface gas rate (STG) of 90841 ft^3/day were specified as the first and second operating constraints, respectively, for the separator gas injection scenario. The composition of the injected separator gas is presented in Table 3.13. Four thousand seven hundred and forty nine (4749) days were specified as the simulation time with daily time step. This brings to an end the dynamic reservoir modelling process. The specified well and recurrent parameters were based on rigorous manual (trial-and-error) flow-stability analysis due to lack of historical production data and the fact that a suitable common rates and BHPs are required

for all the initialised reservoir models to enable adequate performance comparison. At this point, the models are ready to be validated and executed on GEM to simulate the actual reservoir behaviour based on the various fluid models. The models were executed and simulation results analysed and recorded.

Table 3.12: Well Events and Constraints

S/No	Constraint	Limit	Well-4	Well-5	Well-6	Well-7	Well-8	Well-9
1	STO (bbl/day)	Maximum	3619	2019	Injector*	Injector*	2019	2019
2	BHP (psi)	Minimum	2500	2000	Injector*	Injector*	2000	2000

*Injector values are specified in section 3.4.7 of chapter 3.

Table 3.13: Injected Separator Gas Composition

Component	Mole Fraction
CO2	0.006781017
CH4	0.218509978
C2H6	0.024563405
C3H8	0.030727966
IC4	0.010005557
NC4	0.016786574
IC5	0.009199422
NC5	0.009246842
FC6	0.018019486
C7+	0.130356755
Total	**0.474197**

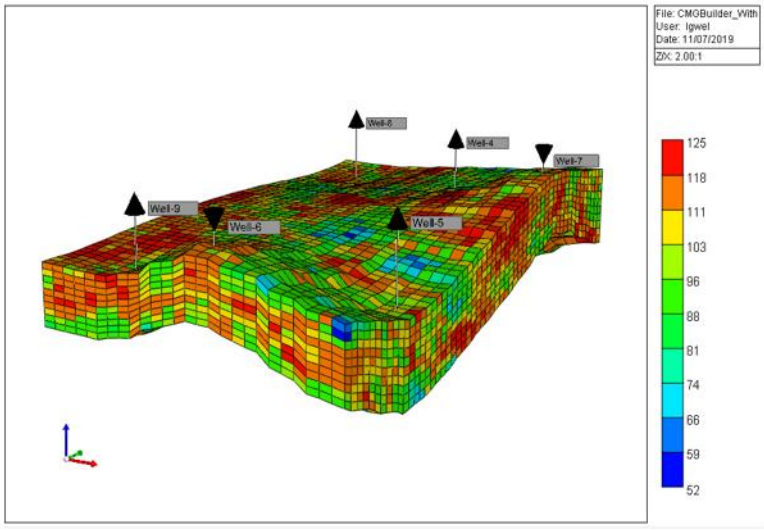

Figure 3.12: Well Locations and Completion in the Reservoir Model

3.8.3 Convergence Test and Numerical Accuracy Analysis

Analysis of convergence testing and numerical accuracy of the various initialised reservoir simulation models are illustrated in Table 3.14, which shows that applied convergence tolerance was adequate and that the simulation results were numerically correct. For example, all the initialised reservoir models indicated zero time step cut and

zero solver failure for a total of 4753 number of time steps, which suggest that the applied convergence tolerance is adequate. Also, the material balance errors indicated by the various models are very low and within acceptable limit, with 0.15 % for the nonisothermal CG initial reservoir models, 0.02 % for the isothermal CG initialised reservoir model, and 0.04% for the constant composition initialised reservoir model.

Table 3.14: Convergence Test and Numerical Accuracy/Refinement Metrics

Parameter	Model				
	Constant Composition	Isothermal	Zero Thermal Diffusion	Haase's	Kempers
Time step (Day)	1.0000	1.0000	1.0000	1.0000	1.0000
Total number of time step	4753	4753	4753	4753	4753
Convergence torance	1.00E-06	1.00E-06	1.00E-06	1.00E-06	1.00E-06
Total Total number of Newton cycles	4753	4757	4755	4755	4755
Total number of solver iterations	43550	33796	35744	35710	35724
Total number of time step cuts	0.0000	0.0000	0.0000	0.0000	0.0000
Total number of solver failures	0.0000	0.0000	0.0000	0.0000	0.0000
Material Balance Error; Weighted by Original Mat In-Place+Injected Mat. (%)	0.0004	0.0002	0.0015	0.0015	0.0015
Implicitness, average (%)	0.4986	0.4986	0.4986	0.4986	0.4986
Implicitness, peak (%)	0.4986	0.5128	0.5199	0.5199	0.5199

3.9 Uncertainty Assessment

According to Hoier and Whitson (2000), when field data are unavailable for history matching, the one-dimensional zero-mas-flux stationary state CG initialised reservoir models can be validated by using “cases” to quantify the range of uncertainties in the estimated in-place quantities. In addition, it has been shown that, if the deterministically (in this case, initialised reservoir models) estimated in-place volumes and the probabilistic (based on Monte Carlo Simulation) values agree significantly, there is an increased confidence in the reserve estimates, thereby validating the model. If the two values differ dramatically, the reservoir model assumptions would need to be reconsidered (Vilanova, 2016; SPE/WPC/AAPG/SPEE/SEG/SPWLA/EAGE, 2017). The uncertainty associated with the CG initialised reservoir model reserve estimates were assessed using CMOST, a CMG software which relies on CMG reservoir simulators to perform uncertainty assessment. CMOST also rely on response surface methodology to build proxy models, which were used to further validate the initialised reservoir models.

The uncertainty assessment (UA) process begins with creating new UA project for each initialised reservoir models (constant composition, isothermal, zero thermal diffusion,

Haase's thermal diffusion, and Kempers thermal diffusion). This involves specification of the project name and importing the base dataset originally created with the applied reservoir simulator. The execution of this initial step enables the creation of the CMOST project file, folder, and study manager for the various reservoir models. Subsequently, new studies are created within the study manager, for the respective models. The UA was performed based on MCS using reservoir simulator. Regressors such as permeability, porosity, water saturation, were created from the reservoir simulation base dataset using CMG Builder. OOIP and OGIP are the two main objective functions considered based on the original time series from the base dataset. A minimum of 300 new experiments was sufficient for the assessment. The simulation job relies on the scheduler in CMG launcher to run. All other default simulation settings were adopted – simulator (GEM), simulator version (2017), maximum run time per job (720 hours). Reduced quadratic model is the response surface model applied in this research to create and match proxy models with the various initialised reservoir simulation responses. To ensure the accuracy of the UA results, the orthogonality value of the designed experiments must be within the orthogonal range (CMOST, 2017). In this work, the orthogonality of the experiments generated for the various reservoir models are within the orthogonal range (0-0.2). The smaller the orthogonality value the better the experimental design quality.

The range of uncertainties in the estimated in-place volumes (OOIP and OGIP) for the various initialised reservoir models were illustrated with non-exceedance cumulative probability distribution curves as follow:

- P10 – there is at least 10 % probability that the volumes actually recovered will be less than the low estimate. This is equivalent to P90 of the probability of exceedance curve
- P50 – there is at least 50 % probability that the volumes actually recovered will be less than or equal the best estimate
- P90 - there is at least 90 % probability that the volumes actually recovered will be less than the high estimate. This is equivalent to P10 of the probability of exceedance curve

3.10 Model Validation

The following methods were used to validate the various initialised reservoir model results:

i. Comparison of the deterministic reserve estimate (reservoir simulation estimate) to the probabilistic (MCS) reserve estimate. The reservoir simulation result is said to be valid if both deterministic and probabilistic estimates agree significantly. If both estimates differ dramatically, the reservoir model assumptions will have to be reconsidered (Vilanova, 2016; SPE/WPC/AAPG/SPEE/SEG/SPWLA/EAGE, 2017).

ii. By quantifying the uncertainty in the estimated in-place volumes using MCS (Hoier and Whitson, 2000),

iii. Response surface methodology – by plotting the simulated in-place volume against proxy model (MCS) predicted in-place volumes (response surface model verification plot or model quality check plot), the validity or otherwise of the initialised reservoir models can be established. The model quality-check plot indicates how meticulously the proxy model predictions match actual reservoir simulation results. The 45-degree line indicate a perfect match between the proxy model and actual reservoir simulation responses. The closeness of the experiments (points) to the 45-degree line shows how perfectly the proxy model matched the reservoir simulation results (CMOST, 2017). The points that are exactly on the 45-degree line are those that are predicted perfectly. The farther away a point is from the 45-degree line, the more its outlier. The indicated training experiments are used by CMOST to create the proxy model while the verification experiments are used to check if the created proxy model is a valid proxy to the actual reservoir simulation responses (CMOST, 2017). Reduced Quadratic Regression Model was used to determine whether the regression model is statistically significant. The model is said to be statistically significant at 5 % probability if the 95 % confidence curves cross the horizontal reference line defined by the mean of response (Sall, 1990).

iv. Experimental design quality of the regression model – the orthogonality of the experimental design gives an indication of the accuracy of the model. A CMOST regression model is assumed valid if the orthogonality of the experimental design quality is within the range of 0-0.2 (CMOST, 2017).

3.11 Sensitivity Analysis

Sensitivity analysis was carried out to determine the parameter(s) in the various initialised reservoir models that was mostly responsible for the observed differences in the estimated

values of the hydrocarbon in-place volumes. The sensitivity of the reservoir models to the effects of model input parameters such as water saturation (s_w), porosity (poro), corner point depths for corner point grids (ZFT), offset of the simulation grid origin in the x-direction (XFT), and offset of the simulation grid origin in the y-direction (YFT), were analysed using CMG CMOST. The effects of these input parameters on the OOIP and OGIP estimated by the various initialised reservoir simulation models were illustrated in tornado diagrams and percentage effect plots. The procedure for sensitivity analysis is the same with that of uncertainty assessment presented in section 3.9.

3.12 Effects of Various EOSs on the Performance of Initialised Reservoir Models

The effect of four (4) different EOSs on the performances of constant composition, isothermal CG, Zero thermal diffusion CG, Haase's thermal diffusion CG, and Kempers thermal diffusion CG initialised reservoir model, respectively, have been considered. The EOSs considered are the PR 1976 EOS with 1976 expression for the constant "α", PR 1978 EOS with 1978 expression for the constant "α", the original SRK EOS, and SRK EOS with the constant "α" proposed by Graboski and Daubert (SRK (G&D)). The fluid modelling procedure is similar to the procedure presented in section 3.6. Simulation outcomes such as estimate OOIP, OGIP, oil and gas recovery factors, are used as performance indicators to assess the effects of the various EOSs on the outcomes of reservoir simulations.

3.13 The Sensitivity of Nonisothermal CG Initialised Reservoir Models to Changes in Temperature Gradient

The value of the temperature gradient in the applied nonisothermal CG initialised reservoir simulation models – zero (passive) thermal diffusion CG initialised reservoir model, Haase's thermal diffusion CG initialised reservoir model, and Kempers thermal diffusion CG initialised reservoir model, were varied from an initial value of 0.002 ^{o}F/ft to 0.5 ^{o}F/ft, 1.0 ^{o}F/ft, 1.5 ^{o}F/ft, 2.0 ^{o}F/ft, and 2.5 ^{o}F/ft, respectively. The effect of these variation on accurate and realistic reserve estimates, demonstrate the importance of accounting adequately for temperature gradient and its concomitant thermal diffusion in CG initialised reservoir model.

CHAPTER 4

RESULTS AND DISCUSSION

4.1 Reservoir Fluid Modelling Based on CG Models

CG models are governed by some fundamental physical principles, such as gravity, temperature gradient, and thermal diffusion. In this section, a comparative evaluation of the technical implications of the individual and combined effects of these fundamental physical principles on the performances of the various CG models based on the study reservoir fluid data (Table 3.2) are presented. CG models considered are the isothermal; zero (passive) thermal diffusion; Haase's thermal diffusion; and Kempers thermal diffusion models, respectively. Performance indicators considered include the reservoir and saturation pressure gradients, C_1 and C_{7+} variation with depth, and GOC variation with depth.

4.1.1 Reservoir and Saturation Pressure Gradient

The trend of the reservoir pressure gradients predicted by the four CG models (isothermal, Zero thermal, Haase's, and Kempers) are presented in Figure 4.1.

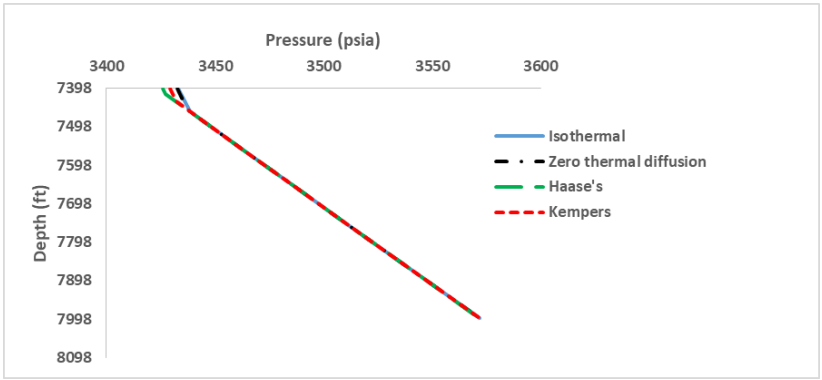

Figure 4.1: Reservoir Pressure Gradients Predicted by the Various CG Models

Figure 4.1 demonstrates that within the gas zone, the reservoir pressure gradient predicted by various models varies relatively. However, there was no major difference in the reservoir pressure gradient predicted by the various models within the oil zone. Within the gas zone, Haase's thermal diffusion model predicted the highest reservoir pressure gradient while the zero thermal diffusion model simulated the lowest. The trend of reservoir pressure gradient predicted by the Kempers model was in between those predicted by Haase's model and zero thermal diffusion model.

Figure 4.2 presents the saturation pressure gradients predicted by the various CG models. Kempers model, zero thermal diffusion model, and isothermal model exhibited similar trends within the gas zone but with distinguishable GOCs. Isothermal GCE model simulated higher saturation pressure gradient within the top gas zone and the bottom oil zone while Haase's thermal diffusion model predicted the least saturation pressure gradient in both zones.

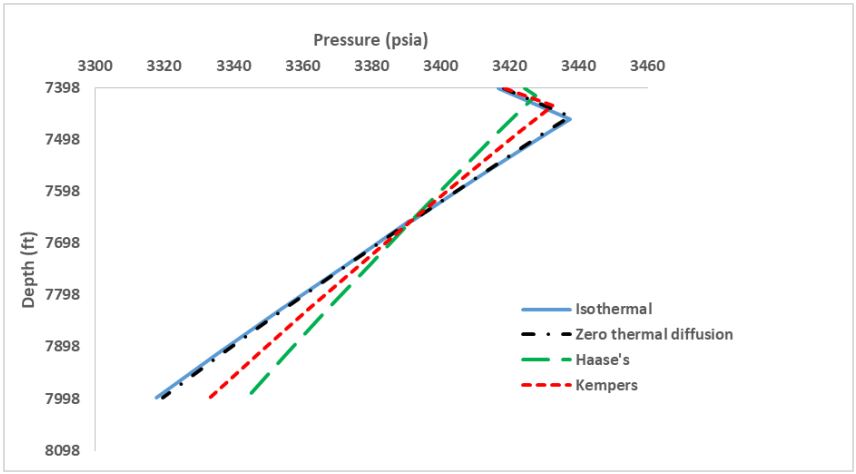

Figure 4.2: Saturation Pressure Gradients Predicted by the Various CG Models

Figure 4.2 indicates that models which accounted for the combined effects of gravity and thermal diffusion (Haase model and Kemper's model) predicted lower saturation pressure gradients in the entire hydrocarbon column. This is because thermal diffusion counteracts gravity effect. Figure 4.2 also shows that without the effect of thermal diffusion, temperature gradient alone as hypothetically assumed in zero thermal diffusion model, only caused a marginal difference in saturation pressure gradient when compared to isothermal model prediction. Another relevant observation from Figure 4.2 is the difference in the saturation pressure gradients predicted by Haase's and Kempers models, respectively. This difference could be attributed to their methods of estimating thermal diffusion factor.

4.1.2 Methane and Heptane plus fraction Gradient

Figures 4.3 and 4.4 presents the trends of C_1 and C_{7+} mole fraction variation with depth, respectively, simulated by the various CG models. Figure 4.3 indicates that isothermal CG model predicted a sharp drop in C_1 mole fraction from the top of the hydrocarbon column to the GOC and then a gradual decrease with increasing depth up to the bottom of the column. Therefore, isothermal CG model suggest that the reservoir gas is very compositionally sensitive with respect to depth than the reservoir oil. The implications of

the high compositional gradation within the gas zone and the marginal compositional variation towards the bottom oil zone as indicated by isothermal CG model would be illustrated more vividly when CG models are coupled with reservoir model for hydrocarbon reserve estimation and reservoir performance prediction. Zero thermal diffusion CG, Haase's thermal diffusion CG, and Kempers thermal diffusion CG models, respectively, indicated very marginal drop in C_1 mole fraction within the predicted gas zones followed by a sharp drop from the various GOC to the depth of 7483.43 ft. The variation in C_1 mole fraction after this depth is quite marginal and gradual with increasing depth. In addition, there is no major difference in C_1 gradation predicted by the various models after this depth (7483.43 ft) and up to the bottom of the hydrocarbon column. Figure 4.3 shows that C_1 mole fraction decreases with increasing depth, which is in agreement with trends reported in the literature (Hoier and Whitson, 2000; Pedersen and Hjermstad, 2015).

Figure 4.4 indicates that C_{7+} mole fraction increased with depth, which is also in agreement with trends reported in referenced literature (Hoier and Whitson, 2000; Pedersen and Hjermstad, 2015). The isothermal CG model shows that gravity effect alone resulted in sharp increase in C_{7+} mole fraction from the top of the hydrocarbon column to the GOC and then a gradual increase with increasing depth up to the bottom of the column. Zero thermal diffusion CG, Haase's thermal diffusion CG, and Kempers thermal diffusion CG models, respectively, indicated very marginal increase in C_{7+} mole fraction within the predicted gas zones followed by a sharp increase from the various GOCs to the depth of 7483.43 ft. The variation in C_{7+} mole fraction after this depth is quite marginal and gradual with increasing depth. The indicated trends by the nonisothermal CG model shows that thermal diffusion counteracts the effect of gravity on compositional variation with depth. Similar to C_1 gradation, there is no major difference in C_{7+} gradation predicted by the various models after 7483.43 ft and up to the bottom of the hydrocarbon column. Figures 4.3 and 4.4 also shows that a temperature gradient of 0.002 ^{o}F/ft was enough to produce thermal diffusion effect that caused noteworthy compositional gradient within the study reservoir. The compositional gradient of other fluid components as predicted by the various CG models are presented in Tables B1-B4 in Appendix B.

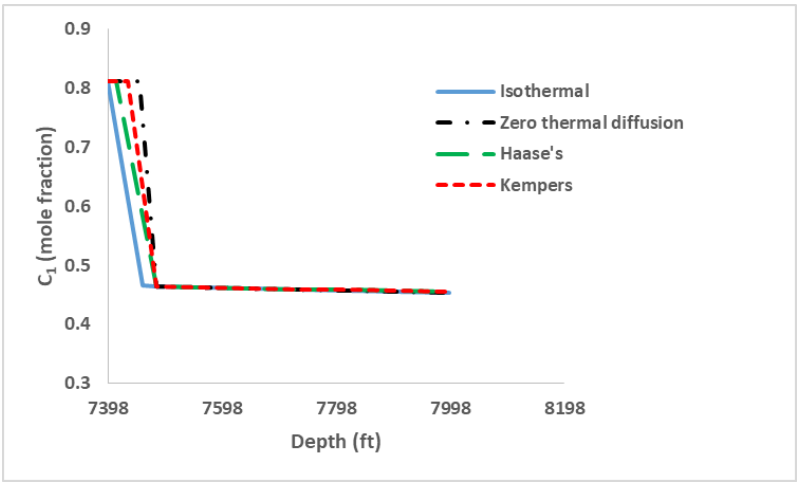

Figure 4.3: C_1 Mole Fraction Variation with Depth Predicted by the Various CG Models

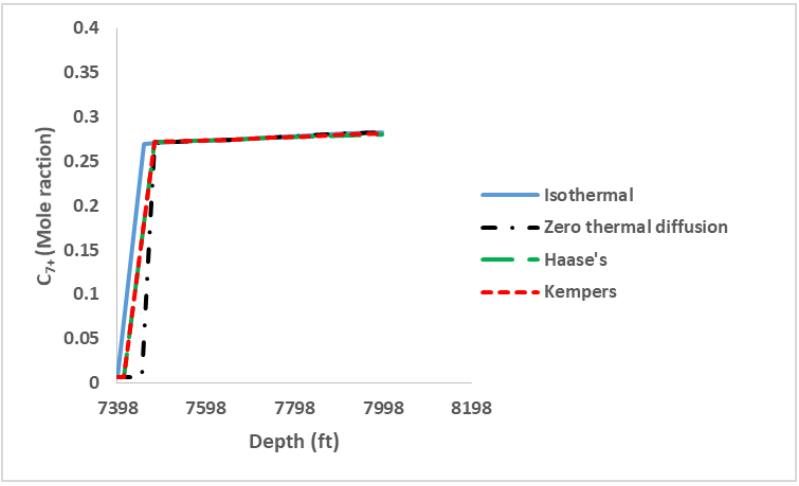

Figure 4.4: C_{7+} Mole Fraction Variation with Depth Predicted by the Various CG Models

4.1.3 Gas-Oil Contacts

Figure 4.5 compares the GOCs predicted by the various CG models. This figure once again illustrates the effects of gravity and thermal diffusion on compositional grading modelling. The effect of the marginal difference between the saturation pressure gradients predicted by isothermal model and zero thermal diffusion model, which was due to gravity and temperature gradient effects (Figure 4.2, section 4.1.1) is a bit more amplified here. Gravity effect resulted in estimation of high GOC value by the isothermal model. A temperature gradient of 0.002 ^{o}F/ft without thermal diffusion did not significantly oppose the effect of gravity, hence, resulting in a marginal reduction in the GOC predicted by zero thermal diffusion model when compared to isothermal model. The noteworthy reduction in the GOCs predicted by Haase's and Kempers thermal diffusion models is an indication that thermal diffusion counteracts the effect of gravity. Therefore, the combined effect of gravity and thermal diffusion in CG models will inevitably produce

more realistic simulation results that would adequately describe compositional grading phenomena in petroleum reservoirs.

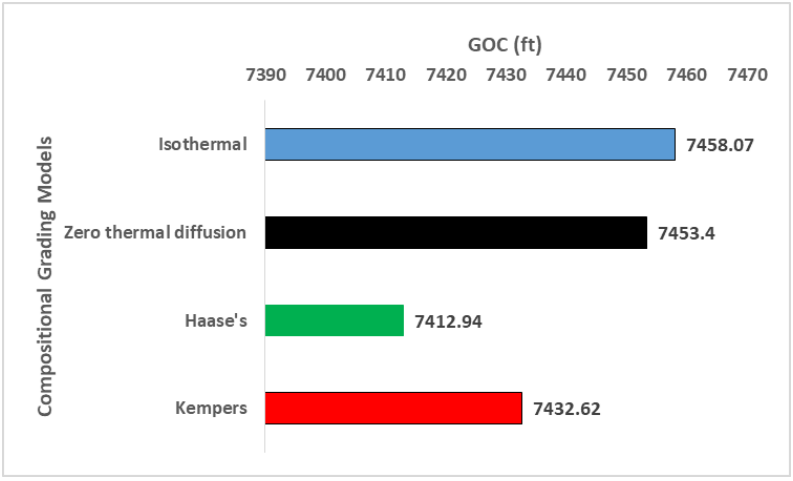

Figure 4.5: Comparison of GOCs Predicted by the Various CG Models

It is important to mention that the observed compositional variations with depth, reservoir and saturation pressure gradient trends, and the predicted GOCs, only apply to the reservoir fluid system investigated in this work. Other reservoir fluid systems such as gas condensate and near critical fluids may behave differently.

4.2 Effect of Temperature Gradient on Compositional Grading

The PVT data and reservoir parameters used for this particular analysis are presented in Table 3.4. These data were used to investigate the effect of vertical temperature gradient variation on GOC prediction, reservoir pressure gradient, saturation pressure gradient, and C_1 and C_{12+} fraction gradation, respectively. The simulation results are presented in Figures 4.6-4.14.

4.2.1 Effect of Temperature Gradient on GOC

The effect of varying temperature gradient on GOC as predicted by the various CG models is presented in Figure 4.6. Vertical temperature gradient was varied from a minimum value of 0.002 ^{o}F/ft to a maximum value of 0.02 ^{o}F/ft. Figure 4.6 shows that at 0.002 ^{o}F/ft, the various CG models predicted GOC trends similar to the trends indicated by the study reservoir shown in Figure 4.5.

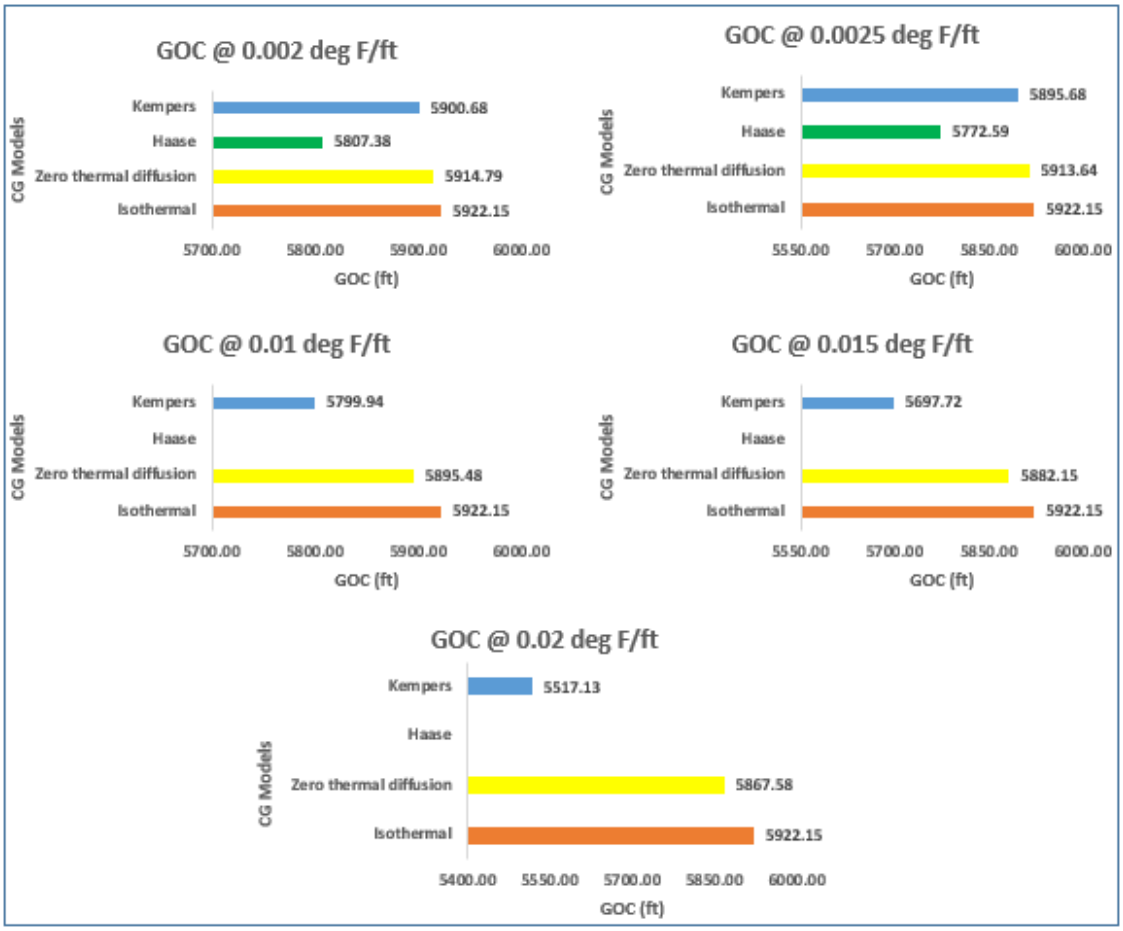

Figure 4.6: The Effect of Temperature Gradient on GOC Predicted by Various CG Models

This similarity is a somewhat confirmation of the initially described GOC behaviour of black oil reservoir fluid from Nigeria, with respect to the various applied CG models (see section 4.1.3). Figure 4.6 also shows that increase in temperature gradient within the reservoir system resulted in concomitant decrease in the GOCs indicated by the various nonisothermal models. Hence, black oil reservoir systems with high temperature gradient will probably indicate low GOCs as indicated. However, the gas condensate reservoir system presented by Pederson and Hjermstad (2015) indicated otherwise. The reason for this different behaviour is beyond the scope of this current study. Figure 4.6 also indicates that although Haase's thermal diffusion CG model predicted the lowest GOC at low temperature gradients, it failed to predict GOC for the reservoir fluid of interest at 0.01 ^{o}F/ft and higher temperature gradient. Consequently, the reservoir fluid system may not be very sensitive to changes in thermal gradient beyond 0.01 ^{o}F/ft, based on Haase's thermal diffusion CG model.

4.2.2 Effect of Temperature Gradient Based on Zero Thermal Diffusion Model

The effects of temperature gradient on reservoir and saturation pressure gradients, respectively, and C_I and C_{12+} gradation based on zero thermal diffusion CG model are presented in Figures 4.7-4.10. Figure 4.7 indicates that incremental temperature gradient has no serious effect on the reservoir pressure gradient. The effect of increasing temperature gradient on saturation pressure gradient is presented in Figure 4.8. It shows that increase in temperature gradient within the reservoir system resulted in decrease in saturation pressure gradient before the GOC and towards the bottom of the hydrocarbon column. Hence, for reservoir system with high temperature gradient, zero thermal diffusion CG model will predict low saturation pressure gradient throughout the hydrocarbon column. Figures 4.9 and 4.10 demonstrates the simulated effects of temperature gradient on C_1 and C_{12+} gradations, respectively, based on zero thermal diffusion CG model. Both figures shows that increasing temperature gradient from 0.002 $^oF/ft$ to a maximum value of 0.025 $^oF/ft$ caused no major changes in the predicted C_1 and C_{12+} variation with depth. Hence, temperature gradient alone without the corresponding thermal diffusion effect, could not sufficiently account for compositional grading phenomena in the studied reservoir system.

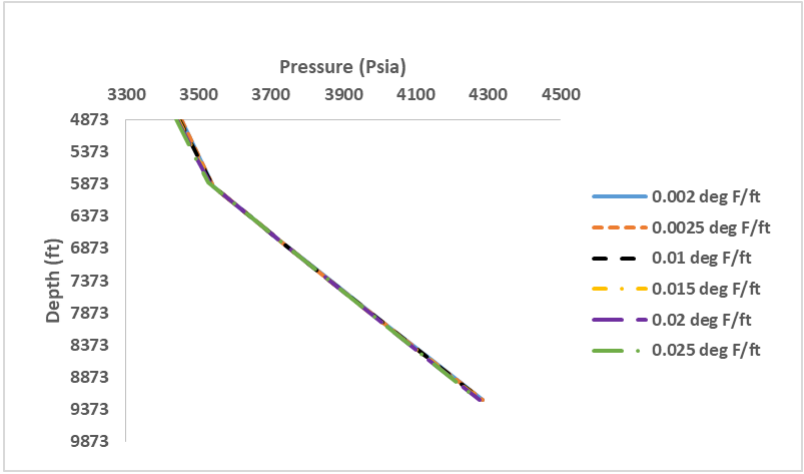

Figure 4.7: The Effect of Temperature Gradient on Reservoir Pressure Gradient Based on Zero Thermal Diffusion CG Models

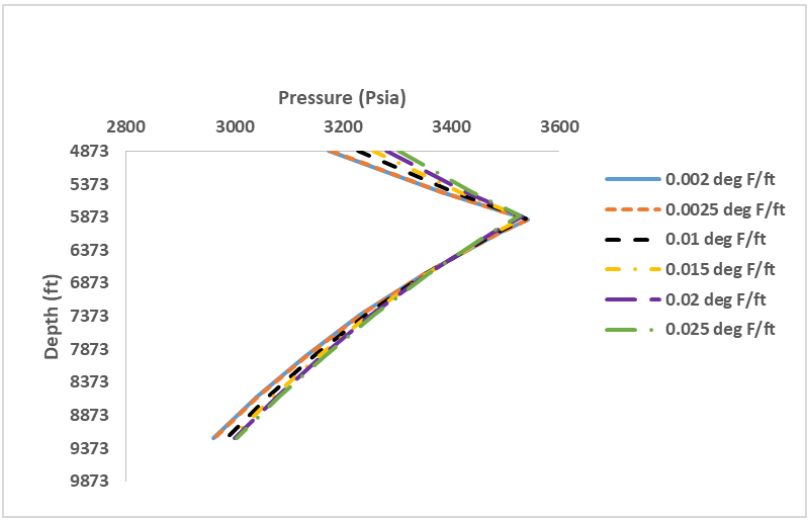

Figure 4.8: The Effect of Temperature Gradient on Saturation Pressure Gradient Based on Zero Thermal Diffusion CG Models

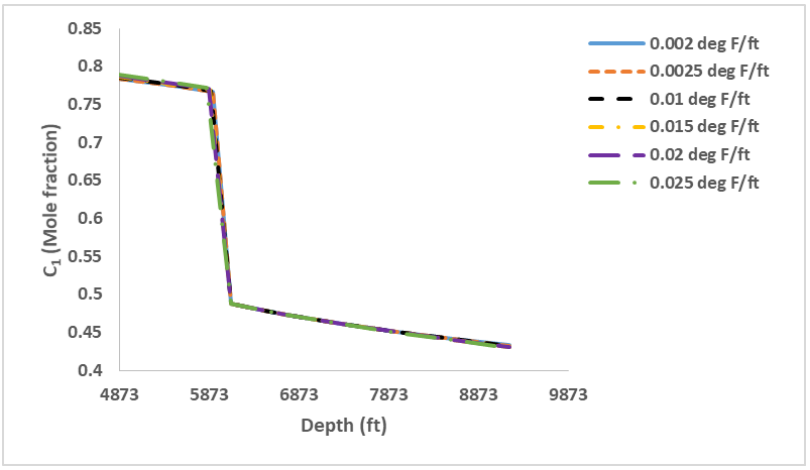

Figure 4.9: The Effect of Temperature Gradient on C_1 Gradation Based on Zero Thermal Diffusion CG Models

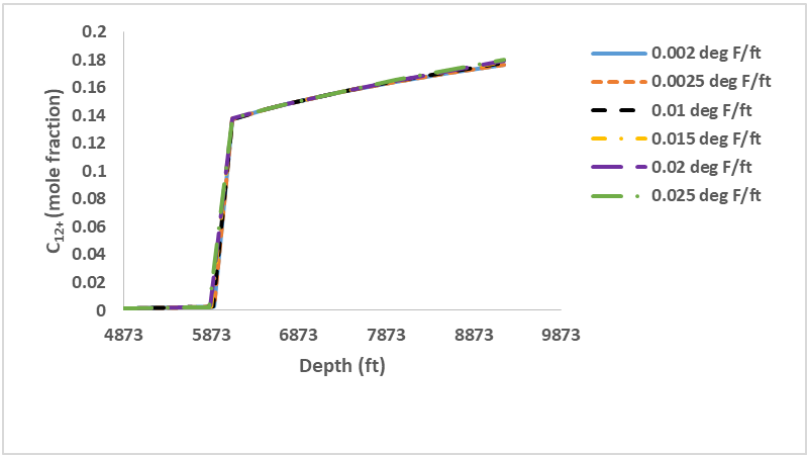

Figure 4.10: The Effect of Temperature Gradient on C_{12+} Gradation Based on Zero Thermal Diffusion CG Models

4.2.3 Effect of Temperature Gradient Based on Kempers Thermal Diffusion Model

Figures 4.11-4.14 illustrates the effects of temperature gradient on reservoir and saturation pressure gradients, respectively, and C_I and C_{12+} gradation based on Kempers thermal diffusion CG model. The effect of increasing temperature gradient on reservoir pressure gradient is presented in Figure 4.11. It shows that from the top of the reservoir to the GOC, increase in temperature gradient resulted in corresponding increase in reservoir pressure gradient. Beyond the GOC and all through to the end of the hydrocarbon column, increase in temperature gradient caused no noticeable changes in reservoir pressure gradient. Contrary to the trends indicated by the zero thermal diffusion CG model, Figure 4.12 shows that increasing temperature gradient resulted to attendant increase in saturation pressure gradient within the top zone of the reservoir and very significant decrease in saturation pressure gradient from the GOC towards the bottom section of the reservoir. Hence, Kempers thermal diffusion CG model indicates that variation in temperature gradient has more pronounced effect on saturation pressure gradient than reservoir pressure gradient. Figure 4.13 illustrates C_1 gradation due to increasing temperature gradient. It indicates that increase in temperature gradient resulted in very marginal gradation within the reservoir top. Beyond the reference depth, increase in temperature gradient caused no noticeable change in C_1 gradation. Figure 4.14 suggest no significant difference in C_{12+} gradation within the cold top zone of the reservoir. However, towards the hot bottom section, increase in temperature gradient resulted to very significant increase in C_{12+} gradation.

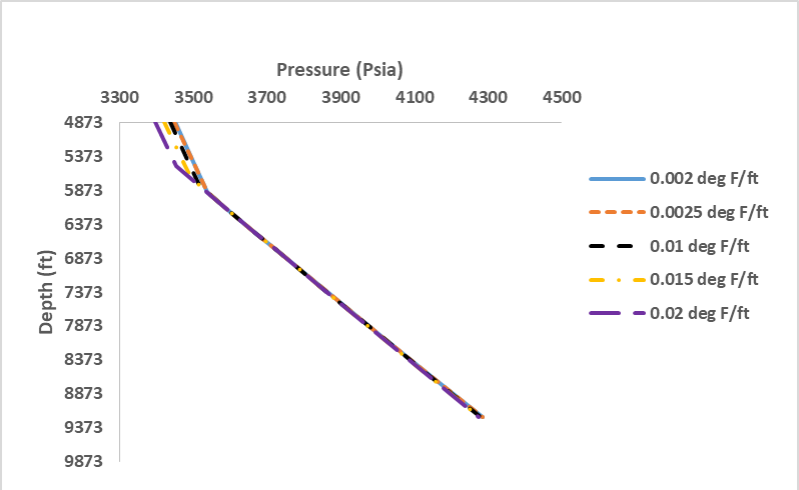

Figure 4.11: The Effect of Temperature Gradient on Reservoir Pressure Gradient Based on Kempers Thermal Diffusion CG Models

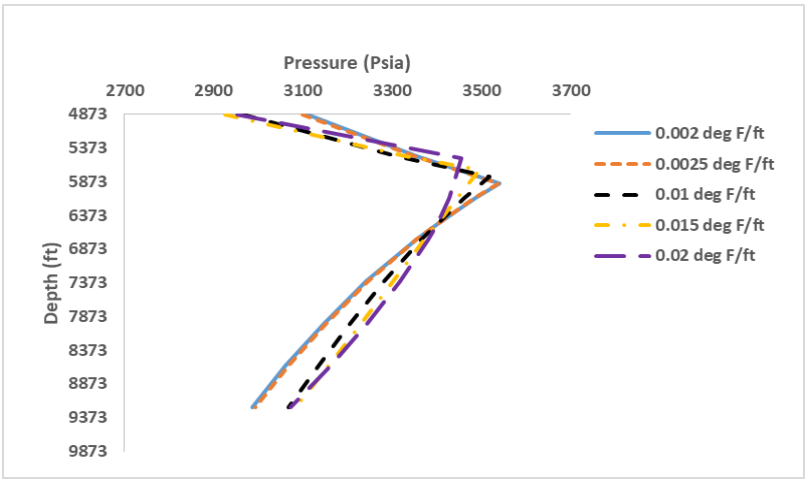

Figure 4.12: The Effect of Temperature Gradient on Saturation Pressure Gradient Based on Kempers Thermal Diffusion CG Models

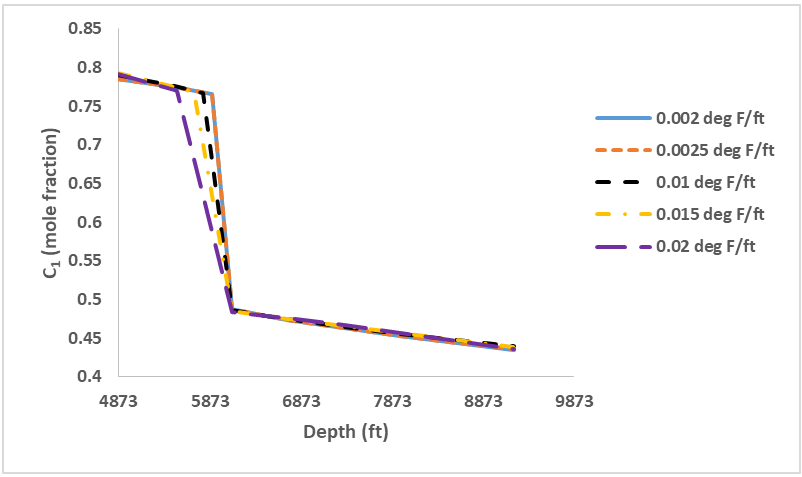

Figure 4.13: The Effect of Temperature Gradient on C_1 Gradation Based on Kempers Thermal Diffusion CG Models

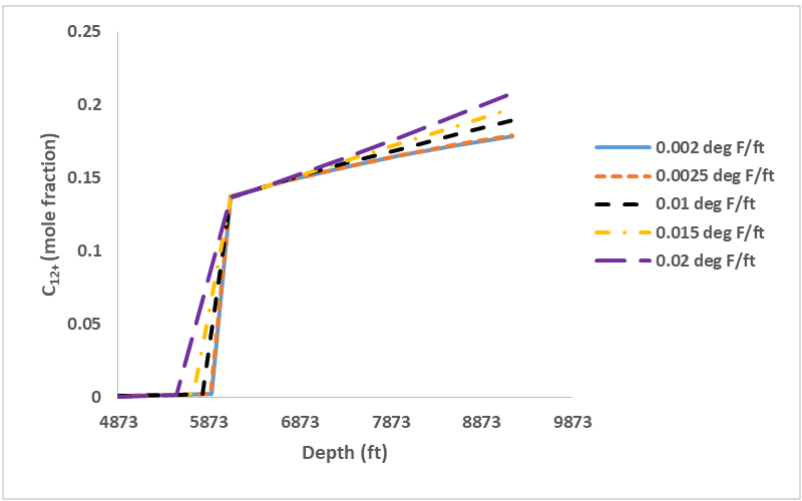

Figure 4.14: The Effect of Temperature Gradient on C_{12+} Gradation Based on Kempers Thermal Diffusion CG Models

The foregoing results and analysis has shown that increase in temperature gradient for the nonisothermal CG models, resulted in noteworthy increase in compositional variation

with depth. This result is in agreement with established fact – high geothermal reservoirs (like near critical reservoirs) exhibit high compositional variation with depth. Therefore, vertical temperature gradient and the associated thermal diffusion force inevitably plays very important role in compositional distribution along the vertical column of the reservoir. Hence, in order to adequately predict or describe compositional grading phenomena in reservoir systems, CG models that takes into account the effect of thermal diffusion amongst other relevant factors is a necessity.

4.3 The Effect of EOSs on the Performances of CG Models

The PVT and reservoir data used for this analysis is presented in Tables 3.5 and 3.6 in Chapter 3. The influence of various EOSs on the capability of applied CG models to accurately predict reservoir pressure gradient, saturation pressure gradient, C_1, and C_{10+} variation with depth, respectively, are considered. Although, the applied reservoir fluid composition consists of fourteen (14) fluid components, only C_1 and C_{10+} were selected as the key components to investigate the influence of the various EOSs on the performances of the applied CG models. This is because C_1 and C_{10+} represents the most dominant light and heavy components, respectively. EOS models available in WinProp and applied in this study include the PR 1976, PR 1978, SRK, and SRK (G&D). Note that detail investigation of the reasons why the various EOS effected the performances of the CG models differently is beyond the scope of this study.

4.3.1 The Effect of EOSs on the Performances of Isothermal CG Model

The effect of EOSs on the performance of isothermal CG model to accurately predict reservoir pressure gradient, saturation pressure gradient, C_1, and C_{10+} variation with depth, respectively, are presented in Figures 4.15-4.18. Figure 4.15 shows the reservoir pressure gradient predicted by the isothermal CG model based on various EOSs and relative to measured (experimental) pressure gradient. It shows that PR 1976, SRK, and SRK (G&D) predicted similar and more accurate trends at the top section of the reservoir. PR 1978 simulated the least accurate reservoir pressure gradient within the top zone. At the bottom section of the reservoir, PR 1978, PR 1976, and SRK simulated the most accurate reservoir pressure gradient. The saturation pressure gradient predicted by isothermal CG model based on the various EOSs and relative to measured data is shown in Figure 4.16. This figure indicated that PR 1978, SRK, and SRK (G&D) similarly overestimated saturation pressure gradient marginally at the top section of the reservoir. PR 1976

underestimated saturation pressure marginally within the same top section. Toward the bottom section of the reservoir, all the EOS models grossly overestimated saturation pressure gradient. Figure 4.17 indicates marginal difference in the C_1 trends simulated by the various EOSs within the top zone of the reservoir. The various EOS models indicate similar C_1 trends towards the bottom section of the reservoir with no significant difference. Figure 4.18 shows the predicted C_{10+} gradation. It shows that the difference between the trends exhibited by the various EOS models is only marginal. The calculated % AAD (statistical analysis) between the experimental values of C_1 and C_{10+} mole % at different depth and the values predicted by the different EOSs based isothermal CG model are presented in Table 4.1, which shows that PR 1976 EOS generated the least % AAD for both C_1 and C_{10+} gradations. These results suggest that, to accurately predict CG using isothermal CG model, the most realistic EOS model for fluid characterisation is PR 1976.

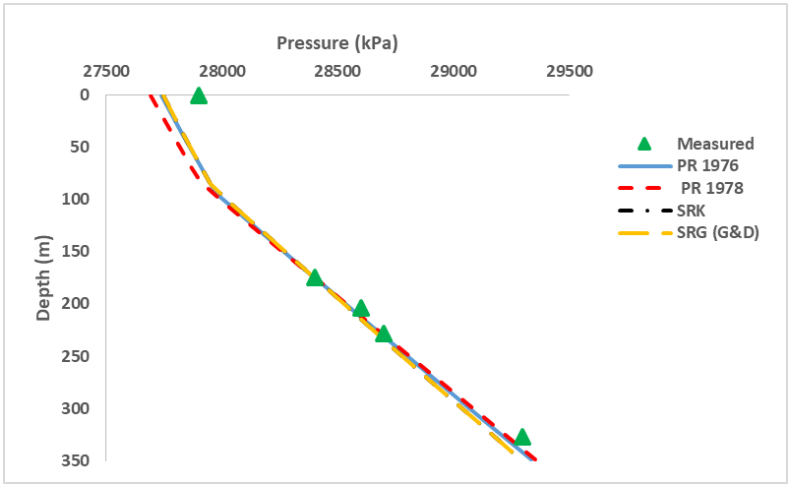

Figure 4.15: Comparison of the Effect of Different EOSs on the Performance of Isothermal CG Model to Accurately Predict Reservoir Pressure Gradient

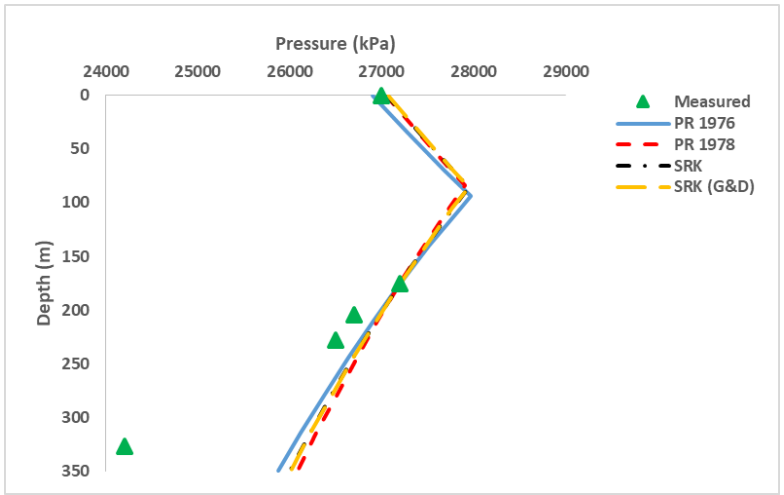

Figure 2.16: Comparison of the Effect of Different EOSs on the Performance of Isothermal CG Model to Accurately Predict Saturation Pressure Gradient

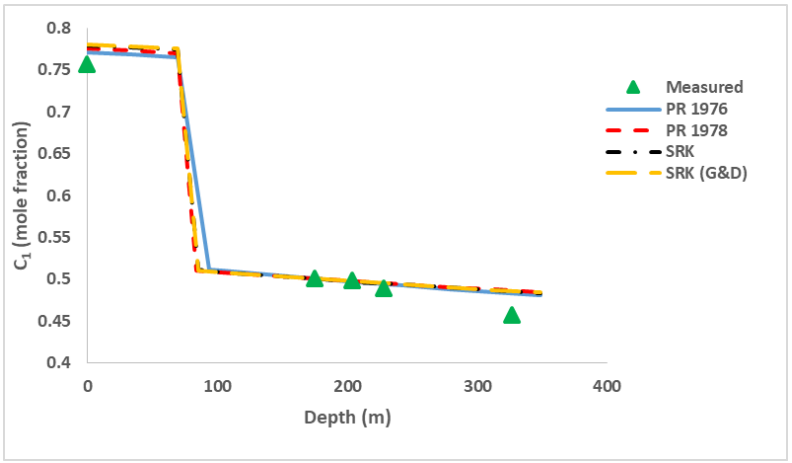

Figure 4.17: Comparison of the Effect of Different EOSs on the Performance of Isothermal CG Model to Accurately Predict C_1 Variation with Depth

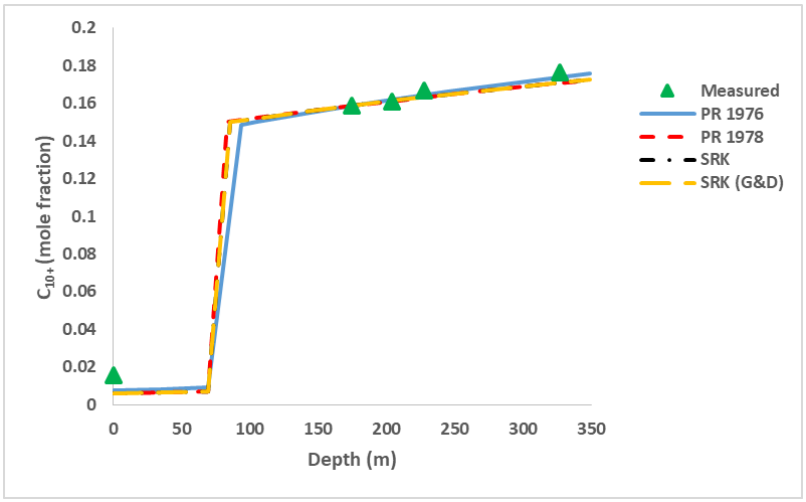

Figure 4.18: Comparison of the Effect of Different EOSs on the Performance of Isothermal CG Model to Accurately Predict C_{10+} Variation with Depth

Table 4.1: Comparison of % AAD Predicted by Various EOSs Based Isothermal CG Model

EOS	% AAD for C_1	% AAD for C_{10+}
PR 1976	1.84	10.75
PR 1978	1.90	11.15
SRK	2.19	13.27
SRK (G&D)	2.22	13.20

4.3.2 The Effect of EOSs on the Performances of Zero Thermal Diffusion CG Model

Figure 4.19 illustrates the reservoir pressure gradient simulated by the various EOSs based zero thermal diffusion CG model were similar to those indicated in Figure 4.15 by isothermal CG model. Figure 4.20 suggest that SRK (G&D) predicted the most accurate saturation pressure gradient at the reservoir top while the other EOS models underestimated saturation pressure gradient within the same section. All the EOS models overestimated saturation pressure gradient at the bottom of the reservoir. The predicted

variation of C_1 with depth predicted by the various EOSs based zero thermal diffusion CG model are presented in Figure 4.21. It shows that PR 1976 and PR 1978 predicted the most accurate C_1 gradation at the reservoir top while at the bottom, all the EOS models similarly overestimated C_1 gradation. Figure 4.22 presents the predicted C_{10+} gradation. It indicates that at both the top and bottom sections of the reservoir, C_{10+} gradation predicted by the various EOS models were all in close agreement with the measured trend. However, statistical analysis of Figures 4.21 and 4.22 presented in Table 4.2 confirmed that each EOS predicted results generated different values of % AAD with PR 1976 EOS estimating the least % AAD. Hence, PR 1976 is also the most suitable EOS for zero thermal diffusion CG model.

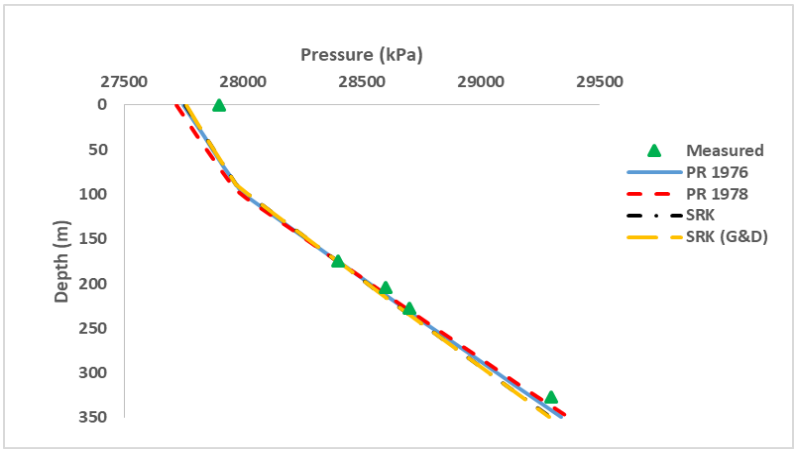

Figure 4.19: Comparison of the Effect of Different EOSs on the Performance of Zero Thermal Diffusion CG Model to Accurately Predict Reservoir Pressure Gradient

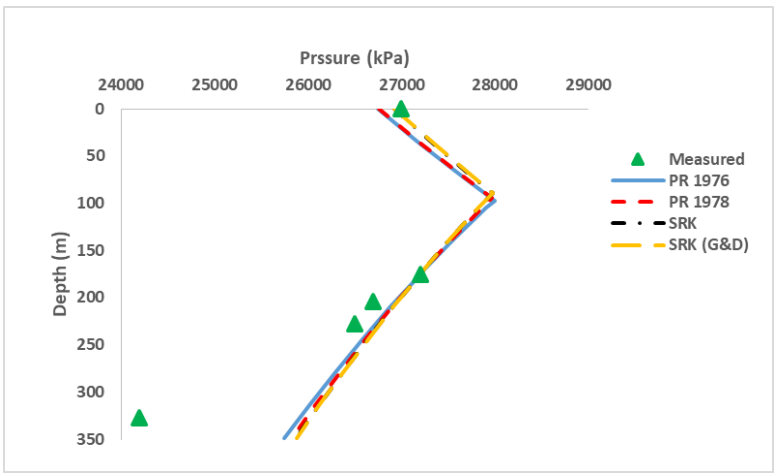

Figure 4.20: Comparison of the Effect of Different EOSs on the Performance of Zero Thermal Diffusion CG Model to Accurately Predict Saturation Pressure Gradient

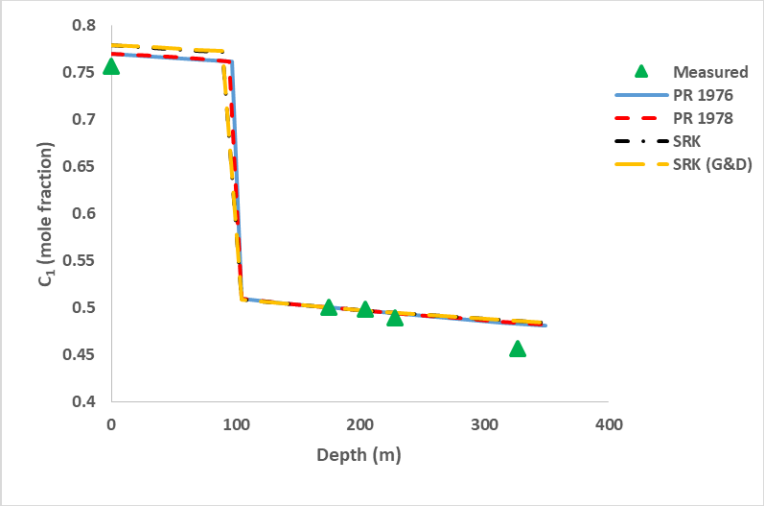

Figure 4.21: Comparison of the Effect of Different EOSs on the Performance of Zero Thermal Diffusion CG Model to Accurately Predict C_1 Variation with Depth

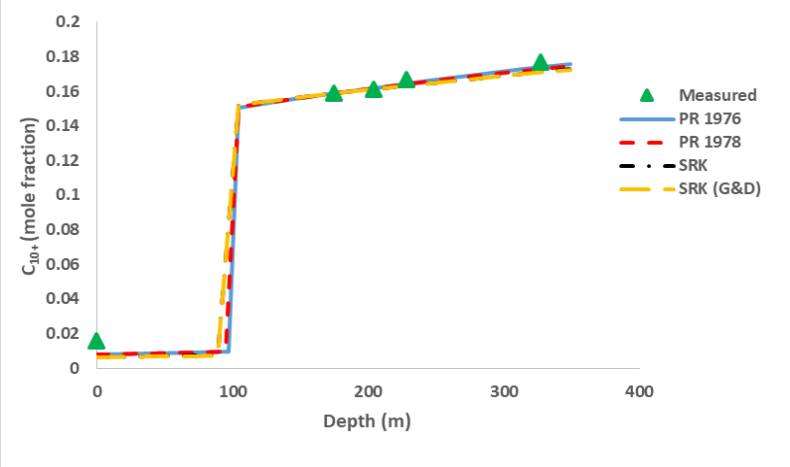

Figure 4.22: Comparison of the Effect of Different EOSs on the Performance of Zero Thermal Diffusion CG Model to Accurately Predict C_{10+} Variation with Depth

Table 4.2: Comparison of % AAD Predicted by Various EOSs Based Zero Thermal Diffusion CG Model

EOS	% AAD for C_1	% AAD for C_{10+}
PR 1976	1.82	10.62
PR 1978	1.89	10.92
SRK	2.17	15.54
SRK (G&D)	2.20	13.22

4.3.3 The Effect of EOSs on the Performances of Haase's Thermal Diffusion CG Model

The reservoir pressure gradients predicted by the various EOS models shown in Figure 4.23, significantly agrees with the measured trend. The saturation pressure gradient predicted by the various EOS models is presented in Figure 4.24. This figure indicates that the various EOS models underestimated the saturation pressure gradient at the reservoir top contrary to the trends indicated by EOS based isothermal and zero thermal

diffusion CG models, respectively. However, at the bottom section of the reservoir, the EOSs based Haase's thermal diffusion CG model predicted saturation pressure gradient that are reasonably close to the measured trend. The simulated variation of C_1 with depth indicated by the various EOSs based Haase's thermal diffusion CG model is presented in Figure 4.25. This figure suggest that at the top of the reservoir, SRK and SRK (G&D) predicted similar C_I gradation trend that is somewhat less accurate than the trends exhibited by PR 1976 and PR 1978. Towards the bottom section of the reservoir, all the EOS models predicted C_1 gradation with significantly similar degree of accuracy. The simulated gradation of C_{10+} illustrated in Figure 4.26 suggest similarity in the trends predicted by the various EOS models at both the top and bottom sections of the reservoir. Despite the observed similarities, statistical analysis of Figures 4.25 and 4.26 presented in Table 4.3 inveterate significant difference in the values of calculated % AAD and shows that PR 1987 is the most suited EOS for Haase's thermal diffusion CG model.

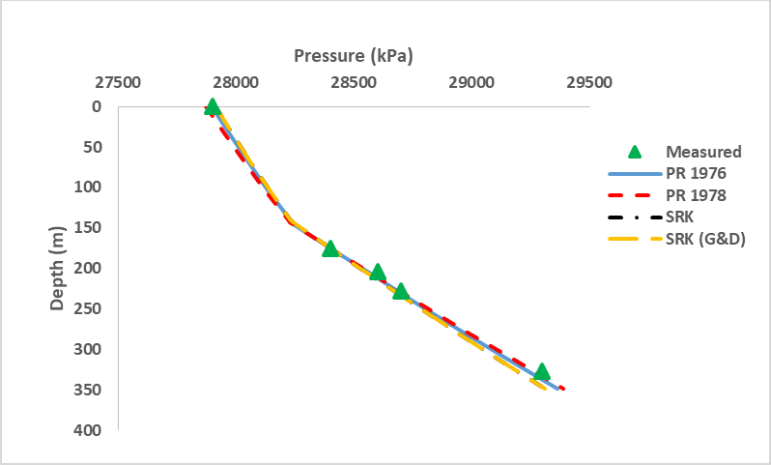

Figure 4.23: Comparison of the Effect of Different EOSs on the Performance of Haase's Thermal Diffusion CG Model to Accurately Predict Reservoir Pressure Gradient

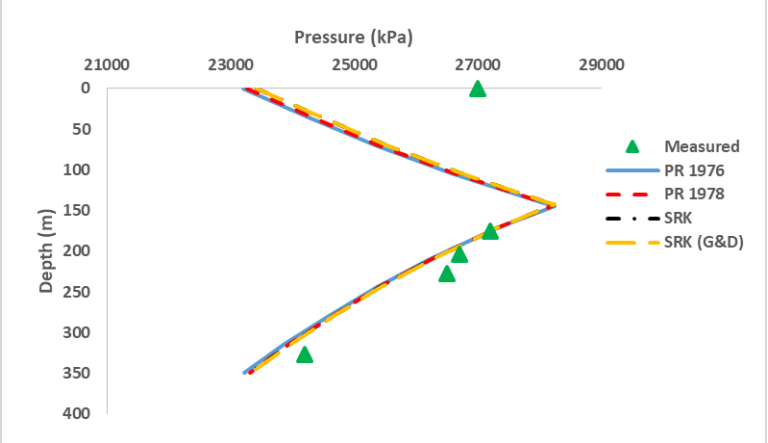

Figure 4.24: Comparison of the Effect of Different EOSs on the Performance of Haase's Thermal Diffusion CG Model to Accurately Predict Saturation Pressure Gradient

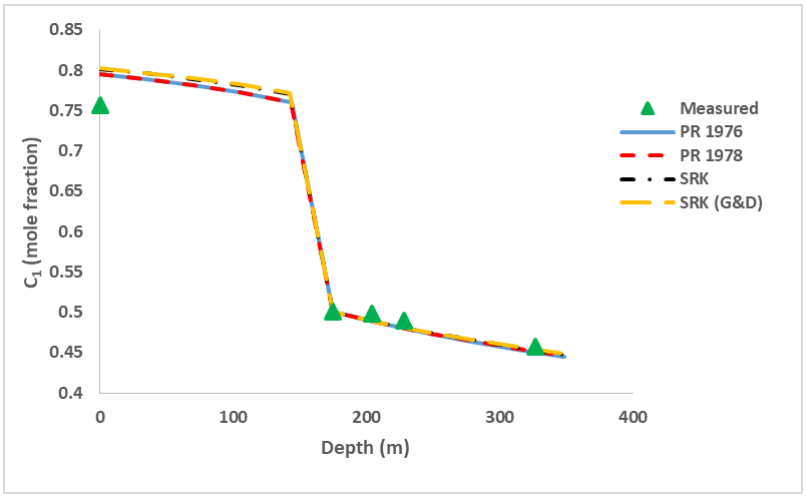

Figure 4.25: Comparison of the Effect of Different EOSs on the Performance of Haase's Thermal Diffusion CG Model to Accurately Predict C_1 Variation with Depth

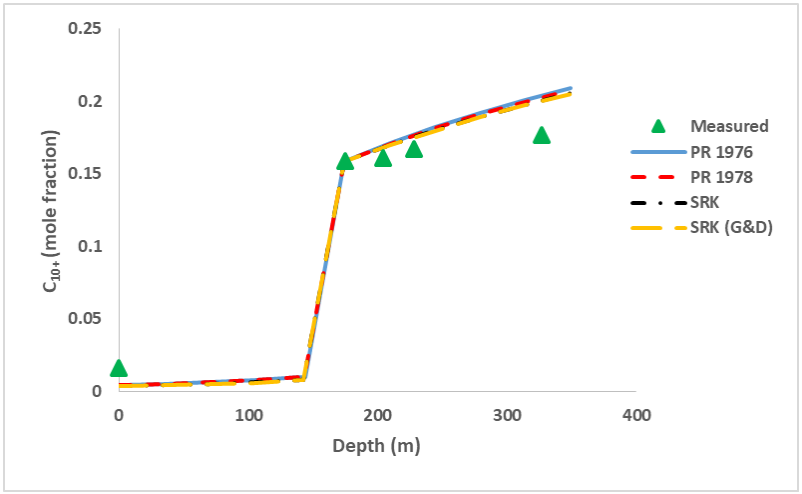

Figure 4.26: Comparison of the Effect of Different EOSs on the Performance of Haase's Thermal Diffusion CG Model to Accurately Predict C_{10+} Variation with Depth

Table 4.3. Comparison of % AAD predicted by various EOSs Based Haase's Thermal Diffusion CG Model

EOS	% AAD for C_1	% AAD for C_{10+}
PR 1976	2.08	19.89
PR 1978	1.97	19.61
SRK	2.04	20.31
SRK (G&D)	2.04	20.22

4.3.4 The Effect of EOSs on the Performances of Kempers Thermal Diffusion CG Model

The simulated effect of the applied EOSs on the performance of Kempers thermal diffusion CG model are presented in Figures 4.27-4.30. Figure 4.27 illustrates the reservoir pressure gradient trends predicted by various EOSs based Kempers thermal diffusion CG model. It shows that the various EOS models predicted marginally different and lower reservoir pressures gradient at the reservoir top while PR 1976, PR 1978, and

SRK predicted similar and more accurate trends towards the bottom section of the hydrocarbon column. Predicted saturation pressure gradients are shown in Figure 4.28 and it indicates that there is no significant difference in the saturation pressure gradient trends predicted by the various EOS models. Figures 4.29 and 4.30 suggests that the C_1 and C_{10+} gradation trends predicted by the various EOS models exhibited analogous trends to the trends presented by Haase's thermal diffusion CG model (Figures 4.25 and 4.26) but with distinct % AAD values. The computed % AAD of the various EOSs are presented in Table 4.4, which shows that PR 1976 EOS with the least % AAD, is the most suitable EOS for Kempers thermal diffusion CG model.

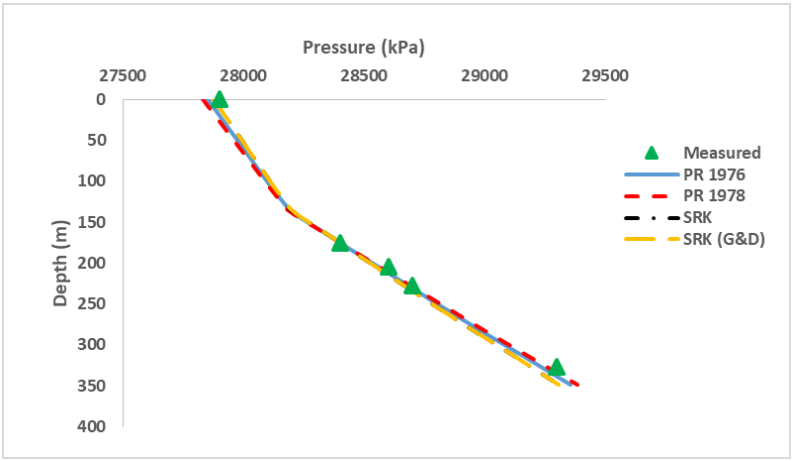

Figure 4.27: Comparison of the Effect of Different EOSs on the Performance of Kempers Thermal Diffusion CG Model to Accurately Predict Reservoir Pressure Gradient

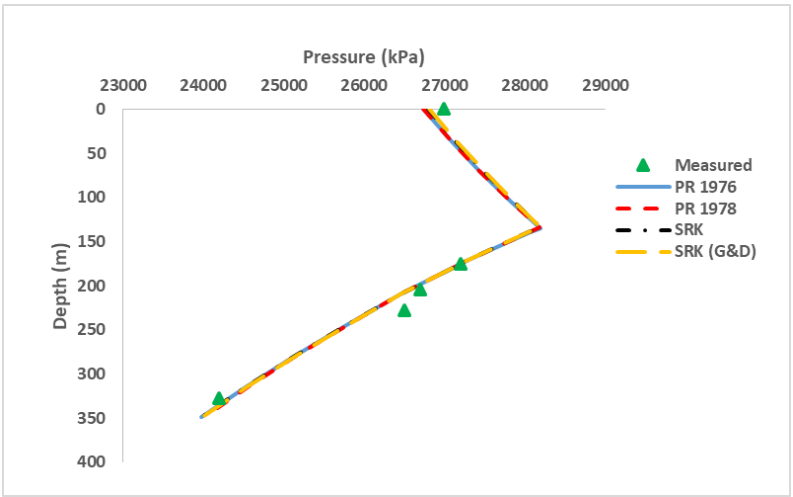

Figure 4.28: Comparison of the Effect of Different EOSs on the Performance of Kempers Thermal Diffusion CG Model to Accurately Predict Saturation Pressure Gradient

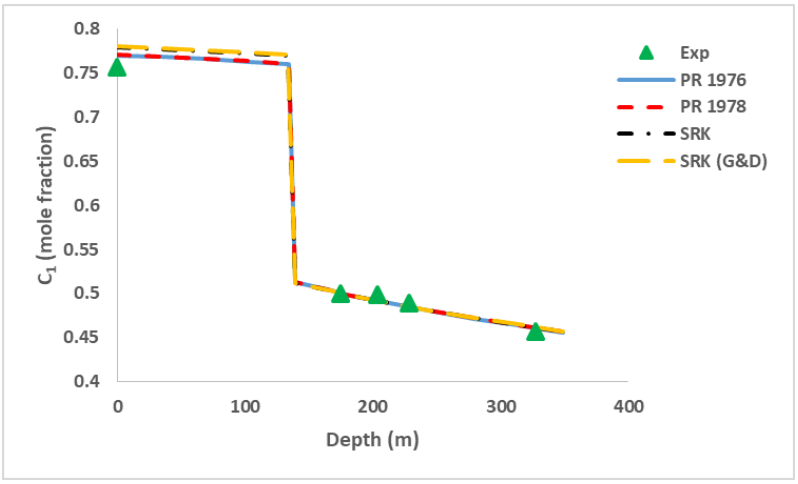

Figure 4.29: Comparison of the Effect of Different EOSs on the Performance of Kempers Thermal Diffusion CG Model to Accurately Predict C_1 Variation with Depth

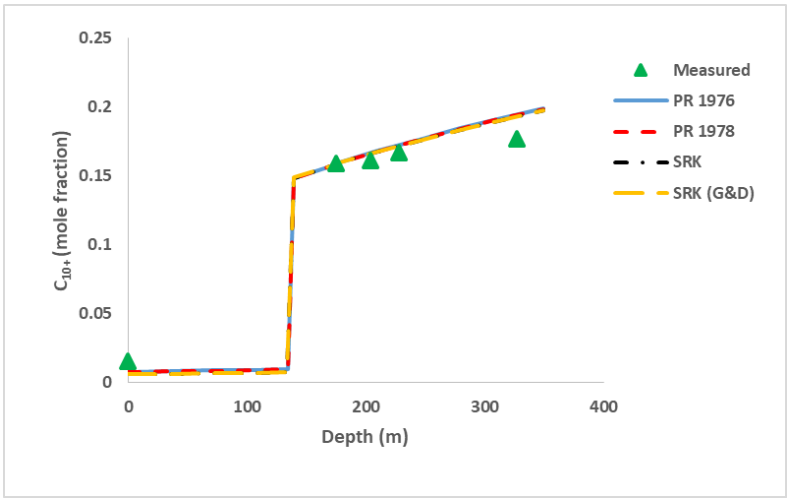

Figure 4.30: Comparison of the Effect of Different EOSs on the Performance of Kempers Thermal Diffusion CG Model to Accurately Predict C_1 Variation with Depth

Table 4.4. Comparison of % AAD Dredicted by Various EOSs based Kempers Thermal Diffusion CG model

EOS	% AAD for C_1	% AAD for C_{10+}
PR 1976	1.01	13.34
PR 1978	1.04	13.40
SRK	1.26	15.23
SRK (G&D)	1.28	15.16

Simulation results from the applied CG models (isothermal model, zero thermal diffusion model, Haase's thermal diffusion model, and Kempers thermal diffusion model) and statistical analysis of the results (%AAD) suggest that selection of a suitable EOS has significant effect on the performances of the applied CG models. Coupling PR 1976 EOS with isothermal model, zero thermal diffusion model, and Kempers thermal diffusion model, respectively, resulted to superior performance of the models. Amongst the applied EOSs for Haase's thermal diffusion model, PR 1978 EOS simulated the most accurate compositional grading with respect to experimental values.

4.4 Reservoir Simulation (Water Injection Scenario)

The simulation results of reservoir models initialised with constant composition fluid model, isothermal CG model, zero (passive) thermal diffusion CG model, Haase's thermal diffusion CG model, and Kempers thermal diffusion CG model, under water injection, are hereby presented and discussed. The only difference in the various initialised reservoir models is the PVT models or compositional grading models. All other parameters within the various initialised reservoir models are the same. This was intended for adequate comparison of the technical implications of the coupled CG models or constant composition PVT fluid model on the performances of resultant reservoir flow models. Technical performance indicators considered are the oil and gas production rates, reserve estimates, oil and gas recovery factors, cumulative oil and gas produced, gas-oil ratio, and average reservoir pressure profile. These technical performance indicators illustrates the implications of implementing the various compositional grading models in reservoir simulation model initialisation.

4.4.1 Reserve Estimates

Results of simulated reservoir volumetric for various initialised models are presented in Figures C1-C5 in Appendix C, which indicated that the various models simulated same total bulk reservoir volume, total pore volume, and total hydrocarbon pore volume, respectively but different original Oil in-place (OOIP) and original Gas in-place (OGIP). The OOIP and OGIP estimated by the various initialised reservoir models are presented in Figures 4.31 and 4.32, respectively. Figure 4.31 indicates that the reservoir model initialised without CG (constant composition) estimated the highest OOIP while Haase's thermal diffusion CG initialised reservoir model estimated the least OOIP. Although, isothermal CG initialised reservoir model estimated OOIP lower than the value predicted by constant composition initialised reservoir model, the value is higher than the OOIP estimated by the various nonisothermal CG initialised reservoir models. There are marginal differences in the OOIPs predicted by the various nonisothermal initialised reservoir models.

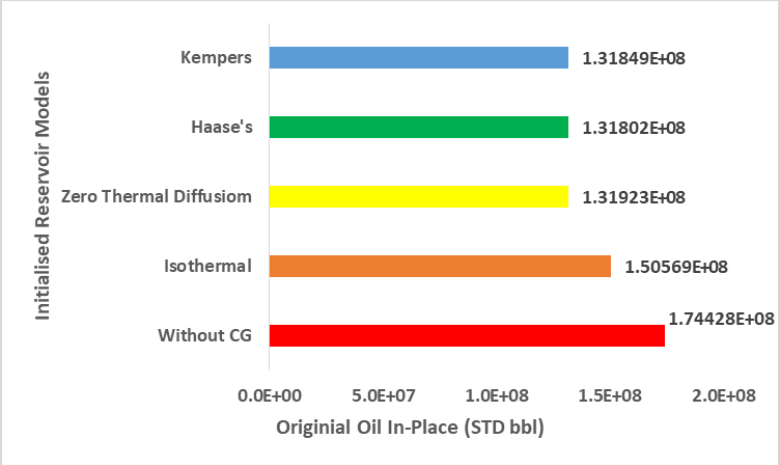

Figure 4.31: Oil Reserve Estimated by Various Initialised Reservoir Models

The results from Figure 4.31 suggest that neglecting CG in reservoir model initialisation and assuming that the compositions of the various reservoir fluid components is the same at any depth along the hydrocarbon column, resulted in high OOIP estimation. This assumption is not tenable, since this work have shown that the compositions of the various fluid components varies with depth. Hence, the constant composition (without CG) initialised reservoir model inevitably overestimated the OOIP. Figure 4.31 also shows that isothermal CG initialised reservoir model which neglects thermal diffusion effect also overestimated the OOIP. Similarly, isothermal assumption, with respect to the study reservoir, is not realistic, since this work has shown that thermal diffusion contributes to compositional gradation in the study reservoir. The zero thermal diffusion CG initialised reservoir model that accounted for both gravity and temperature gradient effects but neglected thermal diffusion effect, estimated marginally higher OOIP than the other nonisothermal models (Haase's and Kempers CG initialised reservoir models). Since it is a hypothetical model, the result is also hypothetical. It can be opined from the forgoing analysis that Haase's and Kempers thermal diffusion initialised reservoir models, which accounted for the combined effect of gravity and thermal diffusion forces estimated the most realistic OOIP since they complied with physical realities (accounting for the effects of gravity and thermal diffusion).

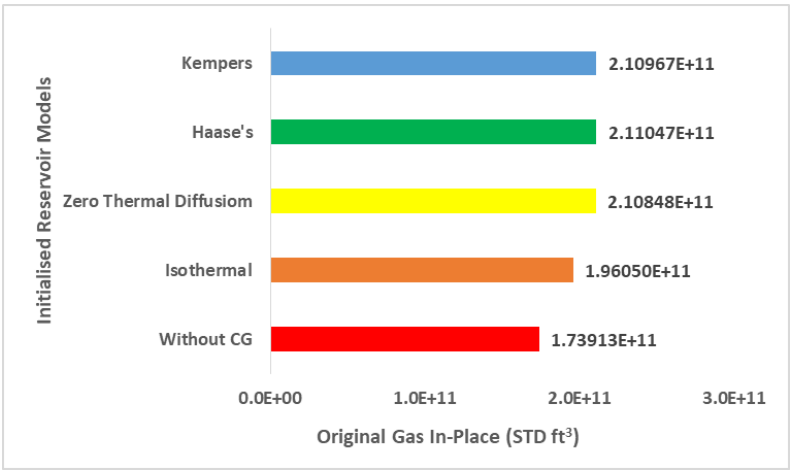

Figure 4.32: Gas Reserve Estimated by Various Initialised Reservoir Models

It is evident from Figure 4.32 that constant composition initialised reservoir model estimated the lowest OGIP with respect to other models. This indicates that, following the previous analogy concerning OOIP, constant composition initialised reservoir model underestimated the OGIP. This suggests that neglecting compositional grading in the initialisation of reservoir simulation model will result in underestimation of OGIP. Figure 4.32 also show that isothermal CG initialised reservoir model estimated higher OGIP than the constant composition initialised reservoir model. However, it estimated a low OGIP than the values indicated by the nonisothermal CG initialised reservoir models. Similarly, following previous analogy with respect to OOIP, neglecting the effects of thermal diffusion and temperature gradient as indicated by the isothermal CG initialised reservoir model, will result in underestimation of OGIP. Figure 4.32 indicates that zero thermal diffusion CG initialised reservoir model, which hypothetically accounted for the effect of temperature gradient but with passive thermal diffusion effect, estimated OGIP value higher than the values indicated by constant composition and isothermal CG initialised reservoir models but marginally lower than the values indicated by other nonisothermal models. Haase's and Kempers thermal diffusion initialised reservoir models estimated the highest OGIP with the value indicated by Haase's model marginally higher than the value predicted by Kempers model.

These results suggests that constant composition (without CG) initialised reservoir model overestimate the OOIP by 13.86 % more than the isothermal model, 24.37 % more than the zero thermal CG model, 24.44 % more than the Haase;s thermal diffusion CG model, and 24.41 % more than the Kempers model. However, it underestimate OGIP by 12.73 % less than the isothermal CG model, 21.24 % less than the zero thermal diffusion CG

model, 21.35 % less than the Haase's thermal diffusion CG model, and 21.31 % less than the Kempers thermal diffusion CG initialised reservoir model. This result has shown once again that neglecting compositional grading in reservoir simulator initialisation has noteworthy technical consequences. It also suggest that neglecting the effect of gravity or thermal diffusion in CG modelling will result in inaccurate estimation of OGIP. It is import to state at this point that these results are attributed only to the current study reservoir system. Other reservoir systems may behave differently.

4.4.2 Oil and Gas Production Rates

Figure 4.33 illustrates that the various initialised reservoir models exhibited similar constant oil production rate behaviour from the start of production. However, the duration of the initial constant oil rate exhibited by the nonisothermal CG initialised reservoir models are shorter than the trends indicated by constant composition and isothermal CG initialised models, respectively. The longer constant oil rate exhibited by the constant composition initialised reservoir model could be attributed to the high OOIP estimated by the model, which is due to the constant composition (without CG) assumption. Consequently, the coupled fluid models are the most likely reasons for the observed differences in the predicted oil rate behaviour of the various initialised reservoir models. This is because the coupled fluid models are the only variable in the various initialised reservoir model, otherwise, they should all indicate the same trends. The observed sharp drop in oil rates exhibited by the various initialised reservoir model after their initial constant rates suggest that due to poor permeability in some sections of the study reservoir, water injection is not the optimal pressure maintenance option for efficient development of the study reservoir.

The simulated gas production rates for the various initialised reservoir models are shown in Figure 4.34. This figure shows that while the nonisothermal CG initialised reservoir model indicate suggestively similar trends, isothermal CG and constant composition initialised reservoir models exhibited different gas rate behaviours. The high gas rates simulated by the nonisothermal CG initialised models is a reflection of the high GOIP estimated by the various noisothermal CG initialised reservoir models. Figure 4.34 also indicates that the constant composition initialised reservoir model, which estimated the least GOIP, also simulated the least initial gas rate (9.571693 $MMft^3$) and the highest ultimate gas rate of 12.008939 $MMft^3$. Note that the simulation end time (2011) does not represent the economic life of the study reservoir but a deliberate decision to minimise

simulation run time and the time taking to analyse simulation results in order to fast track the research work.

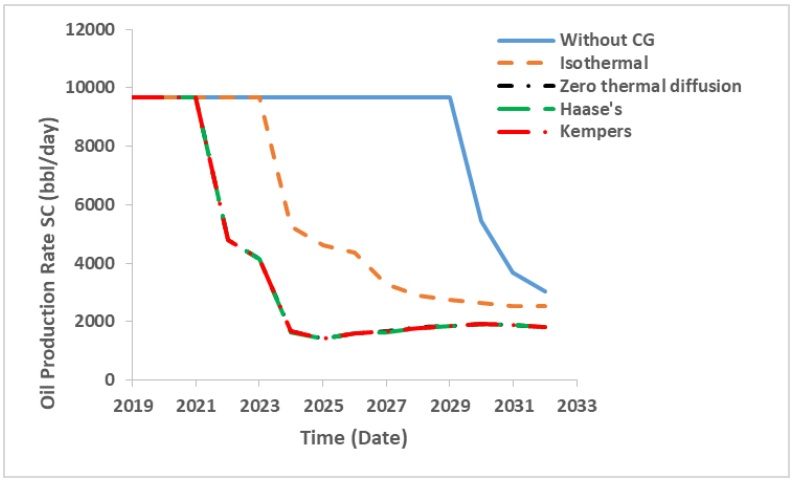

Figure 4.33: Oil Production Rates Predicted by the Various Initialised Reservoir Models under Water Injection

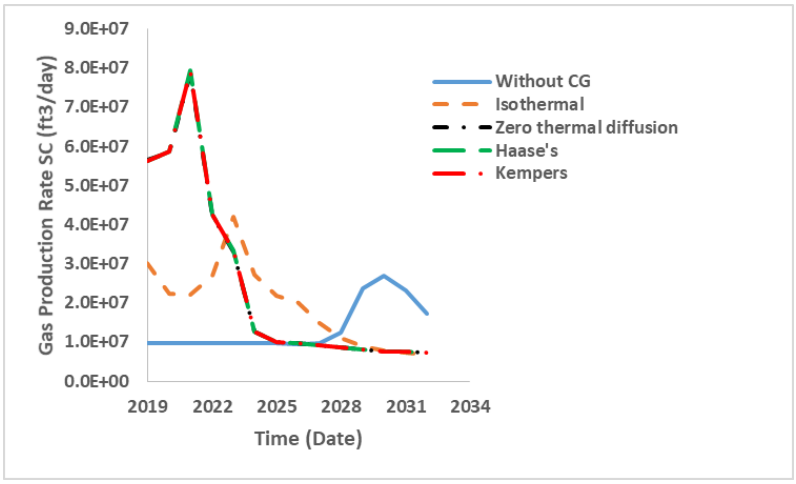

Figure 4.34: Gas Production Rates Predicted by the Various Initialised Reservoir Models under Water Injection

4.4.3 Recovery Factors

The predicted oil and gas recovery factors are illustrated in Figures 4.35 and 4.36, respectively. Figure 4.35 illustrates that the constant composition initialised reservoir model, which estimated high OOIP, also predicted highest oil recovery factor (RF). Isothermal CG initialised model simulated lower oil RF than the constant composition model but significantly higher ultimate RF than the nonisothermal models. There is no significant difference in the oil RF estimated by the various nonisothermal CG initialised models. The ultimate oil RF indicated by the various reservoir models are shown in Table 4.5. Figure 4.35 indicated obvious difference between the oil RF predicted by constant composition initialised reservoir model and isothermal CG initialised reservoir model.

Similarly, there is a clear difference between the oil RF predicted by isothermal CG initialised reservoir model and the nonisothermal CG initialised reservoir models. For example, the ultimate oil RF difference between isothermal CG initialised reservoir model and Haase's thermal diffusion CG initialised model is 0.04875. This value is noteworthy and therefore, suggest that neglecting CG or inadequate account of CG in reservoir model initialisation will have detrimental technical consequences on overall field development decisions and economics.

Figure 4.36 shows that the nonisothermal CG initialised reservoir models, which estimated high GOIP, also predicted the highest gas RF. However, there is no significant difference in the gas RF trends exhibited by the nonisothermal CG initialised reservoir models. Constant composition initialised reservoir model, which simulated the least GOIP, predict the least gas RF with an ultimate value of 0.1114 less than the ultimate RF indicated by isothermal model. The ultimate gas RF simulated by the various initialised reservoir models are tabulated in Table 4.5. Figure 4.36 also shows very clear difference between the gas RF predicted by the constant composition initialised reservoir model and nonisothermal CG initialised reservoir models. The ultimate gas RF difference between Constant composition initialised reservoir model and Haase's thermal diffusion CG initialised model, deduced from Table 4.5, is 0.1733. Again, this value is quite noteworthy and will have very remarkable technical and economic consequences on field development plan.

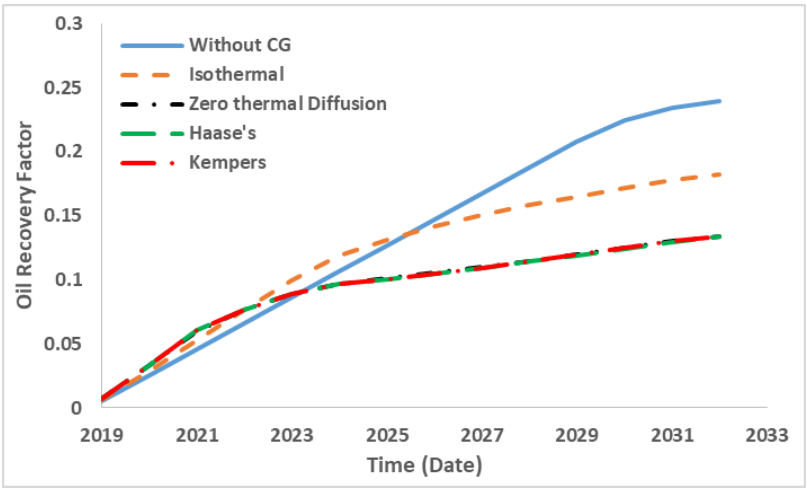

Figure 4.35: Oil Recovery Factor versus Time Predicted by Various Initialised Reservoir Models under Water Injection

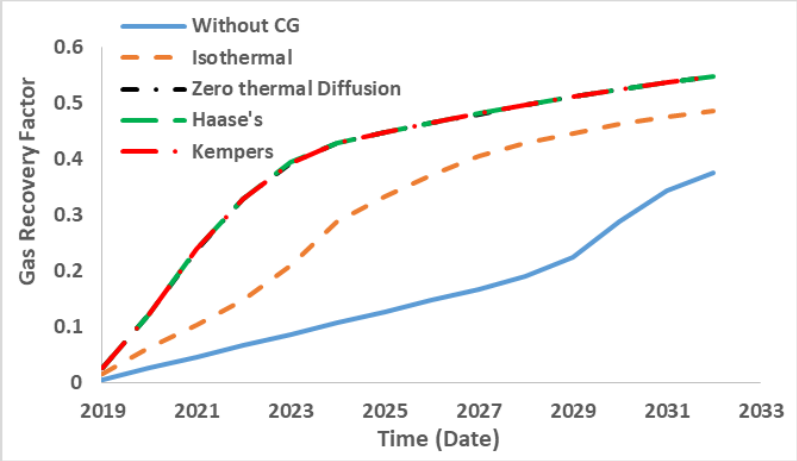

Figure 4.36: Gas Recovery Factor versus Time Predicted by Various Initialised Reservoir Models under Water Injection

Table 4.5: Ultimate Oil and Gas RF Predicted by the Various Initialised Reservoir Models under Water Injection

Models	Ultimate Oil and Gas Recovery Factor	
	Oil	Gas
Constant Composition	0.23929	0.37457
Isothermal	0.18243	0.48597
Zero Thermal Diffusion	0.13412	0.54758
Haase's	0.13368	0.54787
Kempers	0.13388	0.54772

4.4.4 Cumulative Oil and Gas

Predicted cumulative oil and gas produced by the various simulation models are presented in Figures 4.37 and 4.38, respectively. Figure 4.37 shows that the models that neglected the effect of gravity and thermal diffusion (constant composition initialised reservoir model) predicted the highest ultimate cumulative oil, followed by isothermal CG initialised reservoir model, which accounted for the effect of gravity only. The high ultimate cumulative oil predicted by constant composition and isothermal CG initialised reservoir models are due to the high OOIP and high oil RF predicted by the two models. Figure 4.37 also indicates that models that accounted for the combined effect of gravity and temperature gradient or thermal diffusion (nonisothermal CG initialised reservoir models) predicted the least ultimate cumulative oil. There are no weighty differences in the cumulative oil trends exhibited by nonisothermal models as shown in Figure 4.37. A summary of the ultimate cumulate oil simulated by the various initialised reservoir models is presented in Table 4.6.

Contrary to the trends observed in Figure 4.37, Figure 4.38 indicates that nonisothermal CG initialised reservoir models predicted high cumulative gas production relative to isothermal CG initialised reservoir model and constant composition initialised reservoir model. Therefore, for the study reservoir system, the combined effect of gravity and temperature gradient or thermal diffusion resulted in high gas production. Conversely, reservoir model initialised with the assumption of constant composition would result in low gas production. Figure 4.38 also illustrates that isothermal CG initialised reservoir model predicted higher cumulative gas than constant composition assumption but lower cumulative gas than nonisothermal model assumptions. The ultimate cumulative gas simulated by the various initialised reservoir models are summarised in Table 4.6.

Constant composition initialised reservoir model overestimate ultimate cumulative oil by 34.20 % more than the isothermal CG model, 57.61 % more than the zero thermal diffusion CG model, 50.60 % more than the Haase's thermal diffusion CG model, and 57.71 % more than the Kempers thermal diffusion CG model. It underestimated ultimate cumulative gas by 46.26 % less than the isothermal CG, 77.24 % less than the zero thermal diffusion CG model, 77.50 % less than the Haase's thermal diffusion model, and 77.38 % less than Kempers thermal diffusion CG initialised reservoir model. These differences are very noteworthy and should be a major technical concern and the major reason why CG should be adequately accounted for in the study reservoir model. The ultimate cumulative oil produced with isothermal CG initialised reservoir model is higher by 35.53 % than the zero thermal diffusion CG model, 35.86 % than the Haase's thermal diffusion CG model, and 35.74 % than the Kempers thermal diffusion CG initialised reservoir model. The ultimate cumulative gas produced with isothermal CG initialised reservoir model is lower by 21.18 % than the zero thermal diffusion CG model, 21.36 % than the Haase's thermal diffusion CG model, and 21.28 % than the value indicated by Kempers thermal diffusion CG initialised reservoir model. Therefore, isothermal assumption for initialisation of the study reservoir is grossly inadequate, since the results shows that thermal diffusion effect also contributed to the simulated CG.

The ultimate cumulative oil produced by zero thermal diffusion CG initialised reservoir model is greater by 0.42 % than the Haase's thermal diffusion CG model and 0.23 % than the volume indicated by Kempers thermal diffusion CG initialised reservoir model. The ultimate cumulative gas produced by zero thermal diffusion CG initialised model is lower than the volume indicated by Haase's and Kempers thermal diffusion CG models by

0.148 % and 0.082 %, respectively. Therefore, temperature gradient alone, without the corresponding thermal diffusion effect did not adequate describe compositional variation in the study reservoir. The ultimate cumulative oil simulated by Haase's model (which assumed centre of mass for the calculation of thermal diffusion factor) is less by 0.185 % than Kempers model (which assumed centre of volume for calculation of thermal diffusion factor) while the ultimate cumulative gas is greater by 0.067 % than value indicated by Kempers model. Hence, centre of mass assumption favours high gas production while centre of volume assumption supports high oil production.

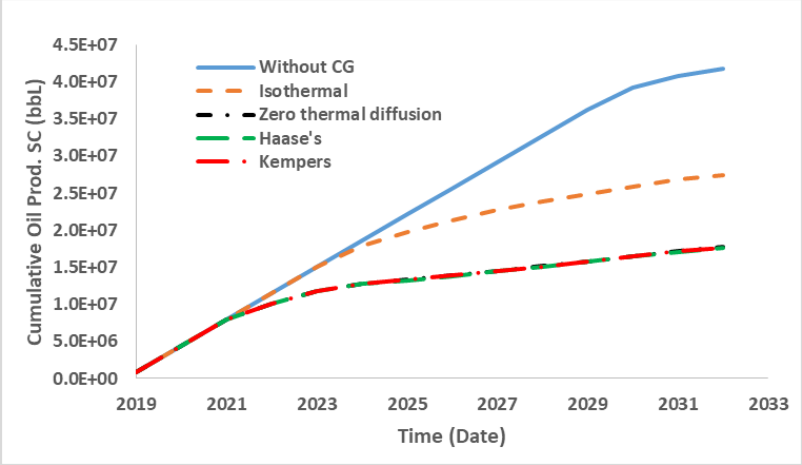

Figure 4.37: Cumulative Oil Produced versus Time Predicted by Various Initialised Reservoir Models under Water Injection

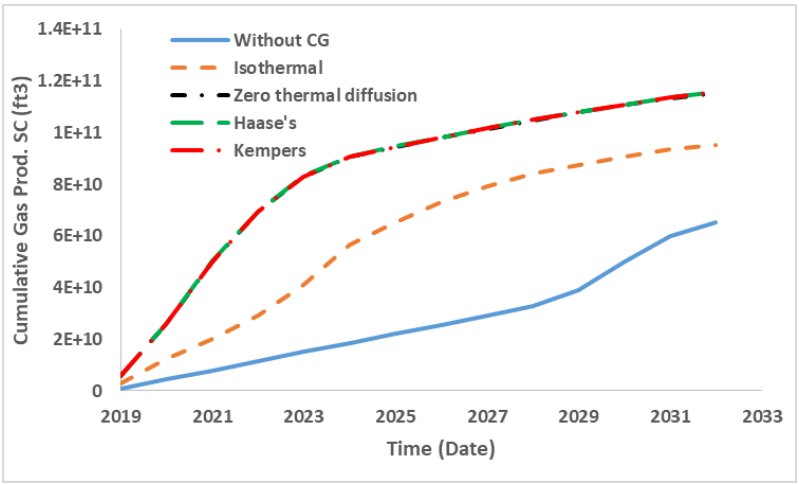

Figure 4.38: Cumulative Gas Produced versus Time Predicted by Various Initialised Reservoir Models under Water Injection

Table 4.6: Ultimate Cumulative Oil and Gas Produced by the Various Initialised Reservoir Models under Water Injection

Models	Ultimate Cumulative Oil and Gas	
	Oil SC (MMbbl)	Gas SC (Bft^3)
Constant Composition	41.740	65.142
Isothermal	27.469	95.275
Zero Thermal Diffusion	17.693	115.456
Haase's	17.619	115.627
Kempers	17.652	115.550

4.4.5 Gas-Oil Ratio

Trends of gas-oil ratio (GOR) predicted by various initialised reservoir models are presented in Figure 4.39. The constant composition initialised reservoir model predicted the lowest initial GOR and the highest ultimate producing GOR, followed by isothermal CG model, which however, indicated the lowest ultimate producing GOR. The nonisothermal models indicated the highest initial GOR but with ultimate GORs in between the values indicated by constant composition and isothermal models, respectively. The high GOR values exhibited by the nonisothermal models are clear reflection of their associated high cumulative gas production. There is no major difference in the predicted GOC behaviour exhibited by the nonisothermal models. Table 4.7 presents the values of the initial and ultimate GOR simulated by the different initialised reservoir models.

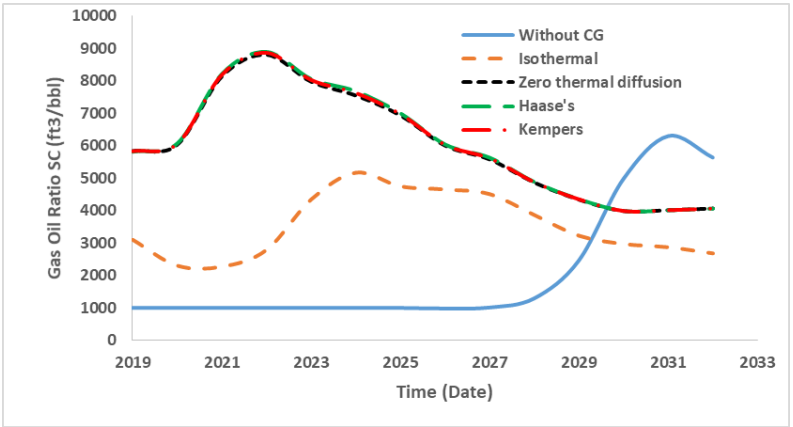

Figure 4.39: Gas Oil Ratio versus Time Predicted by Various Initialised Reservoir Models under Water Injection

Table 4.7: Initial and Ultimate GOR Predicted by the Different Initialised Reservoir Models under Water Injection

Models	GOR SC (ft^3/ bbl)	
	Initial	Ultimate
Constant Composition	997.044	5632.444
Isothermal	3103.399	2684.580
Zero Thermal Diffusion	5833.058	4061.564
Haase's	5808.893	4060.160
Kempers	5821.773	4061.277

4.4.6 Average Reservoir Pressure

The average reservoir pressure behaviour of the various initialised reservoir models, due to depletion and water injection, are illustrated in Figure 4.40. It shows that the pressure profile for the constant composition model increased steadily for about four years from start of production before declining throughout the simulation period. The pressure behaviour for the isothermal model indicated declining rate with production, despite the influence of water injection. The reservoir pressure behaviour of the nonisothermal CG initialised reservoir models indicated similar declining trends from start of production before increasing marginally from the year 2004 and throughout the remaining production period. The general behaviour of the pressure profiles indicated by the various initialised reservoir model can be attributed to the amount of in-place fluid estimated by each model. Models that estimated high oil in-place volumes exhibited improved pressure profiles than those that estimated high OGIP volumes. The decline in average reservoir pressure exhibited by all the models, despite water injection, also demonstrates the limitations of water injection as the pressure maintenance option for the study reservoir.

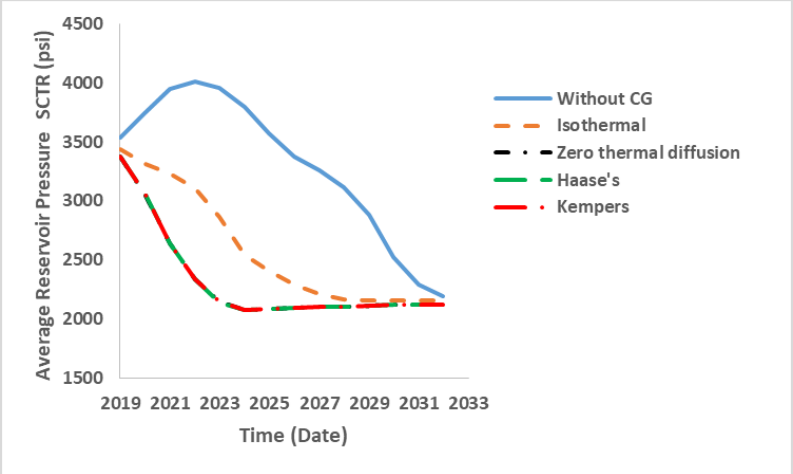

Figure 4.40: Average Reservoir Pressure Profile Predicted by Various Initialised Reservoir Models under Water Injection

4.4.7 Summary of Technical Implications of Simulation Results

The results (cumulative oil and gas produced) suggest that any technical decision made based on production forecast derived from models that ignored or inadequately accounted for compositional grading effect, will inevitably lead to detrimental technical consequences. For instance, field development decisions based on the performances of constant composition or isothermal initialised reservoir models, will lead to wasted investment in the design and procurement of oversized surface and subsurface oil production handling facilities and equipment. Both models suggestively overestimated oil production. Such development decision will also mean the design of undersized surface handling facilities for gas production since constant composition and isothermal CG initialised reservoir models underestimated cumulative gas production. This could lead to more adverse technical consequences such as loses in production or complete operational shutdown due to limited surface handling capacity for unexpected high volume of produced gas. It could also lead to environmental issues such as gas flaring which is still ongoing in some Nigerian oil and gas fields. The economic implications of these results will be presented subsequently.

4.5 Reservoir Simulation (Separator Gas Injection Scenario)

The effect of using separator gas as injection fluid rather than water was investigated in this section. Parameters in the initialised reservoir models remain unchanged. However, the injection fluid was changed from water to separator gas with a maximum BHP of 2700 psi and STG of 90841 ft^3/day as the first and second constraints, respectively. The purpose of comparing the various initialised reservoir model under gas injection scenario is to investigate the influence of gas injection on the performances of the models. It is therefore, possible to determine which pressure maintenance scenario (water or separator gas injection) is more suited for optimal development of the study reservoir. Technical performance indicators considered are the oil and gas production rates, oil and gas recovery factors, cumulative oil and gas produced, and gas-oil ratio.

4.5.1 Oil and Gas Production Rates

Figure 4.41 shows the oil production rates simulated by the different initialised reservoir models, which indicates that separator gas injection influenced the constant composition initialised reservoir model to simulate high and constant oil rate throughout the production period but for the marginal drop in the year 2003. The isothermal model and

the nonisothermal models exhibited initial constant rate of 9676 bbl/day before declining sharply. The isothermal model oil rate declined sharply to 6497.69 bbl/day in the year 2001 before increasing somewhat instantaneously to previous constant rate. Zero thermal diffusion and Kempers thermal diffusion CG initialised reservoir models indicated sharp oil rate decline in the year 2001 to a minimum constant rate of 6057 bbl/day for the period of about five years. Thereafter, the oil rate increased sharply to the initial constant rate of 9676 bbl/day. The oil rate predicted by Haase's thermal diffusion CG model exhibited sharp declining rate in the year 2001 to a minimum constant rate of 6057 bbl/day for about three years before increasing to the initial maximum rate of 9676 bbl/day. These results (Figure 4.41) suggests that the combined effects of gravity, temperature gradient, and thermal diffusion in the nonisothermal CG initialised reservoir models limited the effect of separator gas injection with respect to gas rate for significantly longer duration compared to trends indicated by constant composition and isothermal CG initialised reservoir models.

Separator gas injection has more pronounced effect on the performances of the nonisothermal CG initialised reservoir models than on constant composition and isothermal CG initialised models as illustrated in Figure 4.42. This figure shows that zero thermal diffusion model and Kempers thermal diffusion CG initialised models indicated peak gas rates of 83.086 $MMft^3/day$ 83.327 $MMft^3/day$, respectively, before declining to ultimate rates of 13.214 $MMft^3/day$ 13.208 $MMft^3/day$, respectively. Constant compositional initialised reservoir model simulated the lowest gas production rate.

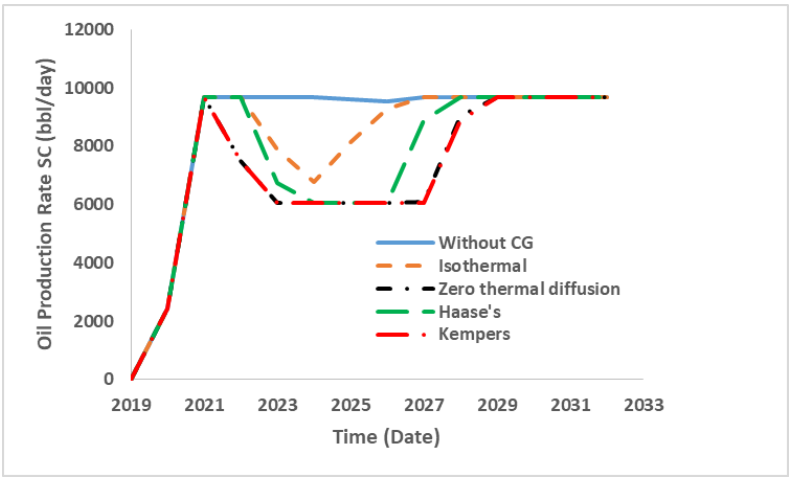

Figure 4.41: Oil Production Rates Predicted by the Various Initialisation Reservoir Models under Separator Gas Injection

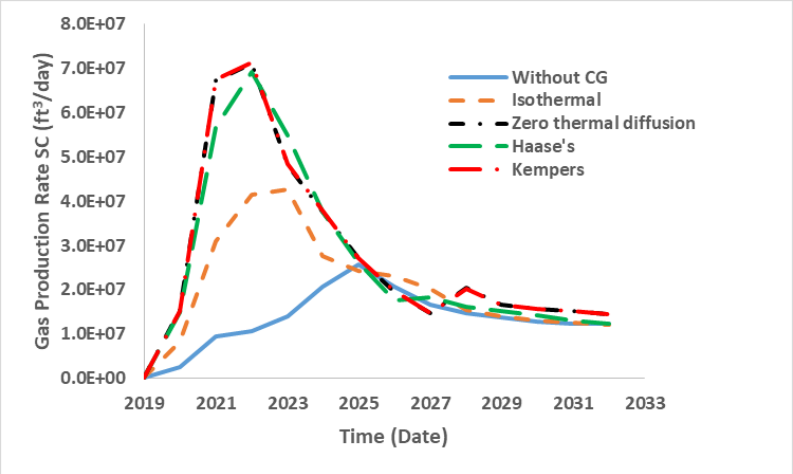

Figure 4.42: Gas Production Rates Predicted by the Various Initialisation Reservoir Models under Separator Gas Injection

4.5.2 Recovery Factors

Figures 4.43 and 4.44 compare the oil and gas RFs, respectively, simulated by the various initialised reservoir models based on separator gas injection. Figure 4.43 shows that contrary to the trend simulated by water injection scenario (Figure 4.35), separator-gas injection influenced the nonisothermal CG initialised reservoir models to simulate higher oil RFs. Haase's thermal diffusion CG initialised model simulated the highest ultimate oil RF, followed by zero thermal diffusion and Kempers thermal diffusion CG initialised reservoir models. Isothermal CG initialised reservoir model also predicted higher oil RF than the constant composition initialised model. The values of the ultimate oil RFs for the various models under separator-gas injection scenario are summarised in Table 4.8.

Similar to water injection case, Figure 4.44 indicates that under separator-gas injection, nonisothermal CG initialised models simulated high gas RFs. Kempers thermal diffusion CG initialised reservoir model indicated the highest ultimate RF, followed by Zero thermal diffusion and Haase's thermal diffusion CG initialised reservoir models. Isothermal CG initialised reservoir model also predicted higher ultimate gas RF than the constant composition initialised reservoir model. Table 4.8 presents the values of the ultimate gas RFs simulated by the respective initialised reservoir models. These results strongly suggest the superiority of gas injection to water injection.

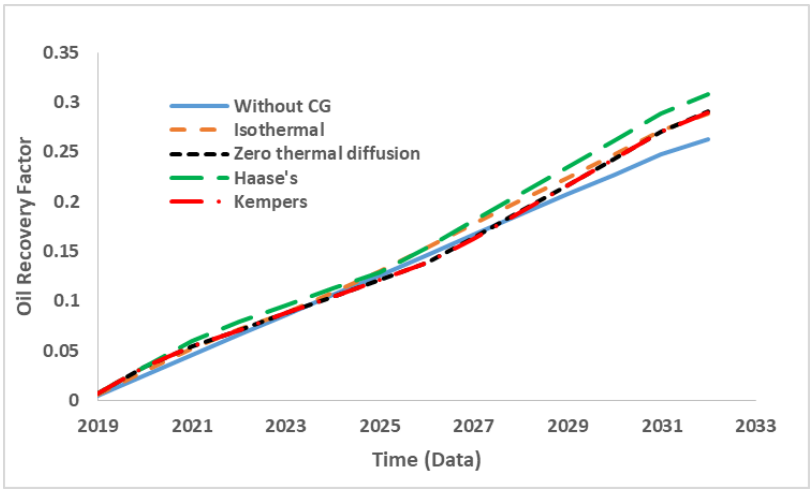

Figure 4.43: Oil Recovery Factors versus Time Predicted by Various Initialised Reservoir Models under Separator Gas Injection

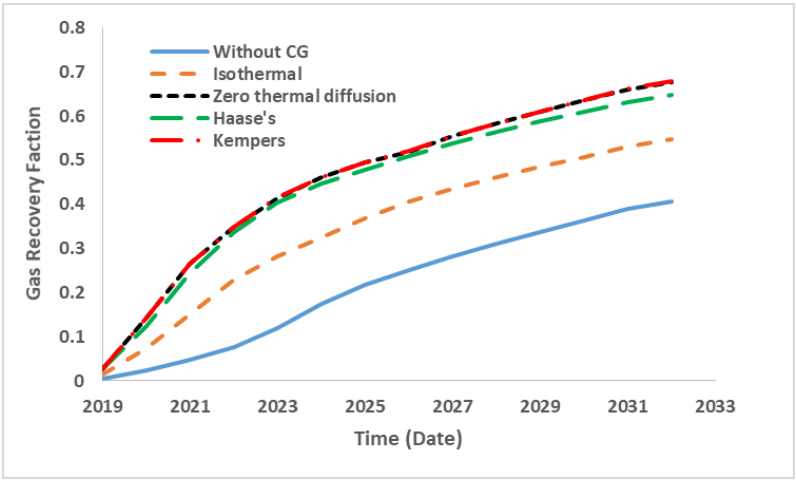

Figure 4.44: Gas Recovery Factors versus Time Predicted by Various Initialised Reservoir Models under Separator Gas Injection

Table 4.8: Ultimate Oil and Gas RF Predicted by the Various Initialised Reservoir Models under Separator Gas Injection

Models	Ultimate Oil and Gas Recovery Factor	
	Oil RF	Gas RF
Constant Composition	0.26293	0.40764
Isothermal	0.28894	0.54684
Zero Thermal Diffusion	0.29040	0.67763
Haase's	0.30818	0.64716
Kempers	0.29015	0.67860

4.5.3 Cumulative Oil and Gas

The cumulative oil and gas predicted by the various models under separator-gas injection scenario are presented in Figures 4.45 and 4.46, respectively. Figure 4.45 indicates marginal differences in ultimate cumulative oil simulated by constant composition, isothermal CG, and Haase's thermal diffusion CG initialised reservoir models, contrary

to the noteworthy difference predicted under water injection scenario (Figure 4.37). There is no major difference in the ultimate cumulative oil predicted by Zero thermal diffusion CG initialised reservoir model and Kempers thermal diffusion CG initialised reservoir model. The values of ultimate cumulative oil predicted by the different reservoir models under separator gas injection are presented in Table 4.9, which indicates that reservoir model that estimated the highest OOIP by ignoring CG effects (constant composition model) also simulated the highest ultimate cumulative oil.

Figure 4.46 shows that contrary to illustrated trends under water injection case, only zero thermal diffusion and Kempers thermal diffusion CG initialised models predicted similar cumulative gas trends. The trend indicated by Haase's thermal diffusion CG initialised model is considerably different from the other nonisothermal models. Similar to the trend indicated under water injection, isothermal CG initialised reservoir model under separator-gas injection, simulated higher cumulative gas than constant composition model. The values of the ultimate cumulative gas predicted by respective initialised reservoir models are recorded in Table 4.9. Figure 4.46 and Table 4.9 shows that the nonisothermal CG initialised reservoir models under separator gas injection, simulated high cumulative gas production. Again, this suggest that nonisothermal CG initialised reservoir models are more suited and sensitive to gas injection than to water injection.

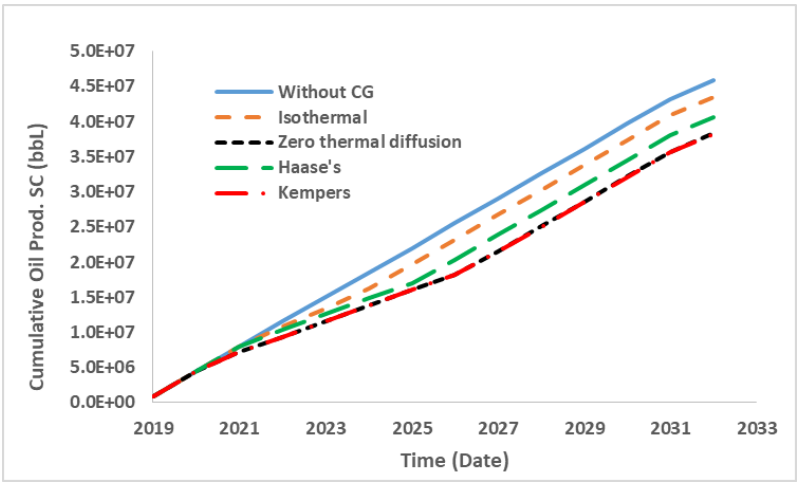

Figure 4.45: Cumulative Oil Produced versus Time Predicted by Various Initialised Reservoir Models under Separator Gas Injection

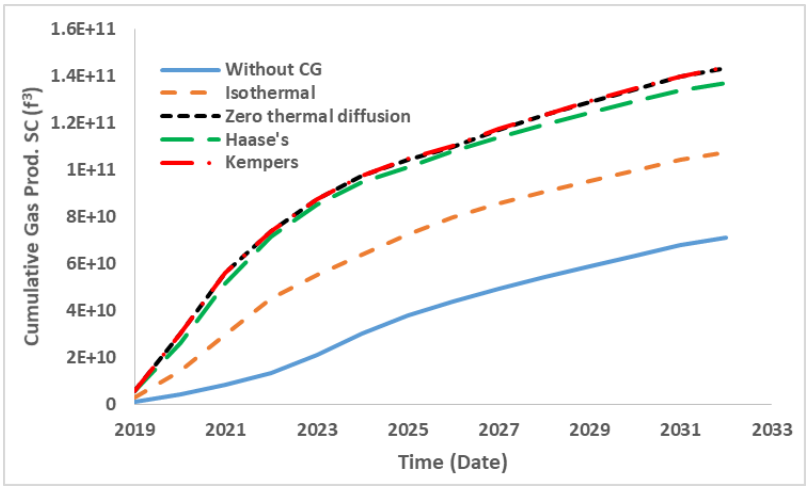

Figure 4.46: Cumulative Gas Produced versus Time Predicted by Various Initialised Reservoir Models under Separator Gas Injection

Table 4.9: Ultimate Cumulative Oil and Gas Produced by the Various Initialised Reservoir Models under Separator Gas Injection

Models	Ultimate Cumulative Oil and Gas	
	Oil SC (MMbbl)	Gas SC (Bft^3)
Constant Composition	45.862	71.271
Isothermal	43.505	107.729
Zero Thermal Diffusion	38.311	143.522
Haase's	40.619	137.225
Kempers	38.256	143.808

4.5.4 Gas-Oil Ratio

Predicted GOR behaviour of the various reservoir models under separator gas injection shown in Figure 4.47 are somewhat different from the observed trends under water injection scenario. Under separator gas injection, constant composition initialised reservoir model predicted the lowest initial GOR. Contrary to water injection case, zero thermal diffusion CG initialised reservoir model also simulated the highest initial and ultimate GOR. The GOR trends exhibited by Haase's thermal diffusion CG initialised reservoir model is rather different from the trends indicated by other nonisothermal initialised model, contrary to the trend indicated under water injection case. Zero thermal diffusion and Kempers thermal diffusion CG initialised reservoir models simulated similar GOR trends but with different initial and ultimate values, respectively. Isothermal CG initialised reservoir model predicted the lowest ultimate GOR. The values of the initial and ultimate GOR simulated by the various initialised models are presented in Table 4.10, which shows that reservoir models that accounted for the combine effects of gravity and thermal diffusion (zero thermal diffusion, Haase's and Kempers models)

generated high initial and ultimate GOR due to their superior production performances under gas injection.

Figure 4.47 shows that the GOR simulated by the various reservoir models exhibited initial increasing trends before declining to their respective ultimate values. The period of increasing GOR was as a result of high gas production with no corresponding increase in oil production. The various GORs started declining when the respective models, due to gas injection, began producing more oil as shown in Figure 4.41 with declining gas rates (Figure 4.42).

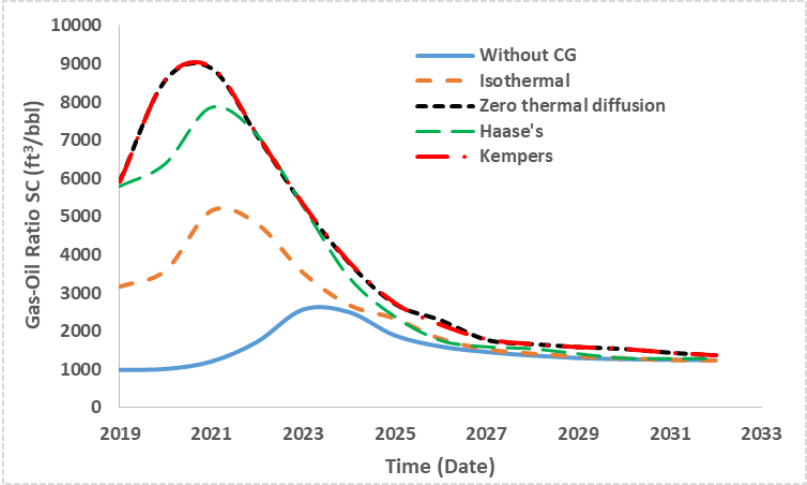

Figure 4.47: Predicted Variation of Gas-Oil Ratio with Time by Various Models under Separator Gas Injection

Table 4.10: Initial and Ultimate GOR Predicted by the Different Initialised Reservoir Models under Separator Gas Injection

Models	GOR SC (ft^3/ bbl)	
	Initial	Ultimate
Constant Composition	989.454	1240.961
Isothermal	3158.570	1215.853
Zero Thermal Diffusion	5938.979	1365.627
Haase's	5782.217	1279.391
Kempers	5915.184	1365.044

4.5.5 Average Reservoir Pressure Profile

Contrary to the average reservoir pressure profile exhibited by the various initialised reservoir models under water injection scenario (Figure 4.40), Figure 4.48 illustrates that after the indicated initial drop in pressure, separator gas injection effectively increased the average reservoir pressure for all the models. This is an indication of the effectiveness of separator gas injection as the optimal pressure maintenance option for the study

reservoir. The observed pressure drop could be attributed to the time lag before the pressure perturbation reach various locations of the four producers.

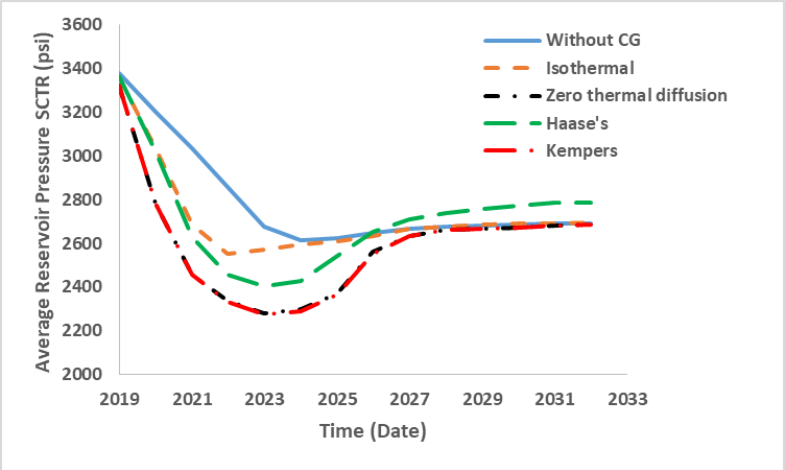

Figure 4.48: Average Reservoir Pressure Profile Predicted by Various Initialised Reservoir Models under Water Injection

4.6 Water Injection versus Separator Gas Injection

The performances of the various initialised reservoir models under water injection and gas injection are presented in Figures 4.49 and 4.50. Figure 4.49 compares the cumulative oil produced by the respective initialised models under water and separator gas injection scenarios while Figure 4.50 compares the cumulative gas produced by the various models under water and separator gas injection. The calculated absolute difference (AD) in the ultimate cumulative oil produced by the various models under water injection and gas injection are summarised in Table 4.11. Table 4.12 presents the AD in the ultimate cumulative gas produced by the respective models under water and gas injection scenarios. Figure 4.49 indicates no major difference between the influence of water injection and gas injection on the performance of constant composition initialised reservoir model, but for the higher ultimate cumulative oil indicated by gas injection scenario. Figure 4.49 and Table 4.11 suggest that separator-gas injection has noteworthy influence on CG initialised reservoir models, resulting in higher ultimate oil production. Haase's thermal diffusion CG initialised reservoir model, with AD of 23.000 MMbbl is the most influenced by gas injection, while constant composition initialised model with AD of 4.122 MMbbl is the least influenced by gas injection. The trends exhibited by the various models in Figure 4.50 indicates that separator-gas injection resulted in better field performance with respect to cumulative gas production, than water injection scenario. Table 4.12 suggest that CG initialised reservoir models were highly sensitive to gas injection and performed better than constant composition model under gas injection

scenario. Kempers thermal diffusion CG initialised reservoir model produced the best ultimate cumulative gas performance under gas injection.

Technically, these results did suggest that separator-gas injection is the optimal pressure maintenance option for efficient development of the study reservoir.

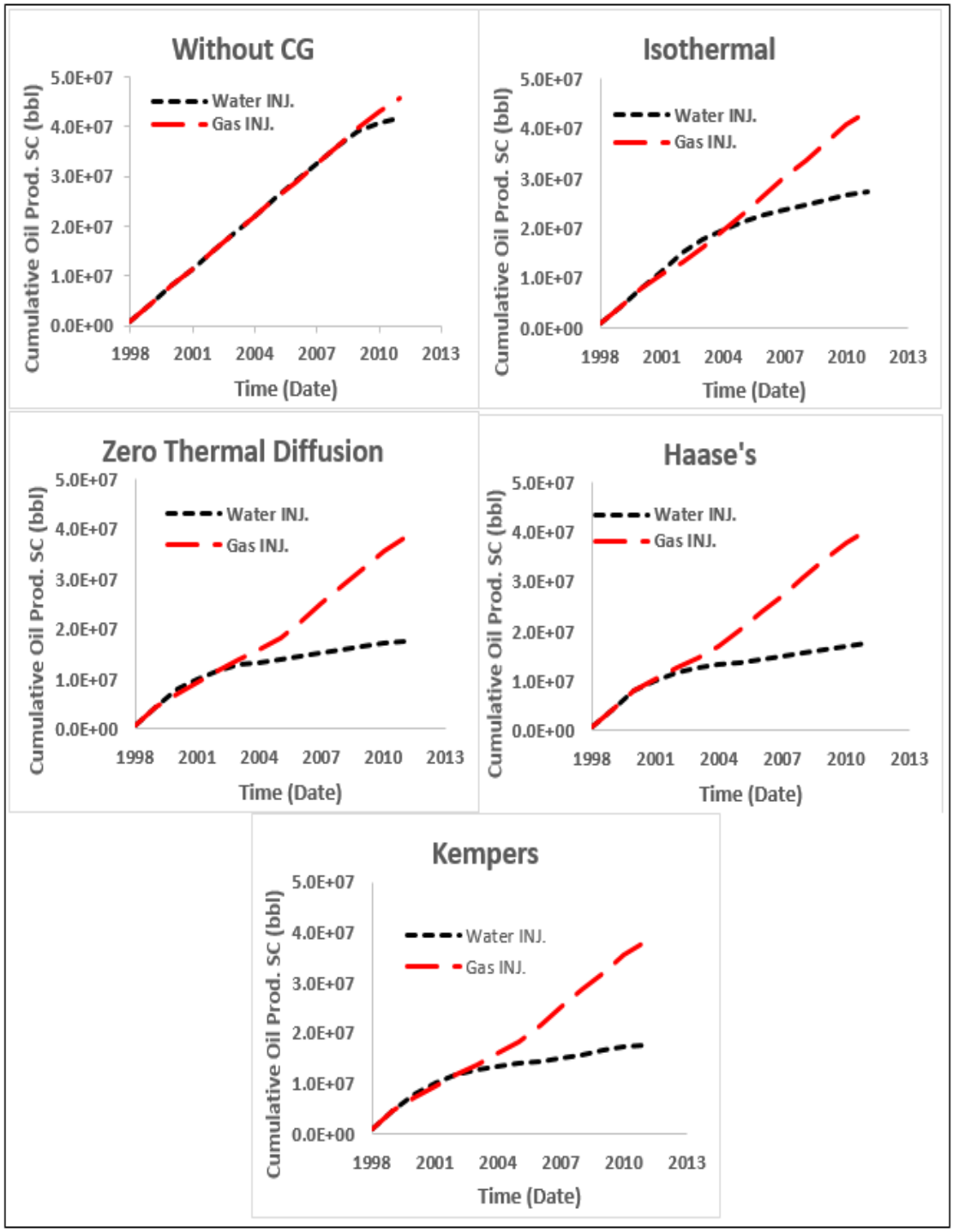

Figure 4.49: Comparison of the Influence of Water and Gas Injections on Cumulative Oil Produced by the Various Initialised Reservoir Models

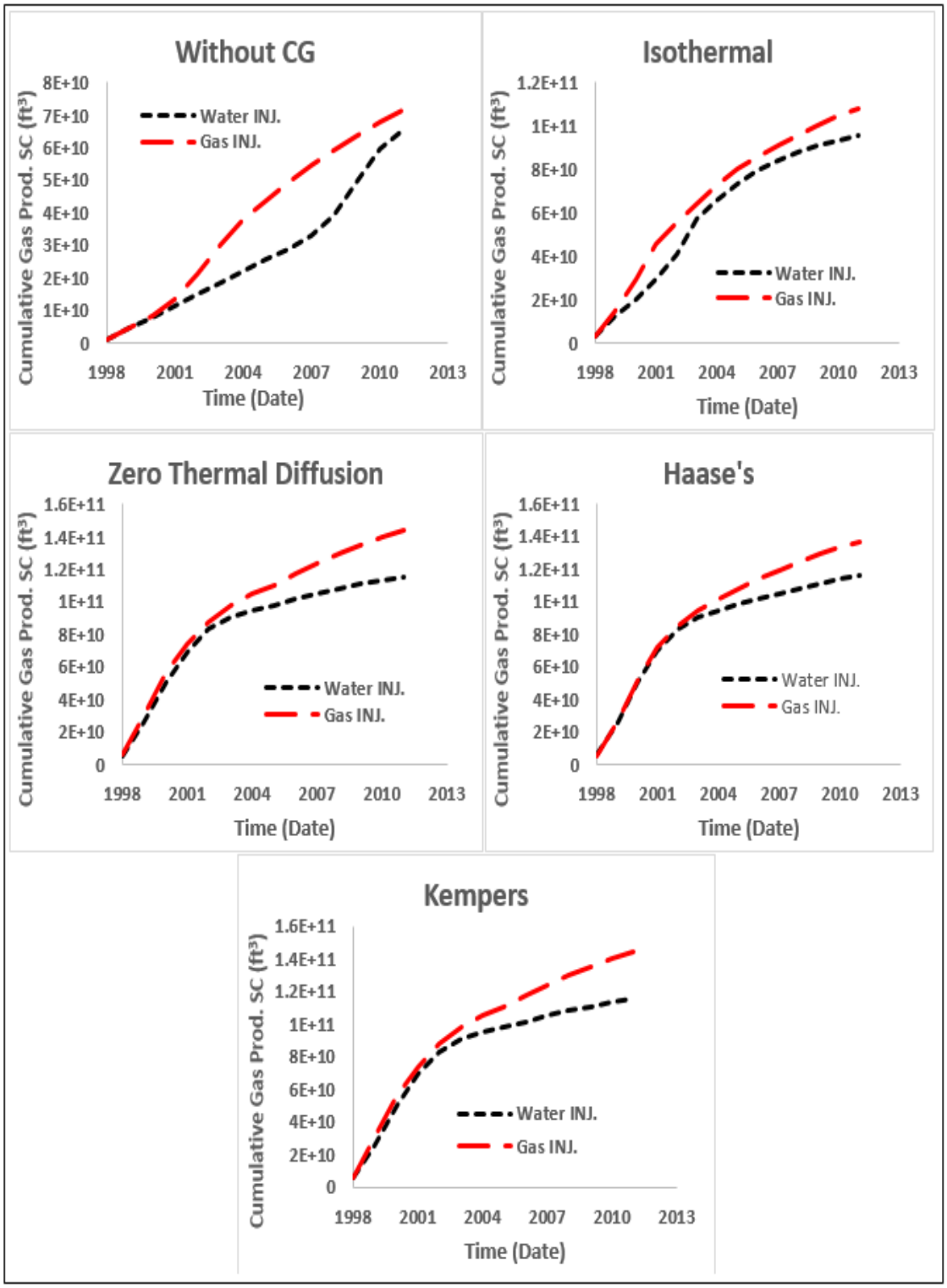

Figure 4.50: Comparison of the Influence of Water and Gas Injections on Cumulative Gas Produced by the Various Initialised Reservoir Models

Table 4.11: Absolute Deviation of Cumulative Oil Produced by Various Initialised Reservoir Models under Water and Separator Gas Injections

Models	Ultimate Cumulative Oil SC (MMbbl)		Absolute Difference (MMbbl)
	Water Inj.	Gas Inj.	
Constant Composition	41.74	45.862	4.122
Isothermal	27.469	43.505	16.036
Zero Thermal Diffusion	17.693	38.311	20.618
Haase's	17.619	40.619	23.000
Kempers	17.652	38.256	20.604

Table 4.12: Absolute Deviation of Cumulative Gas Produced by Various Initialised Reservoir Models under Water and Separator Gas Injections

Models	Ultimate Cumulative Gas SC (Bft^3)		Absolute Difference (Bft^3)
	Water Inj.	Gas Inj.	
Constant Composition	65.142	71.271	6.129
Isothermal	95.275	107.729	12.454
Zero Thermal Diffusion	115.456	143.522	28.066
Haase's	115.627	137.225	21.598
Kempers	115.550	143.808	28.258

4.7 Uncertainty Assessment

In the absence of historical production data for history matching, the range of uncertainties associated with estimated in-place volumes were quantified using Monte Carlo simulation (MCS) to predict the low case estimate (P10), best-case estimate (P50), and high case estimate (P90). The range of uncertainties indicated by the various initialised reservoir models (constant composition, isothermal CG, zero thermal diffusion CG, Haase's thermal diffusion CG, and Kempers thermal diffusion CG) are presented in this section. Obtained MCS results indicated the probability of non-exceedance curves for both OOIP and OGIP estimates for the different initialised reservoir models. The probability distribution curves are illustrated in Figures D1-D10, in Appendix D while the respective range of uncertainties are summarised in Tables 4.13 and 4.14 for OOIP and OGIP, respectively. These figures and Tables shows that the uncertainties associated with the OOIP and OGIP estimates for the different initialised reservoir models were successfully quantified.

Table 4.13: Range of Uncertainties Associated with the Estimated OOIP for the Various Initialised Reservoir Models

Models	Probabilistic OOIP SC (MMbbl)		
	P10	P50	P90
Constant Composition	160.690	174.472	188.394
Isothermal	130.525	150.396	162.642
Zero Thermal Diffusion	121.017	131.721	142.707
Haase's	121.067	131.792	141.56
Kempers	121.081	131.712	142.796

Table 4.14: Range of Uncertainties Associated with the Estimated OGIP for the Various Initialised Reservoir Models

Models	Probabilistic OGIP SC (Bft^3)		
	P10	P50	P90
Constant Composition	160.215	173.956	187.837
Isothermal	180.819	195.916	211.386
Zero Thermal Diffusion	194.367	210.712	227.247
Haase's	194.887	211.036	227.532
Kempers	194.629	210.906	227.501

The results of the UA also demonstrates that the regression model of the various initialised reservoir models are statistically significant. The 95 % confidence curves for both OOIP and OGIP, as illustrated in Figures E1-E10 in Appendix F for the various models, crossed their respective mean of response. Figures E1-E10 shows that the proxy model predicted OOIP and OGIP for the different initialised reservoir models perfectly matched their initialised reservoir model simulated responses. The indicated training and verification experiments, which fall exactly on the 45 degree line, strongly confirmed that the created proxy models are valid proxies of the actual reservoir simulation responses. The experimental design qualities for the proxy models associated with the various reservoir models are within the orthogonal range (0-0.2) as shown in Table 4.15. Table 4.15 also shows that, for the nonisothermal models, Kempers thermal diffusion CG initialised reservoir model indicated the lowest and most orthogonal design quality while zero-thermal diffusion CG initialised reservoir model generated the highest and less orthogonal design quality. However, for the all the models tested, isothermal CG initialised reservoir model (without the thermal diffusion) indicated the most orthogonal design quality.

Table 4.15: Experimental Design Quality for the UA of the Various Initialised Reservoir Models

Models	Orthogonality Value
Constant Composition	0.1336
Isothermal	0.1063
Zero Thermal Diffusion	0.1458
Haase's	0.1439
Kempers	0.1392

4.8 Summary of Reservoir Model Validation

The various initialised reservoir models were validated based on the following procedures:

i. The deterministic reserve estimates are compared to the probabilistic estimates as shown in Tables 4.16 and 4.17 for OOIP and OGIP, respectively. Both Tables suggest no dramatic difference in the estimated in-place volumes, especially with respect to the base case estimates (P50). Hence, reservoir model assumptions and results are valid.

Table 4.16: Comparison of Probabilistic and Deterministic OOIP Estimates

Models	Probabilistic OOIP SC (MMbbl)			Deterministic SC OOIP (MMbbl)
	P10	P50	P90	
Constant Composition	160.215	174.472	188.394	174.428
Isothermal	180.819	150.396	162.642	150.569
Zero Thermal Diffusion	194.367	131.721	142.707	131.923
Haase's	194.887	131.792	141.56	131.802
Kempers	194.629	131.712	142.796	131.849

Table 4.17: Comparison of Probabilistic and Deterministic OGIP Estimates

Models	Probabilistic OGIP SC (Bft^3)			Deterministic OGIP SC (Bft^3)
	P10	P50	P90	
Constant Composition	160.215	173.956	187.837	173.913
Isothermal	180.819	195.916	211.386	196.050
Zero Thermal Diffusion	194.367	210.712	227.247	210.848
Haase's	194.887	211.036	227.532	211.047
Kempers	194.629	210.906	227.501	210.967

ii. The range of uncertainty associated with the estimated in-place volumes for the various initialised reservoir models were successfully quantified (see section 4.7, Tables 4.13 and 4.14).

iii. Response surface model verification plots for OOIP and OGIP associated with the various initialised reservoir models (presented in Appendix E – Tables E1-E10) suggest that the regression models of the various initialised reservoir models are statistically significant at 0.05 probability. The 95 % confidence curves for both OOIP and OGIP crossed the mean of response in all cases. The model quality-check plots also indicates that the proxy model predictions perfectly matched the various initialised reservoir model results. The indicated training and verification experiments are exactly on the 45-degree line, which is an overwhelming indication that the created proxy models are valid proxies of the actual reservoir simulation responses. The summary of fit statistics for the various initialised reservoir models are presented in Tables 4.18 and 4.19 for OOIP and OGIP, respectively. The indicated R^2 values shows that the proxy models perfectly fits actual reservoir model results.

Table 4.18: Summary of Fit Statistics for OOIP

Model	R-Square	R-Square Adjusted	R-Square Predicted	Mean of Response	Standard Error
Constant Composition	1.0000	1.0000	1.0000	1.74650E+08	5984.56
Isothermal	1.0000	1.0000	1.0000	1.50923E+08	171.375
Zero Thermal Diffusion	1.0000	1.0000	1.0000	1.32460E+08	158.082
Haase's	1.0000	1.0000	1.0000	1.31589E+08	167.391
Kempers	1.0000	1.0000	1.0000	1.32368E+08	157.207

Table 4.19: Summary of Fit Statistics for OGIP

Models	R-Square	R-Square Adjusted	R-Square Predicted	Mean of Response	Standard Error
Constant Composition	1.0000	1.0000	1.0000	1.74134E+11	5.964E+06
Isothermal	1.0000	1.0000	1.0000	1.96511E+11	1.235E+07
Zero Thermal Diffusion	1.0000	1.0000	1.0000	2.11714E+11	1.088E+07
Haase's	1.0000	1.0000	1.0000	2.10706E+11	1.154E+07
Kempers	1.0000	1.0000	1.0000	2.11691E+11	1.087E+07

iv. The experimental design quality for proxy models of the initialised reservoir models are within the orthogonal range (0-0.2). Hence, model assumptions and results are valid.

4.9 Sensitivity Analysis

Sensitivity of initialised reservoir models to changes in input variables have been simulated and the results presented in the form of Tornado diagrams and percentage effect plots. The results shows that for all the initialised reservoir models (constant composition, isothermal CG, zero thermal diffusion CG, Haase's thermal diffusion CG, and Kempers thermal diffusion CG), water saturation (s_w), which indirectly accounts for hydrocarbon saturation ($1-s_w$ = hydrocarbon saturation) is the most sensitive input parameter responsible for the estimated reserve volumes. For example, the Tornado diagrams for the constant composition initialised reservoir model for OOIP and OGIP shown in Figures 4.51 and 4.52, respectively, indicates that water saturation (s_w) and porosity (poro) are the input parameters in the initialised reservoir model that are mostly responsible for the estimated OOIP and OGIP. The Tornado diagrams for the other initialised reservoir models exhibited similar trends as shown in Figure F1-F8 in Appendix F. The observed differences in the values of OOIP and OGIP estimated by the various CG models are due to the influence of the CG models on the reservoir fluid formation volume factor, which made the hydrocarbon saturation (compositions of various components) to either increase or reduce in the gas and oil phases, respectively.

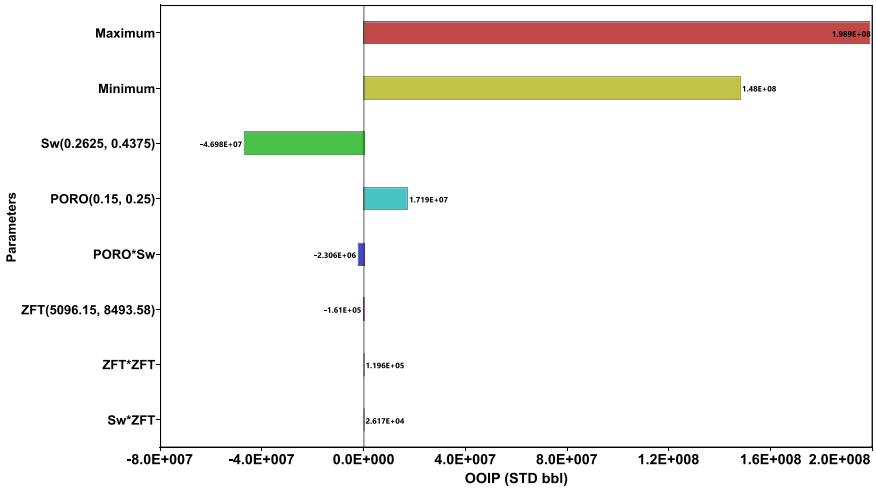

Figure 4.51: Tornado Diagram Showing the Effect of Input Parameters on the OOIP Estimated by Constant Composition Initialised Reservoir Model

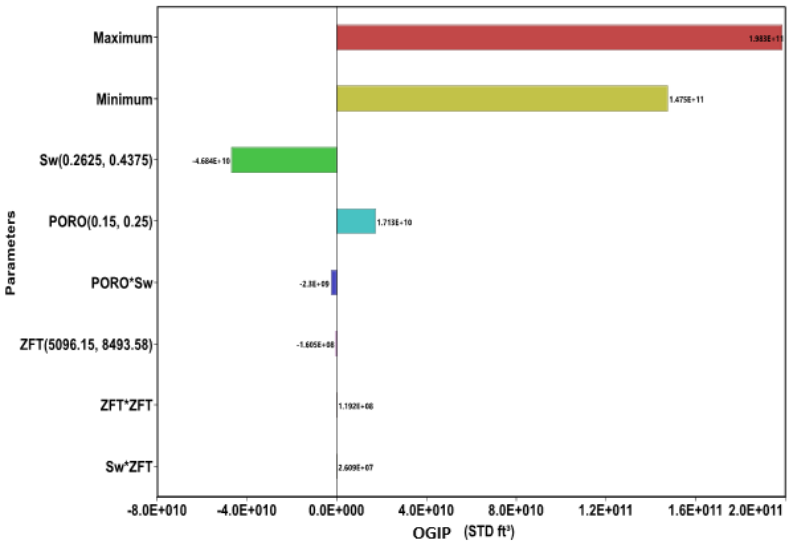

Figure 4.52: Tornado Diagram Showing the Effect of Input Parameters on the OGIP Estimated by Constant Composition Initialised Reservoir Model

Similarly, percentage effect plots for the constant composition initialised reservoir model shown in Figures 4.53 and 4.54 for OOIP and OGIP, respectively, indicates that water saturation had 88 % main effect on estimated OOIP and OGIP while porosity had 12 % main effect on OOIP and OGIP, respectively. Other initialised reservoir models indicated similar trends as illustrated in Figures G1-G8 in Appendix G and summarised in Tables 4.20 and 4.21 for OOIP and OGIP, respectively. Hence, water saturation, which gives an indication of hydrocarbon saturation in the reservoir, is the input parameter that is mostly responsible for the estimated values of OOIP and OGIP. Note that hydrocarbon saturation (OOIP and OGIP) in the study reservoir is a function of compositional variation with depth in the reservoir, which is dependent on the applied fluid model or CG model. Reservoir model initialised with CG model that neglected the effect of temperature gradient and thermal diffusion (isothermal CG model) estimated higher OOIP and lower OGIP than those initialised with nonisothermal CG models.

Table 4.20: Percentage Main Effect of Input Parameters on the OOIP Estimated by Various Initialised Reservoir Models

Models	**Input Parameters**	
	S_w	**Porosity**
Constant Composition	88 %	12 %
Isothermal	85 %	15 %
Zero Thermal Diffusion	82 %	18 %
Haase's	82 %	18 %
Kempers	82 %	18 %

Table 4.21: Percentage Main Effect of Input Parameters on the OGIP Estimated by Various Initialised Reservoir Models

Models	Input Parameter	
	S_w	Porosity
Constant Composition	90 %	10 %
Isothermal	91 %	8.9 %
Zero Thermal Diffusion	91 %	8.9 %
Haase's	91 %	8.9 %
Kempers	91 %	8.9 %

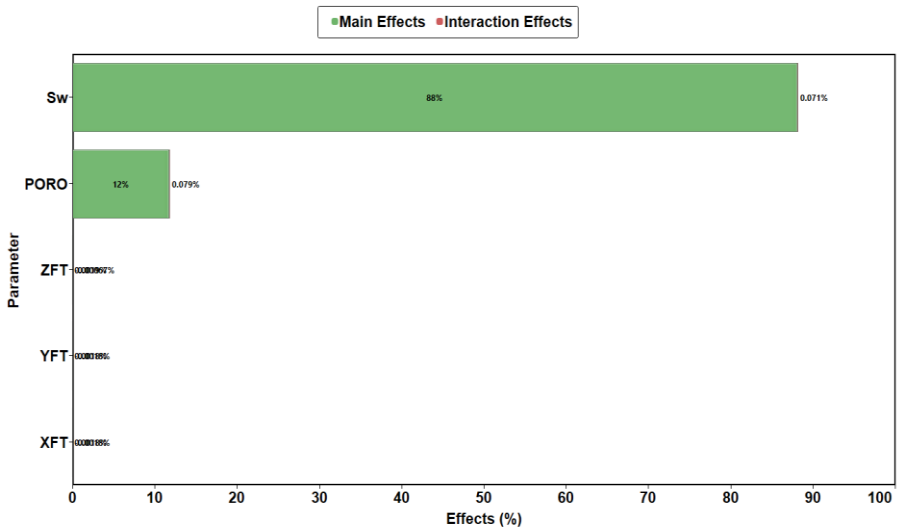

Figure 4.53: Percentage Effect of Input Parameters on the OOIP Estimated by Constant Composition Initialised Reservoir Model

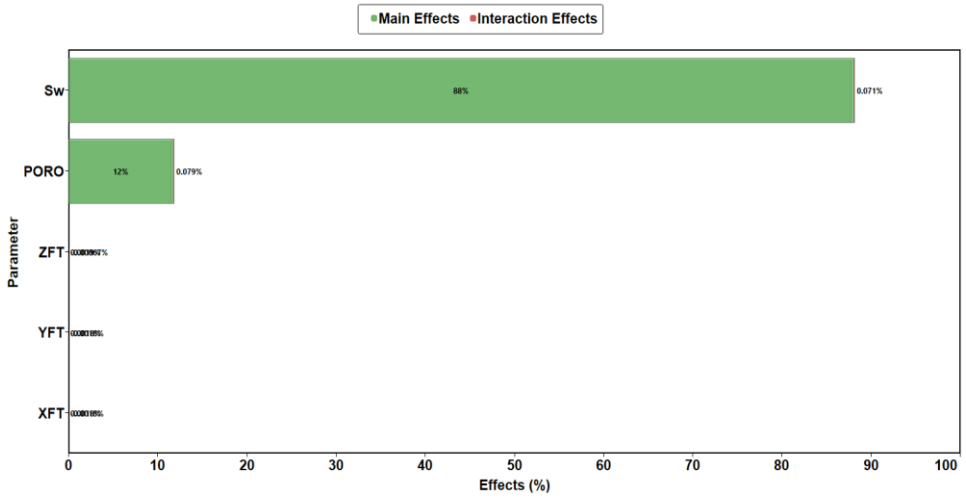

Figure 4.54: Percentage Effect of Input Parameters on the OGIP Estimated by Constant Composition Initialised Reservoir Model

In Figures 4.51-4.54, s_w is the water saturation, poro is the reservoir porosity, ZFT is the corner point depths for corner point grids, XFT is the offset of the simulation grid origin in the x-direction, and YFT is the offset of the simulation grid origin in the y-direction.

4.10 Effect of EOSs on the Performances of Initialised Reservoir Models

Performance indicators such as reserve estimates (OOIP and OGIP), oil recovery factor, and gas recovery factor are used to illustrate the effects of various EOSs on the performance of constant composition, isothermal CG, Zero thermal diffusion CG, Haase's thermal diffusion CG, and Kempers thermal diffusion CG initialised reservoir model, respectively.

4.10.1 Effect of EOSs on Reserve Estimates

Figures 4.55 and 4.56 shows that the various EOSs have different degree of effect on the different initialised reservoir models. For constant composition and zero thermal diffusion initialised reservoir models, the EOSs indicated marginal differences in the estimated OOIP as shown in Figure 4.55. However, Figure 4.55 shows that there are noteworthy differences in the OOIP indicated by the various EOSs for isothermal, Haase's and Kempers initialised reservoir models, respectively, with SRK EOS simulating the highest OOIP when coupled with Haase's model. The date for Figure 4.55 is presented in Table H1 in Appendix H.

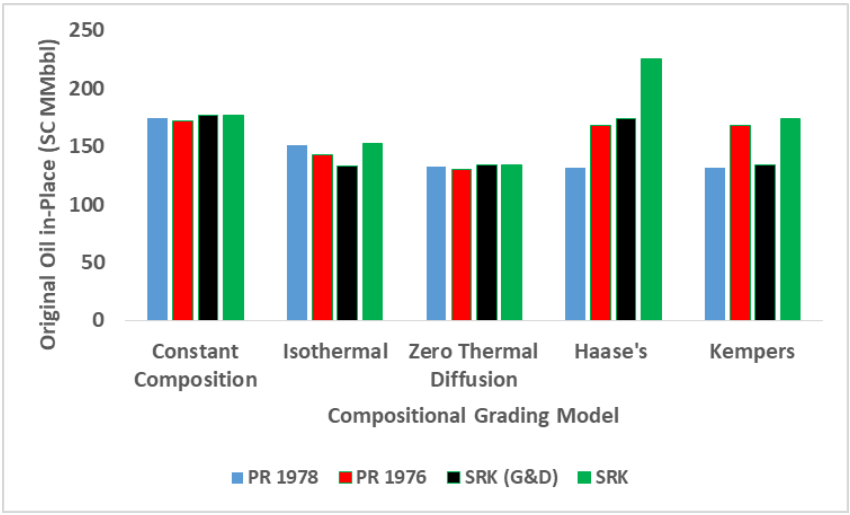

Figure 4.55: Effect of EOSs on OOIP Simulated by Various Initialised Reservoir Models

Figure 4.56 shows that for each initialised reservoir model, the various EOSs simulated different values of OGIP. PR 1978 simulated the highest OGIP for all the initialised reservoir models while SRK (G&D) simulated the lowest. The data for Figure 4.56 is presented in Table H2 in Appendix H. The noteworthy differences in the estimated OOIP and OGIP, which are due to the influence of the various EOSs suggest that applied EOSs has significant effects on the performances of the initialised reservoir models.

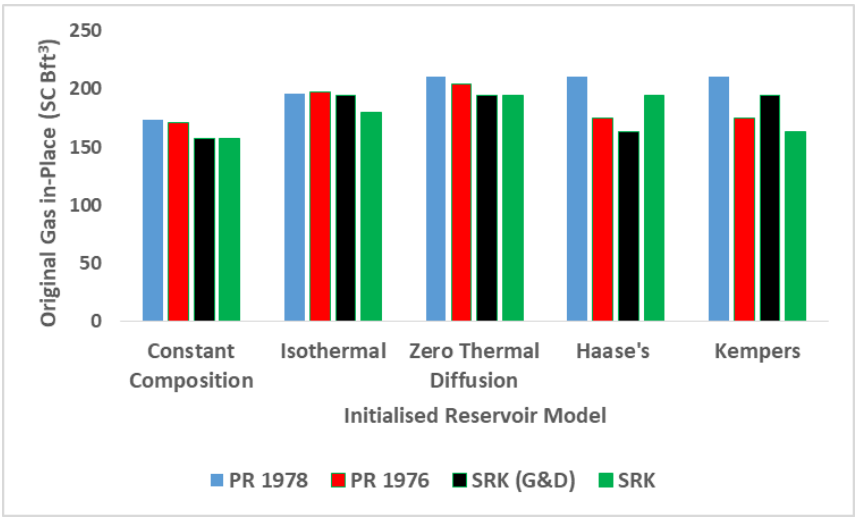

Figure 4.56: Effect of EOSs on OGIP Simulated by Various Initialised Reservoir Models

4.10.2 Effects of EOSs on Recovery Factors

The influence of the various EOSs on oil and gas recovery factors simulated with the constant composition initialised reservoir model are illustrated in Figures 4.57 and 4.58, respectively.

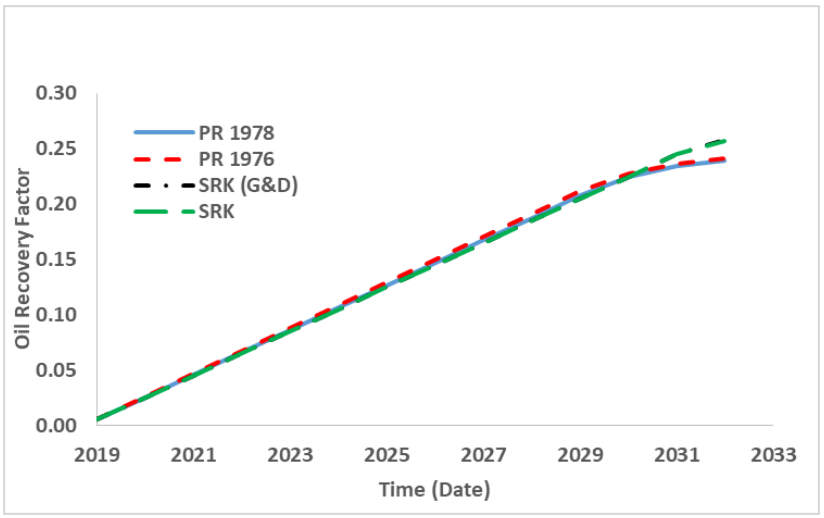

Figure 4.57: The Effects of EOSs on Oil Recovery Factor Predicted by Constant Composition Initialised Reservoir Model

Figure 4.57 illustrates that for constant composition initialised reservoir model, the various EOSs indicated similar oil recovery factor trends from start of production and different ultimate oil recovery factors for the PR EOSs and SRK EOSs (PR 1976 and PR 1978 exhibited approximately similar ultimate recovery factors of 0.239 and 0.242, respectively, while SRK (G&D) and SRK indicated approximately the same ultimate oil recovery factor of 0.257). Similar trends were indicated for the gas recovery factor from start of production as shown in Figure 4.58 but with significantly wide different ultimate gas recovery factors between the PR EOSs and the SRK EOSs ((PR 1976 and PR 1978

exhibited approximately similar ultimate gas recovery factors of 0.375 and 0.383, respectively, while SRK (G&D) and SRK indicated approximately the same ultimate gas recovery factor of 0.307). Therefore, Figures 4.57 and 4.58 suggest that the choice of an EOS is not very critical to the performance of constant composition initialised reservoir model.

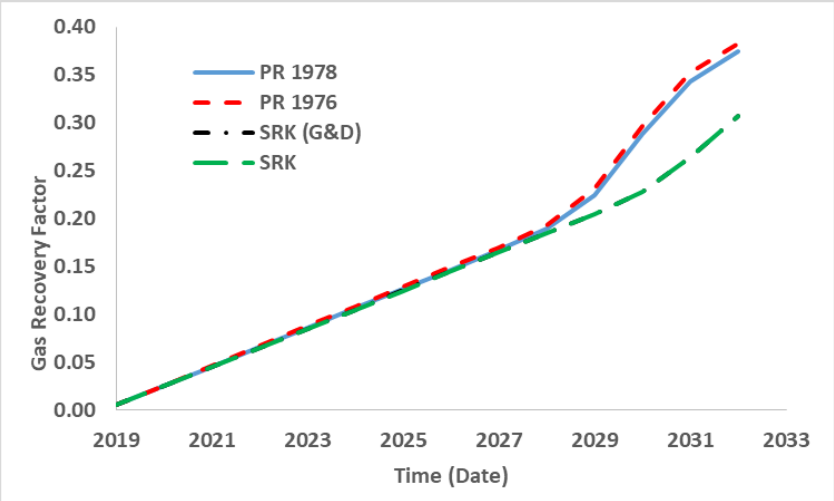

Figure 4.58: The Effects of EOSs on Gas Recovery Factor Predicted by Constant Composition Initialised Reservoir Model

The effects of the applied EOSs on oil and gas recovery factors predicted by isothermal CG initialised reservoir model are illustrated in Figures 4.59 and 4.60, respectively, which shows that the various EOSs resulted in significantly different oil and gas recovery factors. SRK EOS simulated the highest ultimate oil recovery factor while SRK (G&D) EOS simulated the lowest ultimate oil recovery factor as shown in Figure 4.59. A summary of the ultimate oil recovery factors associated with the respective EOSs are presented in Table 4.22.

Table 4.22: Ultimate Oil Recovery Factor Simulated by Applied EOSs Based on Isothermal CG Initialise Reservoir Model

EOS	Ultimate Oil Recovery Factor
PR 1978	0.182
PR 1976	0.195
SRK (G&D)	0.171
SRK	0.204

On the contrary, Figure 4.60 show that SRK (G&D) simulated the highest ultimate gas recovery factor while PR 1976 predicted the lowest. Table 4.23 contains the summary of

the ultimate gas recovery factors predicted by the applied EOSs based on isothermal CG initialised reservoir model.

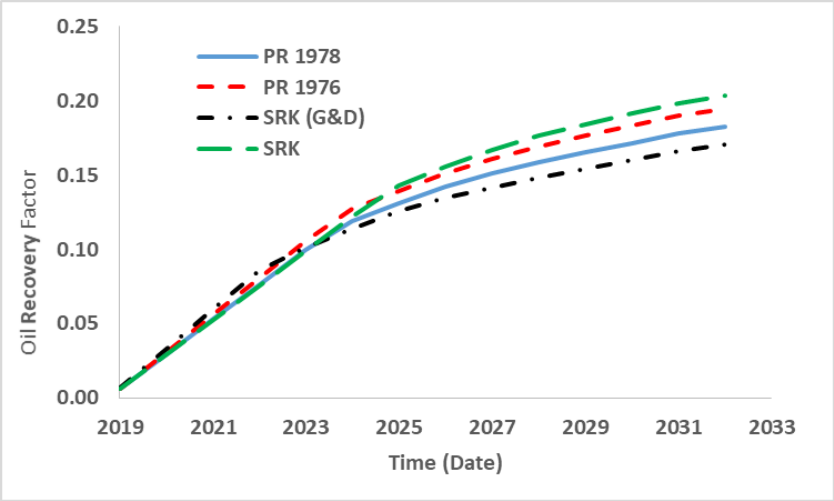

Figure 4.59: The Effects of EOSs on Oil Recovery Factor Predicted by Isothermal CG Initialised Reservoir Model

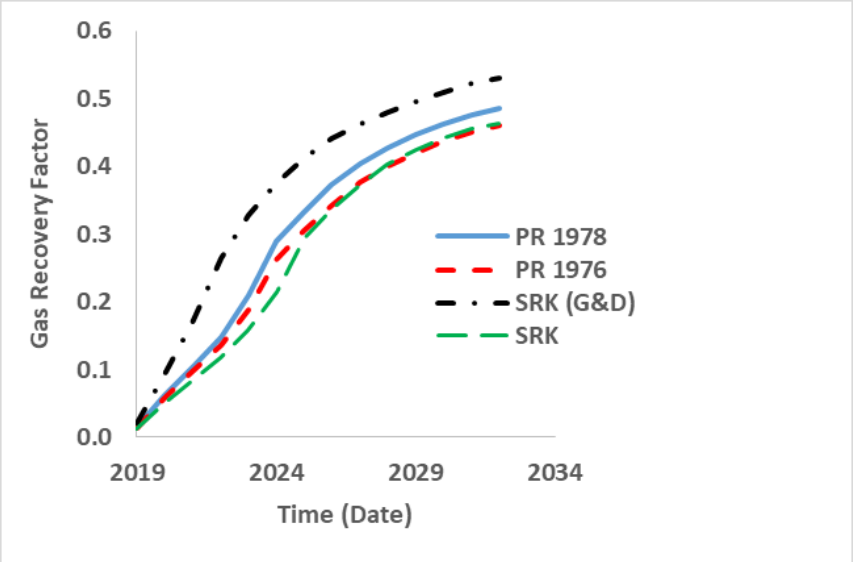

Figure 4.60: The Effects of EOSs on Gas Recovery Factor Predicted by Isothermal CG Initialised Reservoir Model

Table 4.23: Ultimate Gas Recovery Factor Simulated by Applied EOSs Based on Isothermal CG Initialise Reservoir Model

EOS	Ultimate Gas Recovery Factor
PR 1978	0.486
PR 1976	0.461
SRK (G&D)	0.531
SRK	0.464

Figures 4.61 and 4.62 shows the effects of applied EOSs on oil and gas recovery factors, respectively, predicted based on zero thermal diffusion CG initialised reservoir model. Figure 4.61 illustrates that SRK and SRK (G&D) resulted in similar oil recovery trend and highest ultimate oil recovery factor while PR 1976 and PR 1978 simulated similar oil recovery trends with PR 1978 resulting in lowest ultimate oil recovery factor. The values of the ultimate oil recovery factors indicated by the different EOSs are presented in Table 4.23.

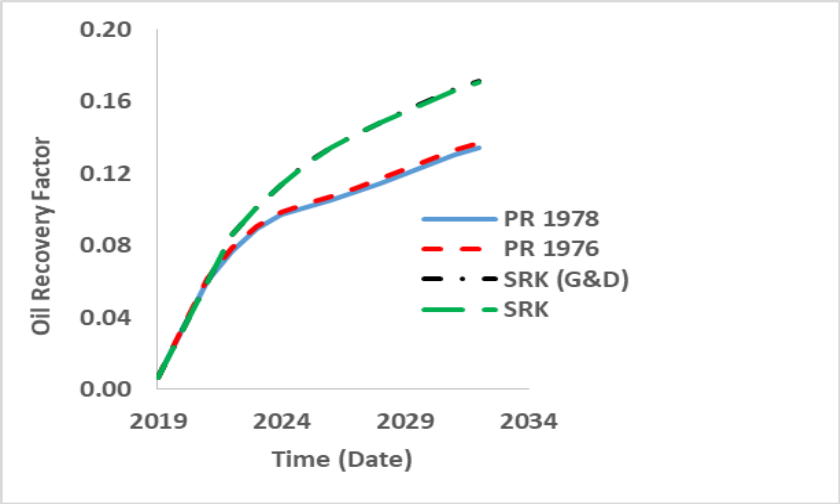

Figure 4.61: The Effects of EOSs on Oil Recovery Factor Predicted by Zero Thermal Diffusion CG Initialised Reservoir Model

Table 4.24: Ultimate Oil Recovery Factor Simulated by Applied EOSs Based on Zero Thermal Diffusion CG Initialise Reservoir Model

EOS	Ultimate Oil Recovery Factor
PR 1978	0.134
PR 1976	0.137
SRK (G&D)	0.171
SRK	0.171

The effects of applied EOSs on the performance of zero thermal diffusion CG initialised reservoir model in predicting realistic gas recovery are illustrated in Figure 4.62 and Table 4.25. Figure 4.62 shows that PR 1976 and PR 1978 resulted in higher and similar gas recovery trends while SRK and SRK (G&D) simulated similar trends. Table 4.25 indicates that PR 1978 simulated the highest ultimate gas recovery factor while (G&D) resulted in the lowest ultimate gas recovery factor.

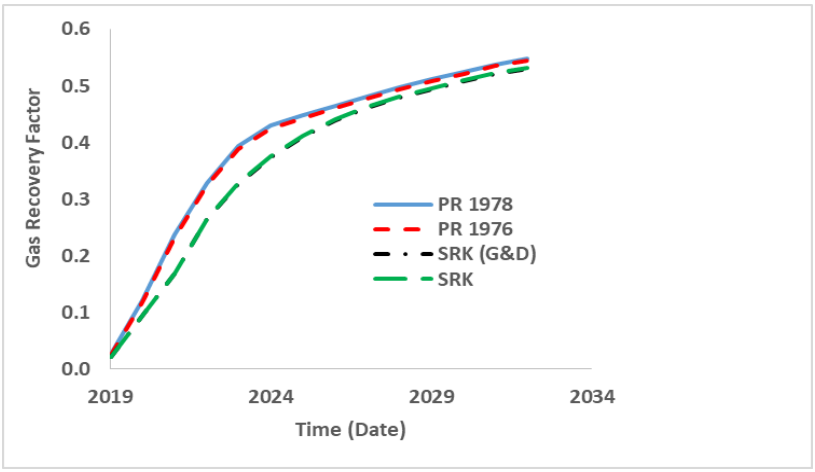

Figure 4.62: The Effects of EOSs on Gas Recovery Factor Predicted by Zero Thermal Diffusion CG Initialised Reservoir Model

Table 4.25: Ultimate Gas Recovery Factor Simulated by Applied EOSs Based on Zero Thermal Diffusion CG Initialise Reservoir Model

EOS	Ultimate Gas Recovery Factor
PR 1978	0.548
PR 1976	0.544
SRK (G&D)	0.531
SRK	0.532

The performances of Haase's thermal diffusion CG initialised reservoir model in predicting realistic oil and gas recovery factors due to the effects of various EOSs are presented in Figures 4.63 and 4.64, respectively. Figure 4.63 shows that SRK (G&D) and PR 1976 exhibited similar oil recovery trends while SRK and PR 1978 exhibited different oil recovery behaviours. Table 4.26 shows that (G&D) resulted in the highest ultimate oil recovery factor while PR 1978 indicated the lowest.

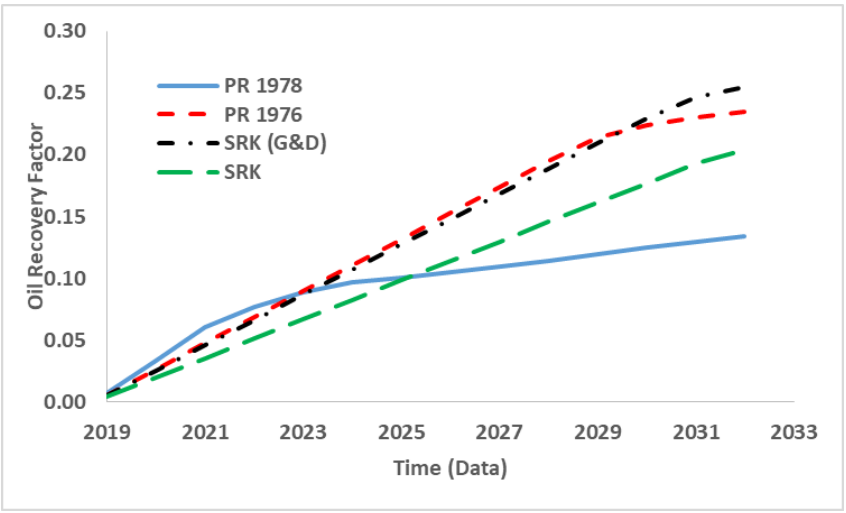

Figure 4.63: The Effects of EOSs on Oil Recovery Factor Predicted by Haase's CG Initialised Reservoir Model

Table 4.26: Ultimate Oil Recovery Factor Simulated by Applied EOSs Based on Haase's CG Initialise Reservoir Model

EOS	Ultimate Oil Recovery Factor
PR 1978	0.134
PR 1976	0.235
SRK (G&D)	0.254
SRK	0.204

The effects of applied EOSs on the performance of Haase's thermal diffusion CG initialised reservoir model in predicting realistic gas recovery are illustrated in Figure 4.64 and Table 4.27, which indicate that PR 1978 resulted in highest gas recovery estimate while SRK resulted in the lowest gas recovery factor estimate. PR 1976 and SRK (G&D) exhibited approximately similar behaviour from the start of production but with PR 1976 indicating higher ultimate gas recovery factor than SRK (G&D).

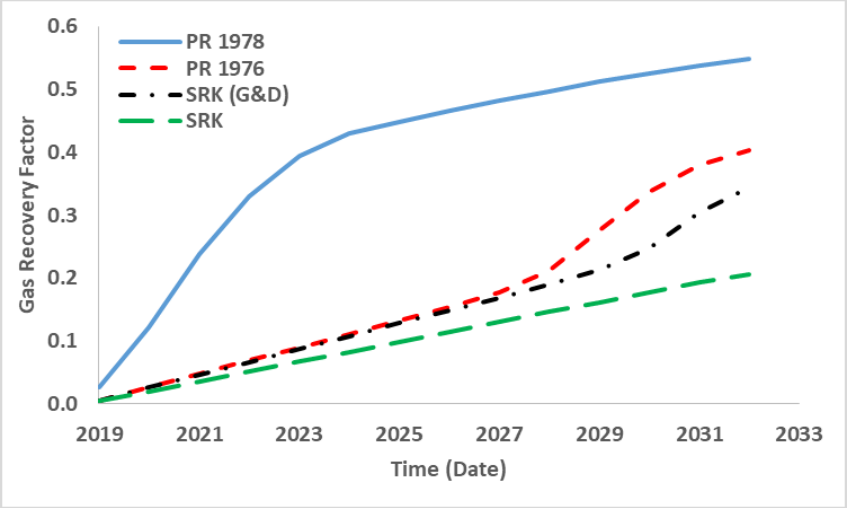

Figure 4.64: The Effects of EOSs on Gas Recovery Factor Predicted by Haase's CG Initialised Reservoir Model

Table 4.27: Ultimate Gas Recovery Factor Simulated by Applied EOSs Based on Haase's CG Initialise Reservoir Model

EOS	Ultimate Gas Recovery Factor
PR 1978	0.548
PR 1976	0.403
SRK (G&D)	0.344
SRK	0.205

Kempers thermal diffusion CG initialised reservoir model response to applied EOSs in terms of oil recovery factor are illustrated in Figure 4.65 and Table 4.28, which shows

that each EOS resulted in significantly different oil recovery outcome with SRK indicating the highest ultimate oil recovery factor and PR 1978 indicating the lowest ultimate oil recovery factor. The response of Kempers thermal diffusion CG initialised reservoir model to applied EOSs in terms of gas recovery factor are demonstrated in Figure 4.66 and Table 4.29, which indicates that PR 1978 resulted in highest gas recovery and that SRK and SRK (G&D) exhibited approximately similar gas recovery behaviour from start of production but with SRK exhibiting the lowest ultimate gas recovery at the end of the simulation period.

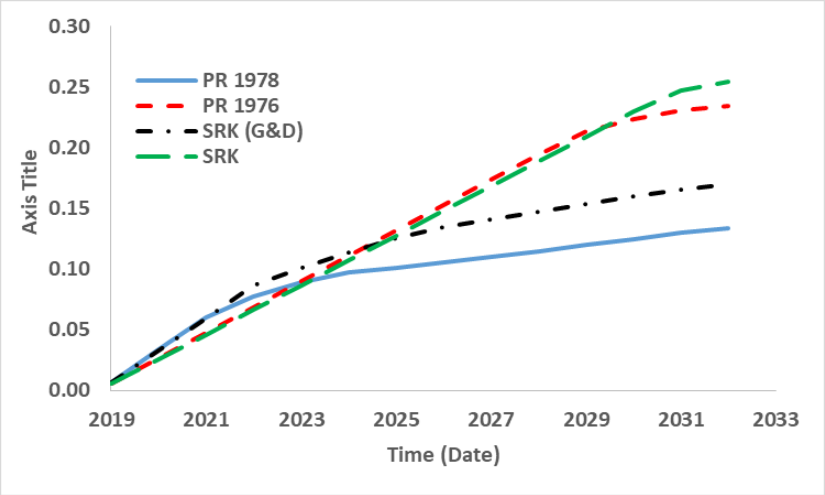

Figure 4.65: The Effects of EOSs on Oil Recovery Factor Predicted by Kempers CG Initialised Reservoir Model

Table 4.28: Ultimate Oil Recovery Factor Simulated by Applied EOSs Based on Kempers CG Initialise Reservoir Model

EOS	Ultimate Oil Recovery Factor
PR 1978	0.134
PR 1976	0.234
SRK (G&D)	0.170
SRK	0.254

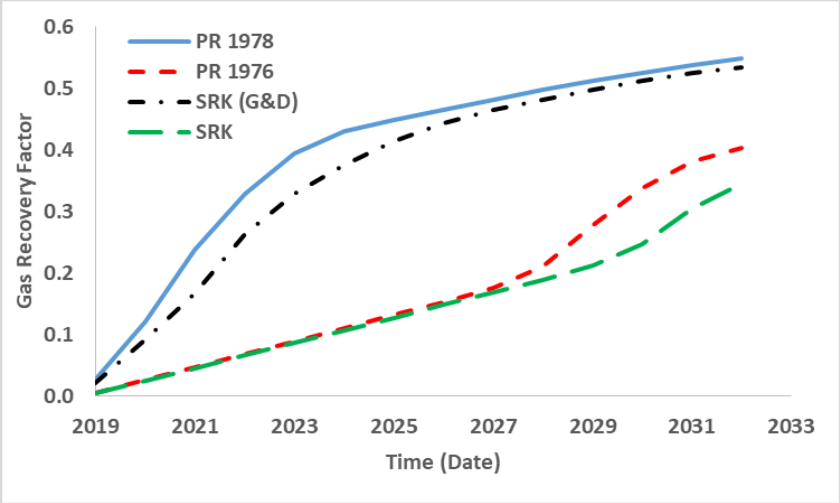

Figure 4.66: The Effects of EOSs on Gas Recovery Factor Predicted by Kempers CG Initialised Reservoir Model

Table 4.29: Ultimate Gas Recovery Factor Simulated by Applied EOSs Based on Kempers CG Initialise Reservoir Model

EOS	Ultimate Gas Recovery Factor
PR 1978	0.134
PR 1976	0.234
SRK (G&D)	0.170
SRK	0.254

The results illustrated in Figures 4.57–4.66 and Tables 4.22–4.29 suggest that, although, the applied EOSs are not very critical to the efficient performances of reservoir models initialised without CG models, they have noteworthy impact on the performances of reservoir models initialised with CG models. Therefore, to effectively predict the performances of compositionally sensitive reservoir, it is important that a sensitivity analysis be carried out to determine the EOS that will guarantee optimal performance.

4.11 The Sensitivity of Nonisothermal CG Initialised Reservoir Models to Changes in Temperature Gradient

The effect of varying the temperature gradient in the applied nonisothermal CG initialised reservoir simulation models – zero (passive) thermal diffusion CG initialised reservoir model, Haase's thermal diffusion CG initialised reservoir model, and Kempers thermal diffusion CG initialised reservoir model, from an initial value of 0.002 ^{o}F/ft to 0.5 ^{o}F/ft, 1.0 ^{o}F/ft, 1.5 ^{o}F/ft, 2.0 ^{o}F/ft and 2.5 ^{o}F/ft, respectively, on realistic OOIP and OGIP estimates, are hereby presented in Figures 4.67 and 4.68, respectively. Figure 4.67 shows that increasing the temperature gradient from 0.002 ^{o}F/ft to 0.5 ^{o}F/ft caused a 30.69

% decrease in the OOIP estimated by zero (passive) thermal diffusion CG initialised reservoir model; 34.14 % increase in OOIP estimated by Haase's thermal diffusion CG initialised reservoir model; and 38.34 % decrease in the OOIP estimated by the Kempers thermal diffusion CG initialised reservoir model. Figure 4.67 also shows that increasing the temperature gradient from 0.5 ^{o}F/ft to 2.5 ^{o}F/ft caused a 22.48 % increase in the OOIP estimated by the Kempers thermal diffusion CG initialised reservoir model; 61.43 % increase in OOIP estimated by Haase's thermal diffusion CG initialised reservoir model; and 44.73 % decrease in the OOIP estimated by zero thermal diffusion CG initialised reservoir model. See Table I1 in Appendix I for the data used in generating Figure 4.67.

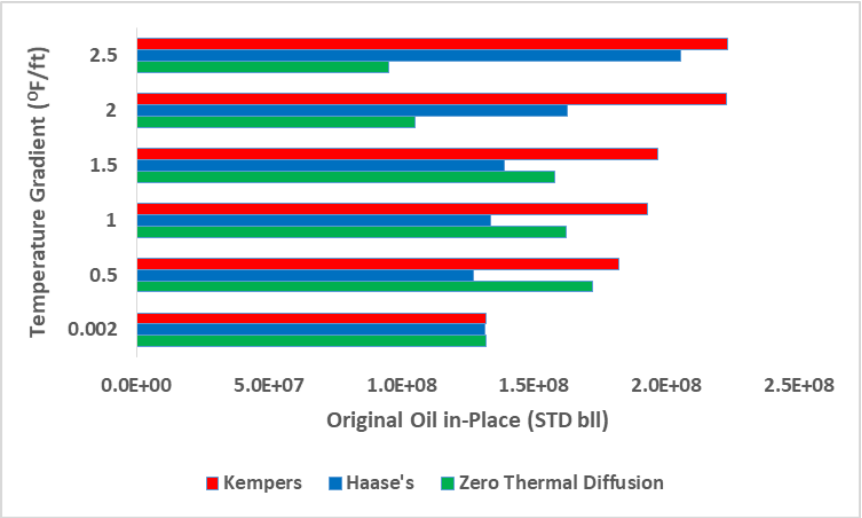

Figure 4.67: The Effect of Varying the Temperature Gradient in the Applied Nonisothermal CG Initialised Reservoir Simulation Models on OOIP

Contrary to observed trends in Figure 4.67, Figure 4.68 shows that increasing the temperature gradient from 0.5 ^{o}F/ft to 2.5 ^{o}F/ft resulted in a 65.79 % decrease in the OGIP estimated by the Kempers thermal diffusion initialised reservoir model; 65.54 % decrease in OGIP estimated by Haase's thermal diffusion CG initialised reservoir model; and 22.28 % increase in the OGIP estimated by zero thermal diffusion CG initialised reservoir model. Figure 4.68 also shows that increasing the temperature gradient from 0.002 ^{o}F/ft to 0.5 ^{o}F/ft caused a 20.19 %, 18.90 %, and 31.49 % increase in the OGIP estimated by zero thermal diffusion CG initialised reservoir model, Haase's thermal diffusion CG initialised reservoir model, and Kempers thermal diffusion initialised reservoir model, respectively. The data associated with Figure 4.68 are presented in Table I1 in Appendix I. The results presented in Figures 4.67 and 4.68 do suggest that temperature gradient and its associated thermal diffusion factor can significantly influence the performances of

nonisothermal CG initialised reservoir models. Hence, need to adequately account for thermal diffusion factor during reservoir simulation model initialisation.

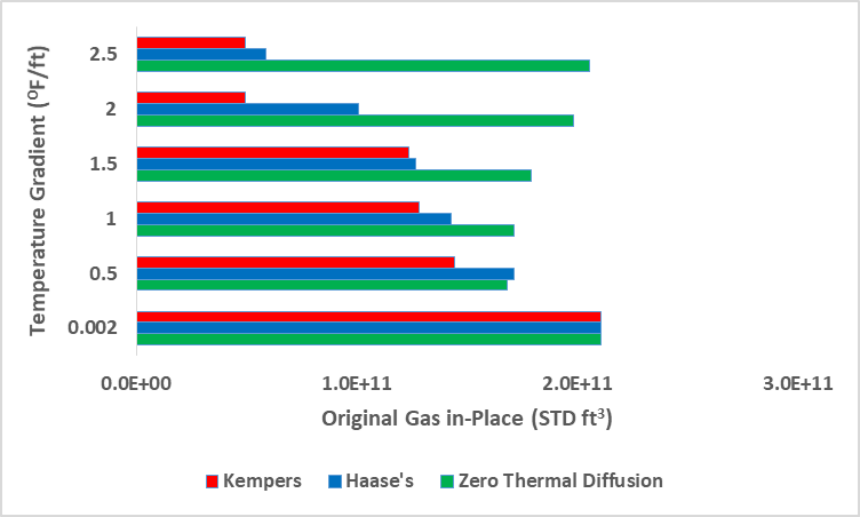

Figure 4.68: The Effect of Varying the Temperature Gradient in the Applied Nonisothermal CG Initialised Reservoir Simulation Models on OGIP

CHAPTER 5

CONCLUSIONS AND FUTURE WORKS

5.1 Conclusions

This study evaluated the performances of petroleum reservoir using CG models with a view to elucidate the technical implications of initialising reservoir simulation models with and without CG models. The research results suggests that inadequate account or complete neglect of compositional grading effect in reservoir simulation model initialisation has significant technical consequences. The results shows that initialising the reservoir model without CG resulted in overestimation of OOIP and cumulative oil production and underestimation of OGIP and cumulative gas production. Constant composition initialised reservoir model overestimate ultimate cumulative oil by 34.20 % more than the isothermal CG model, 57.61 % more than the zero thermal diffusion CG model, 50.60 % more than the Haase's thermal diffusion CG model, and 57.71 % more than the Kempers thermal diffusion CG model. It underestimated ultimate cumulative gas by 46.26 % less than the isothermal CG, 77.24 % less than the zero thermal diffusion CG model, 77.50 % less than the Haase's thermal diffusion model, and 77.38 % less than Kempers thermal diffusion CG initialised reservoir model. The reservoir simulation study also indicated that separator-gas injection is the optimal pressure maintenance option for efficient development of the study reservoir. The results of the sensitivity analysis shows that for all the initialised reservoir models, water saturation (which indirectly accounts for hydrocarbon saturation) with 82-88 % main effects is mostly responsible for the estimated reserve volumes. The observed differences in the values of OOIP and OGIP estimated by the various CG models are due to the influence of the CG models on the reservoir fluid formation volume factor, which made the hydrocarbon saturation (compositions of various components) to either increase or reduce in the gas and oil phases, respectively. Analysis of the effect of various equations of state (EOSs) on the performances of initialised reservoir models suggest that each applied EOSs had significantly different impact on the performances of reservoir models initialised with CG models. Increasing the temperature gradient in nonisothermal CG initialised reservoir models from 0.002 ^{o}F/ft to 2.5 ^{o}F/ft significantly influence the performances of nonisothermal CG initialised reservoir models.

5.2 Future Works

Experimental measurements of compositional grading at different depth in reservoirs within Nigeria are needed in order to adequately compare CG simulation results. PVT data from reservoirs in Nigeria are either recombined surface samples or bottomhole samples taken from a reference depth. There is the need to conduct more CG experimental studies with samples taken from different depths within a reservoir to enable adequate description of CG phenomena in the region. It is important to compare or history-match simulation results with historical production data in order to determine the optimal CG model for a particular reservoir system. Therefore, further simulation studies with comprehensive geologic, geophysical, and engineering data may be required. This study should be extended to other reservoir fluid systems such as gas-condensate and volatile oil reservoir systems, especially in the Niger Delta region of Nigeria where CG studies are inadequately investigated or published. The effect of molecular diffusion and convection were not considered in this current research. Therefore, for non-stationary state reservoir condition, there is the need to investigate the effect of molecular diffusion and natural convection on compositional distribution within the reservoir and the concomitant effect on the performances of coupled reservoir model.

REFERENCE

Abudour, A. M., Mohammad, S. A., Robinson Jr, R. L., & Gasem, K. A. (2012). Volume-translated Peng–Robinson equation of state for saturated and single-phase liquid densities. *Fluid Phase Equilibria*, *335*, 74-87.

Adachi, Y., & Lu, B. Y. (1984). Simplest equation of state for vapor-liquid equilibrium calculation: A modification of the van der Waals equation. *AIChE journal*, *30*(6), 991-993.

Agarwal, R., Li, Y. K., & Nghiem, L. (1987). A regression technique with dynamic-parameter selection or phase behavior matching. In *SPE California Regional Meeting*, Ventura, California, U.S.A., Apr 8-10.

Ahlers, J., & Gmehling, J. (2001). Development of an universal group contribution equation of state: I. Prediction of liquid densities for pure compounds with a volume translated Peng–Robinson equation of state. *Fluid Phase Equilibria*, *191*(1-2), 177-188.

Ahmed, T. (2007). *Equations of State and PVT Analysis: Applications for Improved Reservoir Modeling,* Gulf Publishing Company, Houston, 410-445.

AIAA (1998). Guide for the Verification and Validation of Computational Fluid Dynamics Simulations, AIAA-G-077-1998, Reston, VA, American Institute of Aeronautics and Astronautics.

Ashour, I., Al-Rawahi, N., Fatemi, A., & Vakili-Nezhaad, G. (2011). Applications of equations of state in the oil and gas industry. *Thermodynamics-Kinetics of Dynamic Systems*, *1*, 165-178.

ASME, (2006). Guide for Verification and Validation in Computational Solid Mechanics, The American Society of Mechanical Engineers, ASME V&V 10-2006.

Bath, G. H., Van der Burgh, J., & Ypma, G. J. (1983). RTD 2 (2) Enhanced Oil Recovery in the North Sea. In *11th World Petroleum Congress*, London, UK, Aug 28-Sept 2.

Bath, P. G., Fowler, W. N., & Russell, M. P. (1980). The Brent field, a reservoir engineering review. In *European Offshore Technology Conference and Exhibition*, London, UK, Oct 21-24.

Bedrikovetsky, P. (2013). *Mathematical theory of oil and gas recovery: with applications to ex-USSR oil and gas fields* (Vol. 4). Springer Science & Business Media.

Belery, P., & Da Silva, F. V. (1990). Gravity and thermal diffusion in hydrocarbon reservoirs. *Third Chalk Research Program*, 12.

Biswas, D., & Carey, G. F. (1998). Least-squares finite-element method to predict areal composition variations in large hydrocarbon reservoirs. *SPE Journal*, *3*(04), 307-315.

Bogatyrev, A. F., Makeenkova, O. A., & Nezovitina, M. A. (2015). Experimental study of thermal diffusion in multicomponent gaseous systems. *International Journal of Thermophysics*, *36*(4), 633-647.

Burgess, W. A., Tapriyal, D., Morreale, B. D., Soong, Y., Baled, H. O., Enick, R. M., & McHugh, M. A. (2013). Volume-translated cubic EoS and PC-SAFT density models and a free volume-based viscosity model for hydrocarbons at extreme temperature and pressure conditions. *Fluid Phase Equilibria*, *359*, 38-44.

Carnahan, N. F., & Starling, K. E. (1972). Intermolecular repulsions and the equation of state for fluids. *AIChE Journal*, *18*(6), 1184-1189.

Castro, R. H., Canas, W., Osorio, R., & Soto, C. P. (2009). Definition of Reservoir Compartmentalization Applying Compositional Gradients: Mugrosa B Formation in Middle Magdalena Valley Basin, Lisama Field, Colombia. In *Latin American and Caribbean Petroleum Engineering Conference*, Cartagena de Indias, Colombia, May 31-Jun 3.

Chaback, J. J., & LIRA-GALEANA, C. (1992). Discussions of treatment of variations of composition with depth in gas-condensate reservoirs. *SPE reservoir engineering*, *7*(1), 157-158.

Chien, C. H., Greenkorn, R. A., & Chao, K. C. (1983). Chain-of-rotators equation of state. *AIChE journal*, *29*(4), 560-571.

Cismondi, M., & Mollerup, J. (2005). Development and application of a three-parameter RK–PR equation of state. *Fluid Phase Equilibria*, *232*(1-2), 74-89.

CMG Manual (2017). CMG Builder, Computer Modelling Group LTD.

CMOST (2017). Intelligent Optimization and Analysis Tool, Computer Modelling Group LTD.

Coats, K. H. (1985). Simulation of gas condensate reservoir performance. *Journal of Petroleum Technology*, *37*(10), 1-870.

Danesh, A. (1998). *PVT and phase behaviour of petroleum reservoir fluids* (Vol. 47). Elsevier, 183-192.

de Oliveira Padua, K. G. (1997). Oil composition variation in a large deep water field. In *Latin American and Caribbean Petroleum Engineering Conference*, Rio de Janeiro, Brazil, Aug 30-Sept 3.

Dougherty Jr, E. L., & Drickamer, H. G. (1955). Thermal diffusion and molecular motion in liquids. *The Journal of Physical Chemistry*, *59*(5), 443-449.

England, W. A., Mackenzie, A. S., Mann, D. M., & Quigley, T. M. (1987). The movement and entrapment of petroleum fluids in the subsurface. *Journal of the Geological Society*, *144*(2), 327-347.

Ertekin, T., Abou-Kassem, J. H., & King, G. R. (2001). *Basic applied reservoir simulation* (No. Sirsi) i9781555630898).

Esmaeilzadeh, F., & Roshanfekr, M. (2006). A new cubic equation of state for reservoir fluids. *Fluid Phase Equilibria*, *239*(1), 83-90.

Eun, C. S., Resnick, B. G., & Sabherwal, S. (2012). *International Finance: Global Edition*. McGraw Hill/Irwin.

Everitt, B. S. (2006). *The Cambridge dictionary of statistics*. Cambridge University Press.

Eyitayo, S. I., Lawal, K. A., Ukaonu, C. E., Ovuru, M. I., Sanyaolu, A. A., Otubanjo, M. A., & Matemilola, S. (2017). Using Compositional-Grading Simulations to Assess Gas-Oil Contacts: Practical Cases from the Niger Delta. In *SPE Nigeria Annual International Conference and Exhibition*, Lagos, Nigeria, Jul 31-Aug 2.

Ezekwe, N. (2010). *Petroleum reservoir engineering practice*. Pearson Education.

Faissat, B., Knudsen, K., Stenby, E. H., & Montel, F. (1994). Fundamental statements about thermal diffusion for a multicomponent mixture in a porous medium. *Fluid*

Phase Equilibria, *100*, 209-222.

Fevang, Ø., Singh, K., & Whitson, C. H. (2000). Guidelines for choosing compositional and black-oil models for volatile oil and gas-condensate reservoirs. In *SPE annual technical conference and exhibition*, Dallas, Texas, U.S.A., Oct 1-4.

Firoozabadi, A. (1988). Reservoir-Fluid Phase Behavior and Volumetric Prediction with Equations of State (includes associated papers 18400 and 18579). *Journal of petroleum technology*, *40*(04), 397-406.

Firoozabadi, A., Ghorayeb, K., & Shukla, K. (2000). Theoretical model of thermal diffusion factors in multicomponent mixtures. *AIChE Journal*, *46*(5), 892-900.

Galliero, G., & Montel, F. (2008). Nonisothermal gravitational segregation by molecular dynamics simulations. *Physical Review E*, *78*(4), 041203.

Galliero, G., & Montel, F. (2009). Understanding compositional grading in petroleum reservoirs thanks to molecular simulations. In *EUROPEC/EAGE Conference and Exhibition*, Amsterdam, The Netherlands, Jun 8-11.

Ghorayeb, K., & Firoozabadi, A. (2000). Modeling multicomponent diffusion and convection in porous media. *SPE Journal*, *5*(02), 158-171.

Ghorayeb, K., & Firoozabadi, A. (2000b). Molecular, pressure, and thermal diffusion in nonideal multicomponent mixtures. *AIChE Journal*, *46*(5), 883-891.

Ghorayeb, K., Firoozabadi, A., & Anraku, T. (2003). Interpretation of the unusual fluid distribution in the Yufutsu gas-condensate field. *SPE journal*, *8*(02), 114-123.

Gibbs, J. W. (1906). *The scientific papers of J. Willard Gibbs* (Vol. 1). Longmans, Green and Company.

Gibson, A. P., Sorensen, H., Abdou, M. K., & Sener, I. (2006). New Methods for the Nonequilibrium Initialisation of Reservoir Models with Lateral and Vertical Variations in the Initial Fluid Composition. In *Abu Dhabi International Petroleum Exhibition and Conference*, Abu Dhabi, UAE, Nov 5-8.

Guo, B. (2011). *Petroleum production engineering, a computer-assisted approach*. Elsevier.

Graboski, M. S., & Daubert, T. E. (1978). A modified Soave equation of state for phase equilibrium calculations. 1. Hydrocarbon systems. *Industrial & Engineering Chemistry Process Design and Development*, *17*(4), 443-448.

Haase, R. (1969). *Thermodynamics of irreversible processes*, Addition Wesley, New York.

Haghtalab, A., Kamali, M. J., Mazloumi, S. H., & Mahmoodi, P. (2010). A new three-parameter cubic equation of state for calculation physical properties and vapor–liquid equilibria. *Fluid Phase Equilibria*, *293*(2), 209-218.

Hamoodi, A. N., Abed, A. F., & Grabenstetter, J. (1994). Modeling of a large gas-capped reservoir with areal and vertical variation in composition. In *SPE Annual Technical Conference and Exhibition*, New Orleans, Louisiana, U.S.A., Sep 25-28.

Harmens, A., & Knapp, H. (1980). Three-parameter cubic equation of state for normal substances. *Industrial & Engineering Chemistry Fundamentals*, *19*(3), 291-294.

Hillston, J. (2003). Model validation and verification. Edinburgh: University of Edinburgh.

Hirschberg, A. (1988). Role of asphaltenes in compositional grading of a reservoir's fluid column. *Journal of Petroleum Technology*, *40*(01), 89-94.

Høier, L. (1997). *Miscibility variations in compositionally grading petroleum reservoirs*. Norwegian University of Science and Technology.

Høier, L., & Whitson, C. H. (2000). Compositional grading-theory and practice. In *SPE Annual Technical Conference and Exhibition*, Dallas, Texas, U.S.A., Oct 1-4.

Holt, T., Lindeberg, E., & Ratkje, K. S. (1983). The effect of gravity and temperature gradients on methane distribution in oil reservoirs.

Jacqmin, D. (1987). The interaction of natural convection and gravity segregation in oil/gas reservoirs. In *SPE Annual Technical Conference and Exhibition*, Dallas, Texas, U.S.A., Sep 27-30.

Jacqmin, D. A. V. I. D. (1986). Convection of a Gravity Segregating Fluid Forced by a

Horizontal Temperature Gradient: An Energy Stability Analysis. *Mathematics Applied to Fluid Mechanics and Stability, SIAM Press, Philadelphia*, 263.

Jaramillo, J. M., & Barrufet, M. A. (2001). Effects in the determination of oil reserves due to gravitational compositional gradients in near-critical reservoirs. In *SPE Annual Technical Conference and Exhibition*, New Orleans, Louisiana, U.S.A., Sep 30-Oct 3.

Jhaveri, B. S., & Youngren, G. K. (1988). Three-parameter modification of the Peng-Robinson equation of state to improve volumetric predictions. *SPE reservoir engineering*, *3*(03), 1-033.

Joffe, J., Schroeder, G. M., & Zudkevitch, D. (1970). Vapor-liquid equilibria with the redlich-kwong equation of state. *AIChE Journal*, *16*(3), 496-498.

Joseph, P., & Imo-Jack, O. (2013). Prediction of Oil Rim Presence from Compositional Gradient Theory-A Case Study from Niger Delta Reservoirs. In *SPE Nigeria Annual International Conference and Exhibition*, Lagos, Nigeria, Aug 5-7.

Kempers, L. J. (1989). A thermodynamic theory of the Soret effect in a multicomponent liquid. *The Journal of Chemical Physics*, *90*(11), 6541-6548.

Kiani, M., Osfouri, S., Azin, R., & Dehghani, S. A. M. (2016). Impact of fluid characterization on compositional gradient in a volatile oil reservoir. *Journal of Petroleum Exploration and Production Technology*, *6*(4), 835-844.

Kord, S., & Zobeidi, K. (2007). Effect of compositional grading on reservoir fluid characterization in a giant Iranian oil reservoir. In *Canadian International Petroleum Conference*, Calgary, Alberta, Jun 12-14.

Leahy-Dios, A. (2008). *Experimental and theoretical investigation of Fickian and thermal diffusion coefficients in hydrocarbon mixtures*. Yale University.

Lee, S. T. (1989). Capillary-gravity equilibria for hydrocarbon fluids in porous media. In *SPE Annual Technical Conference and Exhibition*, San Antonio, Texas, U.S.A., Oct 8-11.

Lin, H. M., Kim, H., Guo, T. M., & Chao, K. C. (1983). Cubic chain-of-rotators equation of state and VLE calculations. *Fluid Phase Equilibria, 13*, 143-152.

Liu, J. S., Wilkins, J. R., Al-Qahtani, M. Y., & Al-Awami, A. A. (2001). Modeling a rich gas condensate reservoir with composition grading and faults. In *SPE Middle East Oil Show*, Manama, Bahrain, Mar 17-20.

Luo, S., & Barrufet, M. A. (2004). Compositional gradient: its role in near-critical reservoir development. *Journal of Petroleum Science and Engineering*, *45*(3-4), 193-201.

Mahmoodi, P., & Sedigh, M. (2016). Soave alpha function at supercritical temperatures. *The Journal of Supercritical Fluids*, *112*, 22-36.

Mathias, P. M. (1983). A versatile phase equilibrium equation of state. *Industrial & Engineering Chemistry Process Design and Development*, *22*(3), 385-391.

McCain Jr, W. D. (1990). The Properties of Petroleum Reservoir Fluids. Pennwell Books, Tulsa, Oklahoma.

Michelsen, M. L. (1984). Calculation of critical points and phase boundaries in the critical region. *Fluid Phase Equilibria, 16*(1), 57-76.

Michelsen, M. L. (1985). Saturation point calculations. *Fluid Phase Equilibria*, *23*(2-3), 181-192.

Michelsen, M. L. (1994). A simple method for calculation of approximate phase boundaries. *Fluid phase equilibria*, *98*, 1-11.

Mohammadi, A. H., Eslamimanesh, A., Gharagheizi, F., & Ilani-Kashkouli, P. (2014). Are the reservoir fluid compositional grading data reliable? *Fluid Phase Equilibria*, *363*, 27-31.

Mokhtari, R., & Ashouri, S. (2013). Importance of compositional grading in reservoir development studies: a case study. *Sci Int (Lahore)*, *25*(3), 457-459.

Montel, F. (1993). Phase equilibria needs for petroleum exploration and production industry. *Fluid Phase Equilibria*, *84*, 343-367.

Montel, F., & Gouel, P. L. (1985). Prediction of compositional grading in a reservoir fluid column. In *SPE annual technical conference and exhibition*, Las Vegas, Nevada, U.S.A., Sep 22-26.

Moser, R. D. (1986). Mass transfer by thermal convection and diffusion in porous media. In *10th International Conference on Applied Mathematics,* Austin, Texas, U.S.A.

Muskat, M. (1930). Distribution of non-reacting fluids in the gravitational field. *Physical Review*, *35*(11), 1384.

Nasrabadi, H., Firoozabadi, A., Esposito, R. O., & Vieira, A. J. M. (2008). Interpretation of an unusual bubblepoint pressure variation in an offshore field. In *Europec/EAGE Conference and Exhibition*, Rome, Italy, Jun 9-12.

Nikpoor, M. H., & Chen, Z. (2013). New Methodology for the Modeling of Compositional Grading within the Gas-oil Transition Zone in Petroleum Reservoirs. *Energy Sources, Part A: Recovery, Utilization, and Environmental Effects*, *35*(5), 438-444.

Nikpoor, M. H., Dejam, M., Chen, Z., & Clarke, M. (2016). Chemical–Gravity–Thermal Diffusion Equilibrium in Two-Phase Non-isothermal Petroleum Reservoirs. *Energy & Fuels*, *30*(3), 2021-2034.

Nikpoor, M. H., Kharrat, R., & Chen, Z. (2011). Non-isothermal modeling of compositional grading in petroleum reservoirs, including the effect of plus fraction properties changes with depth. *Pet. Sci. Technol*, *29*, 914-923.

Nikpoor, M. H., Kharrat, R., & Chen, Z. (2013a). The modeling of 3D compositional grading and plus fraction molecular weight change in non-isothermal petroleum reservoirs. *Energy Sources, Part A: Recovery, Utilization, and Environmental Effects*, *35*(2), 99-109.

Nikpoor, M. H., Kharrat, R., & Chen, Z. (2013b). A Comparative Study of Compositional Grading Models in Petroleum Reservoirs. *Energy Sources, Part A: Recovery, Utilization, and Environmental Effects*, *35*(4), 364-369.

Patel, N. C., & Teja, A. S. (1982). A new cubic equation of state for fluids and fluid mixtures. *Chemical Engineering Science*, *37*(3), 463-473.

Pedersen, K. S., & Hjermstad, H. P. (2006). Modeling of large hydrocarbon compositional gradient. In *Abu Dhabi International Petroleum Exhibition and Conference*, Abu Dhabi, UAE, Nov 5-8.

Pedersen, K. S., & Hjermstad, H. P. (2015). Modeling of Compositional Variation with Depth for Five North Sea Reservoirs. In *SPE Annual Technical Conference and Exhibition*, Houston, Texas, U.S.A., Sept 28-30.

Pedersen, K. S., & Lindeloff, N. (2003). Simulations of compositional gradients in hydrocarbon reservoirs under the influence of a temperature gradient. In *SPE Annual Technical Conference and Exhibition*, Denver, Colorado, U.S.A., Oct 5.8.

Pedersen, K. S., Christensen, P. L., Shaikh, J. A., & Christensen, P. L. (2006). *Phase behavior of petroleum reservoir fluids*. CRC press.

Péneloux, A., Rauzy, E., & Fréze, R. (1982). A consistent correction for Redlich-Kwong-Soave volumes. *Fluid phase equilibria*, *8*(1), 7-23.

Peng, D. Y., & Robinson, D. B. (1976). A new two-constant equation of state. *Industrial & Engineering Chemistry Fundamentals*, *15*(1), 59-64.

Privat, R., Jaubert, J. N., & Le Guennec, Y. (2016). Incorporation of a volume translation in an equation of state for fluid mixtures: which combining rule? Which effect on properties of mixing? *Fluid Phase Equilibria, 427*, 414-420.

Rabinowicz, M., Dandurand, J. L., Jakubowski, M., Schott, J., & Cassan, J. P. (1985). Convection in a North Sea oil reservoir: inferences on diagenesis and hydrocarbon migration. *Earth and Planetary Science Letters*, *74*(4), 387-404.

Ratulowski, J., Fuex, A. N., Westrich, J. T., & Sieler, J. J. (2000). Theoretical and experimental investigation of isothermal compositional grading. In *SPE Annual Technical Conference and Exhibition*, Dallas, Texas, U.S.A., Oct 1-4.

Redlich, O., & Kwong, J. N. (1949). On the thermodynamics of solutions. V. An equation of state. Fugacities of gaseous solutions. *Chemical reviews*, *44*(1), 233-244.

Riemens, W. G., Schulte, A. M., & De Jong, L. N. J. (1988). Birba field PVT variations along the hydrocarbon column and confirmatory field tests. *Journal of petroleum technology*, *40*(01), 83-88.

Riley, M. F., & Firoozabadi, A. (1998). Compositional variation in hydrocarbon reservoirs with natural convection and diffusion. *AIChE journal*, *44*(2), 452-464.

Robinson, D. B., & Peng, D. Y. (1978). *The characterization of the heptanes and heavier fractions for the GPA Peng-Robinson programs*. Gas processors association.

Sage, B. H., & Lacey, W. N. (1939). Gravitational concentration gradients in static columns of hydrocarbon fluids. *Transactions of the AIME*, *132*(01), 120-131.

Sall, J. (1990). Leverage plots for general linear hypotheses. *The American Statistician, 44*(4), 308-315.

Schlesinger, S. (1979). Terminology for Model Credibility, Simulation, Vol. 32, No. 3.

Schlumberger (2005). PVTi and ECLIPSE 300, Introduction to PVT Analysis and Compositional Simulation Course, Abingdon Technology Center Training, Dec 12.

Schmidt, G., & Wenzel, H. (1980). A modified van der Waals type equation of state. *Chemical Engineering Science*, *35*(7), 1503-1512.

Schulte, A. M. (1980). Compositional variations within a hydrocarbon column due to gravity. In *SPE annual technical conference and exhibition*, Dallas, Texas, U.S.A., Sept 21-24.

Smalley, P. C., England, W. A., & El Rabaa, A. W. M. (1994). Reservoir compartmentalization assessed with fluid compositional data. *SPE Reservoir Engineering*, *9*(03), 175-180.

Soave, G. (1972). Equilibrium constants from a modified Redlich-Kwong equation of state. *Chemical engineering science*, *27*(6), 1197-1203.

Span, R., Wagner, W., Lemmon, E. W., & Jacobsen, R. T. (2001). Multiparameter equations of state—recent trends and future challenges. *Fluid Phase Equilibria, 183*, 1-20.

SPE/WPC/AAPG/SPEE/SEG/SPWLA/EAGE (2017). Petroleum Resources Management System. https://www.spe.org/industry/docs/Petroleum-Resources-Management-System.pdf?ecid=O~E~~~B2B~Listed@ASX~~201711~4D17FF62DA924A448FCAEF04CEC4541A~

Temeng, K. O., Al-Sadeg, M. J., & Al-Mulhim, W. A. (1998). Compositional grading in the Ghawar Khuff reservoirs. In *SPE Annual Technical Conference and Exhibition*,

New Orleans, Louisiana, U.S.A., Sep 27-30.

Thacker, B. H., Doebling, S. W., Hemez, F. M., Anderson, M. C., Pepin, J. E., & Rodriguez, E. A. (2004). *Concepts of model verification and validation* (No. LA--14167). Los Alamos National Laboratory.

Thiele, E. (1963). Equation of state for hard spheres. *The Journal of Chemical Physics*, *39*(2), 474-479.

Thomas, O. (2007). *Reservoir analysis based on compositional gradients* (Doctoral dissertation, Stanford University).

Tian, J., & Gui, Y. (2003). Modification to the van der Waals equation of state. *Journal of phase equilibria*, *24*(6), 533-541.

Trucano, T. G., Easterling, R. G., Dowding, K. J., Paez, T. L., Urbina, A., Romero, V. J., Rutherford B. M., & HILLS, R. G. (2001). Description of the Sandia validation metrics project.

Tsai, J. C., & Chen, Y. P. (1998). Application of a volume-translated Peng-Robinson equation of state on vapor-liquid equilibrium calculations. *Fluid phase equilibria*, *145*(2), 193-215.

Twu, C. H., Bluck, D., Cunningham, J. R., & Coon, J. E. (1991). A cubic equation of state with a new alpha function and a new mixing rule. *Fluid Phase Equilibria*, *69*, 33-50.

U.S. Department of Energy, (2000). Advanced Simulation and Computing (ASCI) Program Plan," 01-ASCI-Prog-01, Sandia National Laboratories, Albuquerque, New Mexico.

Urbina, A., Hinnerichs, T. D., Hunter, P., O'Gorman, C. C., Rutherford, B. M., & Paez, T. L. (2005). *Validation of mathematical models: an overview of the process* (No. SAND2005-2092C). Sandia National Laboratories.

Valderrama, J. O. (1990). A generalized Patel-Teja equation of state for polar and nonpolar fluids and their mixtures. *Journal of chemical engineering of Japan*, *23*(1), 87-91.

Van Der Waals, J. D., & Rowlinson, J. S. (2004). *On the continuity of the gaseous and liquid states*. Courier Corporation.

Vilanova, J. (2016). A comparison of deterministic and probabilistic methods to improve reserves estimates, Linkedin, Published on 20 September. https://www.linkedin.com/pulse/comparison-deterministic-probabilistic-methods-improve-jordi-vilanova.

Vo, H. X. (2010). Composition variation during flow of gas-condensate wells. *A report submitted to the Department of energy resources engineering of Stanford University.—2010.—441 p*.

Vo, H. X., & Horne, R. N. (2015). Experimental Study of Composition Variation During Flow of Gas-Condensate. In *SPE Annual Technical Conference and Exhibition*, Houston, Texas, U.S.A., Sept 28-30.

Watson, P., Cascella, M., May, D., Salerno, S., & Tassios, D. (1986). Prediction of vapor pressures and saturated molar volumes with a simple cubic equation of state: Part II: The Van der Waals-711 EOS. *Fluid Phase Equilibria*, *27*, 35-52.

Wei, Y. S., & Sadus, R. J. (2000). Equations of state for the calculation of fluid-phase equilibria. *AIChE Journal*, *46*(1), 169-196.

Wheaton, R. J. (1991). Treatment of variations of composition with depth in gas-condensate reservoirs (includes associated papers 23549 and 24109). *SPE Reservoir Engineering*, *6*(02), 239-244.

Whitson, C. H., & Belery, P. (1994). Compositional gradients in petroleum reservoirs. In *University of Tulsa centennial petroleum engineering symposium*, Tulsa, Oklahoma, U.S.A., Aug 29-31.

Whitson, C. H., & Brulé, M. R. (2000). *Phase behavior* (Vol. 20). Richardson, TX: Henry L. Doherty Memorial Fund of AIME, Society of Petroleum Engineers.

Whitson, C. H., Fevang, Ø. & Yang, T. (1999). Gas Condensate PVT: What's Really Important and Why? In *IBC Conference on Optimization of Gas Condensate Fields,* London, UK, Jan 28-29.

Yu, J. M., & Lu, B. C. Y. (1987). A three-parameter cubic equation of state for asymmetric

mixture density calculations. *Fluid Phase Equilibria*, *34*(1), 1-19.

Zudkevitch, D., & Joffe, J. (1970). Correlation and prediction of vapor-liquid equilibria with the redlich-kwong equation of state. *AIChE Journal, 16*(1), 112-119.

Appendix A

Derivation of Equation 2.35

The mathematical framework for the estimation of compositional variation with depth in petroleum reservoirs under the influence of chemical potential, gravitational force, and thermal diffusion were presented by Montel and Gouel (1985); Montel (1993); Faissat et al. (1994); Høier and Whitson (2000). The one-dimensional zero-mass-flow stationary state model proposed by Høier and Whitson (2000) can be written as shown in Eq. A.1 for the combined effects of gravity and thermal diffusion:

$$\sum_{k=1}^{n-1}\left(\frac{\partial \mu_i}{\partial \mathrm{x}_k}\right)\nabla \mathrm{x}_k = J_{Gi} - J_{Ti}\frac{\nabla T}{T} \qquad \text{(A.1)}$$

In Eq. A.1, μ_i is the chemical potential of component i, ∇T is the temperature gradient, T is the system temperature, x is the mole fraction, J_{Gi} accounts for the effect of gravity, and J_{Ti} denotes thermal diffusion factor. The term J_{Gi} is expressed thus:

$$J_{Gi} = (M_i - \rho V_i)g \qquad \text{(A.2)}$$

where M_i is the molecular weight of component i, V_i is the partial molar volume of component i, ρ is mass density, and g is acceleration due to gravity. One necessary constraint to the application of Eq. A.1 either in the form of isothermal model or non-isothermal models, is that the sum of the molar compositions of all fluid components at a given depth along the hydrocarbon column must add up to one (unity). That is:

$$\sum_{i=1}^{n} z_i(h) = 1 \qquad \text{(A.3)}$$

where n is the number of components and z_i is the overall composition of component i. Hence, there are $n+1$ variables at any given depth along the hydrocarbon column. To determine the pressure and molar compositions at any depth will consequently require solving $n+1$ equations consisting $n+1$ variables, with suitable EOS.

Isothermal CG model assumes thermodynamic equilibrium conditions in the reservoir. It neglects the effect of thermal gradient and thermal diffusion (J_{Ti}= 0). Thus, gravity force is the only factor responsible for the distribution of fluid compositions in the reservoir, causing lighter components like methane to migrate towards the top of the reservoir and heavier components to move towards the bottom section. Eq. A.1 can be mathematically

transformed to an isothermal model by expressing it in terms of component fugacity as follows:

$$f_i(h) = f_i(h^o)\exp\left(-\frac{M_i g(h-h^o}{RT}\right) \quad i = 1,2,...,n \tag{A.4}$$

The fugacity of component i can be estimated based on the overall composition of the species, thus:

$$f_i = p_i z_i \varphi_i \tag{A.5}$$

Therefore, Eq. A.4 can be rewritten thus:

$$\left(\varphi_i^h z_i^h p_i^h\right) = \left(\varphi_i^{h^o} z_i^{h^o} p_i^{h^o}\right)\exp\left(-\frac{M_i g(h-h^o}{RT}\right) \quad i = 1,2,...,n \tag{A.6}$$

In Eq. A.4 – A.6, f_i is the fugacity of component i, h^o is the reference depth, h is the depth of interest, R is the universal gas constant, p_i is the pressure of component i, φ_i is the fugacity coefficient of component i, and all other terms are as defined in Eq. A.1. Eq. A.6 is the isothermal CG model applied in this work to simulate compositional variation with depth.

Non-isothermal models considered in this work are the zero thermal diffusion model, Haase's thermal diffusion model, and Kempers thermal diffusion model. Zero or passive thermal diffusion model is a hypothetical model in which the thermal diffusion factor (J_{Ti}) in Eq. A.1 is assumed to be negligible even though thermal gradient exist in the system ($J_{Ti} = 0$, $\nabla T \neq 0$). The temperature, T at a depth (h), was estimated from the knowledge of temperature gradient (∇T).

The basic difference between the various non-isothermal models is the method applied in estimating the thermal diffusion coefficient, (J_{Ti}) in Eq. A.1. Haase's thermal diffusion model is based on centre of mass assumption and is stated thus:

$$J_{Ti} = \frac{1}{M_i} = (M_i H_m - M_m H_i) \tag{A.7}$$

where

$$M_m = \sum_i x_i M_i \tag{A.8}$$

$$H_m = \sum_i x_i H_i \tag{A.9}$$

M_m is molecular weight of the mixture, H_m is molar enthalpy of the mixture, M_i is the molecular weight of component *i* in the mixture, H_i is the partial molar enthalpy of component *i* in the mixture, x_i is the mole fraction of component *i*.

Kempers thermal diffusion model depends on the centre of volume assumption for thermal diffusion coefficient prediction. It is expressed thus:

$$J_{Ti} = \frac{1}{V_i} = (V_i H_m - V_m H_i) \tag{A.10}$$

where,

$$V_m = \sum_i x_i V_i \tag{A.11}$$

where, V_m is the molar volume of the mixture, V_i is the partial molar volume of component i in the mixture.

Belery-da Silva model is an extention of the Dougherty-Drickamer model from binary to multicomponent mixtures. The thermal diffusion factor proposed by Belery-da Silva is expressed thus:

$$J_{Ti} = \frac{1}{2\overline{V}}.(V_i \Delta U_m^* - V_m \Delta U_i^*) \tag{A.12}$$

where,

$$\overline{V} = \frac{M_m}{\sum_i \left(\frac{M_i}{V_i} \right)} \tag{A.13}$$

The partial molar activation energy for component *i* in the mixture (ΔU_i^*), is expressed thus:

$$\Delta U_i^* = \left(\frac{\partial \Delta U_m^*}{\partial n_i} \right)_{p,T,n_k} \tag{A.14}$$

Where n is the number of moles and ΔU_m^* is a function of the viscosity-to-density ratio, given as:

$$\Delta U_m^* \equiv R\left[\left(\frac{\partial \ln(\mu/\rho)}{\partial(1/T)} \right)_{P,\mathrm{xi}} - pT\left(\frac{\partial \ln(\mu/\rho)}{\partial p} \right)_{T,\mathrm{xi}} \right] \tag{A.15}$$

Since chemical potential is a function of pressure, mole fraction and temperature, chain rule can be applied to Eq. A.15 to give:

$$\nabla \mu_i = \left(\frac{\partial \mu_i}{\partial p} \right)_{T,\mathrm{x}} \nabla p + \sum_{k=1}^{n-1} \left(\frac{\partial \mu_i}{\partial \mathrm{x}_k} \right)_{p,T,\mathrm{x}_{k\neq j}} \nabla \mathrm{x}_k + \left(\frac{\partial \mu_i}{\partial T} \right)_{p,\mathrm{x}} \nabla T \tag{A.16}$$

But

$$S_i = -\left(\frac{\partial \mu_i}{\partial T} \right) \tag{A.17}$$

$$\nabla p = \rho g \tag{A.18}$$

Therefore,

$$\nabla \mu_i = V_i \rho . g + \sum_{k=1}^{n-1} \left(\frac{\partial \mu_i}{\partial \mathrm{x}_k} \right)_{p,T,\mathrm{x}_{k\neq j}} \nabla \mathrm{x}_k - S_i \nabla T \tag{A.19}$$

Where S_i is the partial molar entropy of component i in the mixture. Eq. A.18 similarly assumes hydrostatic equilibrium ($\nabla p = \rho g$**)**. Hence, combining Eq. A.1, A.2, and A.19 gives:

$$\nabla \mu_i = M_i . g - S_i \nabla T - J_{Ti} \frac{\nabla T}{T} \tag{A.20}$$

Eq. A.20 (Eq. 2.35 in Chapter 2, section 2.5, page 35) is the CG model applied in this work for both isothermal and non-isothermal scenarios.

Appendix B

Table B1: Compositional Variation with Depth Predicted by Isothermal CG model

Depth (ft)	Composition (fraction)									
	CO_2	C_1	C_2	C_3	iC_4	nC_4	iC_5	nC_5	C_6	C_{7+}
7398	0.014	0.813	0.057	0.05	0.013	0.019	0.008	0.008	0.011	0.007
7458.07	0.014	0.465	0.052	0.065	0.021	0.035	0.019	0.02	0.038	0.27
7483.43	0.014	0.465	0.052	0.065	0.021	0.035	0.019	0.02	0.038	0.271
7568.86	0.014	0.463	0.052	0.065	0.021	0.035	0.019	0.02	0.038	0.273
7654.29	0.014	0.461	0.052	0.065	0.021	0.035	0.019	0.02	0.038	0.275
7655	0.014	0.461	0.052	0.065	0.021	0.035	0.019	0.02	0.038	0.275
7739.71	0.014	0.459	0.052	0.065	0.021	0.035	0.019	0.02	0.038	0.277
7825.14	0.014	0.457	0.052	0.065	0.021	0.035	0.019	0.02	0.038	0.279
7910.57	0.014	0.455	0.051	0.065	0.021	0.035	0.019	0.02	0.038	0.281
7996	0.014	0.453	0.051	0.064	0.021	0.035	0.019	0.02	0.038	0.283

Table B2: Compositional Variation with Depth Predicted by Zero Thermal Diffusion CG model

Depth (ft)	Temp. (^oF)	Composition (fraction)									
		CO_2	**C_1**	**C_2**	**C_3**	**iC_4**	**nC_4**	**iC_5**	**nC_5**	**C_6**	**C_{7+}**
7398	229.49	0.0144	0.8126	0.0568	0.0502	0.0128	0.0194	0.0083	0.0078	0.0112	0.0065
7453.4	229.6	0.0144	0.8118	0.0569	0.0504	0.0129	0.0195	0.0083	0.0078	0.0113	0.0066
7483.43	229.66	0.0143	0.4648	0.0521	0.065	0.0211	0.0354	0.0194	0.0195	0.0379	0.2706
7568.86	229.83	0.0143	0.4628	0.0519	0.0649	0.0211	0.0354	0.0194	0.0195	0.0379	0.2727
7654.29	230	0.0143	0.4608	0.0518	0.0648	0.0211	0.0354	0.0194	0.0195	0.038	0.2749
7655	230	0.0143	0.4608	0.0518	0.0648	0.0211	0.0354	0.0194	0.0195	0.038	0.2749
7739.71	230.17	0.0143	0.4589	0.0517	0.0647	0.0211	0.0354	0.0194	0.0195	0.0381	0.277
7825.14	230.34	0.0143	0.457	0.0515	0.0646	0.0211	0.0354	0.0194	0.0195	0.0381	0.279
7910.57	230.51	0.0143	0.4552	0.0514	0.0645	0.0211	0.0353	0.0194	0.0195	0.0382	0.281
7996	230.68	0.0143	0.4534	0.0513	0.0644	0.021	0.0353	0.0194	0.0195	0.0383	0.283

Table B3: Compositional Variation with Depth Predicted by Haase's Thermal Diffusion CG model

Depth (ft)	Temp. (^oF)	Composition (fraction)									
		CO_2	**C_1**	**C_2**	**C_3**	**iC_4**	**nC_4**	**iC_5**	**nC_5**	**C_6**	**C_{7+}**
7398	229.49	0.0145	0.8123	0.0569	0.0503	0.0128	0.0194	0.0083	0.0078	0.0113	0.0065
7412.94	229.56	0.0145	0.8122	0.0569	0.0503	0.0128	0.0194	0.0083	0.0078	0.0113	0.0066
7483.43	229.66	0.0143	0.4634	0.052	0.0649	0.0211	0.0354	0.0194	0.0195	0.0379	0.2721
7568.86	229.83	0.0143	0.4621	0.0519	0.0649	0.0211	0.0354	0.0194	0.0195	0.038	0.2735
7654.29	230.00	0.0143	0.4608	0.0518	0.0648	0.0211	0.0354	0.0194	0.0195	0.038	0.2749
7655	230.00	0.0143	0.4608	0.0518	0.0648	0.0211	0.0354	0.0194	0.0195	0.038	0.2749
7739.71	203.17	0.0143	0.4595	0.0517	0.0647	0.0211	0.0354	0.0194	0.0195	0.038	0.2763
7825.14	230.34	0.0143	0.4583	0.0516	0.0647	0.0211	0.0354	0.0194	0.0195	0.0381	0.2776
7910.57	230.51	0.0143	0.4571	0.0515	0.0646	0.0211	0.0354	0.0194	0.0195	0.0381	0.2789
7996	230.68	0.0143	0.4559	0.0514	0.0645	0.0211	0.0354	0.0194	0.0195	0.0382	0.2802

Table B4: Compositional Variation with Depth Predicted by Kempers Thermal Diffusion CG model

Depth (ft)	Temp. (^oF)	Composition (fraction)									
		CO_2	**C_1**	**C_2**	**C_3**	**iC_4**	**nC_4**	**iC_5**	**nC_5**	**C_6**	**C_{7+}**
7398	229.49	0.0144	0.8125	0.0568	0.0503	0.0128	0.0194	0.0083	0.0077	0.0112	0.0065
7412.94	229.56	0.0144	0.812	0.0569	0.0504	0.0129	0.0195	0.0083	0.0078	0.0113	0.0066
7483.43	229.66	0.0143	0.464	0.052	0.065	0.0211	0.0354	0.0194	0.0195	0.0379	0.2714
7568.86	229.83	0.0143	0.4624	0.0519	0.0649	0.0211	0.0354	0.0194	0.0195	0.0379	0.2732
7654.29	230	0.0143	0.4608	0.0518	0.0648	0.0211	0.0354	0.0194	0.0195	0.038	0.2749
7655	230	0.0143	0.4608	0.0518	0.0648	0.0211	0.0354	0.0194	0.0195	0.038	0.2749
7739.71	203.17	0.0143	0.4593	0.0517	0.0647	0.0211	0.0354	0.0194	0.0195	0.0381	0.2766
7825.14	230.34	0.0143	0.4578	0.0516	0.0646	0.0211	0.0354	0.0194	0.0195	0.0381	0.2782
7910.57	230.51	0.0143	0.4563	0.0515	0.0646	0.0211	0.0354	0.0194	0.0196	0.0382	0.2798
7996	230.68	0.0143	0.4548	0.0514	0.0645	0.0211	0.0354	0.0195	0.0196	0.0382	0.2814

Appendix C

Table C1: Reservoir Volumetric and Estimated In-Place Volumes Predicted by Constant Composition Initialised Reservoir Model

Item	Unit	Value
Total Bulk Reservoir Volume,	res ft^3	$1.16893x10^{10}$
Total Pore Volume,	res ft^3	$2.37640x10^{9}$
Total Hydrocarbon Pore Volume,	res ft^3	$1.54466x10^{9}$
Original Oil in Place, OOIP	std bbl	$1.74428x10^{8}$
Original Gas in Place, OGIP	std ft^3	$1.73913x10^{11}$

Table C2: Reservoir Volumetric and Estimated In-Place Volumes Predicted by Isothermal CG Initialised Reservoir Model

Item	Unit	Value
Total Bulk Reservoir Volume,	res ft^3	$1.16893x10^{10}$
Total Pore Volume,	res ft^3	$2.37640x10^{9}$
Total Hydrocarbon Pore Volume,	res ft^3	$1.54466x10^{9}$
Original Oil in Place, OOIP	std bbl	$1.50569x10^{8}$
Original Gas in Place, OGIP	std ft^3	$1.96050x10^{11}$

Table C3: Reservoir Volumetric and Estimated In-Place Volumes Predicted by Zero Thermal Diffusion CG Initialised Reservoir Model

Item	Unit	Value
Total Bulk Reservoir Volume,	res ft^3	$1.16893x10^{10}$
Total Pore Volume,	res ft^3	$2.37640x10^{9}$
Total Hydrocarbon Pore Volume,	res ft^3	$1.54466x10^{9}$
Original Oil in Place, OOIP	std bbl	$1.31923x10^{8}$
Original Gas in Place, OGIP	std ft^3	$2.10848x10^{11}$

Table C4: Reservoir Volumetric and Estimated In-Place Volumes Predicted by Haase's Thermal Diffusion CG Initialised Reservoir Model

Item	Unit	Value
Total Bulk Reservoir Volume,	res ft^3	$1.16893x10^{10}$
Total Pore Volume,	res ft^3	$2.37640x10^{9}$
Total Hydrocarbon Pore Volume,	res ft^3	$1.54466x10^{9}$
Original Oil in Place, OOIP	std bbl	$1.31802x10^{8}$
Original Gas in Place, OGIP	std ft^3	$2.11047x10^{11}$

Table C5: Reservoir Volumetric and Estimated In-Place Volumes Predicted by Kempers Thermal Diffusion CG Initialised Reservoir Model

Item	Unit	Value
Total Bulk Reservoir Volume,	res ft^3	$1.16893x10^{10}$
Total Pore Volume,	res ft^3	$2.37640x10^{9}$
Total Hydrocarbon Pore Volume,	res ft^3	$1.54466x10^{9}$
Original Oil in Place, OOIP	std bbl	$1.31849x10^{8}$
Original Gas in Place, OGIP	std ft^3	$2.10967x10^{11}$

Appendix D

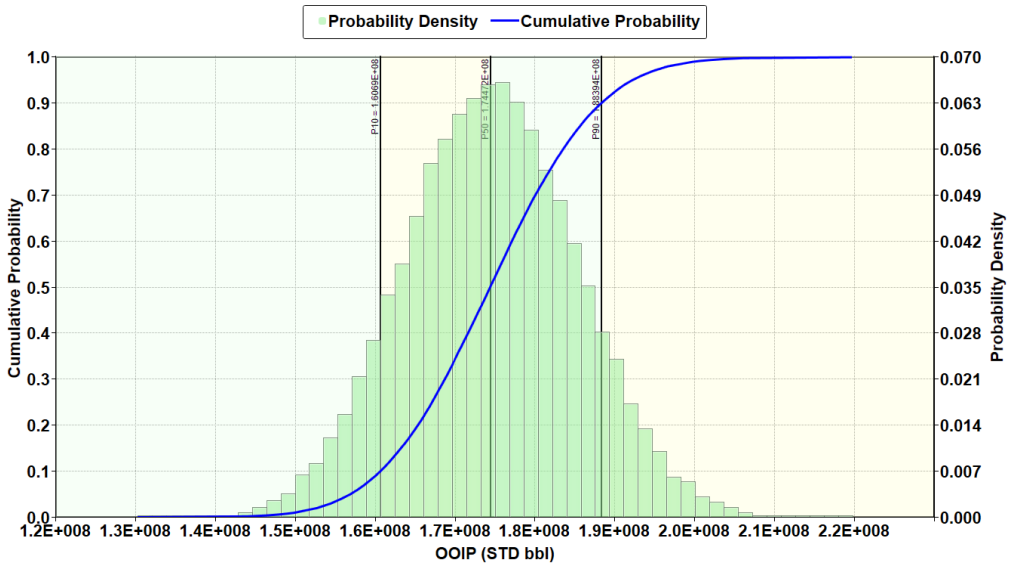

Figure D1: OOIP Probability Distribution Estimated by Constant Composition Initialised Reservoir Model

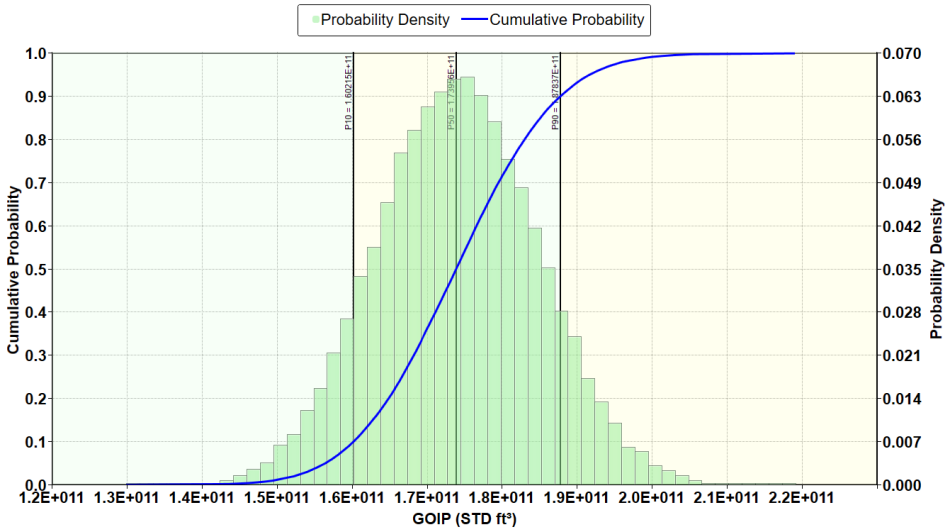

Figure D2: OGIP Probability Distribution Estimated by Constant Composition Initialised Reservoir Model

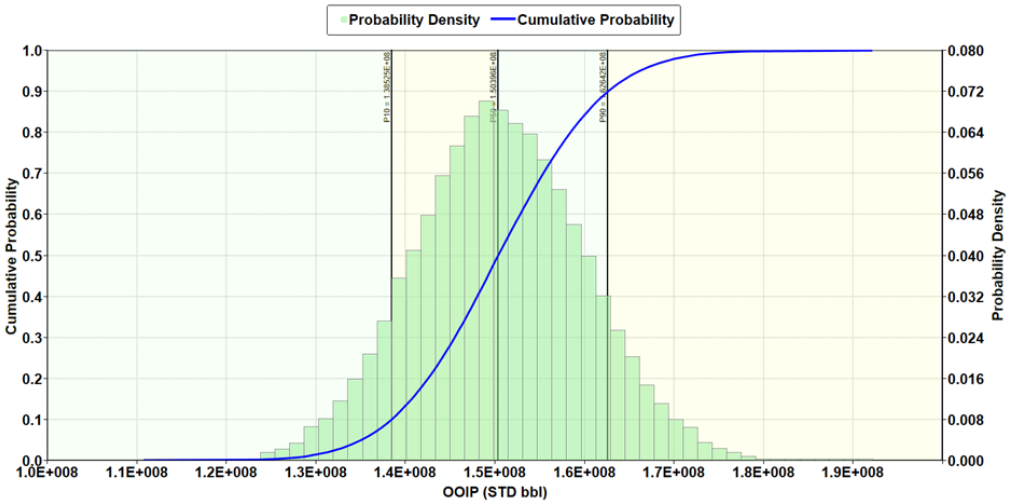

Figure D3: OOIP Probability Distribution Estimated by Isothermal CG Initialised Reservoir Model

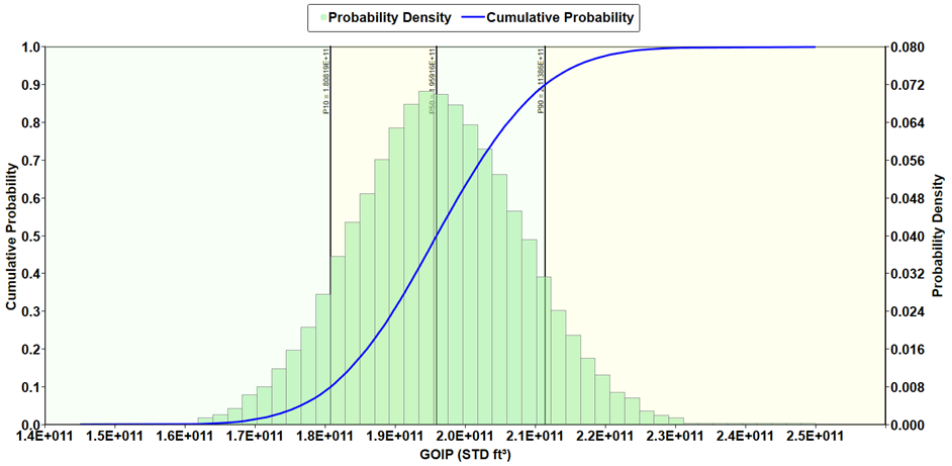

Figure D4: OGIP Probability Distribution Estimated by Isothermal CG Initialised Reservoir Model

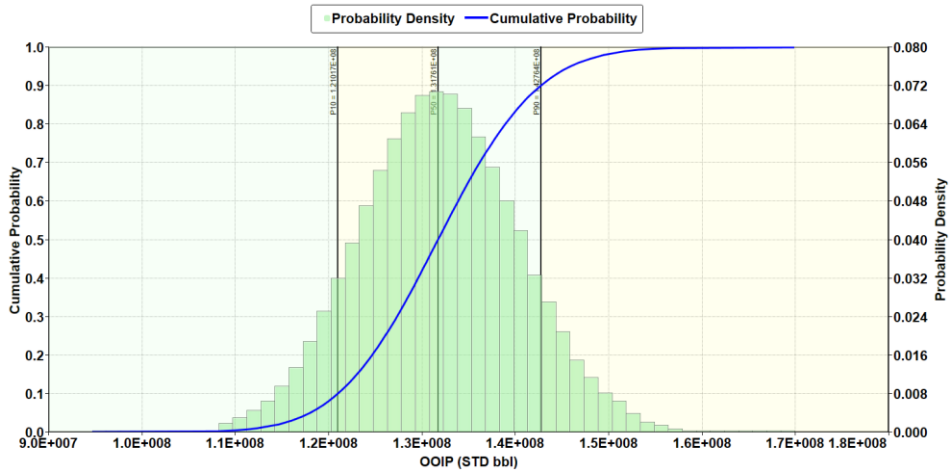

Figure D5: OOIP Probability Distribution Estimated by Zero Thermal Diffusion CG Initialised Reservoir Model

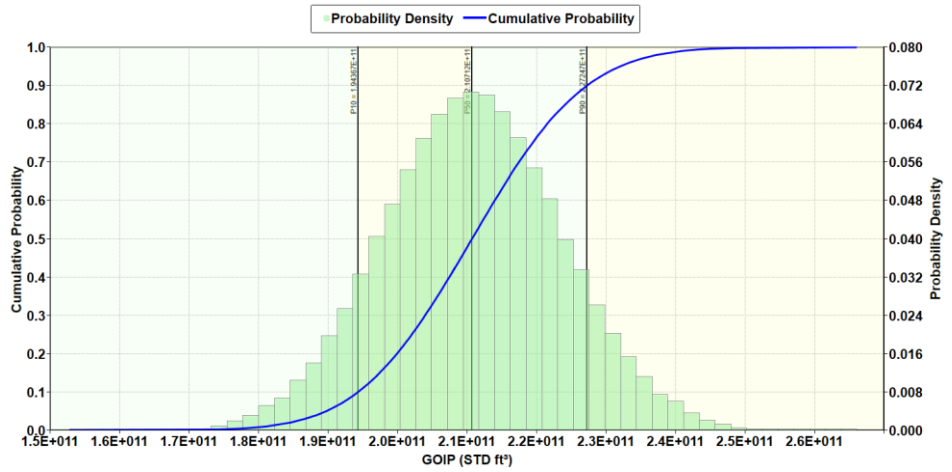

Figure C6: OGIP Probability Distribution Estimated by Zero Thermal Diffusion CG Initialised Reservoir Model

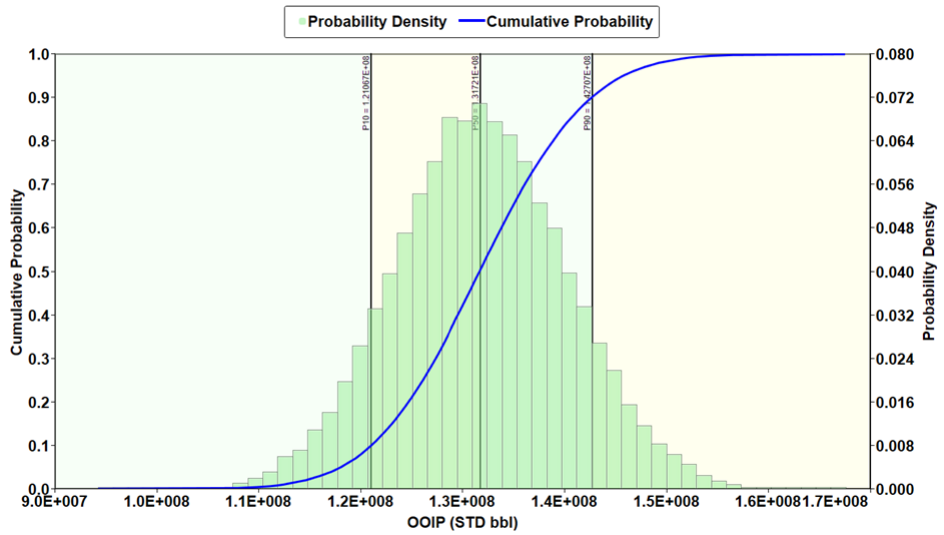

Figure D7: OOIP Probability Distribution Estimated by Haase's Thermal Diffusion CG Initialised Reservoir Model

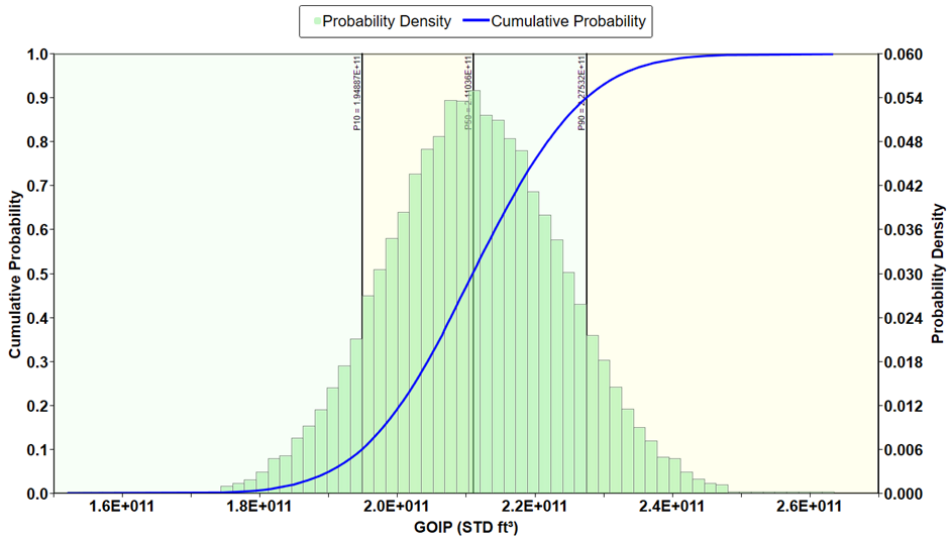

Figure D8: OGIP Probability Distribution Estimated by Haase's Thermal Diffusion CG Initialised Reservoir Model

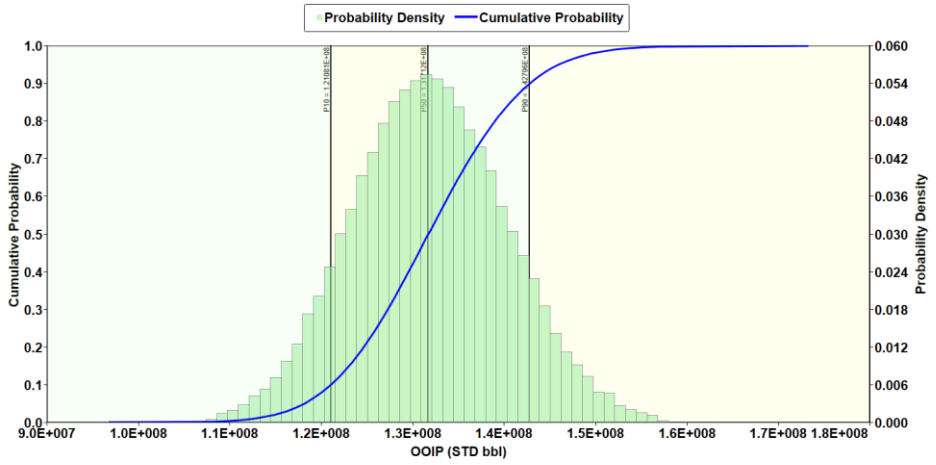

Figure D9: OOIP Probability Distribution Estimated by Kempers Thermal Diffusion CG Initialised Reservoir Model

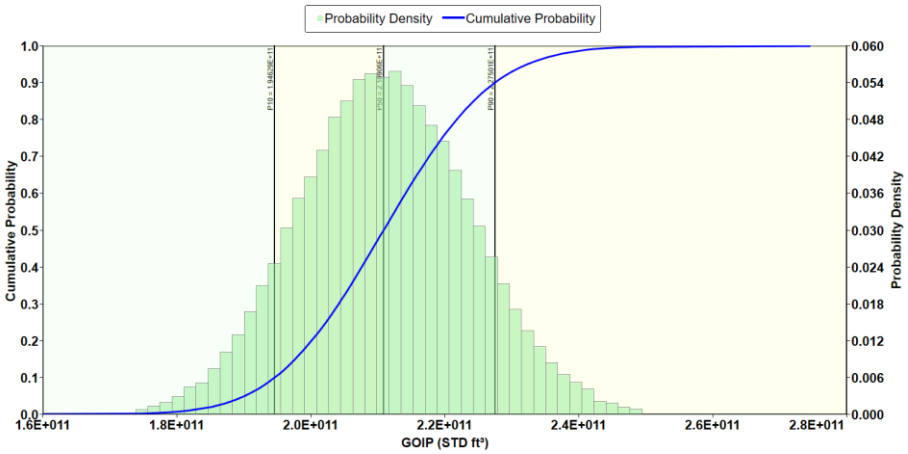

Figure D10: OGIP Probability Distribution Estimated by Kempers Thermal Diffusion CG Initialised Reservoir Model

Appendix E

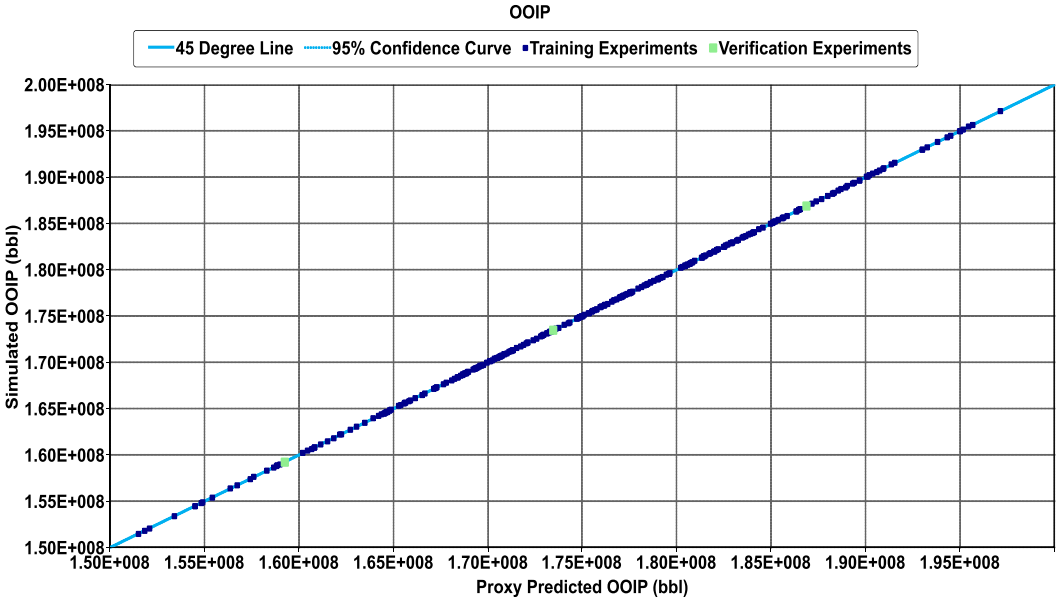

Figure E1: OOIP Response Surface Model Verification Plot for Constant Composition Initialised Reservoir Model

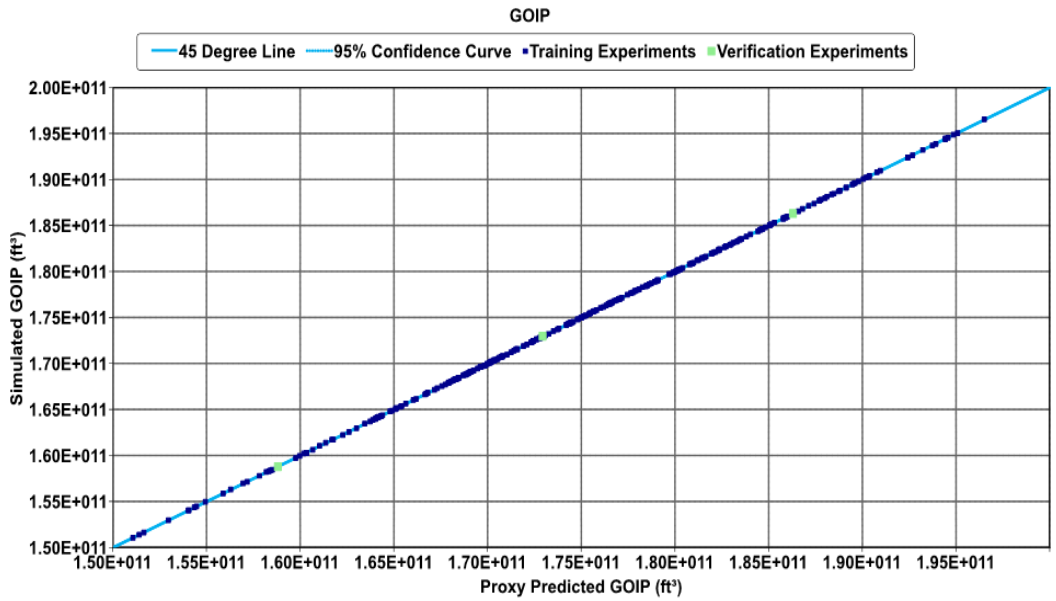

Figure E2: OGIP Response Surface Model Verification Plot for Constant Composition Initialised Reservoir Model

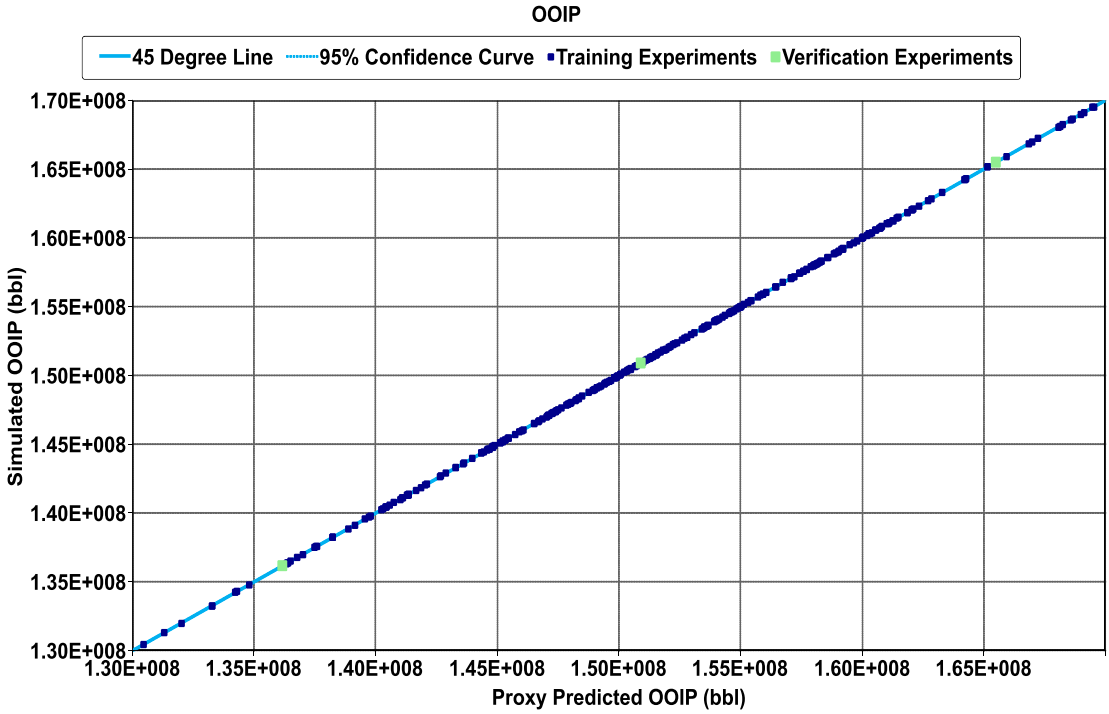

Figure E3: OOIP Response Surface Model Verification Plot for Isothermal CG Initialised Reservoir Model

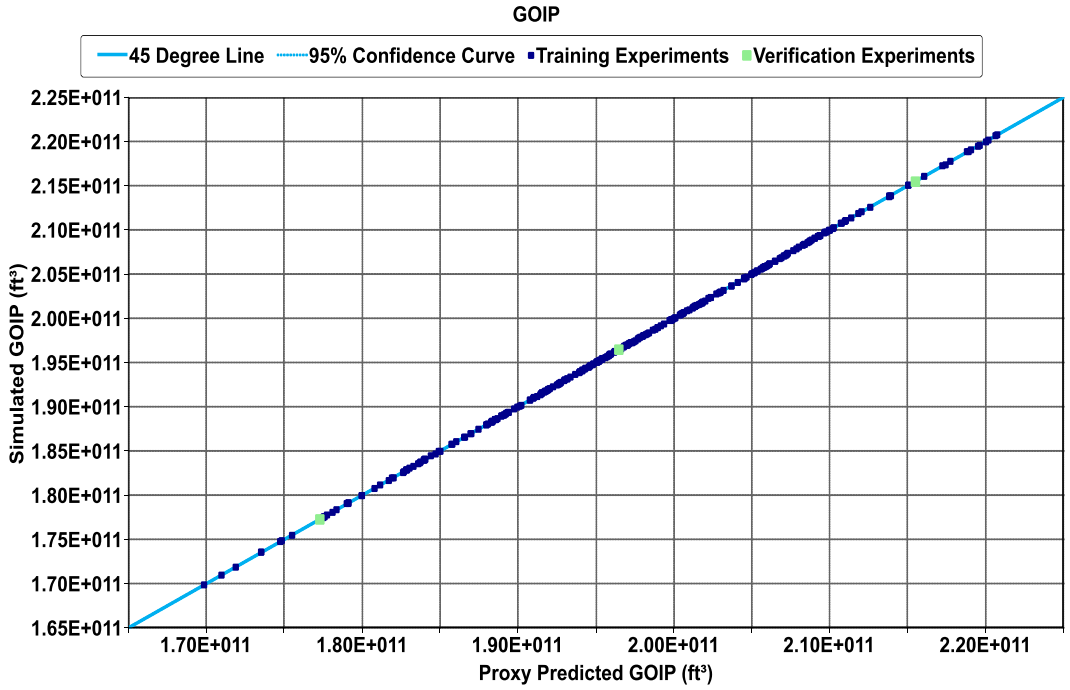

Figure E4: OGIP Response Surface Model Verification Plot for Isothermal CG Initialised Reservoir Model

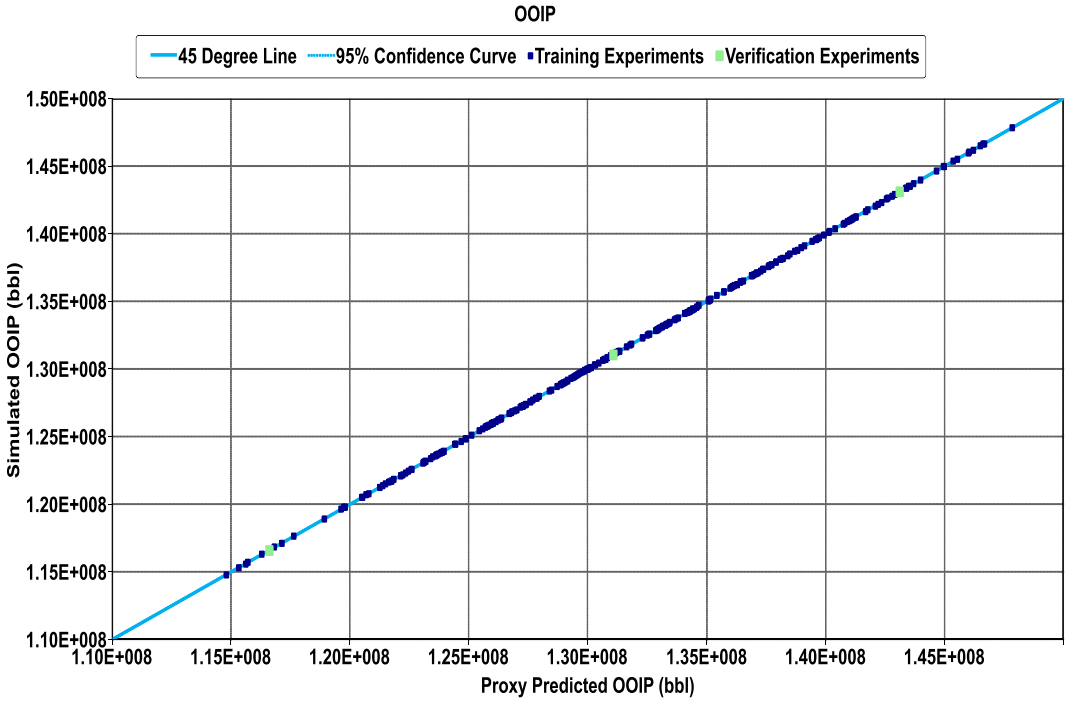

Figure E5: OOIP Response Surface Model Verification Plot for Zero Thermal Diffusion CG Initialised Reservoir Model

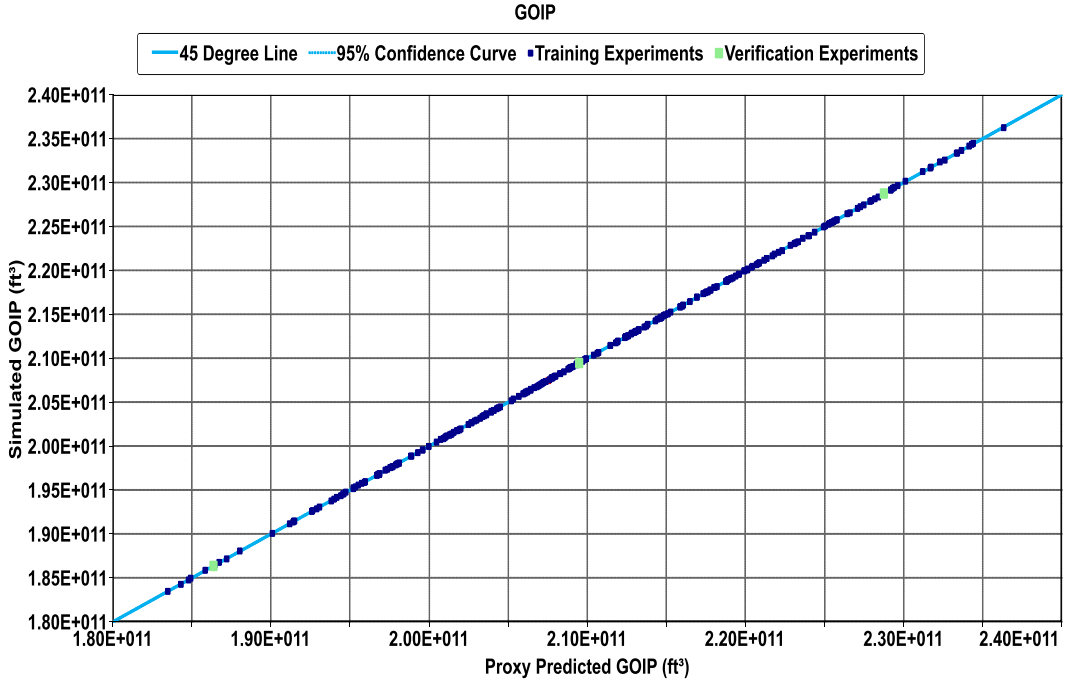

Figure E6: OGIP Response Surface Model Verification Plot for Zero Thermal Diffusion CG Initialised Reservoir Model

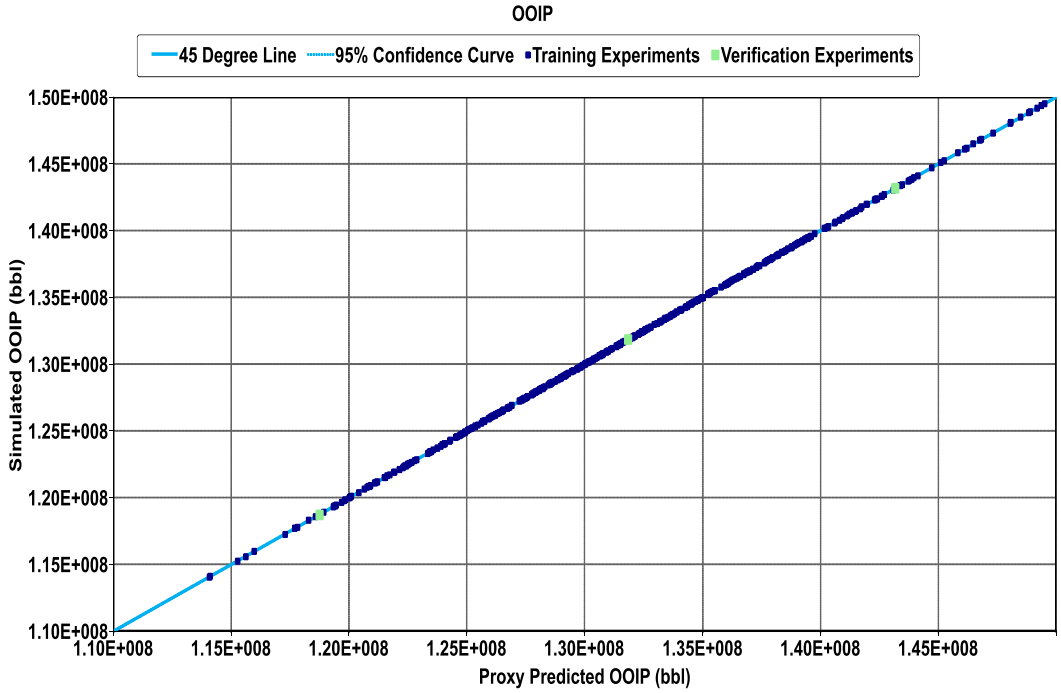

Figure E7: OOIP Response Surface Model Verification Plot for Haase's Thermal Diffusion CG Initialised Reservoir Model

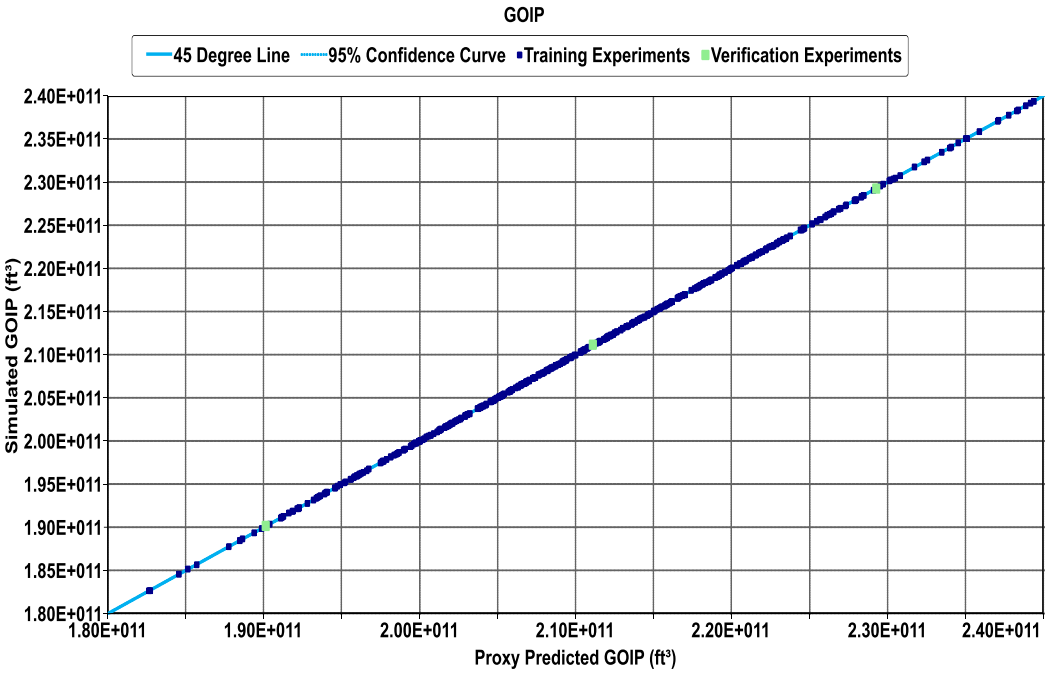

Figure E8: OGIP Response Surface Model Verification Plot for Haase's Thermal Diffusion CG Initialised Reservoir Model

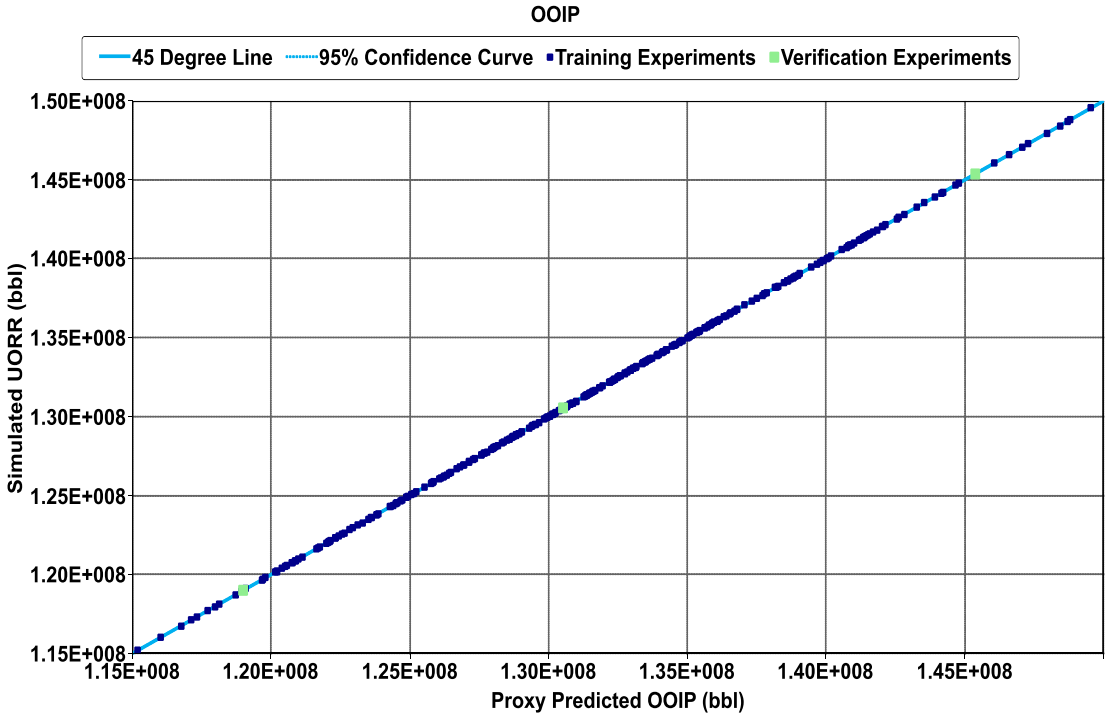

Figure E9: OOIP Response Surface Model Verification Plot for Kempers Thermal Diffusion CG Initialised Reservoir Model

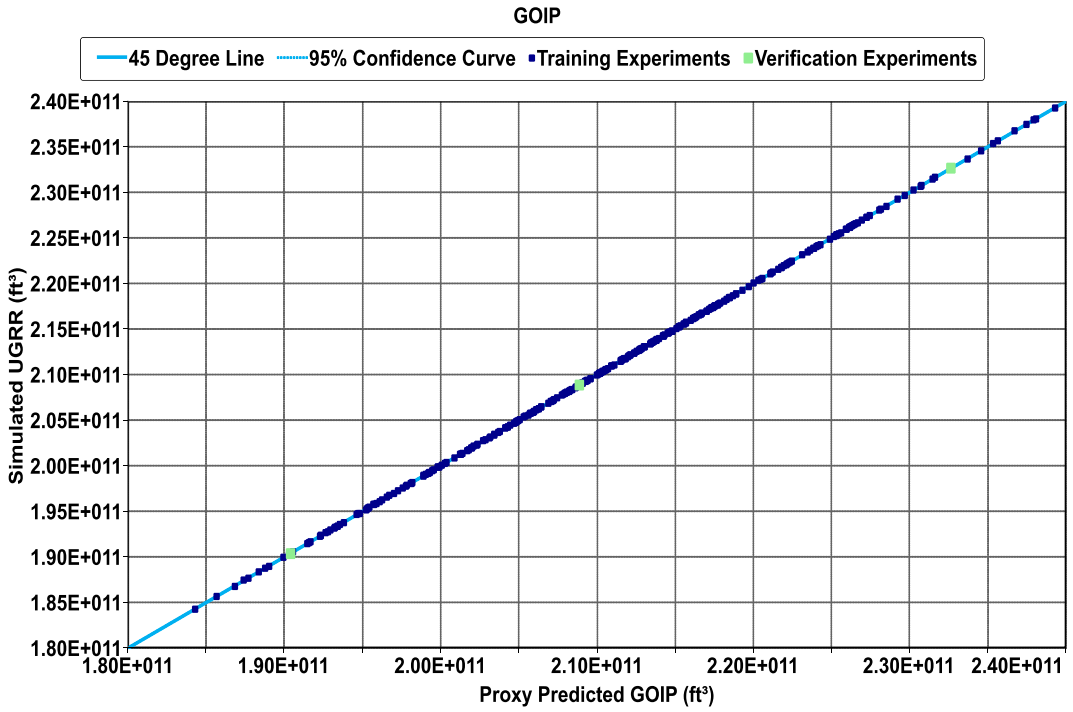

Figure E10: OGIP Response Surface Model Verification Plot for Kempers Thermal Diffusion CG Initialised Reservoir Model

Appendix F

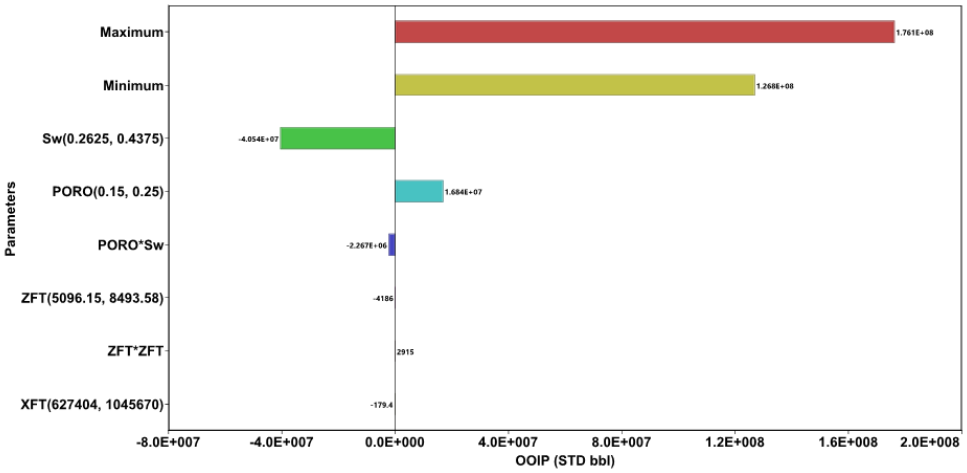

Figure F1: Tornado Diagram Showing the Effect of Input Parameters on the OOIP Estimated by Isothermal CG Initialised Reservoir Model

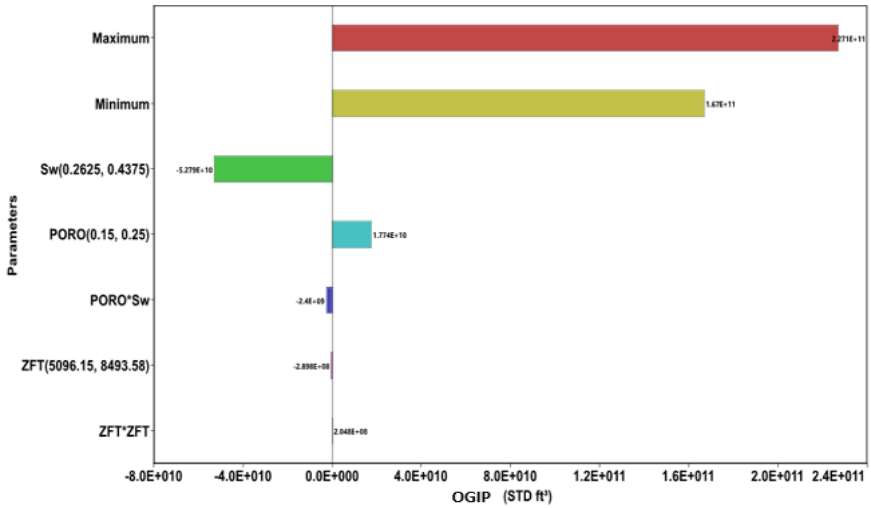

Figure F2: Tornado Diagram Showing the Effect of Input Parameters on the OGIP Estimated by Isothermal CG Initialised Reservoir Model

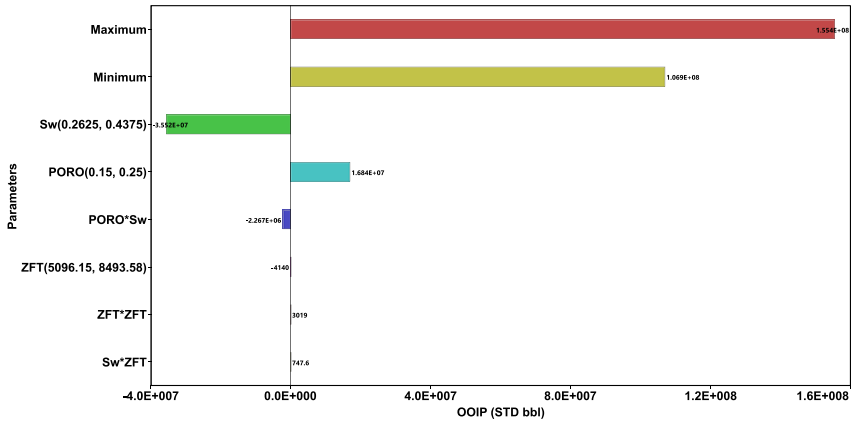

Figure F3: Tornado Diagram Showing the Effect of Input Parameters on the OOIP Estimated by Zero Thermal Diffusion CG Initialised Reservoir Model

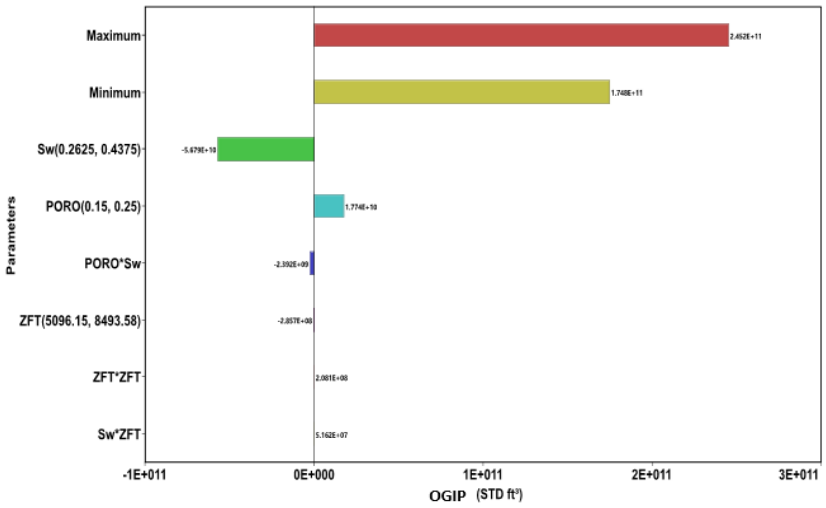

Figure F4: Tornado Diagram Showing the Effect of Input Parameters on the OGIP Estimated by Zero Thermal Diffusion CG Initialised Reservoir Model

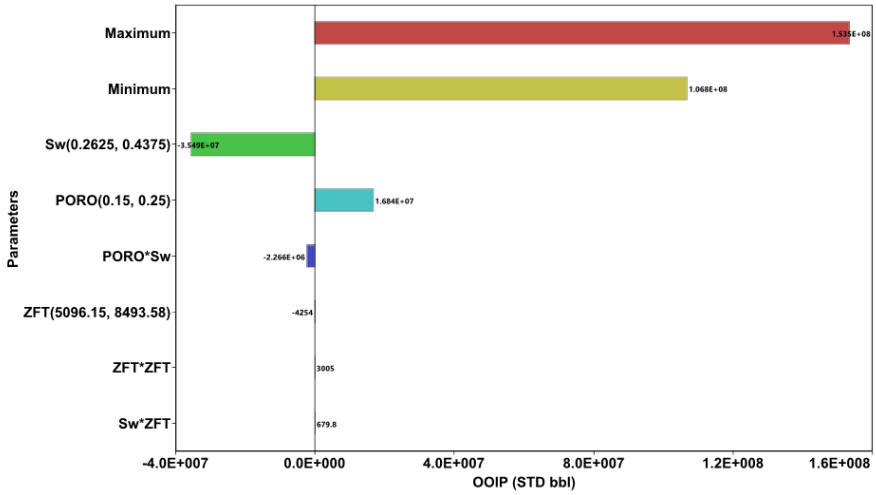

Figure F5: Tornado Diagram Showing the Effect of Input Parameters on the OOIP Estimated by Haase's Thermal Diffusion CG Initialised Reservoir Model

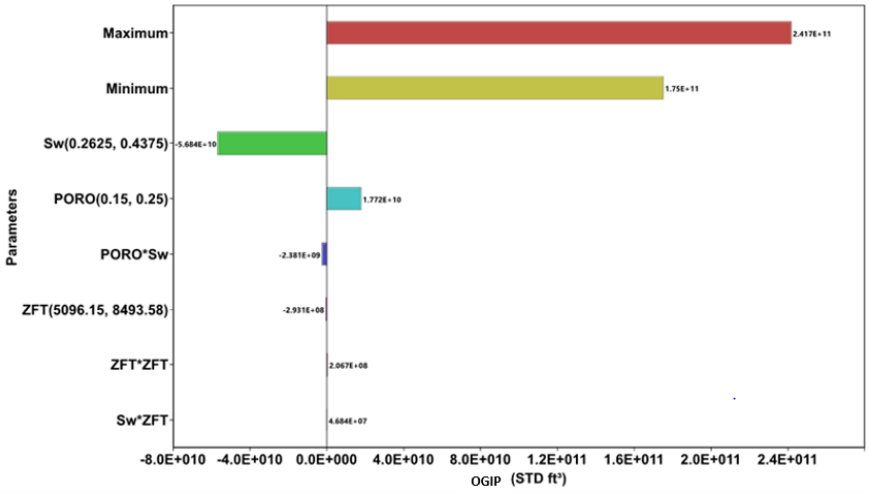

Figure F6: Tornado Diagram Showing the Effect of Input Parameters on the OGIP Estimated by Haase's Thermal Diffusion CG Initialised Reservoir Model

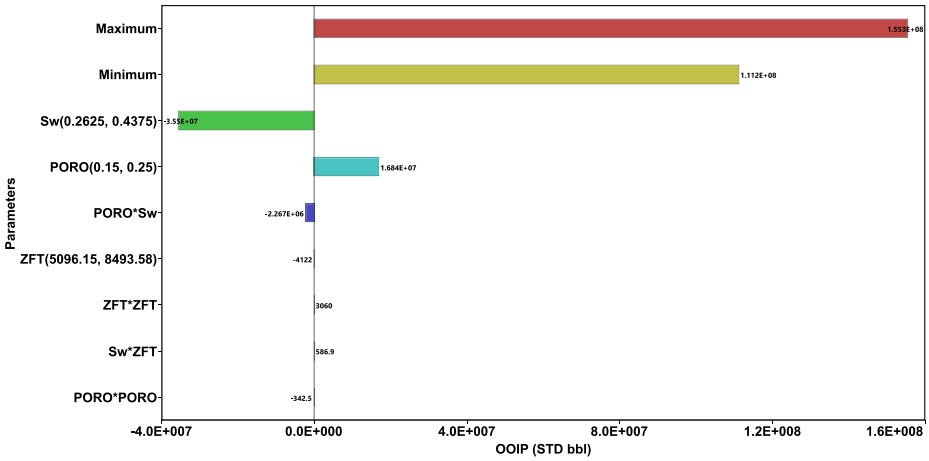

Figure F7: Tornado Diagram Showing the Effect of Input Parameters on the OOIP Estimated by Kempers Thermal Diffusion CG Initialised Reservoir Model

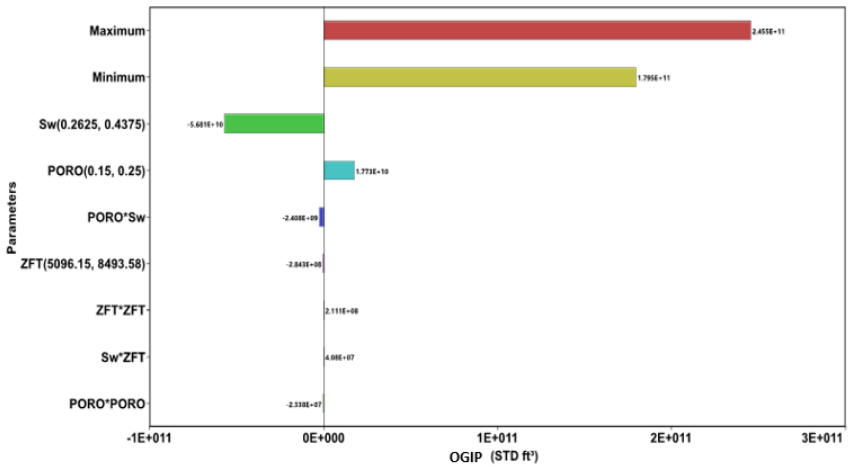

Figure F8: Tornado Diagram Showing the Effect of Input Parameters on the OGIP Estimated by Kempers Thermal Diffusion CG Initialised Reservoir Model

Appendix G

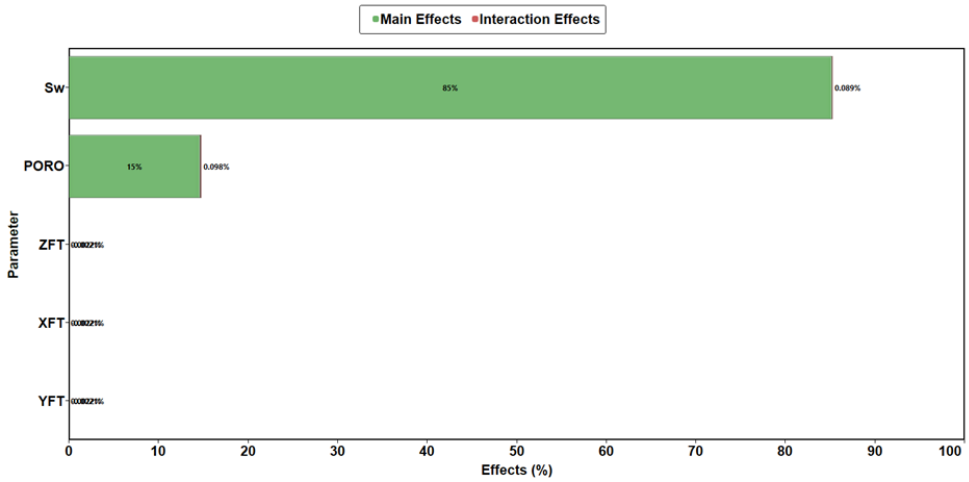

Figure G1: Percentage Effect of Input Parameters on the OOIP Estimated by Isothermal CG Initialised Reservoir Model

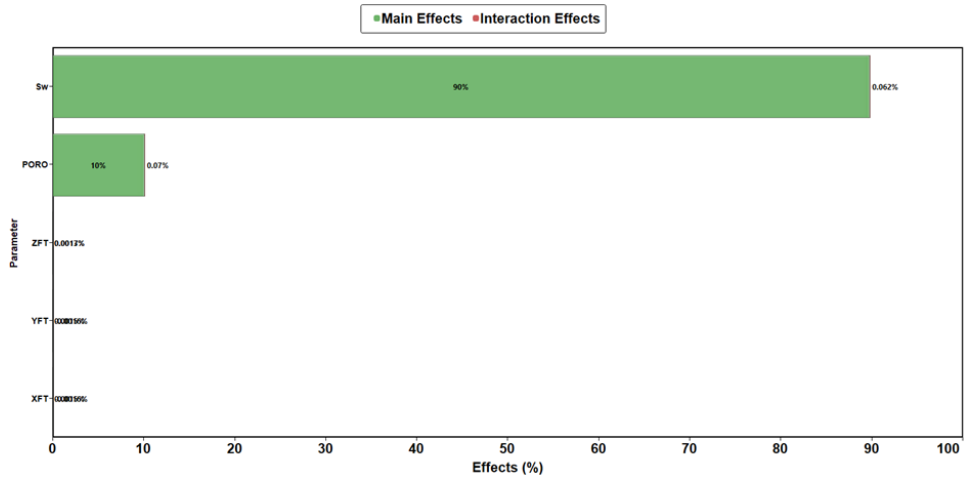

Figure G2: Percentage Effect of Input Parameters on the OGIP Estimated by Isothermal CG Initialised Reservoir Model

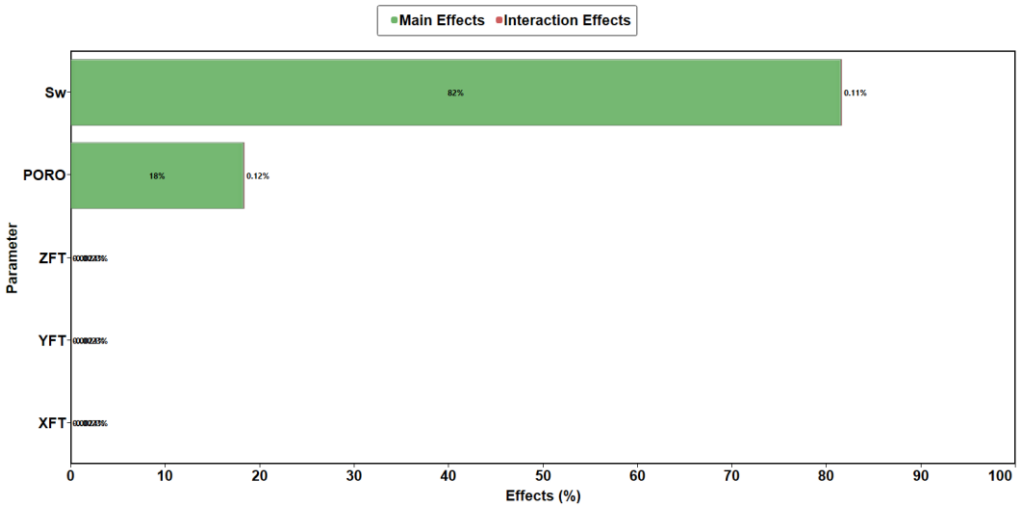

Figure G3: Percentage Effect of Input Parameters on the OOIP Estimated by Zero Thermal Diffusion CG Initialised Reservoir Model

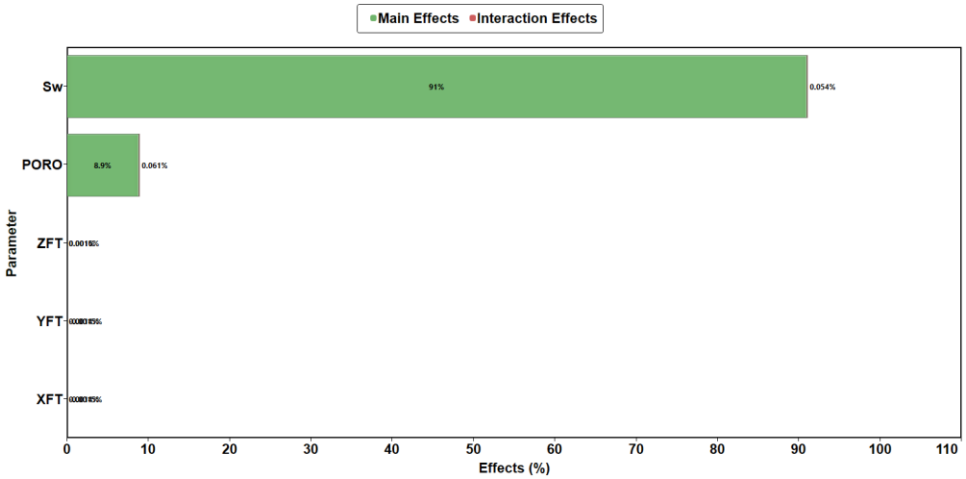

Figure G4: Percentage Effect of Input Parameters on the OGIP Estimated by Zero Thermal Diffusion CG Initialised Reservoir Model

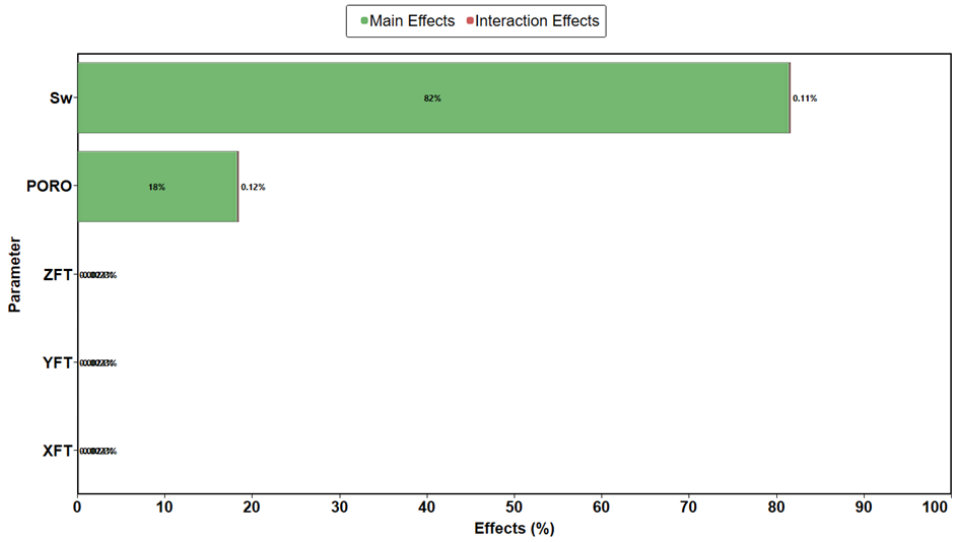

Figure G5: Percentage Effect of Input Parameters on the OOIP Estimated by Haase's Thermal Diffusion CG Initialised Reservoir Model

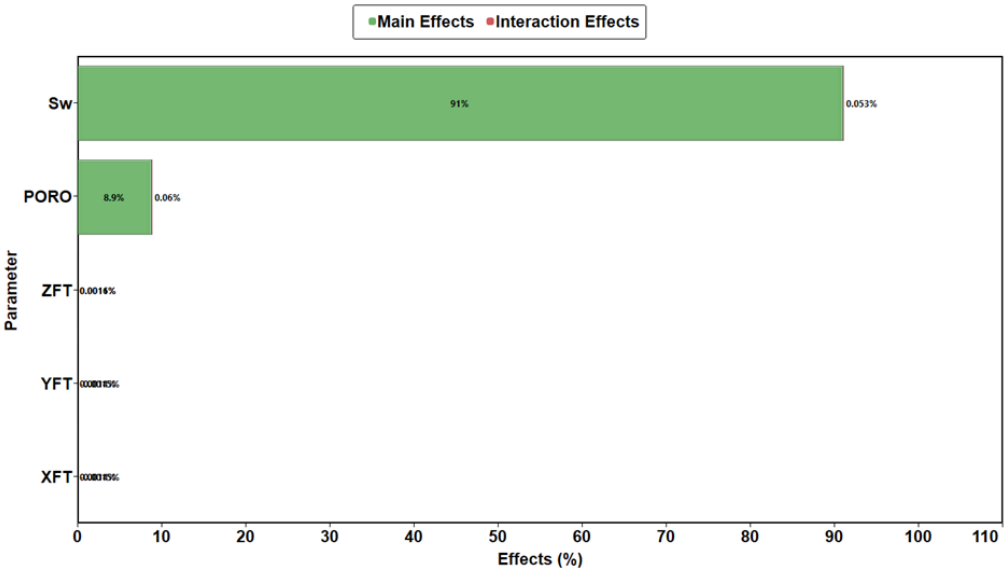

Figure G6: Percentage Effect of Input Parameters on the OGIP Estimated by Haase's Thermal Diffusion CG Initialised Reservoir Model

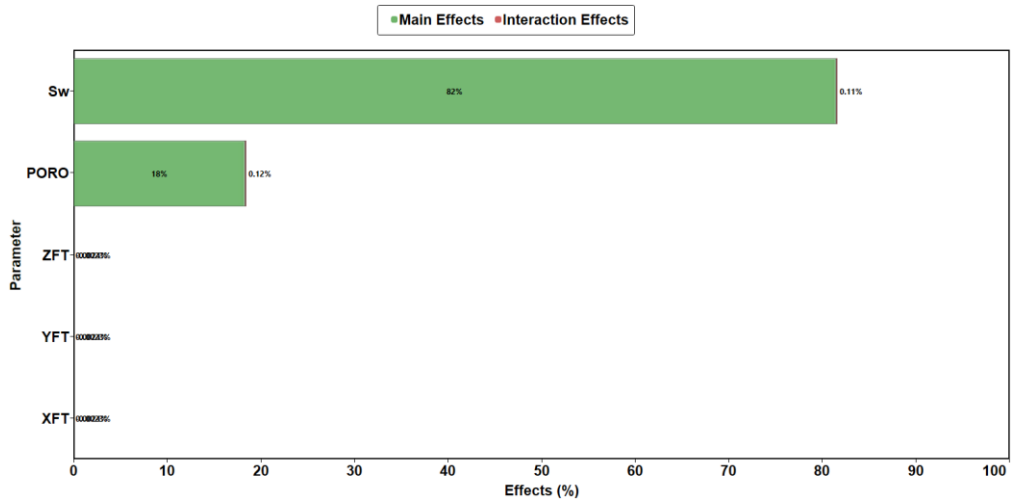

Figure G7: Percentage Effect of Input Parameters on the OOIP Estimated by Kempers Thermal Diffusion CG Initialised Reservoir Model

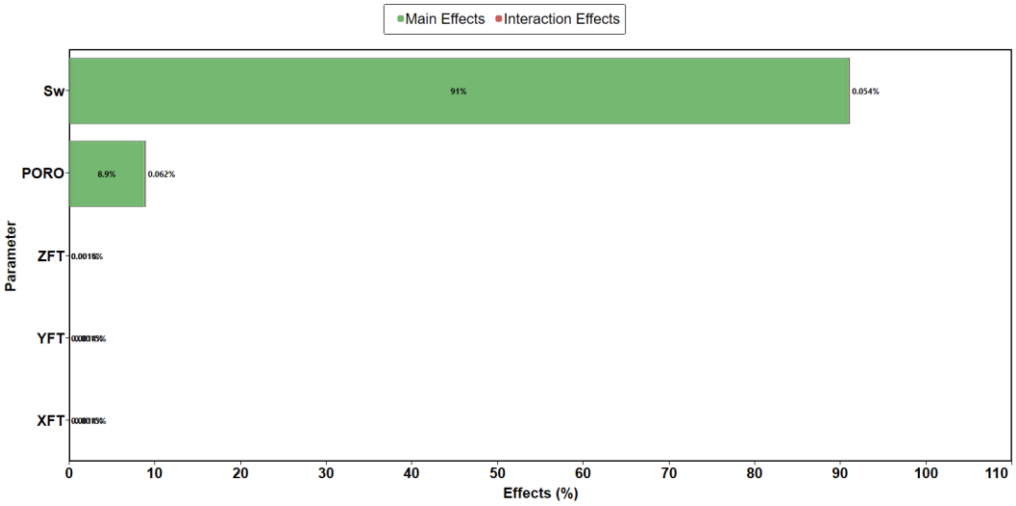

Figure G8: Percentage Effect of Input Parameters on the OGIP Estimated by Kempers Thermal Diffusion CG Initialised Reservoir Model

Appendix H

Table H1: OOIP Estimated by Different EOSs Based on Various Initialised Reservoir Model

Model	**OOIP Estimated with Different EOSs (STD MMbbl)**			
	PR 1978	**PR 1976**	**SRK (G&D)**	SRK
Constant Composition	174.428	171.417	176.843	177.031
Isothermal	150.569	142.358	133.286	152.431
Zero Thermal Diffusion	131.923	129.608	133.451	133.605
Haase's	131.802	167.889	173.277	224.861
Kempers	131.849	167.901	133.676	173.473

Table H2: OGIP Estimated by Different EOSs Based on Various Initialised Reservoir Model

Model	**OGIP Estimated with Different EOSs (STD Bft3)**			
	PR 1978	**PR 1976**	**SRK (G&D)**	SRK
Constant Composition	173.913	171.417	157.778	157.635
Isothermal	196.05	197.947	194.569	179.795
Zero Thermal Diffusion	210.848	204.789	194.364	194.289
Haase's	211.047	175.404	163.364	194.525
Kempers	210.967	175.386	194.525	163.214

Appendix I

Table I1: The OOIP Estimated by Applied Nonisothermal CG Initialised Reservoir Models at Different Temperature Gradients

Model	OOIP (SC bbl) at Different Temperature Gradient					
	0.002	0.5	1	1.5	2	2.5
Zero Thermal Diffusion	1.3192×10^{8}	1.7237×10^{8}	1.6234×10^{8}	1.5798×10^{8}	1.0534×10^{8}	9.5272×10^{7}
Haase's	1.3180×10^{8}	1.2725×10^{8}	1.3372×10^{8}	1.3875×10^{8}	1.6261×10^{8}	2.0549×10^{8}
Kempers	1.3185×10^{8}	1.8236×10^{8}	1.9285×10^{8}	1.9674×10^{8}	2.2269×10^{8}	2.2342×10^{8}

Table I2: The OGIP Estimated by Applied Nonisothermal CG Initialised Reservoir Models at Different Temperature Gradients

Models	OGIP (SC ft^3) at Different Temperature Gradient					
	0.002	0.5	1	1.5	2	2.5
Zero Thermal Diffusion	2.1085×10^{11}	1.6828×10^{11}	1.7146×10^{11}	1.7943×10^{11}	1.9837×10^{11}	2.0584×10^{11}
Haase's	2.1105×10^{11}	1.7117×10^{11}	1.4284×10^{11}	1.2654×10^{11}	1.0069×10^{11}	5.8999×10^{10}
Kempers	2.1097×10^{11}	1.4453×10^{11}	1.2821×10^{11}	1.2387×10^{11}	4.9568×10^{11}	4.9441×10^{10}

Form UPR16

FORM UPR16

Research Ethics Review Checklist

Please include this completed form as an appendix to your thesis (see the Research Degrees Operational Handbook for more information

Postgraduate Research Student (PGRS) Information			**Student ID:**	up796720	
PGRS Name:	IKECHI IGWE				
Department:	School of Energy and Electronic Engineering	**First Supervisor:**	Dr. Jebraeel Gholinezhad		
Start Date: (or progression date for Prof Doc students)	01/10/2016				
Study Mode and Route:	Part-time ☐ Full-time ☒	MPhil ☐ PhD ☒		MD ☐ Professional Doctorate ☐	

Title of Thesis:	Petroleum Reservoir Performance Evaluation Based on Compositional Grading Models
Thesis Word Count: (excluding ancillary data)	32,972

If you are unsure about any of the following, please contact the local representative on your Faculty Ethics Committee for advice. Please note that it is your responsibility to follow the University's Ethics Policy and any relevant University, academic or professional guidelines in the conduct of your study

Although the Ethics Committee may have given your study a favourable opinion, the final responsibility for the ethical conduct of this work lies with the researcher(s).

UKRIO Finished Research Checklist:
(If you would like to know more about the checklist, please see your Faculty or Departmental Ethics Committee rep or see the online version of the full checklist at: http://www.ukrio.org/what-we-do/code-of-practice-for-research/)

a) Have all of your research and findings been reported accurately, honestly and within a reasonable time frame?	YES ☒ NO ☐
b) Have all contributions to knowledge been acknowledged?	YES ☒ NO ☐
c) Have you complied with all agreements relating to intellectual property, publication and authorship?	YES ☒ NO ☐
d) Has your research data been retained in a secure and accessible form and will it remain so for the required duration?	YES ☒ NO ☐
e) Does your research comply with all legal, ethical, and contractual requirements?	YES ☒ NO ☐

Candidate Statement:		
I have considered the ethical dimensions of the above named research project, and have successfully obtained the necessary ethical approval(s)		
Ethical review number(s) from Faculty Ethics Committee (or from NRES/SCREC):		E770-9532-B645-7B80-A4C0-B32E-66B4-4616
If you have *not* submitted your work for ethical review, and/or you have answered 'No' to one or more of questions a) to e), please explain below why this is so:		
Signed *(PGRS)*:		**Date:** 14/09/2020

UPR16 – April 2018

Certificate of Ethics Review

Certificate of Ethics Review

Project Title:	PETROLEUM RESERVOIR PERFORMANCE EVALUATION BASED ON COMPOSITIONAL GRADING MODELS
User ID:	796720
Name:	Ikechi Igwe
Application Date:	20/07/2018 19:13:50

You must download your certificate, print a copy and keep it as a record of this review.

It is your responsibility to adhere to the University Ethics Policy and any Department/School or professional guidelines in the conduct of your study including relevant guidelines regarding health and safety of researchers and University Health and Safety Policy.

It is also your responsibility to follow University guidance on Data Protection Policy:

- General guidance for all data protection issues
- University Data Protection Policy

You are reminded that as a University of Portsmouth Researcher you are bound by the UKRIO Code of Practice for Research; any breach of this code could lead to action being taken following the University's Procedure for the Investigation of Allegations of Misconduct in Research.

Any changes in the answers to the questions reflecting the design, management or conduct of the research over the course of the project must be notified to the Faculty Ethics Committee. **Any changes that affect the answers given in the questionnaire, not reported to the Faculty Ethics Committee, will invalidate this certificate.**

This ethical review should not be used to infer any comment on the academic merits or methodology of the project. If you have not already done so, you are advised to develop a clear protocol/proposal and ensure that it is independently reviewed by peers or others of appropriate standing. A favourable ethical opinion should not be perceived as permission to proceed with the research; there might be other matters of governance which require further consideration including the agreement of any organisation hosting the research.

GovernanceChecklist
A1-BriefDescriptionOfProject: This research is absolutely computer based modelling and simulation using Petroleum reservoir simulators (software) and raw numerical data from industrial archives to estimate hydrocarbon reserves and predict reservoir performance, respectively. The technical and economic implications of the various isothermal and non-isothermal compositional grading models to accurately predict hydrocarbon reserves and reservoir performance will be advised.
A2-Faculty: Technology
A3-VoluntarilyReferToFEC: No

Certificate Code: E770-9532-B645-7B80-A4C0-B32E-66B4-4616 Page 1